EXTREME WAVE HEIGHT ESTIMATION FOR OCEAN ENGINEERING APPLICATIONS IN THE GULF OF MEXICO

A Dissertation

by

CHAN KWON JEONG

Submitted to the Office of Graduate Studies of
Texas A&M University
in partial fulfillment of the requirements for the degree of

DOCTOR OF PHILOSOPHY

May 2011

Major Subject: Ocean Engineering

Extreme Wave Height Estimation for Ocean Engineering

Applications in the Gulf of Mexico

EXTREME WAVE HEIGHT ESTIMATION FOR OCEAN ENGINEERING APPLICATIONS IN THE GULF OF MEXICO

A Dissertation

by

CHAN KWON JEONG

Submitted to the Office of Graduate Studies of
Texas A&M University
in partial fulfillment of the requirements for the degree of

DOCTOR OF PHILOSOPHY

Approved by:

Co-Chairs of Committee,	Vijay Panchang
	Patrick Lynett
Committee Members,	Billy L. Edge
	Kuang-An Chang
	Vivek Sarin
Head of Department,	John Niedzwecki

May 2011

Major Subject: Ocean Engineering

ABSTRACT

Extreme Wave Height Estimation for Ocean Engineering

Applications in the Gulf of Mexico. (May 2011)

Chan Kwon Jeong, B.S., HongIk University, Korea;

M.S., Inha University, Korea

Co-Chairs of Advisory Committee: Dr. Vijay Panchang
Dr. Patrick Lynett

Recent hurricanes in the Gulf of Mexico (e.g., Ivan, Dennis, Katrina, Rita and Ike) were observed to develop wave conditions that were near or exceeded the predicted 100-year conditions. As a result, many offshore facilities, as well as coastal infrastructure, which were designed to withstand the 100-year condition, were damaged. New estimates of extreme conditions, which incorporate recently observed maxima, are needed to provide better guidelines for design of coastal and offshore structures. Berek et al. (2007) have used modeled data to develop new criteria, but these estimates can be very sensitive to the data and to the statistical methods used in the development. Berek's estimates also do not cover the entire Gulf of Mexico. We have developed updated estimates of the 100-year extreme wave conditions for the entire Gulf of Mexico using a more comprehensive approach. First, the applicability of standard parametric wind models was examined and appropriate adjustments to the Rankine vortex model were developed to reduce the wind field errors during hurricane conditions. The adjusted winds reduced the error by up to 25 % compared to the original Rankine vortex model.

To obtain reliable wave data, merged wind fields were generated using the NCEP/NCAR Reanalysis 1 project modeled wind data for background wind and the parametric wind model for hurricane conditions. Next, the SWAN wave model was used for the 51-year period from 1958 to 2008 along with multiple statistical methods (Gumbel, Weibull and GEV-Generalized Extreme Value distribution). The effect of the recent hurricane season (2004-2008) shows that maximum 100-year wave height values and their distribution changes. A resampling technique (bootstrap) is used to evaluate and select the optimum statistical method to estimate more appropriate extreme wave conditions.

ACKNOWLEDGEMENTS

It is hard to exaggerate my gratitude to my Ph.D. supervisor, Dr. Vijay Panchang. With his enthusiasm, his inspiration, and his kind consideration, he helped me finish my Ph.D. study and guided me to the right path as an engineer. During my dissertation-writing period, I would have been lost if I had not had his advice, good teaching and encouragement.

I would like to thank my committee co-chair, Dr. Lynett and my committee members, Dr. Edge, Dr. Chang, and Dr. Sarin, for their guidance and kind assistance throughout the course of this research. I wish to thank in addition Dr. Miller, Dr. Horrillo and Mr. Singhal.

I wish to thank my wife, Jahyun, for providing a loving environment with two daughters, Jeana and Yuna.

Finally, thanks to my deceased mother and father for their encouragement, support and love.

TABLE OF CONTENTS

LIST OF FIGURES

FIGURE Page

FIGURE Page

LIST OF TABLES

CHAPTER I

INTRODUCTION

The accurate prediction of winds and waves in the ocean and in coastal regions is critical for the safe and effective design of coastal and offshore structures, prediction of sediment transport, marine operations, and maritime safety. In addition, accurate characterization of the wave climate and estimates of waves during extreme events are needed to anticipate environmental impacts as well as for use in structural design. Obtaining reliable and adequate data is always a major part of engineering studies.

The Gulf of Mexico (GOM), shown in Fig. 1.1, is an area of extensive and diverse ocean activities. The region supports large commercial and sport fisheries, large-scale shipping, and gas and oil exploration and production. The region is also subject to topical storms and hurricanes. During recent past, strong hurricane winds in the GOM have generated waves of unusual height relative to those that have been predicted from previous long-term studies (API, 2000). During hurricane Ivan in 2004, "maximum" wave heights as high as 27.9 m were recorded by Wang et al. (2005), who suggest that even larger waves may have occurred. During hurricane Ivan, "significant" wave heights (SWH's) of nearly 16 m were recorded at a National Data Buoy Center (NDBC) measurement site before the buoy malfunctioned. These wave heights are well in excess of the 100-year return period estimate (Panchang and Li, 2006). Comparably

---

This dissertation follows the style of *Journal of Waterway, Port, Coastal, and Ocean Engineering*.

large (and at some locations, larger) wave heights were recorded again during hurricane Katrina in 2005. The extreme storm surge, wind, and wave conditions, which have been documented and analyzed in part by Hovis (2005) and by Panchang and Li (2006), caused damage to the extensive oil and gas facilities in the Gulf of Mexico. Approximately 190 oil platforms were destroyed or severely damaged, disrupting the nation's energy supplies for months and causing economic losses to the tune of hundreds of millions of dollars (Clayton 2007). Other significant storms during recent years include hurricanes Ivan (September 2004), Dennis (July 2005), Katrina (August 2005), Rita (September 2005), and Ike (September 2008).

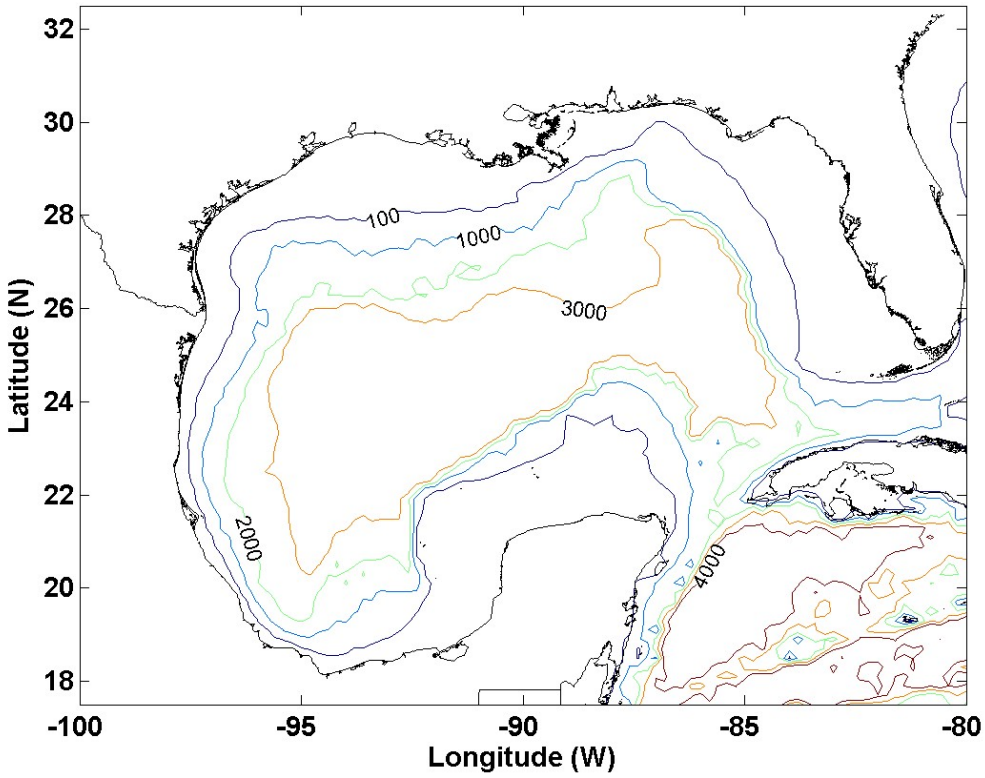

Fig. 1.1. Gulf of Mexico and bathymetry (m).

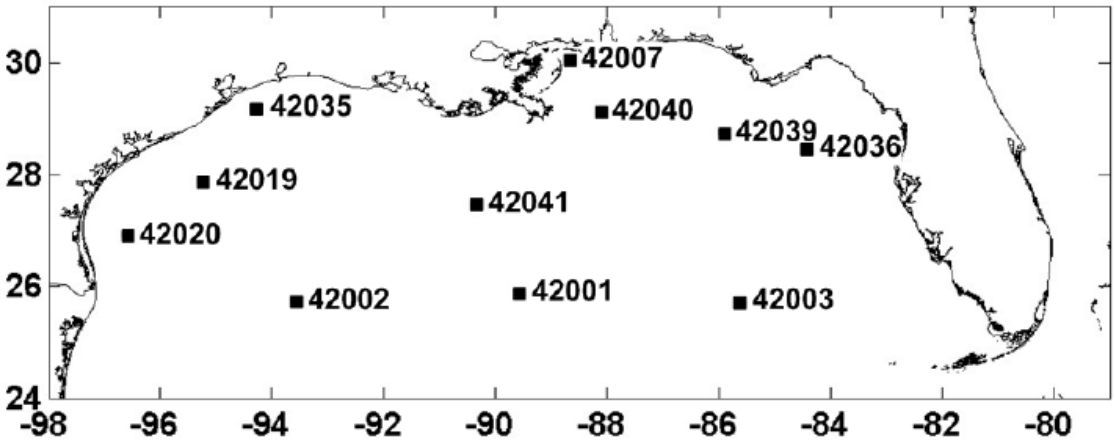

Fig.1.2. Approximate NDBC buoy locations in the Gulf of Mexico.

The NDBC maintains eleven wave measurement buoys in the GOM from which measured wave data can be obtained (Fig. 1.2). For this study, hourly values were available for time periods ranging between 7 and 33 years at these locations. Table 1.1 provides a summary of these data and includes the highest and second highest SWHs recorded at the indicated locations. When the measured maximum waves are associated with a recent storm, the name has been included. It is clear from Table 1.1 that, at seven of the buoy locations (42001, 42003, 42007, 42019, 42035, 42039, and 42040) the 2004-2008 hurricane seasons produced SWHs larger than any of those previously recorded. The height difference between the previous largest SWH and those recorded during the 2004 to 2008 seasons are substantial at three of the buoy locations (42039, 42040, and 42007). The previous largest SWH recorded at these locations were 9.3 m (in 1998), 10.8 m (in 1998), and 4.9 m (2002), respectively. Although two of these locations have relatively short datasets, the differences are notable at the locations of buoys 42007 and

42040; at the latter buoy location, large SWH's were recorded even during hurricane Ivan also (15.96 m). At the other three locations, the differences are marginal.

Table 1.1. Wave data description in the Gulf of Mexico.

Buoy	Year	Depth (m)	Maximum SWH (m)	2ND largest SWH (m)
42001	1976 – 2008 (33)	3246.0	11.63 (Sep 2005) - Rita	11.2 (Oct 2002)
42002	1976 – 2008 (33)	3566.2	9.70 (Sep 1988)	8.4 (Nov 1980)
42003	1977 – 2008 (32)	3233.0	11.04 (Sep 2004) - Ivan	10.7 (Nov 1985)
42007	1981 – 2008 (28)	14.0	9.09 (Sep 2004) - Ivan	5.64 (Aug 2005) - Katrina
42019	1990 – 2008 (19)	82.3	6.3 (Sep 2008) - Ike	5.92 (Sep 2005) - Rita
42020	1990 – 2008 (19)	88.1	8.20 (Aug 1999)	6.79 (Oct 1996)
42035	1993 – 2008 (16)	13.7	7.1 (Sep 2008) - Ike	4.7 (Sep 2005) - Rita
42036	1994 – 2008 (15)	54.5	8.60 (Oct 1995)	6.9 (Jan 1994)
42039	1995 – 2008 (14)	291.4	12.05 (Sep 2004) - Ivan	10.6 (Jul 2005) - Dennis
42040	1995 – 2008 (14)	443.6	16.91 (Aug 2005) - Katrina	15.96 (Sep 2004) - Ivan
42041	1999 – 2005 (7)	1055.7	12.31 (Oct 2002)	8.56 (Sep 2004) - Ivan

As a result of the observation of these extremely large waves, the American Petroleum Institute (API) has started efforts to reexamine the specification of design conditions for offshore structures in this area. These efforts, described by Berek et al. (2007) used a combination of synthetic hindcast (modeled) wind and wave information (including the most recent period) and the Weibull distribution (with the peak over threshold method) to estimate the n-year return period wind and wave conditions. In some regions of the GOM, these new estimates suggest substantial increases in wave height and wind speed; relative to API's current estimates of the 100-year design conditions, the maximum increase is as much as 6.4 m in the 100 –year significant wave height (denoted by SWH_{100}) and 5 m/s in the wind speeds. According to the API (2000), the maximum SWH_{100} was 12m; according to the API (2007), the maximum SWH_{100} is 15.8m.

Because such extreme value estimates can be sensitive to (1) the data and (2) the statistical method used to generate them and, because the API calculations do not cover the entire Gulf, in this thesis, we have tried to provide additional estimates by using 51 years of detailed numerical simulation data and multiple statistical methods. This is also important because significant wave heights generated during hurricane Ike (2008) equaled on exceeded API's new estimates at some locations. In fact, the API study does not include storms after 2006. Our additional estimates helps the engineer make informed decisions and assess the uncertainty associated with the results.

The quality of data is a fundamental element for this study. Although measured data are the best source for metocean studies, individual measurement sites are widely distributed and the lengths of records are relatively short or discontinuous. As a result, measured data are usually insufficient to characterize waves over large ocean areas. An alternative method of data development is to use numerical models to calculate the wave conditions based on measured or modeled winds. This method of wave-data development is well established and has been widely applied. Besides the API (Berek et al. 2007), several recent examples include the work of Oliveira (2002) who used a mild-slope wave equation model to estimate the wave climate near Rio de Janeiro for beach evolution studies, Pontes et al. (2005) who developed a near-shore atlas for wave energy calculations in Portugal, Millar et al. (2006) who used the model SWAN (Simulating WAves Nearshore) to examine the impacts of wave energy farms off the UK coast, and Harris and Coleman (1998) who used hindcast obtained with energy-balance model to estimate shelf sediment mobility.

For the modeling of waves, as described above, the reliability of wind data is a critically important factor. Berek et al. (2007) have generated the data by hindcasting select storms for the period 1950-2006 using proprietary modeling tools. However, synthetic data can generally be vulnerable to many modeling related errors (e.g. Rogers et al. 2007; Cardone et al. 1992*)* and no details of their errors are available. Most wave models can produce accurate wave results when provided with realistic surface wind input, but the measured and modeled resolution of normal weather systems is too coarse to represent the rapidly changing velocities and directions within hurricanes. Parametric models of wind distribution and intensity are commonly used to estimate the surface wind fields based on hurricane parameters provided by the National Hurricane Center in the Atlantic basin hurricane database (or HURDAT). This dataset is available from 1851 to present. Most parametric models provide good estimates of maximum wind speed values, but the spatial distribution of the winds is often represented as symmetrical around the central area which is substantially different from the real hurricane wind distribution. Asymmetric wind models have been attempted to more realistically represent the actual wind distribution (Georgiou 1985) and McAfee and Pearson (2006) proposed adjustments to the parametric model schemes suitable for the mid-latitudes. For the mid-Atlantic region, Xie el al. (2006) also developed an asymmetric model based on the Holland model, and Liu et al. (2007) tested the differences of modeled wind waves between symmetric and asymmetric wind input by using SWAN. Though some of these attempts were improvements on common parametric wind models, they do not cover all hurricane wind patterns nor do they adequately provide wind speeds at specific

locations. In particular, GOM hurricanes were not systematically studied. Moreover, data required by the adjustments proposed by Xie el al. (2006) are not available, in HURDAT dataset. For the reconstruction of reliable historical wind and wave data, alternative methods must be examined.

In addition to reliable metocean data, the application of suitable statistical methods is important to characterize extreme events. The n-year estimates can be highly sensitive to the chosen statistical method, and to the "threshold" in the peak-over-threshold method that is commonly used for extreme estimation (Van Vledder et al. 1993). Berek et al (2007) have chosen, a priori, the Weibull distribution. The question of whether this is the best distribution for the data has not been addressed, nor has the sensitivity to the threshold.

The main objective of this thesis is carry out a comprehensive study for estimating the variability inherent in the SWH_{100} estimates resulting from the use of different sets of data and different statistical methods for the entire Gulf of Mexico. A 51-year numerical wave hindcast (1958 – 2008) was developed and appropriately chosen statistical methods were investigated. Buoy data were also used to validate both individual storm simulations and the SWH_{100} estimates. While generating SWH_{100} estimates suitable for design, the following questions must be addressed:

1. How well do commonly used parametric wind models (such as the Holland, Rankine vortex, and SLOSH models) reproduce GOM hurricanes?
2. Are adjustments to parametric wind models needed, as suggested by other researchers (e.g. Xie et al. 2006, McAfee et al. 2006)?

3. What is the effect of errors in the wind modeling on the modeled SWHs?
4. How do SWH_{100} values obtained by modeling compare with those obtained from buoy data? What is the effect of modeling errors on the SWH_{100}?
5. What is the variability associated with the choice of other distributions? For estimation of extreme wave conditions, three commonly used extreme value distribution functions (Gumbel, Weibull, and Generalized Extreme Value) were evaluated to select the optimum statistical method for extreme condition estimates.
6. Which model is the most appropriate in different areas? This is usually a difficult and subjective problem, but recent developments by Li et al. (2008) have provided more robust and quantitative ways based on the Jack-knife or the Bootstrapping methods, for such identification. By following their approach, the most appropriate model can be selected based on the engineer's preference, rather than limiting oneself to any pre-selected model, as done by Berek et al. (2007).
7. What is the effect of data length on the estimates? Buoy data are available for varying time periods, whereas model results were developed here for 51 years.
8. What is the effect of the recent (2004-2008) extreme hurricane season on the estimates of SWH_{100}?
9. Beside the API recommendations, are alternative estimates available to the engineer?

The thesis is organized as follows. Chapter II provides details about available wind and wave information in the GOM. It also examines the perform of three commonly used parametric wind models when applied to recent storms. Substantial differences were found. Chapter III describes adjustments to the Rankine vortex model to obtain more reliable hurricane winds. The wave modeling methodology used to obtain wave characteristics at appropriately fine resolution, modeling errors, adjustments, and validation of the calculated wave heights are described in Chapter IV. Chapter V introduces statistical methods for extreme wave estimations, and the validation of the statistical estimates using model data and buoy data is presented in Chapter VI. This involves using a model dataset that is limited to the length of the buoy data. In Chapter VII, the entire 51 years of model data are used to obtain SWH_{100}, using three distributions, and the behavior of each is examined. This helps identify the most appropriate SWH_{100} estimate at each grid point. Chapter VIII summarizes the results of this study.

CHAPTER II

AVAILABLE WIND INFORMATION IN THE GULF OF MEXICO AND PARAMETRIC WIND MODELING

2.1 Introduction

Wind and wave measurements have been made in the Gulf of Mexico at a number of sites maintained by the National Oceanic and Atmospheric Administration. These data have been archived and are available through the National Data Buoy Center. These data are collected at fixed locations, however, and numerical modeling is needed to obtain data at other locations. Four types of wind fields (on different spatial and temporal grids) are available for developing the wave estimates:

1) The National Center for Environmental Prediction (NCEP) uses the most sophisticated models available to produce wind fields every 6 hours. In the Gulf of Mexico, the simulations are made using the NCEP "Western North Atlantic" and "North Atlantic Hurricane" models, which creates wind fields on $0.25° \times 0.25°$ grids. These simulations represent perhaps the best estimates of wind fields for the entire Gulf of Mexico; however they are not available prior to 1999. Thus, alternative sources of wind data must be explored because for this study wave hindcasts are needed for the period prior to 1999.

2) NCEP and National Center for Atmospheric Research (NCAR) have developed the "Reanalysis" wind field dataset, using a combination of mathematical models and

assimilation of all available data (Kalnaya et al. 1996). An example is shown in Fig. 2.1 (left) for hurricane Gordon. These wind fields are available for the period starting in 1948 at a temporal resolution of 6 hours. Because the spatial resolution is coarse (2.5° × 2.5°), some features of a hurricane may not be well represented by these data, despite their use in large areas such as the Atlantic (Music and Nickovic 2008; Cieślikiewicz and Paplińska-Swerpel 2008; Pilar et al. 2008; Wang and Swail 2002; Wang et al. 2004).

3) A comprehensive wind dataset representing all available hurricane measurements has been developed by the National Hurricane Center (Powell et al. 1996 & 1998). This dataset, called H*Wind, is available for the post-1994 period, and has been widely used by researchers for various applications (e.g. Kennedy et al. 2010; Powell et al. 2010). An example is shown in Fig. 2.1 (right) for hurricane Gordon. It is an estimate of the wind field based on all available observations, viz. aircraft-based, land-based, sea-based, and satellite-based. Based on a standardization technique to process data from diverse sources, it provides wind fields at a resolution of approximately 6 km. As may be expected, this dataset is not continuous (except in the recent past), does not cover all hurricanes is limited to the immediate vicinity of the hurricane, and is available at irregular time steps.

4) A dataset containing a limited set of storm parameters has been developed by NOAA for a period going back to 1851. But more details are available only after 1950. This dataset, called HURDAT, provides information at 6-hour intervals, information such

as the location of the storm center (LatC, LonC), storm direction (θ_s), storm speed (V_s), maximum wind speed (V_m), and storm central pressure (P_c). These data do not provide details of a complete wind field, but only storm parameters.

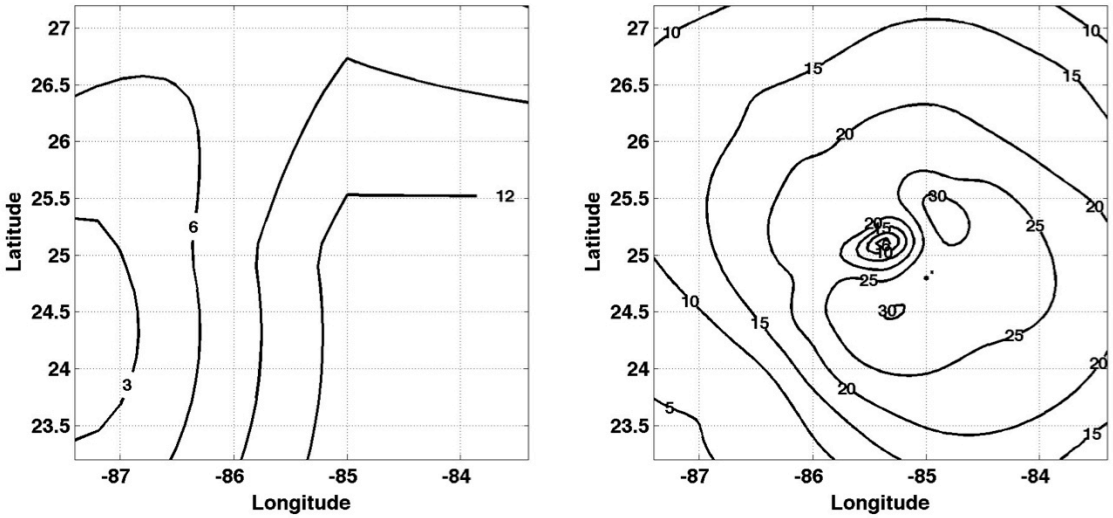

Fig. 2.1. Wind-field contours (m/s) for hurricane Gordon, 0000 UTC 17 September 2000; Reanalysis (left), and H*Wind field (right).

For recreating historical wind fields on a continuous basis for a grid covering the entire Gulf of Mexico the H*Wind and the Reanalysis wind fields are not completely adequate. Therefore, we develop wind fields using parametric formulations that depend on a limited set of parameters (HURDAT). This approach has been used, for instance, by Phadke et al. (2003) for simulating tropical cyclones near Hawaii, and by McAfee and Pearson (2006) for simulating mid-Atlantic hurricanes.

2.2 Parametric wind models

Hurricane winds change rapidly in speed and direction. For numerical simulation purposes, parameterized models are developed and are widely used to represent complex hurricane wind fields. MacAfee and Pearson (2006) have summarized five parametric models: The Rankine Vortex (RV) model (with modifications as presented by Phadke et al., 2003), the SLOSH model (Houston and Powell, 1994), the Holland (1980) model, the vortex simulation model (DeMaria et al. 1992), and the Willoughby and Rahn (2002) model. In general, these models provide the wind speed $V(x,y)$ as a function of hurricane parameters V_m and P_c and also of the other model-calculated quantities such as the radius to maximum wind (R_m), sea level pressure at the last closed isobar (P_n), etc. (Different numerical models use different parameters). The three models used here are described in the following,

(a) The Rankine vortex (denoted by RV) model provides a radially symmetric hurricane wind field as follows:

$$V = \begin{cases} V_m \left(\dfrac{R}{R_m} \right)^B, & R < R_m \\ V_m \left(\dfrac{R_m}{R} \right)^B, & R \geq R_m \end{cases} \tag{2.1}$$

where V_m is the maximum wind speed, R is the radial distance from the storm center, R_m is the radius to maximum winds, and B is a shape parameter (≈ 0.5). The radius to maximum winds (R_m in km) has been described by MacAfee and Pearson (2006) as a

function of the latitude (φ in degrees), the central pressure (*mb*), and the pressure along the last closed isobar (P_n in *mb*) as follows:

$$\ln R_{\mathrm{m}} = 2.636 - 0.00005086(P_n - P_c)^2 + 0.0394899\varphi \tag{2.2}$$

$$\text{where} \quad P_n = P_c - 20.69 + 1.33V_{\mathrm{m}} + 0.11\varphi \tag{2.3}$$

The importance of properly introducing asymmetry to the RV model has been emphasized by Liu et al. (2007). This is done by making an adjustment to V due to storm translation. The net motion-adjusted wind velocity can then be obtained as:

$$V_{RV} = \left\{ \left(-V\cos\theta_r\right)^2 + \left[V\sin\theta_r + \frac{V_s R_m R}{\left(R_m^2 + R^2\right)} \right]^2 \right\}^{1/2} \tag{2.4}$$

where θ_r is the angle between the storm direction and the radius to a particular grid point, and V is the model wind speed estimated from Eq. 2.1.

A circular wind flow pattern for the wind direction is assumed and a cross-isobaric flow correction β proposed by Bretschneider (1972) was applied to each grid point (See example is shown in Fig. 2.2):

$$\beta = \begin{cases} 10^\circ + \left(1 + \dfrac{R}{R_m}\right), & R < R_m \\ 20^\circ + 25^\circ\left(\dfrac{R}{R_m} - 1\right), & R_m \le R < 1.2R_m \\ 25^\circ, & R \ge 1.2R_m \end{cases} \tag{2.5}$$

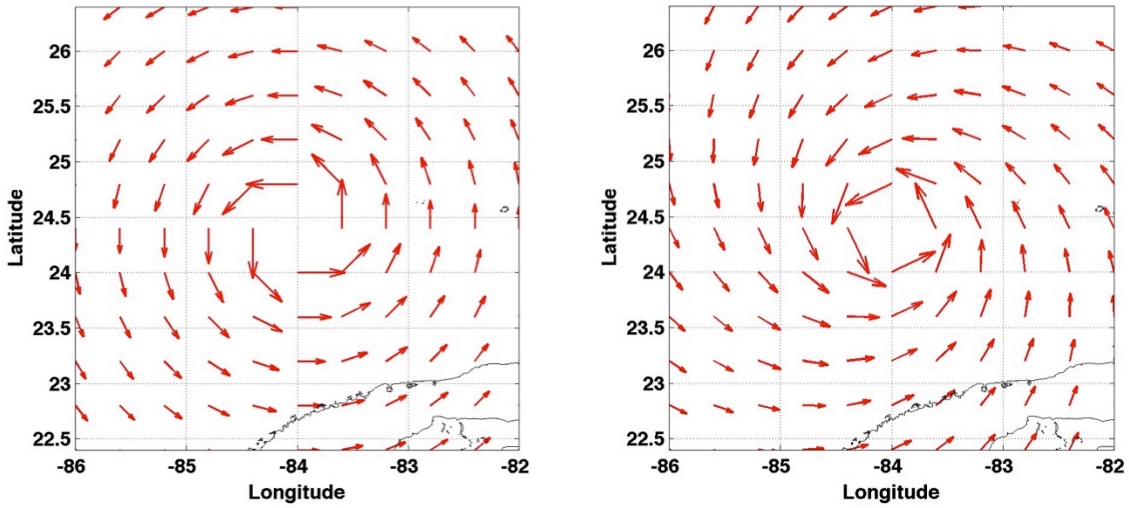

Fig. 2.2. A circular wind flow pattern (left) and a cross-isobaric flow correction β applied wind flow pattern.

(b) The SLOSH model essentially replaces Eq. 2.1 with the following,

$$V = V_{\max} \frac{2 \cdot R \cdot R_{\max}}{(R_{\max}^2 + R^2)} \tag{2.6}$$

(c) The Holland model essentially replaces Eq. 2.1 with the following,

$$V = \left\{ \left(\frac{R_{\max}}{R} \right)^B \frac{B(P_n - P_c)}{\rho} \exp\left[-\left(\frac{R_{\max}}{R} \right)^B \right] + \frac{R^2 f^2}{4} \right\}^{1/2} - \frac{Rf}{2} \tag{2.7}$$

2.3 Application of parametric models and recent hurricanes

As an example, for the parameters of hurricane Katrina, HURDAT provides the following information:

Month	Day	Hour	LatC	LogC	Dir.	Translational speed: V_s (km/h)	Max wind speed: V_m (km/h)	Pressure: P_c (mb)	Type
8	28	12	25.7	87.7	300	. . 18 .	270	909	Category 5

These HURDAT parameters were used with various parametric models to produce the wind field plots for hurricane Katrina shown in Fig. 2.3. Typically the basic models yield a symmetric pattern about the center as shown on the left side of the figure. Asymmetry may also be introduced parametrically (based on Eq. 2.4), which leads to the plots shown on the right side of Fig. 2.3.

For a detailed quantitative examination, five prominent Gulf of Mexico hurricanes that occurred during the period from 2004-2008 were chosen. These are Ivan (2004), Katrina (2005), Rita (2005), Dolly (2008), and Ike (2008). At the location of some of the NDBC buoys, wave heights recorded during four of these storms were larger than those recorded prior to 2004. In some cases, the SWH exceeded the predicted100-year wave condition (Panchang and Li, 2006; Jeong and Panchang, 2008). HURDAT details of these hurricanes provide a total of 56 snapshots (Table 2.1). (In fact, more snapshots are available in the HURDAT dataset, but the others extend over regions outside the Gulf of Mexico, including over land. Thus they are not considered). These snapshots cover the entire range of hurricane development stages (from the “tropical

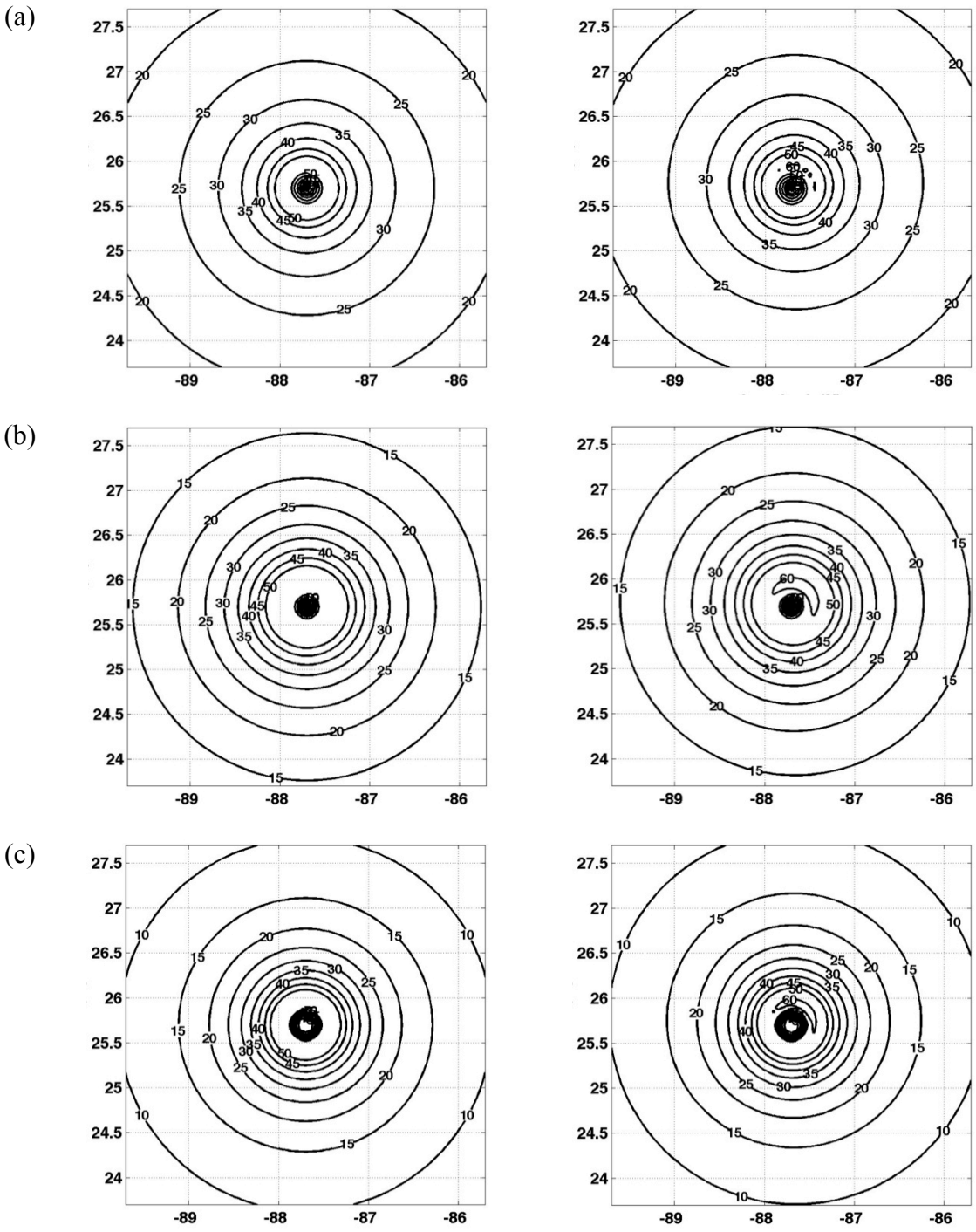

Fig. 2.3. Symmetric (left) and asymmetric (right) wind speeds (m/s) during hurricane Katrina (1200 UTC 28 Aug. 2005); (a) Rankine Vortex model; (b) SLOSH model; (c) Holland model.

storm" category to category 5; central pressures ranging between 902 *mb* and 1005 *mb*; and wind speeds varying between 85 km/h and 285 km/h). Also, these storms were chosen because they had the most largest number of HURDAT snapshots for validation.

Some results of the wind fields calculated using the RV model (Eqs. 2.1-2.5) for the parameters in Table 2.1 are shown Fig. 2.4a and Fig. 2.5a. The results represent one snapshot from each of the five storms. The corresponding H*Wind datasets are shown in Fig. 2.4b and Fig. 2.5b. Comparison shows that the parametric model needs adjustment to obtain a better match with the data. In particular, for some storms the "bean shape" in the core is insufficiently developed and the distribution of the velocity contours is tighter (smaller) than the data (e.g., the plots show considerable under estimation in many areas, especially on the right side of the hurricane). Figure 2.6 shows the wind speed along the central East-West radial, calculated using the RV model (Eq. 2.1-2.5), as well as the SLOSH (Eq. 2.6) and Holland model (Eq. 2.7). All three models show discrepancies from the H*Wind data, indicating the need for adjustment. Wind speed errors are as large as 15 m/s. The SWH was calculated for the location of NDBC buoy 42040 using the RV model winds and the SWAN wave model for hurricane Katrina, and compared to the measured wave data. As can be seen in Fig. 2.7, the RV winds led to an under-estimate of the wave heights by near 5m at the peak of the storm.

Table 2.1. HURDAT dataset for five hurricanes.

IVAN - 2004									
Month	Day	Hour	Lat.	Log.	Dir.	Translational speed (km/h)	Max wind speed (km/h)	Pressure (mb)	Type
9	13	0	19.5	82.8	300	12	260	916	Category 5
9	13	6	19.9	83.5	300	12	260	920	Category 5
9	13	12	20.4	84.1	310	12	260	915	Category 5
9	13	18	20.9	84.7	310	12	260	912	Category 5
9	14	0	21.6	85.1	330	12	260	914	Category 5
9	14	6	22.4	85.6	330	16	260	924	Category 5
9	14	12	23	86	330	12	230	930	Category 4
9	14	18	23.7	86.5	325	14	220	931	Category 4
9	15	0	24.7	87	335	18	220	928	Category 4
9	15	6	25.6	87.4	340	16	220	935	Category 4
9	15	12	26.7	87.9	340	20	215	939	Category 4
9	15	18	27.9	88.2	345	22	215	937	Category 4
KATRINA - 2005									
Month	Day	Hour	Lat.	Log.	Dir.	Translational speed (km/h)	Max wind speed (km/h)	Pressure (mb)	Type
8	26	18	24.9	82.6	250	9	160	968	Category 2
8	27	0	24.6	83.3	245	12	165	959	Category 2
8	27	6	24.4	84	255	11	175	950	Category 2
8	27	12	24.4	84.7	270	11	185	942	Category 3
8	27	18	24.5	85.3	280	9	185	948	Category 3
8	28	0	24.8	85.9	300	11	185	941	Category 3
8	28	6	25.2	86.7	300	14	230	930	Category 4
8	28	12	25.7	87.7	300	18	270	909	Category 5
8	28	18	26.3	88.6	305	18	280	902	Category 5
8	29	0	27.2	89.2	330	18	260	905	Category 5
8	29	6	28.2	89.6	340	18	230	913	Category 4
RITA - 2005									
Month	Day	Hour	Lat.	Log.	Dir.	Translational speed (km/h)	Max wind speed (km/h)	Pressure (mb)	Type
9	21	0	24.1	82.7	280	18	175	967	Category 2
9	21	6	24.2	84	275	20	205	955	Category 3
9	21	12	24.2	85.2	270	18	220	941	Category 4
9	21	18	24.3	86.2	275	16	270	920	Category 5
9	22	0	24.5	86.9	285	11	280	897	Category 5
9	22	6	24.8	87.6	295	12	285	897	Category 5
9	22	12	25.2	88.3	300	12	260	908	Category 5
9	22	18	25.6	89.1	300	14	230	913	Category 4
9	23	0	26	89.9	300	14	220	915	Category 4
9	23	6	26.5	90.7	305	14	215	924	Category 4
9	23	12	27.1	91.5	310	16	215	927	Category 4
9	23	18	27.8	92.3	315	16	205	930	Category 3

Table 2.1. Continued.

DOLLY - 2008									
Month	Day	Hour	Lat.	Log.	Dir.	Translational speed (km/h)	Max wind speed (km/h)	Pressure (mb)	Type
7	21	18	22.8	90.4	305	31	85	1005	T-Storm
7	22	0	23	92	280	25	85	1000	T-Storm
7	22	6	23.2	93.3	280	22	85	999	T-Storm
7	22	12	23.7	94.1	305	14	100	993	T-Storm
7	22	18	24.3	94.9	310	16	110	990	T-Storm
7	23	0	24.9	95.7	310	16	120	982	Category 1
7	23	6	25.4	96.2	320	11	130	982	Category 1
IKE - 2008									
Month	Day	Hour	Lat.	Log.	Dir.	Translational speed (km/h)	Max wind speed (km/h)	Pressure (mb)	Type
9	10	0	23.1	84	300	12	120	968	Category 1
9	10	6	23.4	84.6	300	11	130	964	Category 1
9	10	12	23.8	85.2	305	11	150	959	Category 1
9	10	18	24.2	85.8	305	11	160	958	Category 2
9	11	0	24.7	86.4	310	12	160	944	Category 2
9	11	6	25.1	87.1	300	12	160	945	Category 2
9	11	12	25.5	88	295	16	160	946	Category 2
9	11	18	25.8	88.9	290	14	160	952	Category 2
9	12	0	26.1	90	285	18	160	954	Category 2
9	12	6	26.4	91.1	285	18	165	954	Category 2
9	12	12	26.9	92.2	295	20	175	954	Category 2
9	12	18	27.5	93.2	305	18	175	954	Category 2
9	13	0	28.3	94	320	18	175	952	Category 2

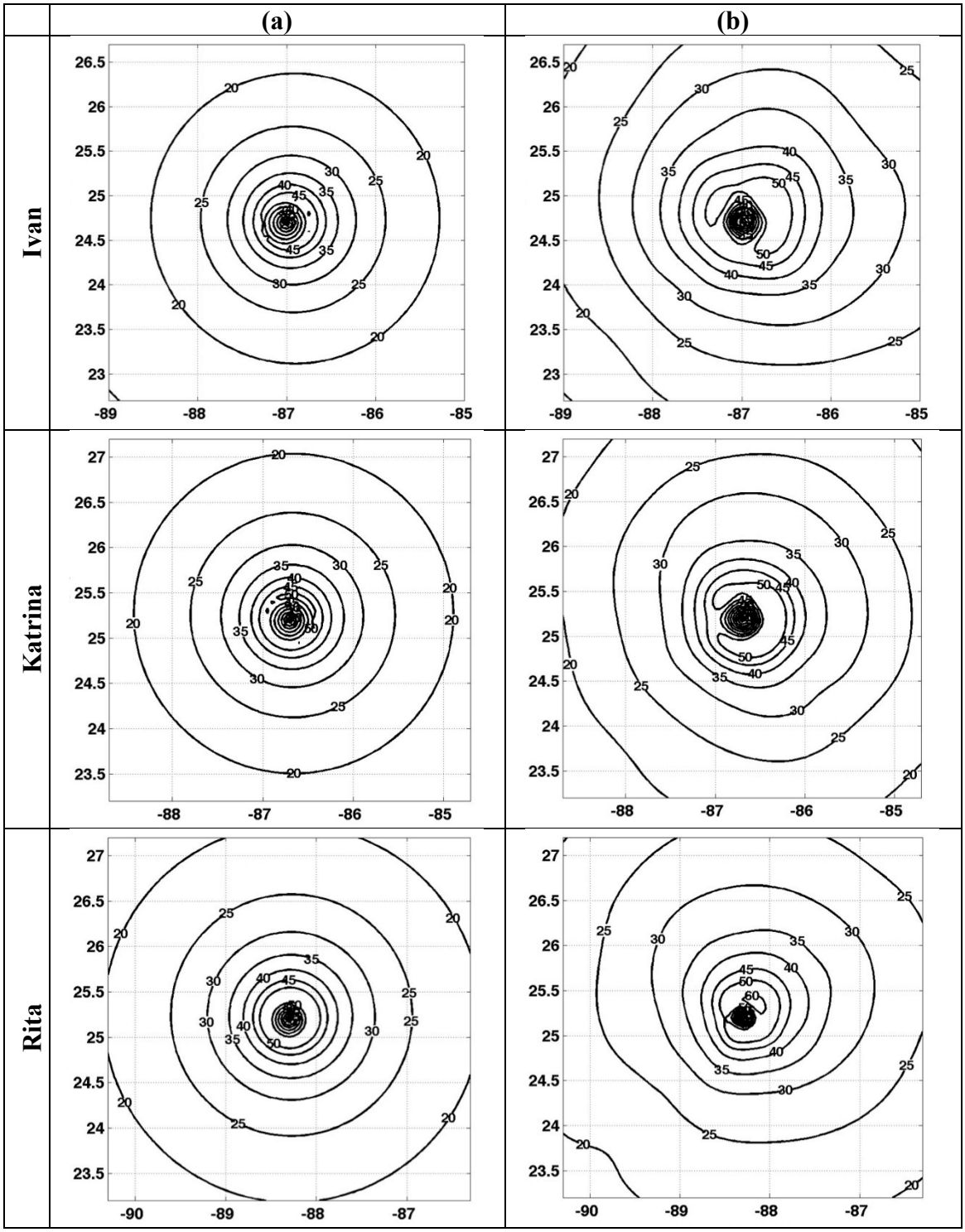

Fig. 2.4. Wind fields for hurricane Ivan, Katrina, and Rita (a) asymmetric RV model (b) H*Wind.

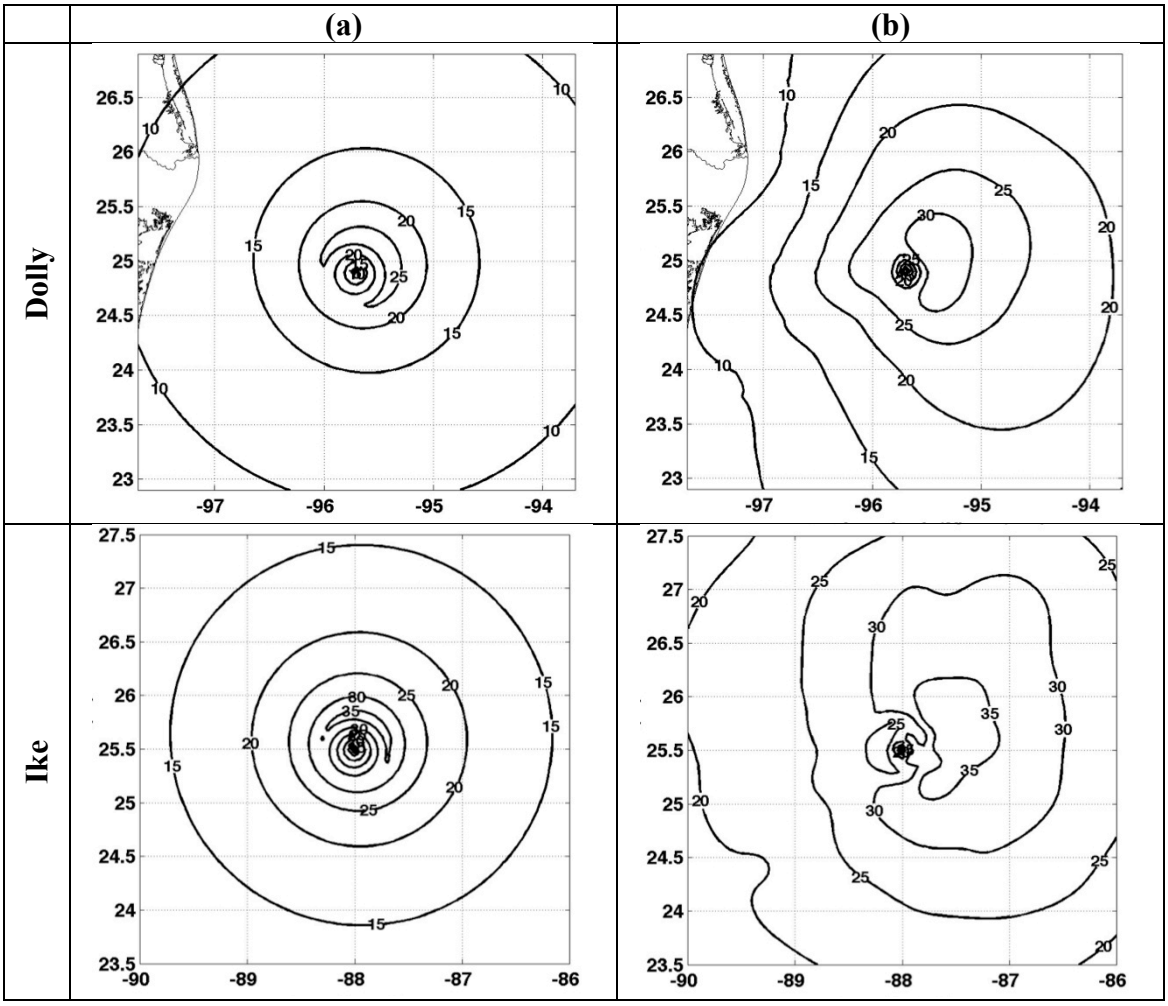

Fig. 2.5. Wind fields for hurricane Dolly and Ike (a) asymmetric RV model (b) H*Wind.

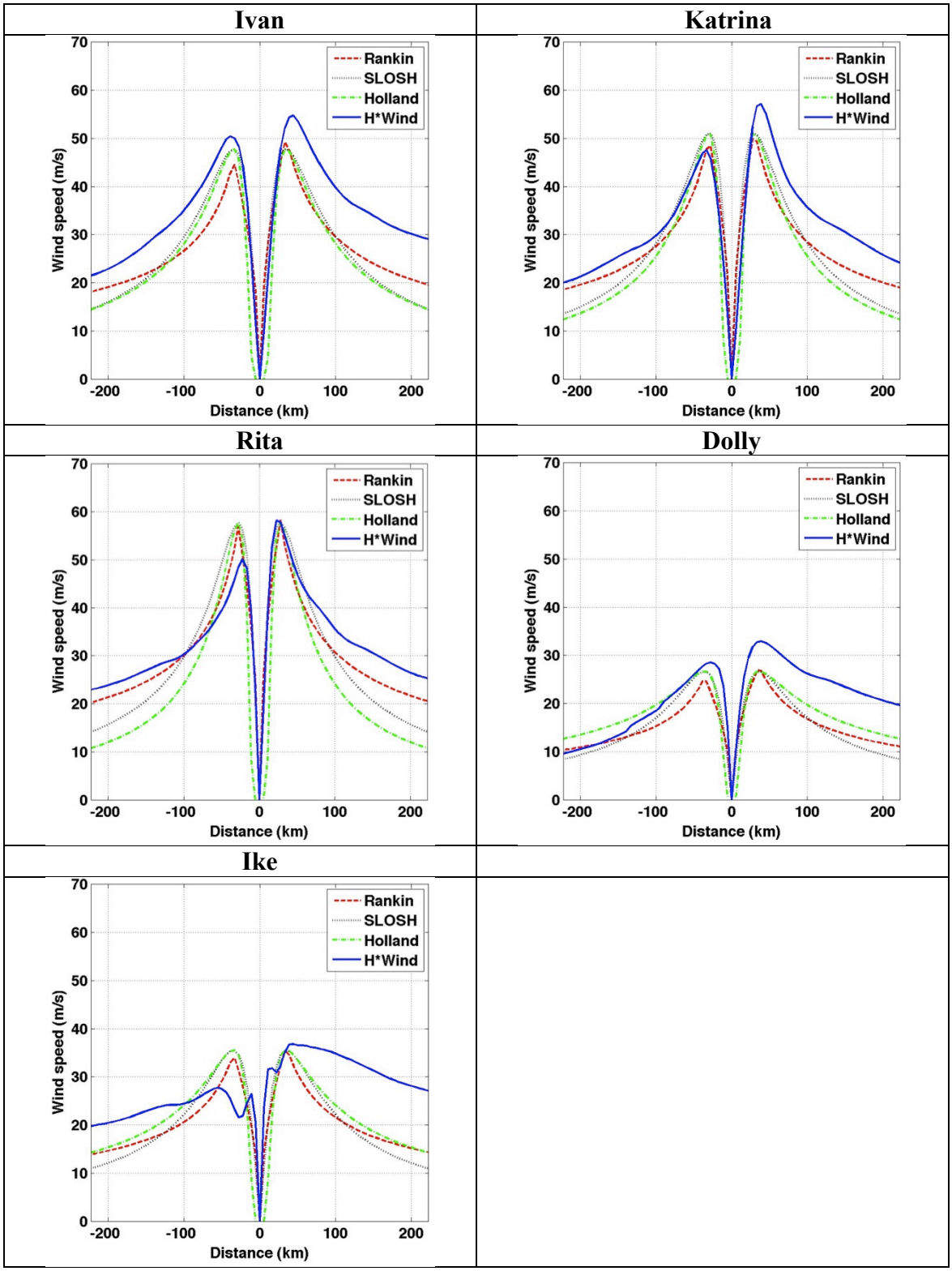

Fig. 2.6. Modeled and measured wind velocities along the central transact.

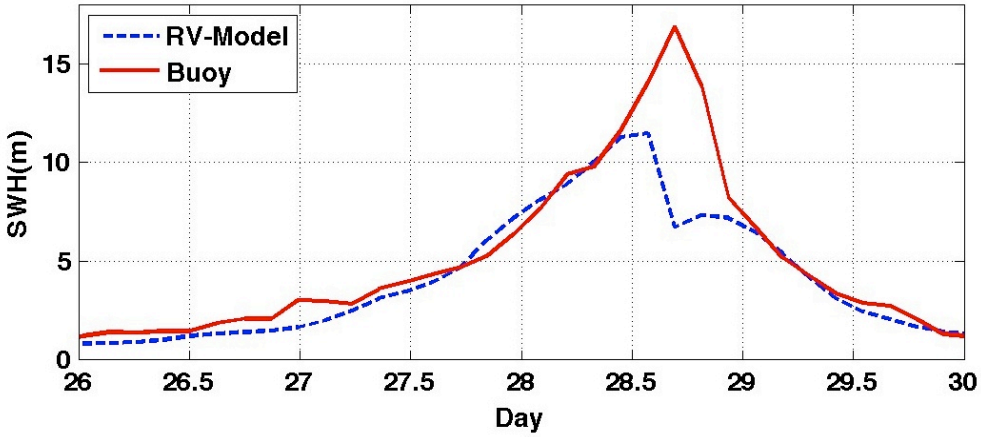

Fig. 2.7. SWH comparison plot during hurricane Katrina (August 2005) at NDBC buoy 42040.

CHAPTER III

ADJUSTMENTS TO THE RANKINE VORTEX MODEL

3.1 Introduction

Chapter II showed that there is mismatch between modeled and measured winds. This type of mismatch has been observed in other studies also (Phadke et al. 2003;MacAfee and Pearson 2006; Xie et al. 2006). Typically adjustments have to be made to suit individual cases or locations by using data to develop alternative equations. For example, Xie et al. (2006) made adjustments to the Holland model based on four mid-Atlantic hurricanes. Instead of treating $R_m \neq f(\theta)$, they described it as power series of θ, and the constants were determined on a case-by-case basis using wind speeds at specific locations. For our work, such details are not available (especially for the pre-1994 period). MacAfee and Pearson (2006) also made adjustments, which were tailored for mid-latitude applications. Even with adjustments, there is no consensus on which model should be used. It is not reasonable to expect any one model to reliably reproduce every hurricane. For the purpose of recreating historical wind fields in the Gulf of Mexico, here we focus on the RV model (described in 2.3). This choice is based on the conclusions of Phadke et al. (2003) who found that the first three models produced the same results in the core of the hurricane, but the RV model had better overall agreement with data outside the core. The performance of this model was examined in Chapter II against data from five recent hurricanes. The observed discrepancies between model and measurement are used in this chapter to make adjustments to the RV model. The

performance of the adjusted model is then examined using wind data from twelve other hurricanes. The effect of the modified wind fields on wave simulation is also examined.

For the five hurricanes examined in Chapter II, in general, the RV-model results were frequently similar to H*Wind for strong hurricanes (e.g. for P_c < 930 *mb*) but in other instances both the shapes and the magnitudes were incorrect. The observed differences between modeled and measured data were used to develop empirical correction factors, $d(\theta)$ and C_B.. The first correction factor can modify the RV-modeled hurricane shape and the second correction factor can modify the size and velocity distributions. The net wind field V_{CRV} is obtained in two stages as follows:

$$V_{RV1} = V_{RV} \cdot d(\theta) \tag{3.1}$$

$$V_{CRV} = V_{RV1} \cdot C_B \tag{3.2}$$

3.2 Development of correction factor $d(\theta)$

A detailed examination of the modeled and H*Wind plots indicated that the comparison was acceptable for low P_c values (Fig. 3.1, top). But for higher values of P_c the hurricane shape was more deformed relative to the modeled shape (Fig. 3.1, bottom); the hurricane was less circular in shape and developed a more pronounced bean-shaped central feature than in the model.

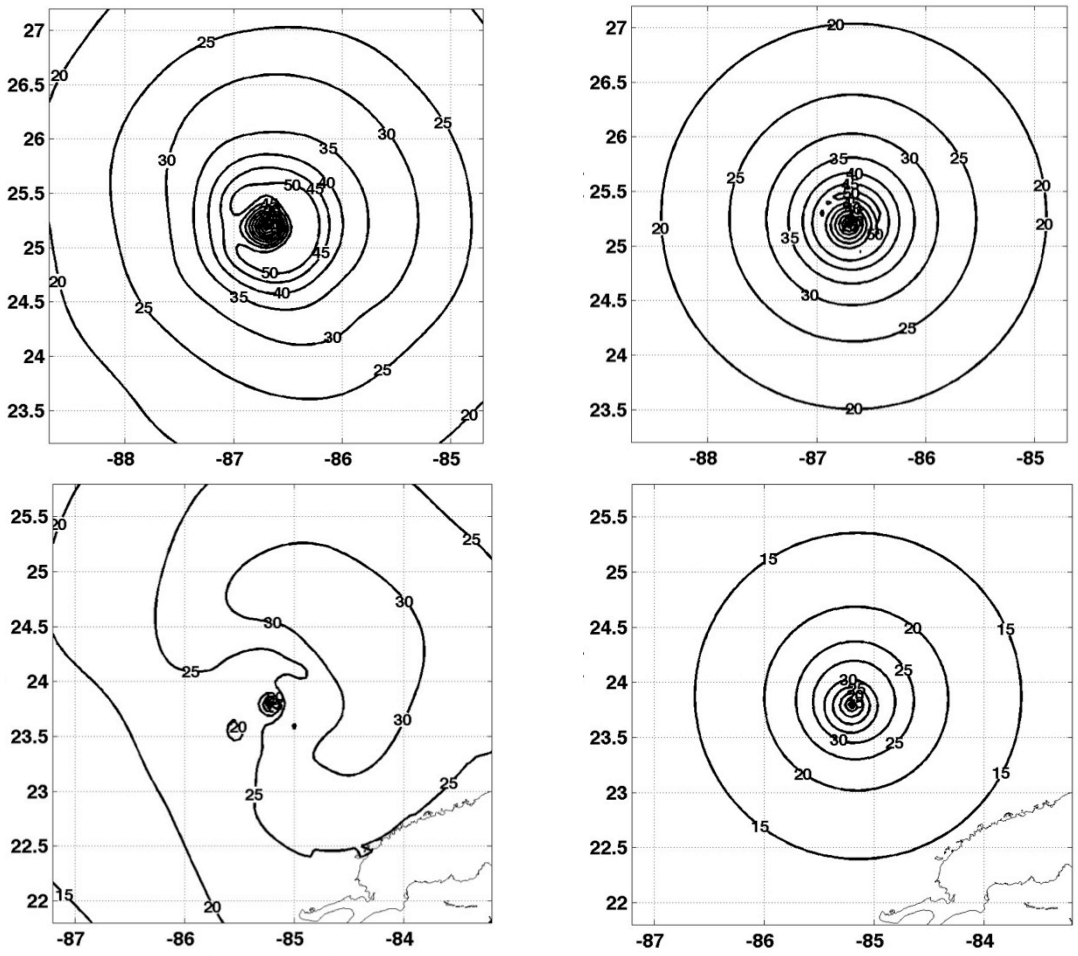

Fig. 3.1. H*Wind (left) and RV-model (right) wind speeds (m/s): Katrina (0600 UTC 28 August. 2005), $P_c = 930$ (top); Ike (1200 UTC 10 September. 2008), $P_c = 959$ (bottom).

To accommodate these features, it is necessary to appropriately deform the modeled RV contour shapes. Since the RV model produces largely circular contours, the values of H*Wind data velocities along any circle (after appropriate normalization) can be used as a measure of the required deformation *d(θ)*. For example, denoting the H*Wind velocities at three points *P*, *Q* and *B* along a circle (shown in Fig. 3.2) by V_P, V_Q, and V_B respectively, the ratio $d_P = V_P / V_B$ and $d_Q = V_Q / V_B$ can be used as a measure of the deviation of the contour from a circle. A circle with radius $4R_m$ is nominally

selected for this purpose, and $d(\theta)$ are estimated at selected points on the circle. These estimates are used to calculate the deformation $d(\theta)$ at other points by curve-fitting.

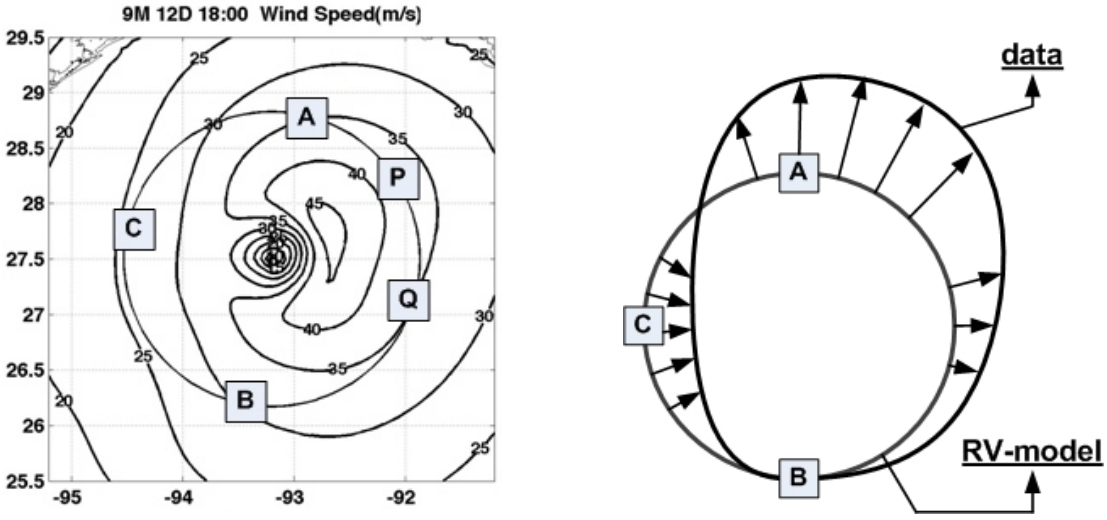

Fig. 3.2. Deformation schematic.

To be specific, the point with smallest velocity on this circle was denoted by "*C*". Two other points (*A* & *B*) were located on the circle so as to create radii perpendicular to the one to *C* (Fig. 3.2 left). Using point *B* as the base velocity ratios $d_A=V_A/V_B$ and $d_C=V_C/V_B$ were estimated to provide measures of deformation at these points. These data are provided in Table 3.1 in the form of averages for each storm.

Table 3.1. Deformation ratio.

	Number of HWIND wind field data	$d_A=\left(\overline{V_A/V_B}\right)$	$d_B=\left(\overline{V_B/V_B}\right)$	$d_C=\left(\overline{V_C/V_B}\right)$
Ivan	12	1.114	1	0.842
Katrina	11	1.142	1	0.875
Rita	13	1.166	1	0.872
Dolly	7	1.180	1	0.703
Ike	13	1.160	1	0.838
Average		1.152	1	0.826

The values of d_A for the 56 plots were found to vary in a relatively small range ($\pm 4\%$) around the average. So the average (≈ 1.15) was used as the deformation factor. On the other hand the ratio d_C showed more variability (varying between -16% and +6% around the average) and was found to depend on central pressure (Fig. 3.3). Since $930 \leq P_c \leq 970$ for most of the cases examined, a best-fit line was used to define this deformation ratio as follows:

$$\begin{aligned} d_C &= 0.8 + 0.2\alpha \quad && \text{for} \quad && 930 \leq P_c \leq 970 \\ d_C &= 1, && \text{for} && P_c \leq 930 \\ d_C &= 0.8, && \text{for} && P_c \geq 970 \end{aligned} \tag{3.3}$$

where $\alpha = (970 - P_c) / 40$.

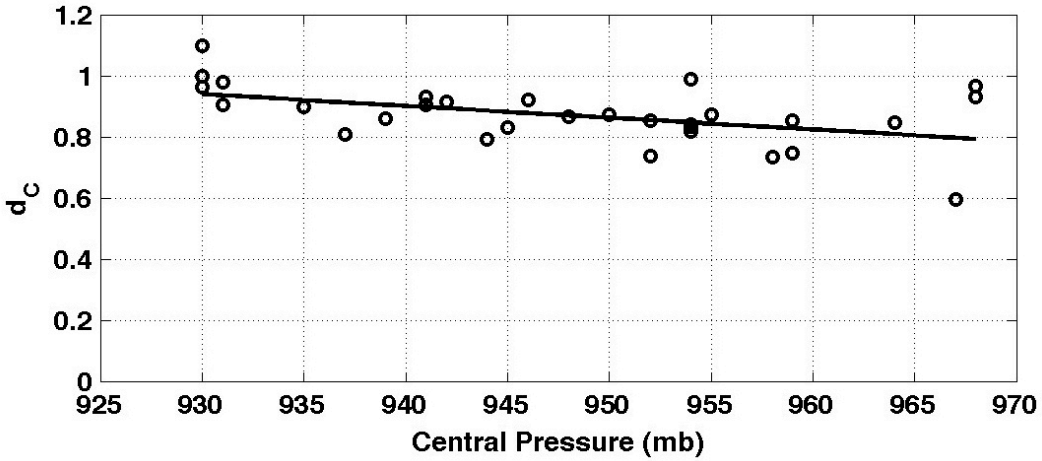

Fig. 3.3. Best-fit line for d_c v/s P_c.

It is now necessary to find $d(\theta)$ using the deformation at A, B, and C (d_A, d_B, and d_C), for which reference to Fig. 3.4 is made. The right curve between A and B was described by $d(\theta)=a_1\theta+b_1$, where d_A and d_B (i.e. information at $\theta=0$ and $\theta=\pi$) are used

to determine a_1 and b_1. The left half was described by $d(\theta)=a_2 \cos(2\theta)+b_2$ for $\pi<\theta<3/2\pi$ and $d(\theta)=a_3 \cos(2\theta)+b_3$ for $3/2\pi<\theta<2\pi$, and a_2 and b_2 are obtained from d_B and d_C, and a_3, b_3 are from d_C and d_A. These calculations lead to

$$\begin{aligned} d(\theta) &= 1.15-(0.15/\pi)\theta, && 0<\theta\le\pi \\ d(\theta) &= 1-(1-d_c)\sin^2\theta && \pi<\theta\le\frac{3}{2}\pi \\ d(\theta) &= d_c+(1.15-d_c)\cos^2\theta, && \frac{3}{2}\pi<\theta\le 2\pi \end{aligned} \tag{3.4}$$

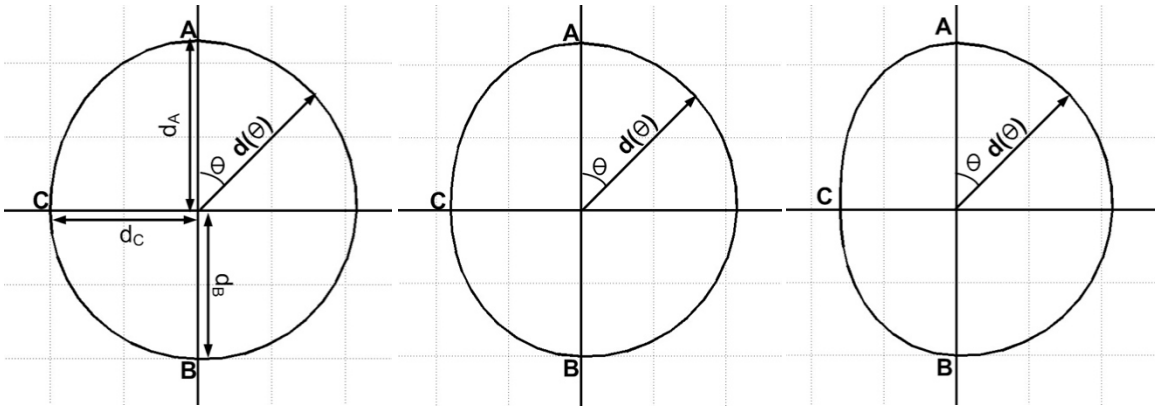

P_c =930 mb P_c =948 mb P_c =970 mb

Fig. 3.4. *d(θ)* for different central pressure.

Multiplying the RV model velocities by $d(\theta)$ changes the largely circular contour shape;, however, it is first necessary to determine the locations that most closely correspond to *A*, *B* and *C* on the modeled contours. For the parametric model, (based on Eq. 4) the radius to point *A* is theoretically in the same direction as the storm direction. However, the data show that this is not always true. The actual storm direction can be found from the 56 H*Wind plots (Fig. 3.5). Generally, strong hurricane conditions

agreed with this theoretical expectation (storm direction and radius to A are in one line) but for other hurricanes, the storm speed, storm direction and central pressure affect the orientation of A, B, and C. Using the 56 plots we attempted to determine the angles between the radius to A and the storm track (θ_c). Unfortunately there was no simple pattern. Therefore the data points were placed into 6 categories based on storm direction. While no meaningful difference between the two vectors was observed for $0 < \theta < 180$, for the other sectors, the difference varied with P_c and V_s. The results are summarized in Table 3.2. The net θ used in eq. (7) is therefore the sum of θ_r and θ_c.

Figure 3.6 shows plots for wind fields pertaining to H*Wind, the RV model, the RV model with the $d(\theta)$ correction before applying the θ_c correction, and the RV model with the corrected θ. The hurricane shape in Fig. 3.6d is clearly substantial improvement over the basic RV model. However, the hurricane size and the velocity distribution are not well matched; thus, further adjustment is required.

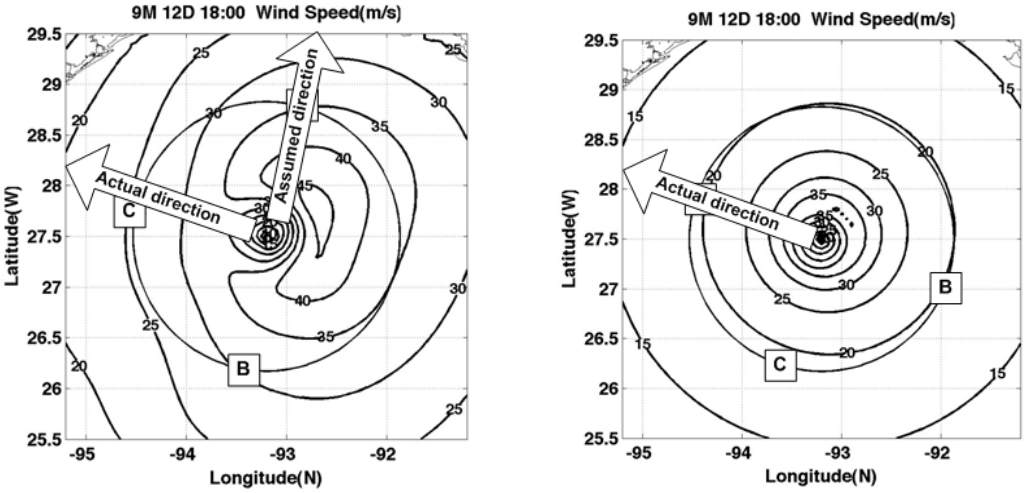

Fig. 3.5. Hurricane Ike (2008, $\theta_d = 305°$); H*Wind (left), RV-model (right).

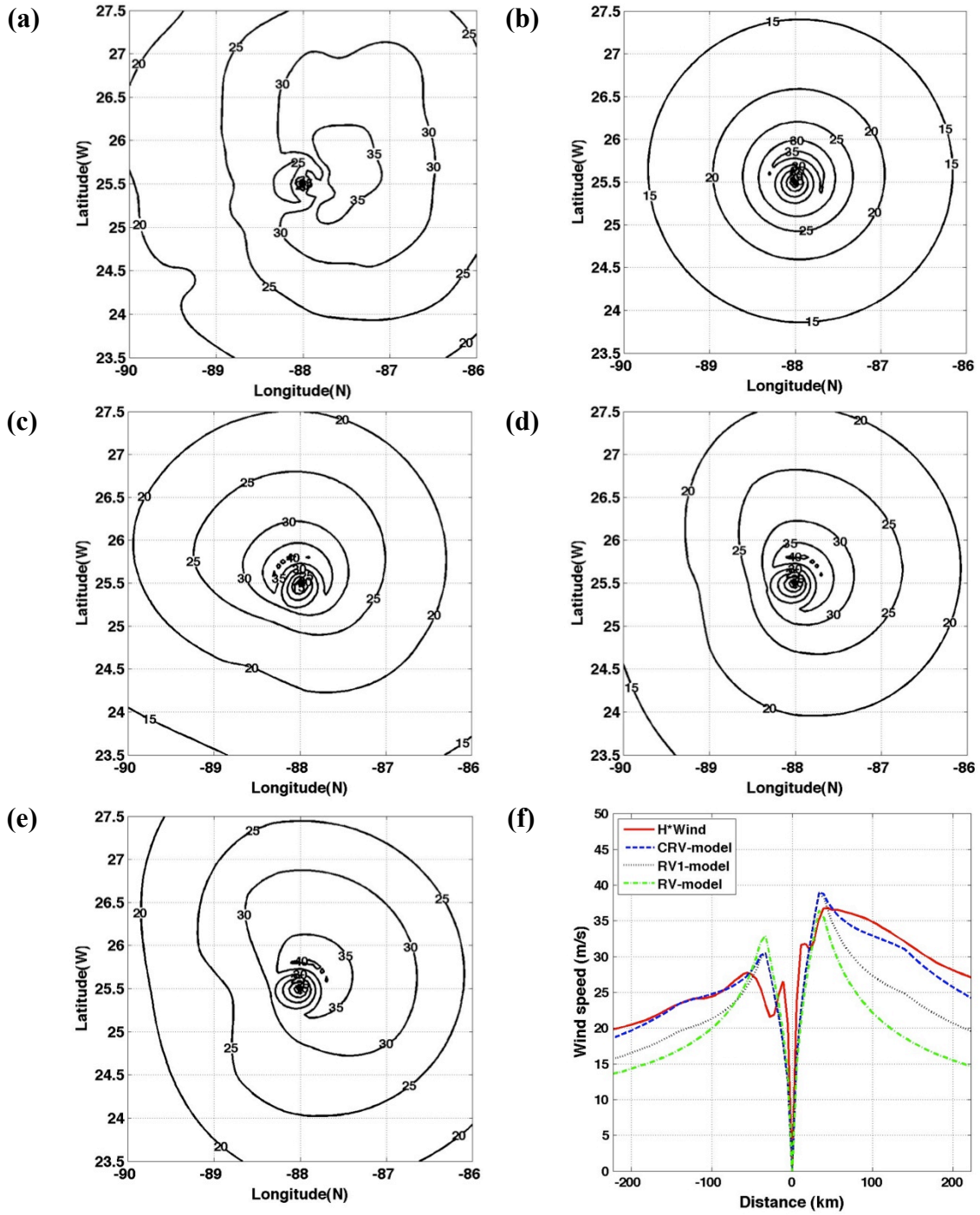

Fig. 3.6. Wind speeds (m/s) for hurricane Ike at UTC 1200 11 September 2008; $\theta_D = 295°$, $V_S = 4.44$ m/s, $P_C = 946$ mb (a) H*Wind, (b) RV-model, (c) before angle correction with $d(\theta)$, (d) after angle correction with d(θ), (e) after application of both correction factors, and (f) comparison along the central transect.

Table 3.2. Storm direction corrections vary with central pressure and translation speed.

Sector	$P_c(mb)$	$V_s(m/s)$	θ_c
$180 < \theta < 255$			–90
$255 < \theta < 285$		$V_s \le 3.88$ $V_s > 3.88$	90 $90 - 60 \cdot (1-\gamma)$
$285 < \theta < 315$	$P_c \ge 970$	$V_s > 3.88$	$60 \cdot (1-\gamma)$
	$P_c < 970$	$V_s \le 3.88$ $V_s > 3.88$	$60 \cdot \alpha$ $60 \cdot \alpha + 60 \cdot (1-\gamma)$
$315 < \theta < 340$	$P_c \ge 970$	$V_s > 3.88$	$60 \cdot (1-\gamma)$
	$P_c < 970$	$V_s \le 3.88$ $V_s > 3.88$	$60 \cdot \alpha$ $60 \cdot (1-\gamma)$
$340 < \theta < 360$		$V_s > 3.88$	$60 \cdot (1-\gamma)/2$
$*$ α is defined in eq. 6 $\gamma = (5.55 - V_S)/1.67$ (for $3.88 \le V_s \le 5.55$), $\gamma = 0$ (for $V_s > 5.55$), and $\gamma = 1$ (for $V_s < 3.88$)			

3.3 Development of correction factor C_B

Mismatch at any grid point in the modeled velocity V_{RV1} are due to two reasons. The first is that modeled velocity is not at 10 m elevation, whereas H*Wind is; the second is due to errors in the hurricane size and velocity distribution. The first error is addressed as a function of r, and the second as a function of both r and θ. In other words, we provide a correction to the V_{RV1} using a correction factor C_B that includes both sources of errors, defined as

$$C_B(r,\theta) = f_1(r) + f_2(r,\theta) \tag{3.5}$$

The function $f_1(r)$ was chosen as a constant ($\cong 0.8$) by Phadke et al. (2003). Figure 3.7 shows an example of the RV modeled wind and the corresponding data along

the central transect for hurricane Katrina (0600 UTC, 8/27/2005), with an adjustment by a factor of 0.8 (Fig.3.7b). It is obvious that this adjustment leads to an underestimation of wind velocity outside the core. An examination of several such plots suggested that instead of using a constant, the following function worked better:

$$f_1(r) = 0.8 + 0.2\left(\frac{r - R_m}{3R_m}\right), \quad \text{for} \quad R_m \le r \le 4R_m$$
$$f_1(r) = 1, \quad \text{for} \quad r > 4R_m \tag{3.6}$$
$$f_1(r) = 0.8, \quad \text{for} \quad r < R_m$$

This leads to an improvement as shown in Fig. 3.7c.

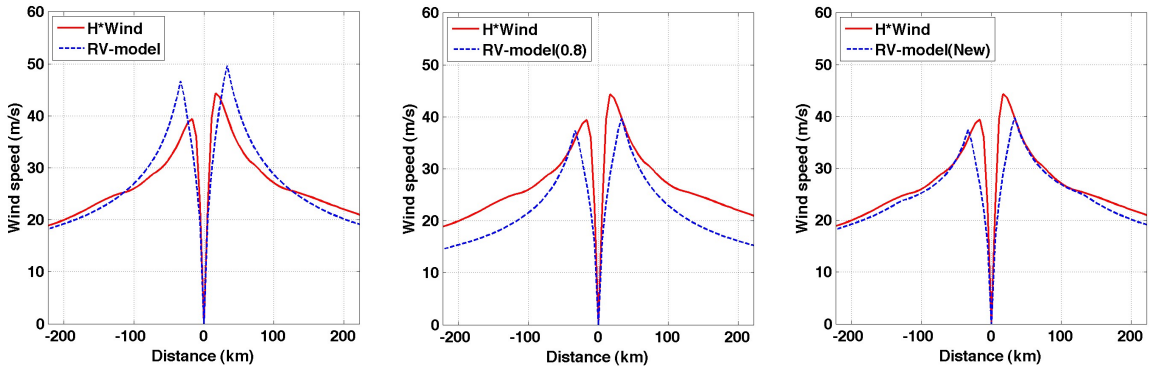

(a) **(b)** **(c)**

Fig. 3.7. Wind speed along the central transect for (a) H*Wind and RV model, (b) H*Wind and RV-model with 10-meter elevation correction factor ($\cong 0.8$), and (c) H*Wind and RV-model with the 10-meter elevation correction factor (from eq. 9).

As to the correction necessitated by varying storm sizes, the function $f_2(r,\theta)$ was for simplicity described as

$$f_2(r,\theta) = F_2(r) \cdot E(\theta) \tag{3.7}$$

In order to estimate $F_2(r)$ and $E(\theta)$, the discrepancies $\Delta(r,\theta)$ between V_{RV1} and H*Wind at approximately 100 points along four radii (corresponding to $\theta = 0°$, $90°$, $180°$, and $270°$) were determined. For each of the radii, the maximum discrepancy Δ_m was calculated.

In general, two patterns were observed as shown in Figs. 3.8 and 3.9. For the storms, which had a maximum wind speed between 36 m/s and 50 m/s, the maximum discrepancy Δ_m occurred at approximately $r = 4R_m$. Figure 3.8 (right) shows a composite of all discrepancies for such cases. A regression analysis was used to fit the following curve to correct these errors:

$$\frac{\Delta(r,\theta)}{\Delta_m(r,\theta)} = 0 \qquad \text{for} \qquad r < R_m$$

$$\frac{\Delta(r,\theta)}{\Delta_m(r,\theta)} = -0.0218r^3 + 0.1017r^2 + 0.281r - 0.3609 \qquad R_m < r < 4R_m \tag{3.8}$$

$$\frac{\Delta(r,\theta)}{\Delta_m(r,\theta)} = 0.000333r^3 - 0.01639r^2 + 0.1204r + 0.7565 \qquad 4R_m < r < 15R_m$$

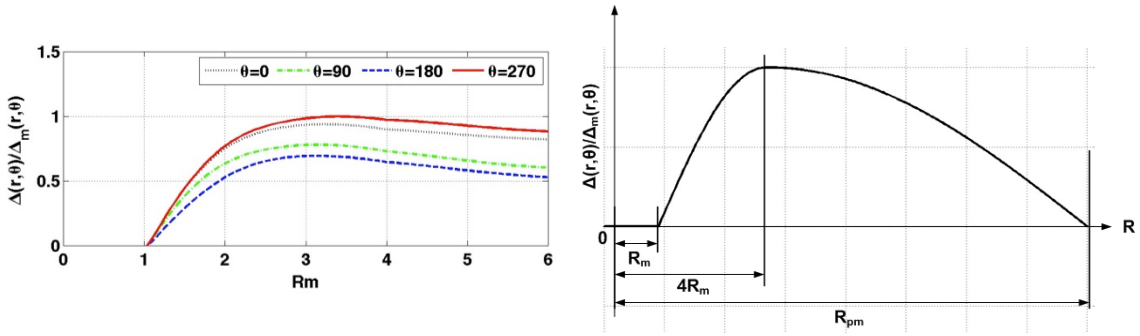

Fig. 3.8. Model-data discrepancies for hurricane Ike, $V_m = 48.6$ m/s (left); best-fit curve based on 400 data point (right).

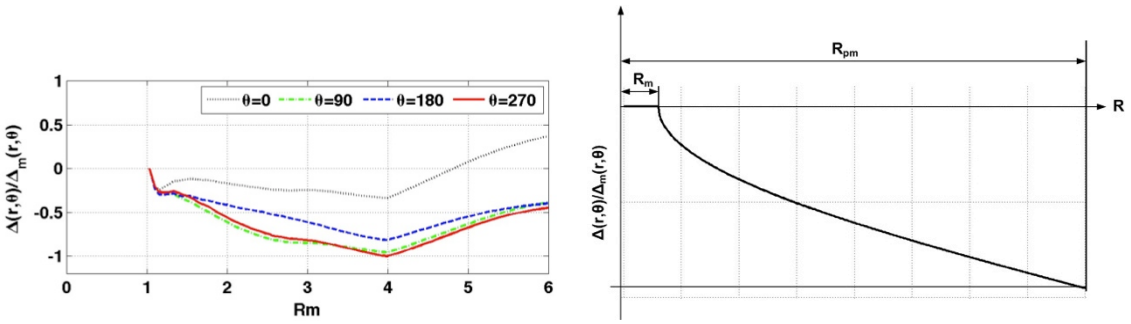

Fig. 3.9. Model-data discrepancies for hurricane Rita with $V_m = 79.2$ m/s (left); best-fit curve based on 400 data point (right).

Note that the left hand side of Eq. 11 is a measure of $F_2(r)$ because

$$\frac{\Delta(r,\theta)}{\Delta_m(r,\theta)} = \frac{F_2(r)\cdot E(\theta)}{F_2(4R_m)\cdot E(\theta)} = \frac{F_2(r)}{F_2(4R_m)}$$

For $V_m > 70 m/s$, the pattern is largely reversed and the data (Fig. 3.9) suggested using the following form:

$$\frac{\Delta(r,\theta)}{\Delta_m(r,\theta)} = 4.868e^{-5}r^4 - 0.001871r^3 + 0.02643r^2 - 0.2104r + 0.115 \qquad (3.9)$$

For maximum wind speeds between 50 m/s and 70 m/s, the discrepancy between the modeled wind speed and H*Wind was small.

For the functional form of $E(\theta)$, the maximum discrepancy Δ_m (at $r = 4R_m$) at $\theta = 0°$, 90°, 180°, and 270° was used. These four locations are denoted by A, B, C, and D, and the discrepancies at these locations are denoted by Δ_m^A, Δ_m^B, Δ_m^C, and Δ_m^D and are plotted in Fig. 3.10. A curve was fitted to the values at these four locations to estimate $E(\theta)$ for other values of θ, in a maner analogovs to that for $d(\theta)$.

An examination of the data showed that these discrepancies varied with V_m e.g. see Fig. 3.10.

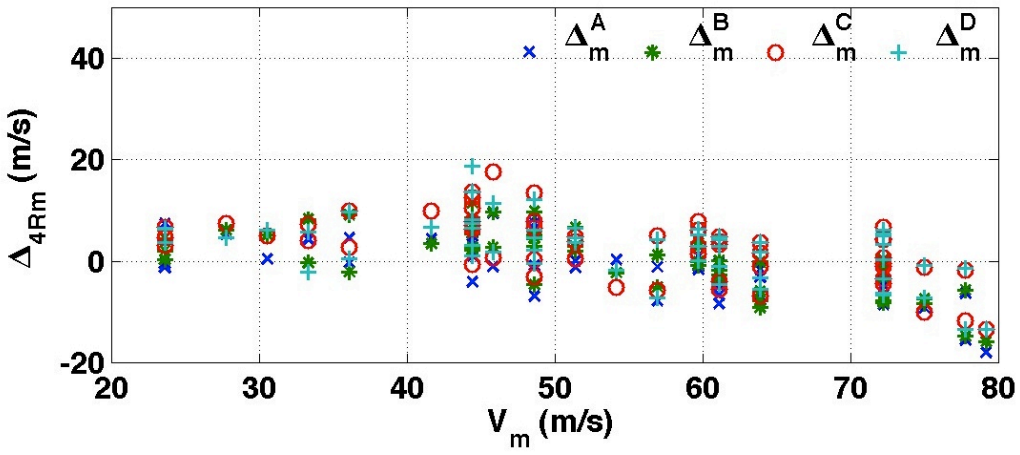

Fig. 3.10. Wind speed differences at r = 4Rm versus maximum wind speed.

As was the case for the radial error, the parameters showed different characteristics for large wind speeds (V_m > 60 m/s) and for moderate wind speeds (36 m/s < V_m < 50 m/s). For simplicity, straight lines were fitted to obtain Δ_m^D and Δ_m^B as follows.

$$\Delta_m^B = 0.4(V_m - 70)/10 \quad \text{for} \quad V_m > 70$$

$$\Delta_m^B = 0.9(50 - V_m)/20 \quad \text{for} \quad 36 < V_m < 50 \qquad (3.10a)$$

$$\Delta_m^B = 0 \quad \text{otherwise}$$

$$\Delta_m^D = 0.5(V_m - 60)/20 \quad \text{for} \quad V_m > 60$$

$$\Delta_m^D = 0.7(50 - V_m)/20 \quad \text{for} \quad 36 < V_m < 50 \qquad (3.10b)$$

$$\Delta_m^D = 0 \quad \text{otherwise}$$

In general, we found that $\Delta_m^A \approx \Delta_m^C \approx (\Delta_m^B + \Delta_m^D)/2$.

With these parameterizations, the function $E(\theta)$ was defined as $E(\theta) = a_1 \cos(2\theta) + b_1$ for $0 < \theta < \pi$ and $E(\theta) = a_2 \cos(2\theta) + b_2$ for $\pi < \theta < 2\pi$, where the constants a_1, a_2, b_1 and b_2 are determined from the conditions $E(\theta) = \Delta_m^D$ at $\theta = 3/2\pi$ and $E(\theta) = \Delta_m^B$ at $\theta = \pi/2$. The final form of E(theta) reduced to:

$$\begin{aligned} E(\theta) &= [(\Delta_m^D - \Delta_m^B) \cdot \cos 2\theta + (3\Delta_m^B + \Delta_m^D)]/4 \qquad 0 < \theta < \pi \\ E(\theta) &= [(\Delta_m^B - \Delta_m^D) \cdot \cos 2\theta + (\Delta_m^B + 3\Delta_m^D)]/4 \qquad \pi < \theta < 2\pi \end{aligned} \tag{3.11}$$

To summarize, a detailed examination of five storms (approximately 56 plots) suggested that the 10m elevation wind could be obtained by adjusting the RV model as follows:

$$V_{CRV} = V_{RV} \cdot d(\theta) \cdot C_B \tag{3.12}$$

The effect of this second adjustment may be seen in Figs. 3.6 (e and f), for hurricane Ike, and in Fig 3.11 for hurricane Katrina. We note that in the case of hurricane Katrina, the shape obtained by the original RV-model is reasonable, although for both storms, our final adjusted velocities are significantly improved as compared to the original RV model results. Details are provided in APPENDIX A. The effect of our modification on the wave heights for hurricane Katrina is shown in Fig. 3.12; the differences are of a magnitude sufficient to influence extreme wave height calculations.

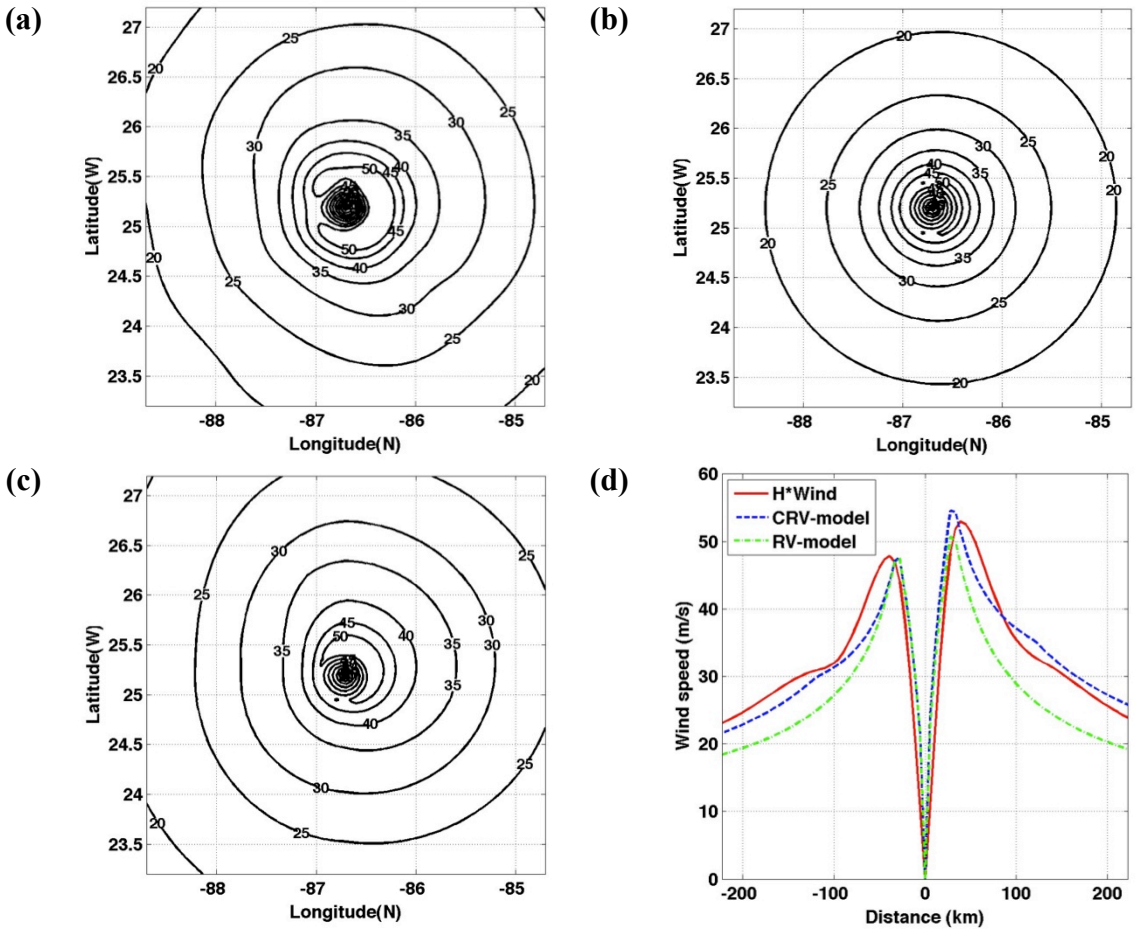

Fig. 3.11. Wind speeds during hurricane Katrina (0600 UTC 28 August 2005);(a) H*Wind, (b) RV-model, (c) CRV-model (d) comparison along the central transect.

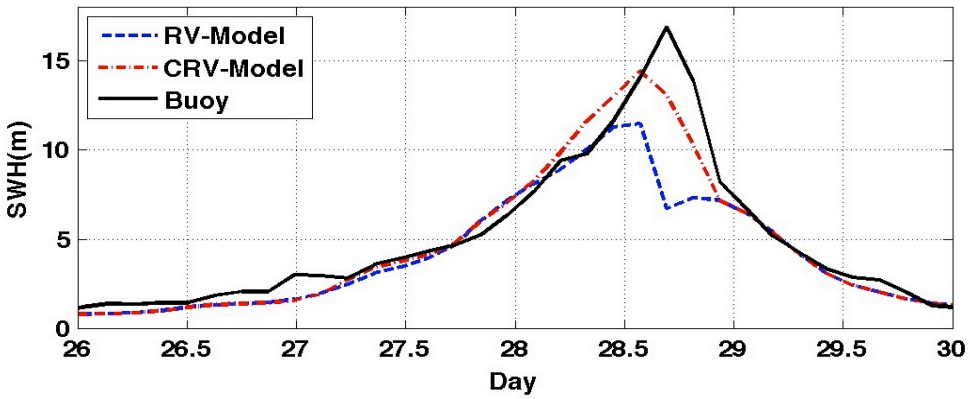

Fig. 3.12. SWH comparison plot during hurricane Katrina (August 2005) at NDBC buoy 42040.

3.4 Validation and effect on wave fields

As noted earlier, the Reanalysis wind fields are available on a 6-hourly basis, dating back to 1948, and have been used for wave and storm-surge hindcasting by others (e.g., Music and Nickovic 2008; Cieślikiewicz and Paplińska-Swerpel 2008; Pilar et al. 2008; Wang et al. 2002 & 2004; Sebastião et al. 2008). However, the coarse resolution (2.5°× 2.5°) can be expected to adversely impact the wind and wave hindcasts in hurricane conditions. For example, considering the case of hurricane Gordon mentioned in Chapter II, winds resulting from the modified RV model are shown in Fig. 3.13 (left). The wave hindcast that results from these wind fields are compared with data from buoy 42003 in Fig. 3.13 (right). It is clear that the Reanalysis winds do not provide accurate wave height predictions and that the modified RV model results in better wave predictions, with maximum difference of the order of 4 m.

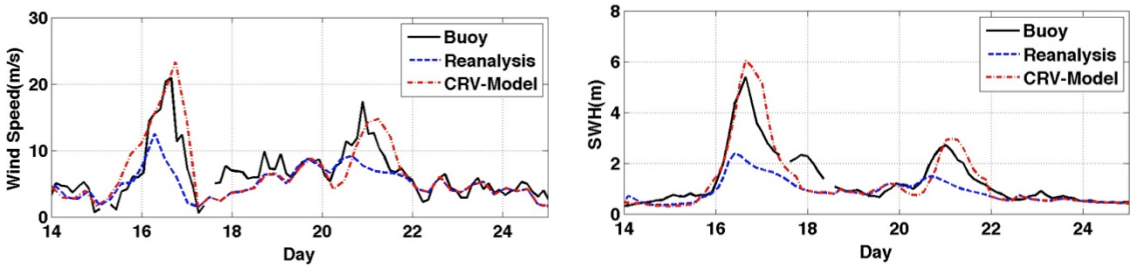

Fig. 3.13. Wind (left) and SWH (right) speed during September 2000 at NDBC buoy 42003.

The parametric model equation (Eq.12) was tested against 17 storms (107 plots) covering a period from 1961 to 2008 (Table 3.3); these formed a subset of the entire

H*Wind dataset. The others were not chosen because numerical data were not available for them or because they contained too many land points.

Table 3.3. Selected 17 hurricane list.

No.	Name	Storm Period	Number of HWIND storm snapshots chosen
1	Carla (1961)	Sep. 03. 12:00 – Sep. 16. 00:00	2
2	Georges (1998)	Sep. 15. 12:00 – Oct. 01. 06:00	9
3	Gordon (2000)	Sep. 14. 12:00 – Sep. 21. 06:00	5
4	Isidore (2002)	Sep. 14. 18:00 – Sep. 27. 18:00	5
5	Lili (2002)	Sep. 21. 18:00 – Oct. 04. 12:00	4
6	Ivan (2004)	Sep. 02. 18:00 – Sep. 24. 06:00	12
7	Arlene (2005)	Jun. 08. 18:00 – Jun. 14. 06:00	4
8	Dennis (2005)	Jul. 04. 18:00 – Jul. 18. 06:00	3
9	Emily (2005)	Jul. 11. 00:00 – Jul. 21. 12:00	6
10	Katrina (2005)	Aug. 23. 18:00 – Aug. 31. 06:00	9
11	Rita (2005)	Sep. 18. 00:00 – Sep. 26. 06:00	10
12	Wilma (2005)	Oct. 15. 18:00 – Oct. 26. 18:00	12
13	Alberto (2006)	Jun. 10. 06:00 – Jun. 19. 06:00	3
14	Dean (2007)	Aug. 13. 06:00 – Aug. 23. 00:00	2
15	Dolly (2008)	Jul. 20. 12:00 – Jul. 27. 00:00	4
16	Gustav (2008)	Aug. 25. 00:00 – Sep. 05. 12:00	5
17	Ike (2008)	Sep. 01. 06:00 – Sep. 15. 12:00	12

For each snapshot V(x,y) was calculated using Equation (12) for a matrix containing 81×81 points on each side (at a resolution of approximately 5 km) covering a $4° \times 4°$ region (approximately 6561 grid points per snapshot). Wind speeds from the modified RV model and the original RV models were compared with H*Wind data for these grid points for each snapshot. The absolute percentage errors (i.e. (H*Wind data – model wind)/H*Wind data) were calculated (see Table 3.4). In general, in 14 out of 17 cases, the modified RV model (V_{CRV}) produces wind velocities far lower than the

original model. Ignoring small differences (say less than 10%) which occur in eight cases, eight of the remaining nine showed significant improvements, while only one (i.e. hurricane Dennis) showed an increased deterioration relative to the original RV model. The maximum improvement is for hurricane Dean (30%). Unfortunately, for the two cases with maximum discrepancies (i.e. Dennis and Dean), very few snapshots being available. In addition, a detailed comparison of both parametric wind fields against H*Wind data was conducted for hurricane Georges (1998), and results are in shown in Fig. 3.14.

Table 3.4. Absolute percentage errors for 17 hurricanes.

No.	Name	N	AE (CRV-model)	AE (RV-model)
1	Carla	2	15%	20%
2	Georges	9	12%	26%
3	Gordon	5	22%	26%
4	Isidore	5	37%	45%
5	Lili	4	23%	16%
6	Ivan	12	11%	24%
7	Arlene	4	32%	34%
8	Dennis	3	38%	20%
9	Emily	6	26%	20%
10	Katrina	9	9%	20%
11	Rita	10	10%	16%
12	Wilma	12	11%	30%
13	Alberto	3	19%	24%
14	Dean	2	12%	42%
15	Dolly	4	20%	33%
16	Gustav	5	8%	22%
17	Ike	12	14%	39%

The results indicate clearly that the CRV-model wind speed contour shape shows a better match with H*Wind than the RV-model plot. The wave fields resulting from the

two numerically generated wind fields are shown in Fig. 3.14 (bottom). For both wind fields and wave fields, although the maximum values are largely the same, the spatial patterns are different, leading to a maximum of about ±1.8m difference in wave height estimates at some locations. A difference of the order of about 3.5m in the maximum SWH results for hurricane Katrina (see Fig. 3.12 where buoy data are also shown) and of about 4m for hurricane Ike (not shown). Such large differences have the potential to affect calculations of extreme wave statistics.

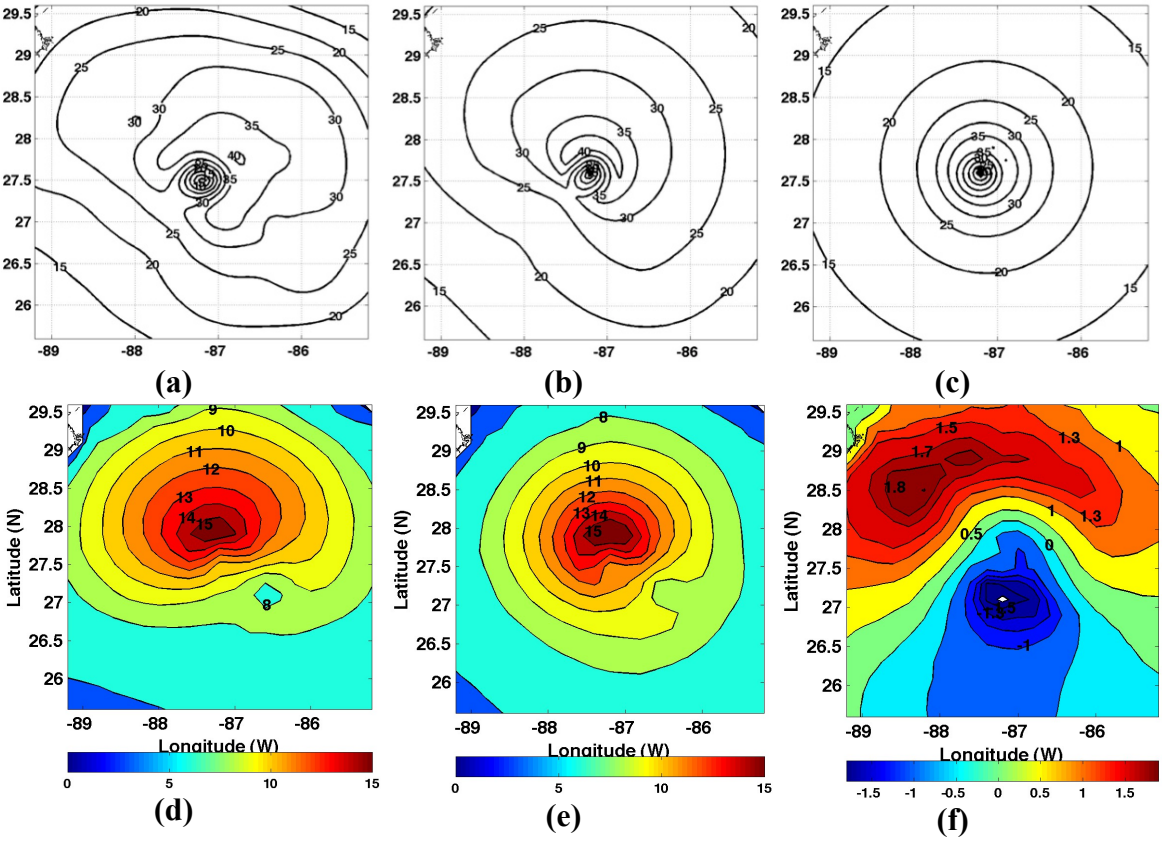

Fig. 3.14. Wind speeds and SWH's during hurricane Georges (at 0600 UTC 27 September 1998): (a) H*Wind, (b) CRV-model wind, (c) RV-model wind, (d) SWH (m) using CRV-model wind, (e) SWH (m) using RV-model wind, (f) the difference SWH (m) between (d) and (e).

Finally, the effect of the two wind fields (V_{RV} and V_{CRV}) on the 100-yr return period SWHs (defined by SWH_{100}) are examined. These extreme wave height calculations were made by fitting the Gumbel distribution to 51 years of simulations (1958 – 2008). The purpose of this exercise was merely to study the differences; actual estimates of SWH_{100} would depend on the type of statistical model used, and other factors which will be discussed in a separate paper. The results (Fig. 3.15) show considerable differences in the spatial patterns. These differences (of the order of 4 m at some locations, see Fig. 3.15c) are substantial relative to the SWH_{100} and also to the values used by API (2000).

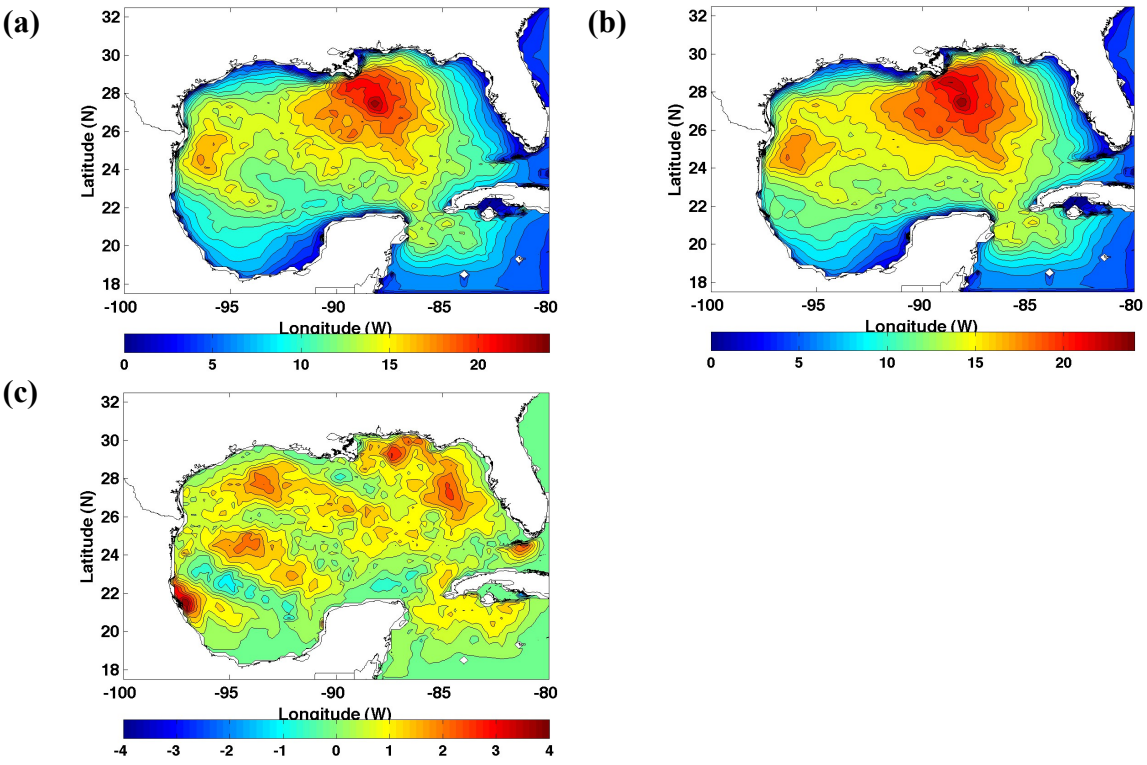

Fig. 3.15. SWH_{100} (m) for the Gulf of Mexico estimated using (a) RV-model wind, (b) CRV-model wind, (c) differences between (a) and (b).

CHAPTER IV

GENERATION OF MODELLED WAVE DATA

4.1 Introduction

Wave model data for the Gulf of Mexico is in fact produced by NOAA's National Center for Environmental Prediction, but as part of a large-scale simulation for the entire western North Atlantic. The well-established and validated energy-balance mathematical model WAVEWATCH is used for this purpose along with simulated wind-fields. For a large domain such as the western North Atlantic, the resolution is coarse and a grid of 0.25° is used by NOAA. Obviously, for the certain hurricane conditions, the resulting information is not enough for representing the intricacies of extreme conditions of the Gulf of Mexico. To make up for these limitations, NOAA developed the North Atlantic Hurricane model but results are available only from 2000. Hindcasting with other methods is needed to provide data for extreme wave estimation for long return periods.

4.2 Wave modeling

To provide the required wave data, we used the third generation wave-prediction model SWAN (Simulating Wave in the Nearshore), developed at the Technical University of Delft (Booij et al. 1999; Ris et al. 1998; and Ris et ai. 1999). The model is based on the spectral action balance equation and includes the total rate of change of wave action, frequency shift and refraction induced by depth and currents the effects of generation, dissipation (due to breaking, bottom-friction, and white-capping), and nonlinear wave-wave interactions. Reflections and diffraction are incorporated in an approximate

manner (Booij et al. 1997). The governing equation is solved using finite differences for a spectral or parametric input specified along the boundaries (Booij et al. 1999; Ris et al. 1998). The model has been widely used and validated by several investigators (e.g. Rogers et al. 2002; Booij et al. 1999; Zubier et al. 2003; Li et al. 2005).

First, the Reanalysis winds were used as model input, with a time-step of 12 minutes. The model domain is the entire Gulf of Mexico from 18°N to 32°N and from 80°W to 100°W. The spatial resolution is 0.2° × 0.2° (101 × 76 grid points) and the discrete spectrum consists of 24 directions ($\Delta\theta = 15°$) and 24 frequencies (from 0.04 to 0.4Hz, with a logarithmic increment). Bathymetry resolution is 2 minutes (601×451 grid points). It was obtained from NGDC.

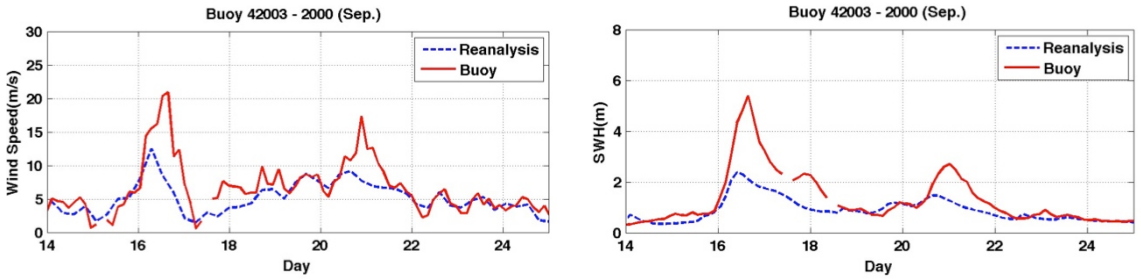

Fig. 4.1. Time series of wind speed (left) and SWH (right) comparison during September 2000 at NDBC buoy 42003.

The Reanalysis data provide a sufficient temporal wind record but are limited for wave hindcasts in hurricane conditions because of the coarse spatial resolution (2.5° × 2.5°). For example, considering the case of hurricane Gordon, winds resulting from the Reanalysis are shown in Fig. 4.1 (left). The wave hindcast that results from these wind fields are compared with data from buoy 42003 in Fig. 4.1 (right). It is clear that the

Reanalysis winds are inadequate for reliable wave height predictions for hurricane condition.

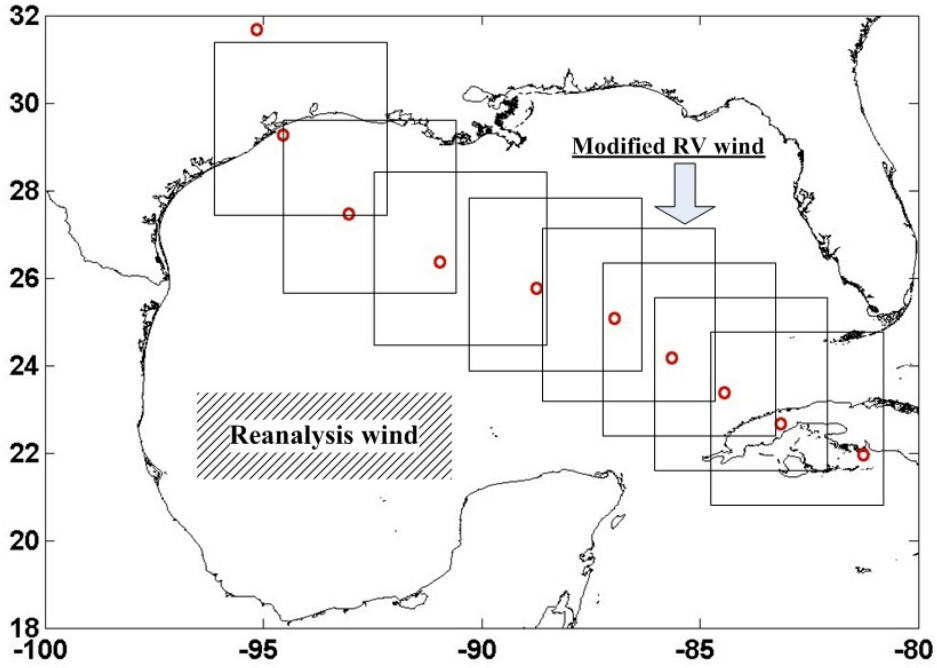

Fig. 4.2. Combined wind scheme for storm conditions.

For supplementing this coarse resolution, the modified RV winds were used to replace the Reanalysis winds in the hurricane area covering a 4° × 4° region (0.05° × 0.05° resolution). Nonetheless, the reanalysis winds can be used to provide the "background" wind fields, viz. the wind fields outside the hurricane and also the wind fields that existed before the onset of the hurricane (Fig. 4.2). The benefits of incorporating such background wind fields have been indicated by Liu et al (2007). Therefore we have constructed a composite wind field dataset by merging the parametric model winds with the reanalysis winds (the latter are interpolated onto a 0.05° grid).

From 1958 to 2008, 145 HURDAT data are available for GOM area. However, data are incomplete for 18 hurricanes, so 127 hurricanes were included in this study. Details are provided in APPENDIX B.

4.3 Basic results: Individual storms

Even with the modified RV model, some difficulties remain while modeling the hurricanes. The HURDAT dataset provides the location of the storm center at 6-hour intervals. Here we have connected these locations by a straight line, which is assumed to be the storm track, and simulations are made for intermediate times by placing the storm center on this line by interpolation. This leads to problems in some instances. For example, during hurricane Ike, Fig.4.3 shows that the simulated SWHs at the location of buoy 42001 did not successfully simulate the two peaks.

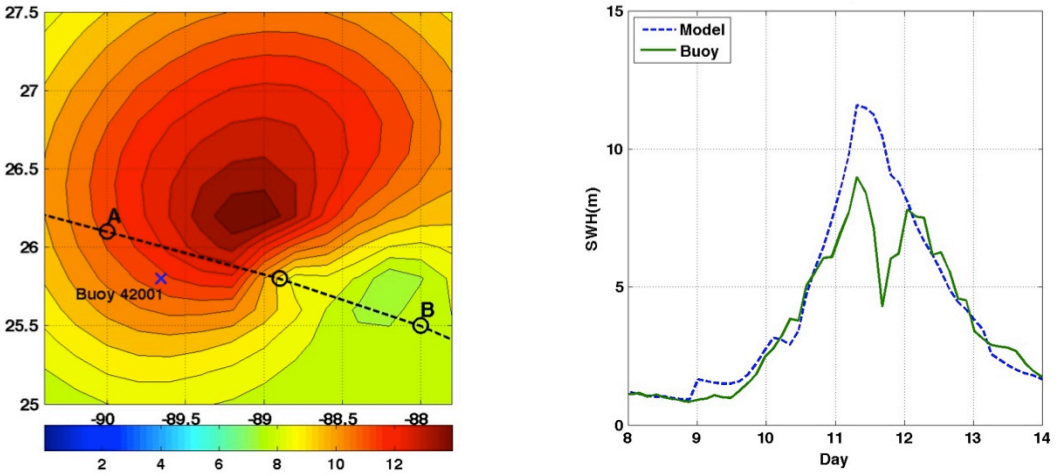

Fig. 4.3. SWH contour (left), and SWH comparison at the buoy location 42001(right).

The two peaks indicate that the buoy is close to the actual storm track (possibly with the eye of the storm passing in the vicinity). However, the assumption of AB as the assumed storm track yields a simulation at the buoy location with only one peak and substantial differences in wave heights. Thus, the actual storm track could be off by as much 30 km (based on this example).

The problems of storm track uncertainty has been addressed by Heideman and Mitchell (2009) using a technique called grid point pooling. This involves collecting estimates from several points in a preselected area, and then using them for statistical analysis. However, as Heideman and Mitchell (2009) state, this violates the statistical independence, because each storm is included multiple times. They have recommended some general guidelines to obtain reasonable results, including a selection of spatially homogeneous regions, which is subjective and difficult.

Since the SWHs show great variability in the vicinity of the storm center, we applied a smoothing of the simulated SWHs by using model data from 2 grid points on all four sides of a given point. Sample results are shown in Figs. 4.4 and 4.5 for hurricane Ivan. Figure 4.5 also includes data from the eleven buoys. The comparisons, shown in Fig. 4.5 indicate that the model simulations are fairly realistic and show some SWHs larger than 10 m. But the SWHs at buoy 42007 are larger than model data. Several factors could adversely affect the modeling effort and the comparisons. The first is the storm surge effect, which we have ignored in the simulation. This effect consists of water level changes and surface currents, which can modify the waves in shallow water. A more likely source of errors may be due to inaccuracies in the wind-fields in the

near-shore areas arising from the presence of islands (near 42007) and other subgrid-scale topographic features. Other possible reasons for modeling errors are inaccurate representations of the bathymetry and some modeling limitations (e.g. Rogers et al. 2007). There can also be data problems. Bender et al. (2008) observed over estimation of about 3.31m higher measurements at buoy 42007 during hurricane Katrina and reported that possible measurement errors occur as a result of swell in shallow water, heeling of the buoy caused by wind and currents, and the failure to tilt-correct the accelerometer data.

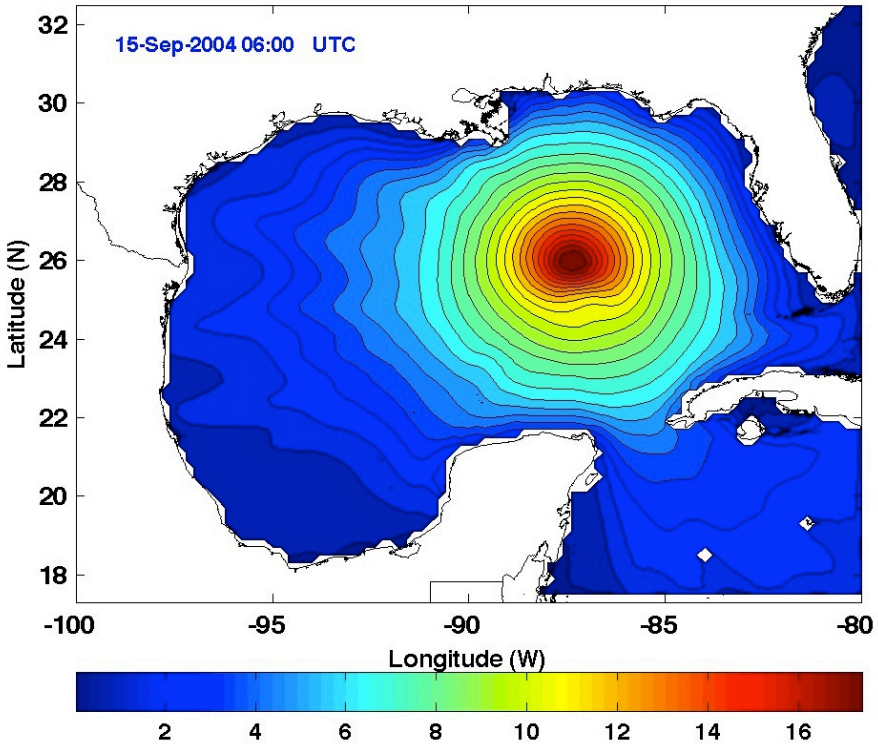

Fig. 4.4. SWH result for hurricane Ivan.

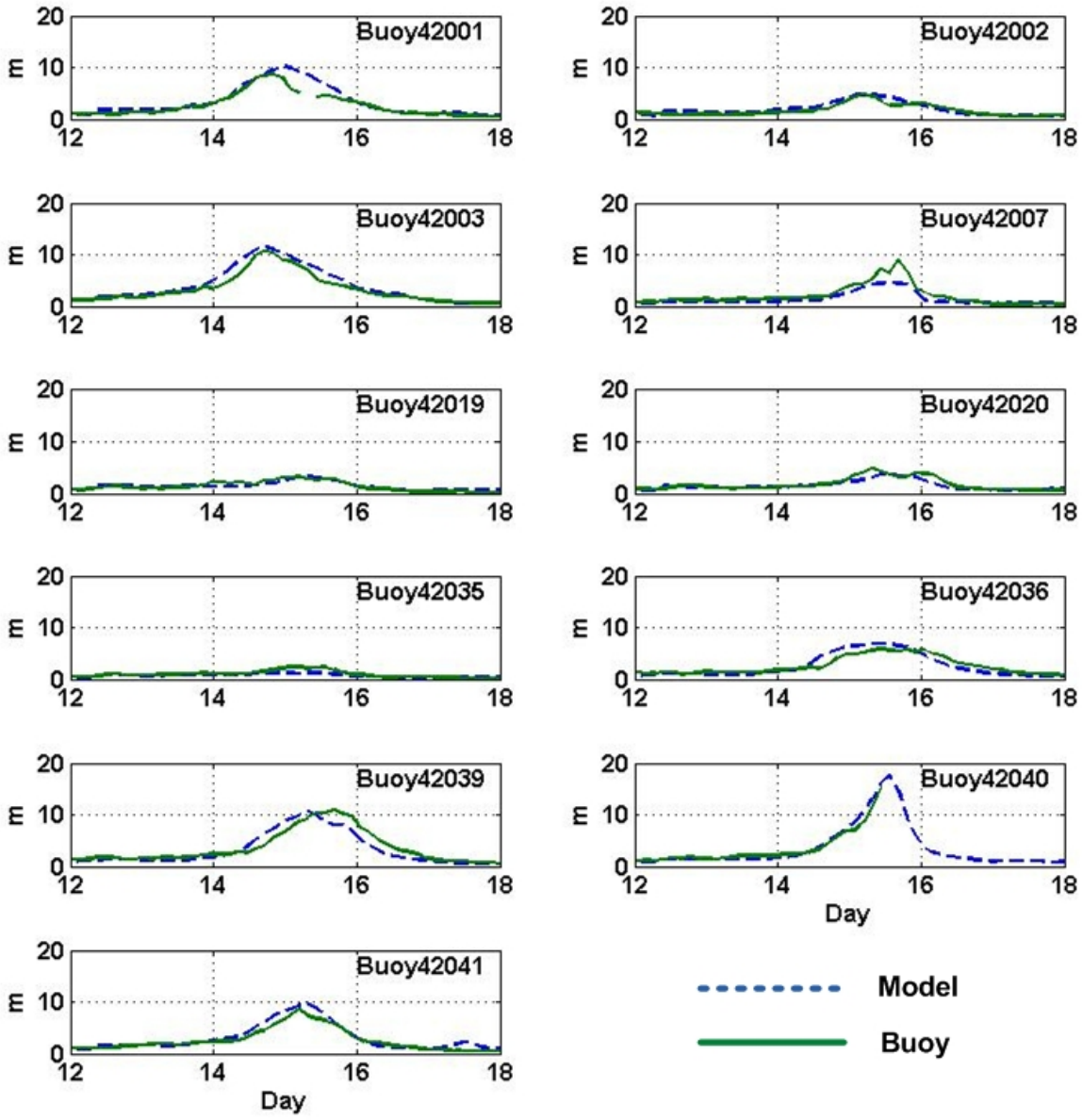

Fig. 4.5. SWH comparisons.

Additional comparison of model SWH with historical data are shown in Fig. 4.6. The data were collected from a fixed platform near Louisiana during hurricane Camille, which passed within 23km of the platform (Earle 1975). These data are older than all NDBC data. The measured maximum SWH is 13.45m and model SWH is 14.65m. Note

that data are available only for a part of the hurricane. The model calculations are reasonably accurate especially if you take the storm track uncertainty into consideration.

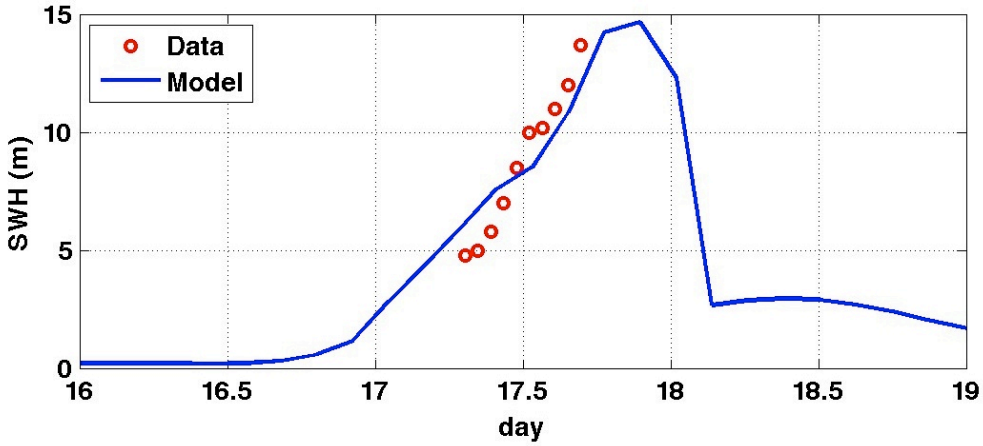

Fig. 4.6. SWH comparison during hurricane Camille (August 1969).

4.4 Basic results: 51 years

Simulations were performed for 51 years (1958 - 2008), and 127 hurricanes are re-constructed by the modified RV model. Since it is the maxima in specific time intervals that influence the extreme wave statistics, it is necessary to assess the quality of such maxima. Here we choose monthly maxima for assessing the simulations. Figure 4.7 shows a comparison of the monthly maxima at the location of the eleven buoys.

In order to make the comparison, we have used a total of 2760 data points. Instances where the buoy stopped recording have not been included in the comparison. For the comparison, the model data from the grid point that is the closest to the buoy has been used. The comparison in Fig. 4.7 (left) shows that most of the model data and buoy data are fairly close to the slope one line. In fact, the slope of best-fit line is

approximately 0.82 (Fig. 4.7). However, in the case of larger wave heights the predicted wave heights appear to be larger than data. We, therefore, decided to filter the data into two wave height bins for further analysis.

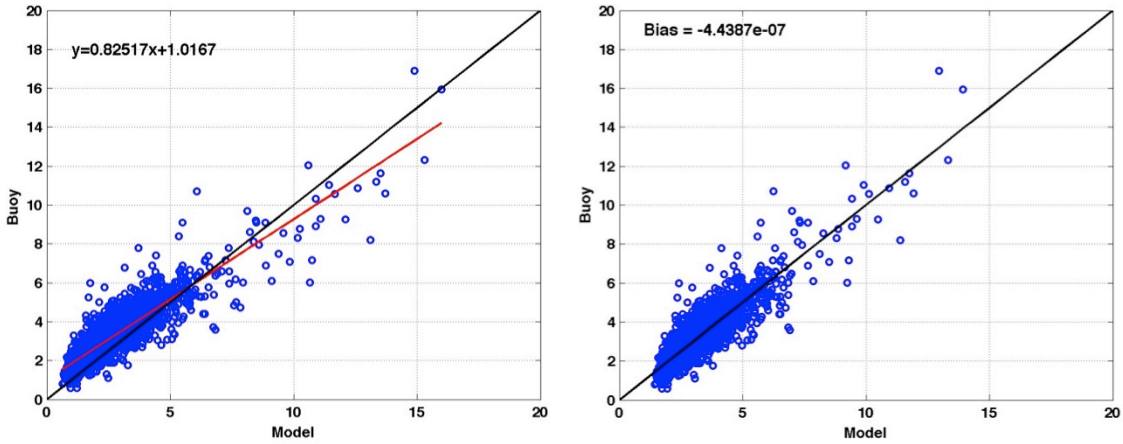

Fig. 4.7. Comparison of monthly maxima for the eleven NDBC buoy.

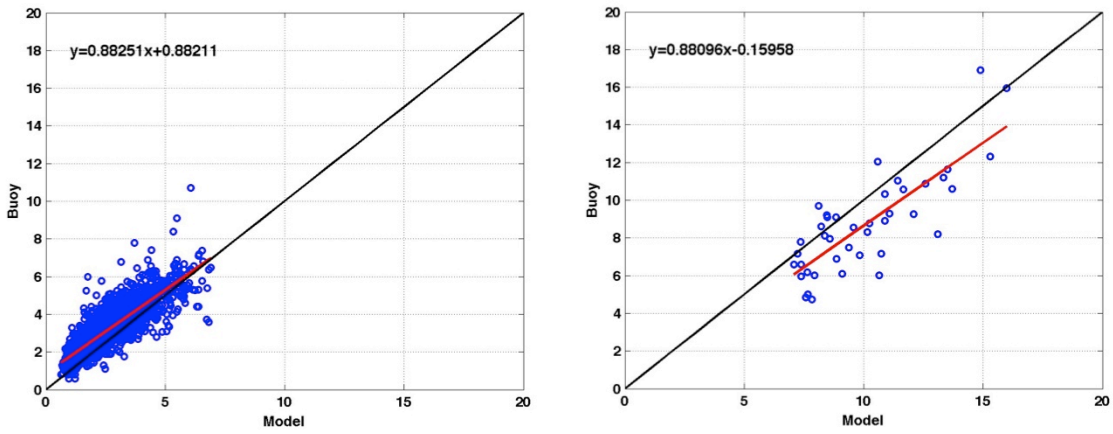

Fig. 4.8. Best fitting curve for two groups of monthly maxima.

Since larger wave height are of importance in the extreme value statistics, we separated the 2760 points into two sets, those larger than 7m and those smaller than 7m and the best fit line obtained each one. (Fig.4.8) The formula from the best-

fit line can be used to modify the simulated wave heights in order to bring them closer to the buoy values. The modified results are shown in Fig. 4.7 (right) for all eleven buoys and the comparison appears fairly reasonable.

Using the simulations for the pre-2004 period and for the period including the 2004-2008 hurricane season, the maximum SWH obtained from the simulations at each of the 7676 grid points was determined. The maximum modeled SWH's for each location in the Gulf of Mexico are shown in Fig. 4.9 for two periods (1958-2003 and 1958-2008).

The distribution of the maxima (Fig. 4.9) has changed slightly (mostly between 85 and 90 longitude), but the frequency of large waves shows a greater change. Figure 4.10 shows the number of times the SWH exceeded 10m in the Gulf of Mexico; the frequency and spatial extent of these large waves clearly increased during 2004-2008. The maximum number of events exceeding 10 m in SWH during first 46 years is 8, but of the order of 12 or more the last 4 years (2004 – 2008). The largest modeled SWH's occurred in 1969 (Camille), with a simulated value of approximately 18 m in the offshore areas (27° 5'N, 87° 8'W). Note that in Figs 4.9 there is some patchiness. That is, there are high spots interspersed amidst areas of slightly lower SWH's. This is due to the output protocol where the data were output every 3 hours. For example, the maximum SWH's along a region from the tip of the Yucatan peninsula to Brownsville were all due to hurricane Allan (1980). If the output is obtained every 1 hour, the patchiness is reduced (Fig. 4.11). This feature does not affect the SWH_{100} calculations substantially because they are based on 51 years of data (and not one snapshot as in Figs 4.9).

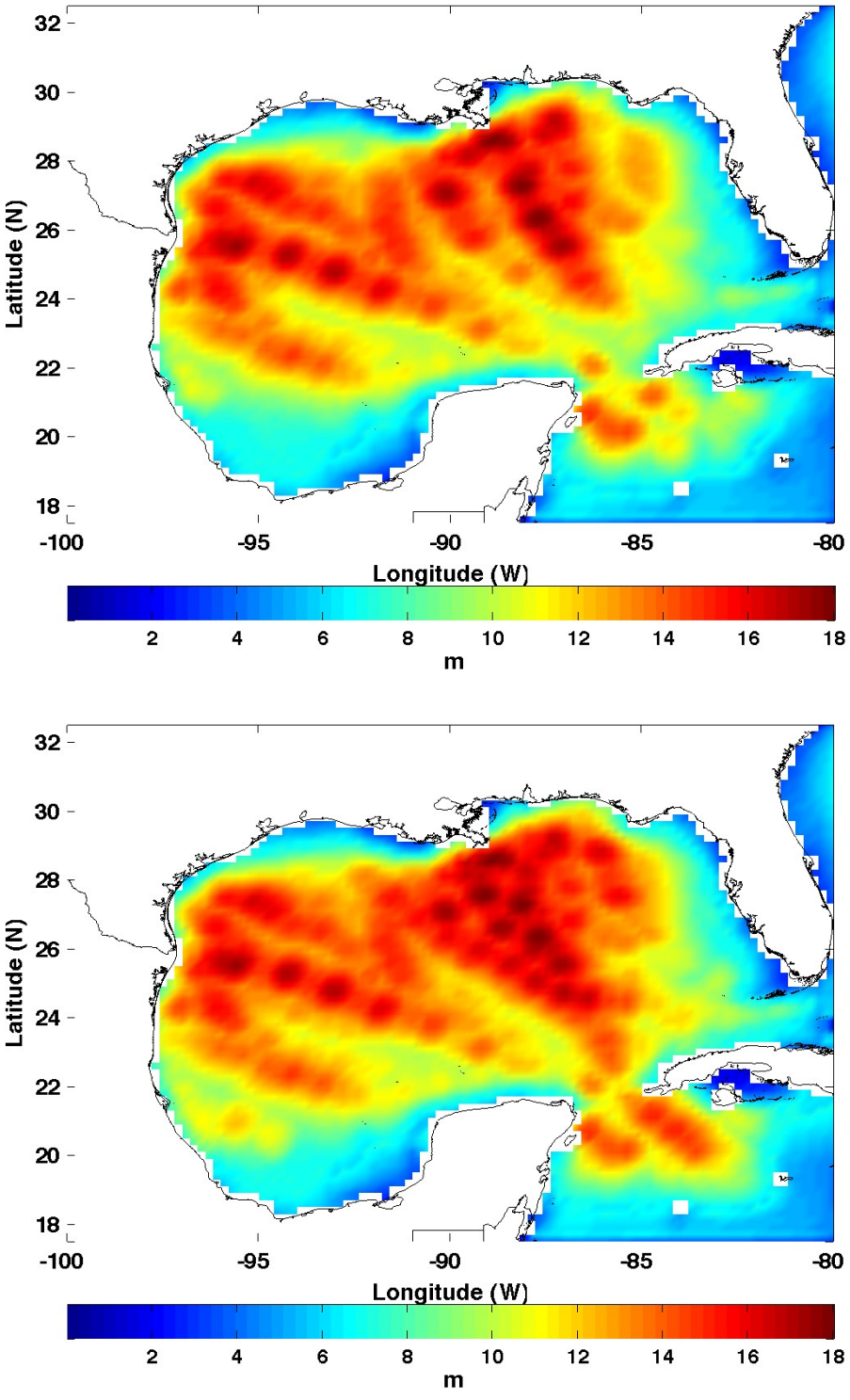

Fig. 4.9. Maximum SWH (m) for 46 years (top) and 51 years (bottom).

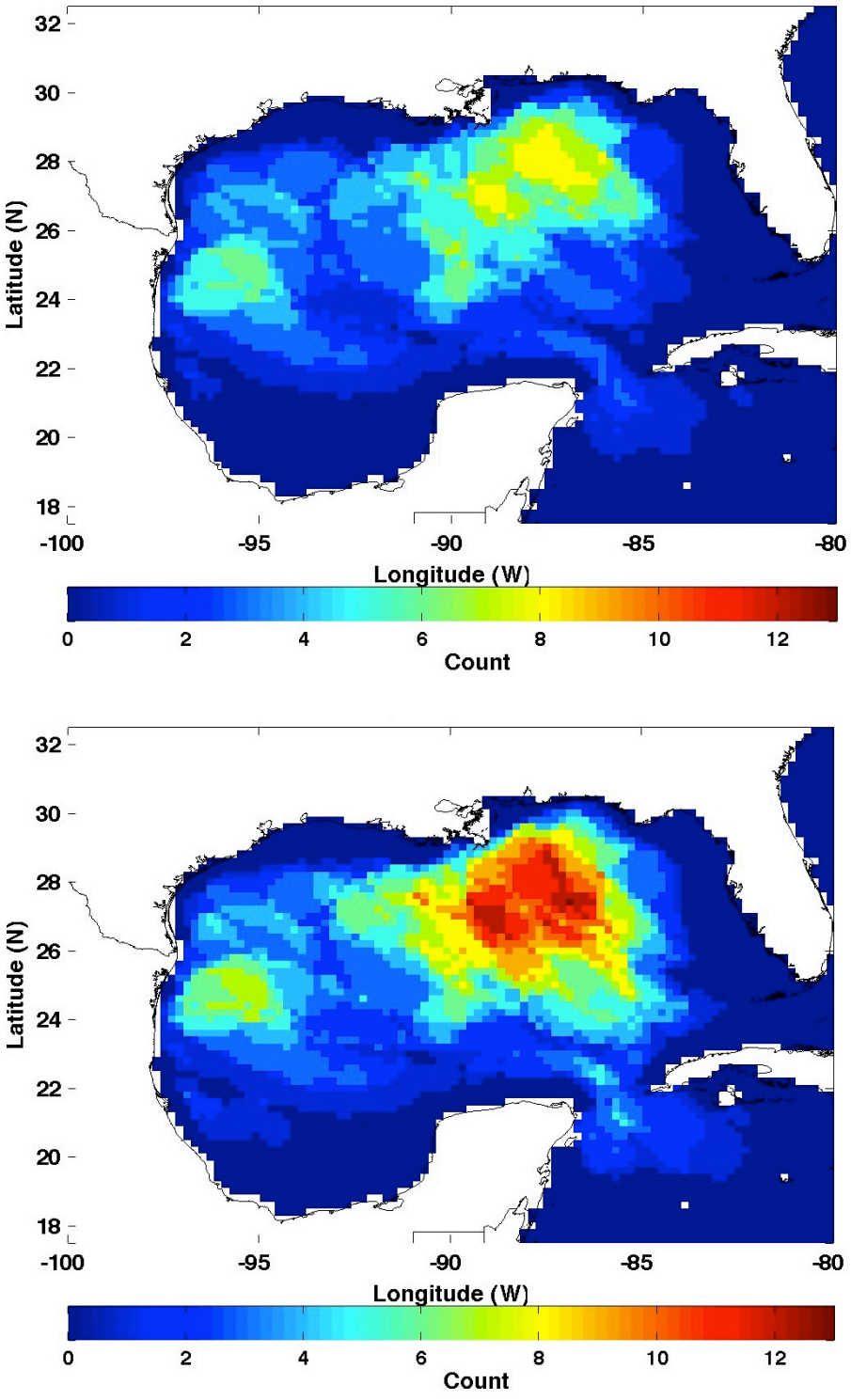

Fig. 4.10. Number of times SWH > 10 m: 1958 - 2003 (top), and 1958 - 2008 (bottom).

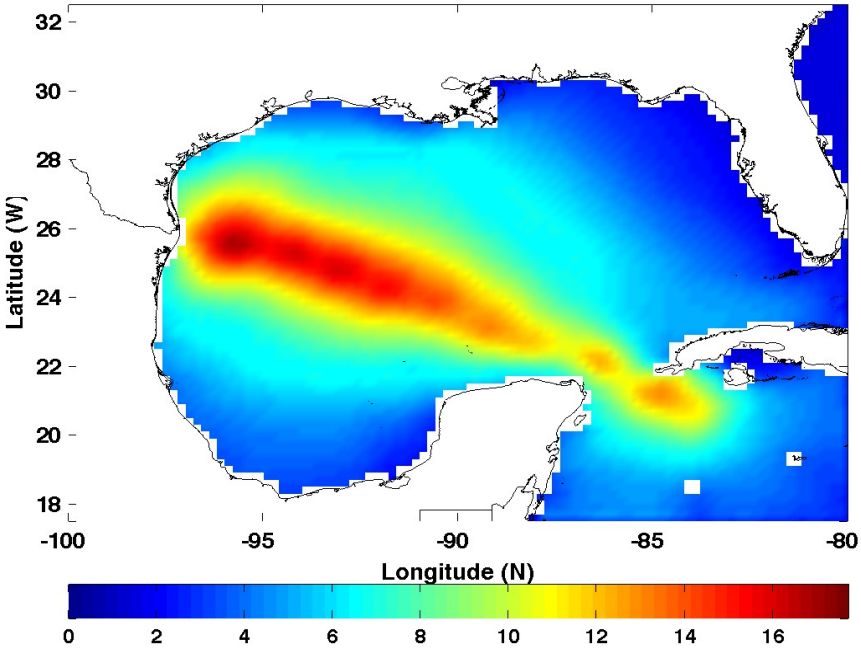

Fig. 4.11. Maximum SWH (m) for hurricane Allan (1980).

Figure 4.12 describes the entire Gulf of Mexico SWH trend based on the mean of each grid point's annual maximum average. This plot indicates an approximately 0.6 cm increase per year in wave height. Fig. 4.13 shows the trend in the annual maxima for each grid points. The blue dots denote an area of decreasing trend and the red dots denote an area of increasing trend.

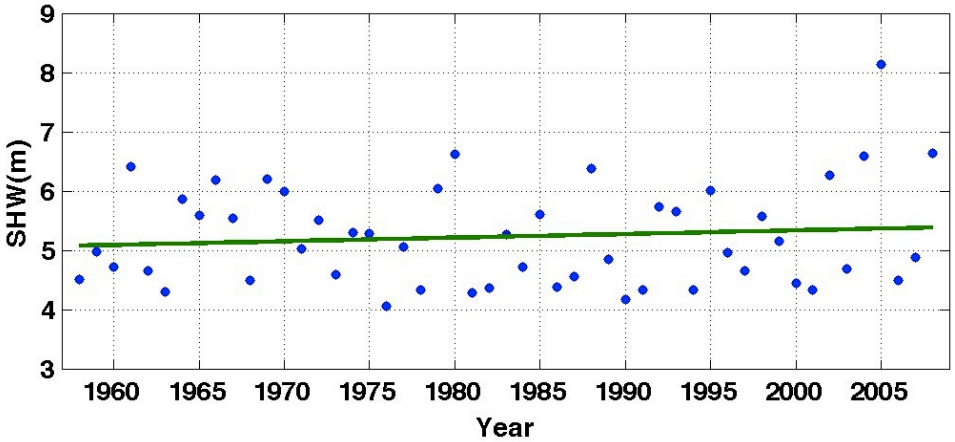

Fig. 4.12. Trend using mean of entire annual maxima.

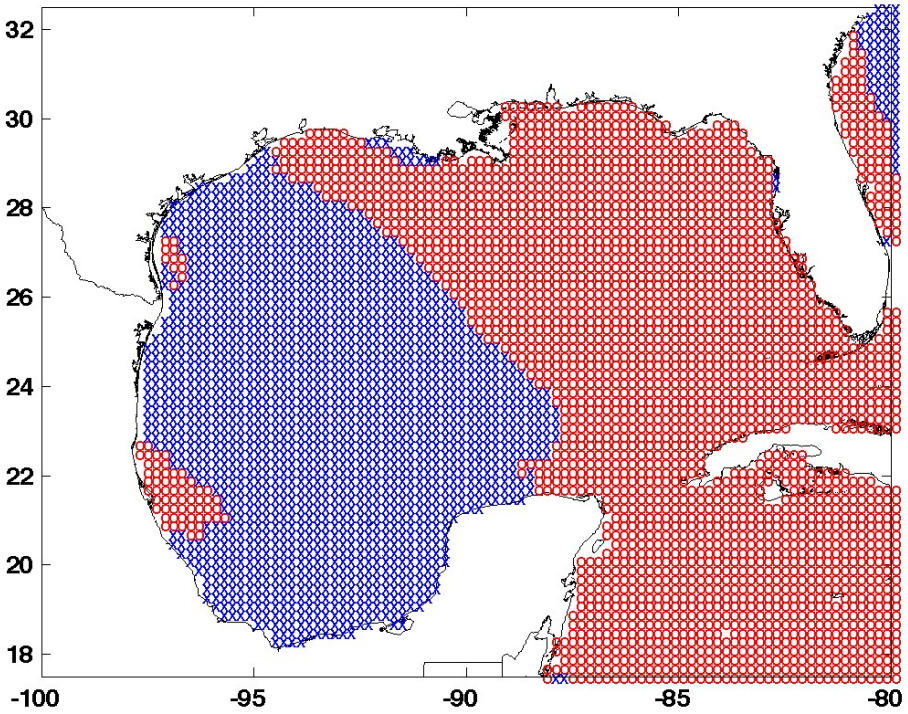

Fig. 4.13. Increase and decrease trend distribution (Blue: decrease trend point, Red: increase trend point).

CHAPTER V

STATISTICAL METHODS

5.1 Introduction

Estimating the extreme wave statistics at each location is usually done by fitting a distribution to the extremes in successive time intervals and then using the distribution to estimate the probability of occurrence associated with a specified SWH. Although several distributions can be used for this purpose (e. g. Sorenson 1993), the most common appear to be the Gumbel and the Weibull distributions (e.g. Petruaskas and Aagaard 1971; Sobey and Orloff 1995; Panchang et al. 1990; Panchang et al. 1999; Perez et al. 2003; Pontes et al. 2005). In recent years, the use of the Generalize Extreme Value (GEV) has been proposed for ocean engineering applications and coastal flood hazard analysis by Guedes Soares (2004) and FEMA (2004).

5.2 Extremal distribution

The cumulative density functions (CDF) for three distributions are as follows:

$$\text{Gumbel:} \qquad F(x;\mu,\sigma) = \exp\left[-\exp\left[-\left(\frac{x-\mu}{\sigma}\right)\right]\right]$$

$$\text{Weibull:} \qquad F(x;\mu,\sigma,\xi) = 1-\exp\left[-\left(\frac{x-\mu}{\sigma}\right)^{\xi}\right], \quad x>\mu \tag{5.1}$$

$$\text{GEV:} \qquad F(x;\mu,\sigma,\xi) = \exp\left\{-\left[1+\xi\left(\frac{x-\mu}{\sigma}\right)\right]^{-1/\xi}\right\}$$

where F stands for the probability of the SWH being less than a given number x , and the variables σ, μ, ξ represent the scale, location and shape parameters, respectively. The left hand side of CDF is related to the "recurrence interval" or the "return period" N (in years) through

$$F\,(SWH < SWH_{N}) = 1 - \frac{1}{SN}$$

where S is the number of data points per year and SWH_N is the SWH associated with a return period of N years. A rule of thumb, permits extrapolation to duration that is approximately 3 times as long as the length of the data when using the customary annual maxima (Borgman 1975).

To use the above equations, however, the parameters ξ, σ, and μ must be estimated for a given set of data (say x_1, x_2, x_3, …, x_n). This is accomplished by the method of maximum likelihood. This involves first constructing the likelihood function

$$L(\mu,\sigma,\xi)=\prod_{i=1}^{m} f(x_i;\mu,\sigma,\xi) \tag{5.2}$$

where, f is probability density function (PDF), and then maximizing $\ell = log(L)$: for instance, for the GEV, we have:

$$f(x;\mu,\sigma,\xi) \;= \frac{1}{\sigma}\left(1+\xi\left(\frac{x-\mu}{\sigma}\right)\right)^{-(1+1/\xi)} \exp\left\{-\left[1+\xi\left(\frac{x-\mu}{\sigma}\right)\right]^{-1/\xi}\right\} \tag{5.3}$$

$$\ell(\mu,\sigma,\xi) = -m\log\sigma - \left(1+1/\xi\right)\sum_{i=1}^{m}\log\left[1+\xi\left(\frac{z_i-\mu}{\sigma}\right)\right] - \sum_{i=1}^{m}\left[1+\xi\left(\frac{z_i-\mu}{\sigma}\right)\right]^{-1/\xi} \tag{5.4}$$

where $\xi \neq 0$,

The following nonlinear equations are solved to determine ξ, σ, and μ:

$$\frac{\partial \ell}{\partial \mu}=0, \quad \frac{\partial \ell}{\partial \sigma}=0, \quad \frac{\partial \ell}{\partial \xi}=0$$

$$\frac{\partial \ell}{\partial \mu}=\frac{1}{\sigma}\sum_{i=1}^{m}\left[\frac{\xi+1-A^{-1/\xi}}{A}\right]=0, \qquad A=\left[1+\xi\left(\frac{x_i-\mu}{\sigma}\right)\right]$$

$$\frac{\partial \ell}{\partial \sigma}=-\frac{m}{\sigma}+\frac{1}{\sigma^2}\sum_{i=1}^{m}\left[\frac{\xi+1-A^{-1/\xi}}{A}\cdot\left(x_i-\mu\right)\right]=0, \tag{5.5}$$

$$\frac{\partial \ell}{\partial \xi}=-\frac{1}{\xi^2}\sum_{i=1}^{m}\left[\frac{\xi+1-A^{-1/\xi}}{A}\left(\frac{x_i-\mu}{\sigma}\right)\xi-\ln A\cdot(1-A^{-1/\xi})\right]=0$$

Similar equations result for the other two distributions. As to the choice of data used to fit the various distributions, the classical approach involves the use of a subset corresponding to the annual maxima (e.g. Carter and Challenor, 1981); this can generally be expected meet to the requirement of the extremal distributions that the extremes be drawn from samples (in this case, annual data) which belong to the same population.

5.3 Choice of distribution

Usually, a number of subjective measures are used to identify the preferred model. Not only is this tedious, but this also constrains one to the chosen model when comparing multiple time-frames. Recent developments by Li & Reeve (2008) have provided more robust and quantitative ways based on the 'Jack-knife' or the 'Bootstrap' resampling methods with the error norm for such identification. By following their approach, the most appropriate model can be selected by the engineer, rather than limiting oneself to any pre-selected model, as done by Berek et al. (2007).

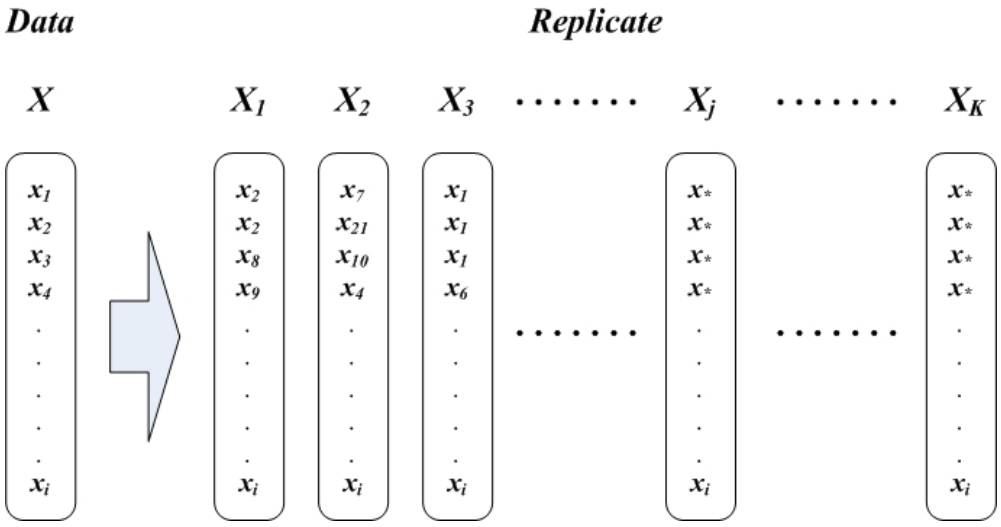

Fig. 5.1 Bootstrap resampling method.

The bootstrap resampling method is similar to Monte Carlo simulation. We randomly select *n* data points from the original sample (Fig. 5.1). Thus, this method can create new and statistically similar resampled datasets a large number of times. A similar resampling method, the Jacknife method, can also be used but the bootstrap resampling method is selected because the degree of randomness in the bootstrap resampling is greater, and the stability of the optimized parameters has been rigorously tested by Li and Reeve (2008).

In this study, the weighted error norms of the maximum likelihood optimizations for each of the three CDFs are calculated as the average of *K*=500 bootstrap replicates. The weighted error norm of standard error is (Linhart and Zucchini 1986):

$$E\left\langle \Delta_i\left(\bar{Q}_j\right)\right\rangle = E\left\langle \max_{1\le i\le m}\left|\left[\frac{i}{m+1}\right]^h - G_{\bar{Q}_i}\left(r_{ij}\right)^h\right|\right\rangle, \tag{5.6}$$

where E stands for the expected value, $\bar{Q}$ is optimized parameter, $G_{\bar{Q}}$ is the CDF for the

selected distribution, r_1, r_2, **…**, r_m are the ordered data X in increasing magnitude, and j =1, 2, …, K represents the K samples.

The distribution with the smallest error norm is to be preferred. The parameter h, controls the emphasis that we place on different parts of the data while fitting the distribution to the data. When h=1.0, both the lower tail and the upper tail are equally important. For h<1, emphasis is placed on the lower tail, while for h>1, emphasizes the upper tail where 'extreme' events occur.

These computations were made at all points in the Gulf of Mexico. The resulting SWH_{100} and best distribution depending on the error norm are shown in Chapter VII.

CHAPTER VI

APPLICATION OF STATISTICAL METHOD TO MODEL AND BUOY DATA: VALIDATION

6.1 Introduction

Models are an effective way to create a long-term database for extreme wave height estimation. They have the advantage of providing data on a regular grid, and as described in Chapter IV for a long period (51 years) on a continuous basis, which allows the creation of data consisting of annual maxima required in the classical method of extremal analysis. However, even when we used the best models, there will be errors (as seen in Chapter IV). The effect of the errors on the estimated SWH_{100} must be determined. If the overall modeled dataset is long, one can expect the effect of individual modeling errors on SWH_{100} to be small. If the dataset is short, or if even one or two errors are very large, one can expect a greater impact on the estimated SWH_{100}.

Fortunately, in the GOM, there are 11 NDBC wave buoys (Fig.1.2). As shown in Table 1.1 some of them have been recording data since 1976, creating a database that is sufficiently long for SWH_{100} estimation. In some cases the rule of thumb for extrapolating to duration three times the length of the data (Borgman 1975) is satisfied. In fact Palao et al. (1994) and Panchang et al. (1999) have used these data to obtain such estimates.

While buoy data may appear to have no problems such as modeling errors, note that there are other problems with them. Typical problems found were as follows. Frequently there are gaps in the data (Table 6.1). The gaps are sometimes for several

months (which include the hurricane season) or for several hours (including in some cases the peak of a storm). Other problems include a location change. This is deliberate sometimes (location shifted by NOAA), and sometimes (per our judgment), the buoy has drifted several miles in a storm (During hurricane Ike, buoy 42035 drifted approximately 40km). If the buoy is located near the storm track, where the wave height variability is greater, the effect on a pre-chosen point (we used a single location for each buoy) can be substantial. Finally, the quality of the measurements may have changed over the years, and recently Bender et al. (2008) suggested that the data could sometimes be wrong. He proposed that buoy 42007 might have overestimated the SWH by as much as 3m because of heeling of the buoy during Katrina. Therefore, even though the buoys provide 'data', estimates obtained from these cannot be considered as the 'absolute', but perhaps a more 'reliable' value compared with models.

Another point to be noted is that when making comparisons between model and buoy SWH_{100} is that buoy location does not usually coincide with a model grid point. The closest model grid point to the buoy was used, and the distance between the two varied between 3.6km and 20km (Table 6.2). Again, if the location happens to be near the storm track, the variability can create big differences in two estimates.

The data from all eleven buoys were carefully examined. Obvious problems were identified. When data during hurricane months was missing, model results for those months were used to assess the usability of a particular buoy. If model results (or HURADT data) suggested that very large SWH's may have occurred, the remaining buoy data is not useful for SWH_{100} estimation. A summary of the examination is

provided in Table 6.1. On the basis of this, data from buoy 42041 was discarded. For the other 10 buoys, the annual maxima were used with the Gumbel, Weibull and GEV distributions as described in Chapter V.

Table 6.1. Summary of the eleven buoy data.

Buoy	Total data avail.	Missing data	Comments
42001	1976 – 2008 (33)	1976 - 1978 (Bad quality) 2007 (Jan. – Feb.)	NA
40002	1976 – 2008 (33)	1976 (Jan. – Sep.) 1977 (Aug. – Sep.) 1978 (Aug.) – 1979 (Nov.) 1980 (Aug.) 1999 (Jan. – Feb.) 2001 (Jan. – Aug.) 2005 (Jul.)	Three large SWHs (~10m) are missing (1977, 1980, and 2005). At other times, when data are missing, model results indicate mostly small SWH's, but sometimes of the order of 5m.
42003	1977 – 2008 (32)	1977 (Jan. – Jun.) 1986 (Nov.) – 1987 (Apr.) 1987 (Dec.) – 1988 (Apr.) 1994 (Sep.) – 1995 (Jan.) 1996 (Sep.) – 1997 (May) 2005 (Aug. – Sep.) 2008 (Aug. – Nov.)	One large SWH (~10m) is missing. (2008) At other times, when data are missing, model results indicate mostly small SWH's, but sometimes of the order of 5m.
42007	1981 – 2008 (28)	1981 (Oct.) – 1983 (Jan.) 1983 (Apr. – Dec.) 1987 (Jan. – Apr.) 1990 (Aug.) – 1996 (Sep.)	When data are missing, model results indicated fairly small SWH's (< 3.5m)
42019	1990 – 2008 (19)	1990 (Jan. – May) 2000 (jan. – Jun.)	NA
42020	1990 – 2008 (19)	1990 (Jan. – May) 1993 (Aug. – Nov.) 1997 (Feb. – Oct.)	NA
42035	1993 – 2008 (16)	NA	~ 40 km buoy drift during hurricane Ike.
42036	1994 – 2008 (15)	2005 (Jul.) 2007 (Feb. – Sep.)	One large SWH (~10m) is missing. (2005)
42039	1995 – 2008 (14)	1995 (all)	Annual maximum data from 1996 are used.
42040	1995 – 2008 (14)	1995 (Jan. – Nov.)	
42041	1999 – 2005 (7)	1999 (Jan. – Nov.) 2001 (March) – 2002 (April) Disestablished after 2005 (April)	Almost half the data are missing.

6.2 Results and discussion

Estimates of SWH_{100} were obtained for the period excluding the year 2004-2008 and then by including them. Results were obtained using both buoy data and model data. The model data length chosen corresponded to the earliest and latest buoy data availability. The results are shown in Table.6.2.

Table. 6.2. Estimated SWH_{100} (m).

Buoy No.	Data	Δ (km)	No. of Year	(a) before 2004			(b) including 2004 - 2008		
				Gumbel	Weibull	GEV	Gumbel	Weibull	GEV
42001	Buoy	20	28/33	10.62	10.95	12.84	12.64	12.32	14.74
	Model			11.65	12.63	14.2	12.90	14.31	16.1
42002	Buoy	12.4	28/33	10.36	9.49	10.47	9.80	9.12	9.82
	Model			12.11	12.45	14.56	11.95	12.76	14.25
42003	Buoy	16.1	27/32	10.64	11.24	12.62	12.44	12.43	14.25
	Model			12.27	13.24	15.03	13.44	14.92	16.09
42007	Buoy	3.6	23/28	5.75	7.02	5.78	7.61	10.4	10.53
	Model			6.71	8.2	8.07	7.16	8.0	7.92
42019	Buoy	5.4	14/19	7.18	6.20	6.26	7.25	6.80	6.88
	Model			8.52	8.98	10.0	8.51	9.30	9.71
42020	Buoy	12.8	14/19	8.05	9.40	10.90	9.02	9.94	10.47
	Model (a)			12.37	11.26	14.83	12.59	12.90	17.19
	Model (b)			8.03	8.1	10.0	9.9	10.5	13.5
42035	Buoy	7.7	11/16	5.94	7.55	6.59	6.76	7.53	7.44
	Model			5.37	5.67	6.4	6.24	6.75	7.39
42036	Buoy	9.2	10/15	9.9	11.52	10.28	9.57	8.90	8.84
	Model			9.21	10.77	9.36	10.8	13.08	10.78
42039	Buoy	10.1	8/13	11.0	11.9	13.01	14.49	19.2	17.8
	Model			11.3	12.39	13.53	14.15	19.24	17.3
42040	Buoy	9.8	8/13	13.2	16.35	19.45	21.9	31.2	31.8
	Model			13.02	14.85	19.1	18.48	23.45	24.56

Several features are apparent in these results. First, at most locations, the SWH_{100} estimates obtained using buoy data and model data are close to each other, especially for the Gumbel and Weibull distributions for the most part. The differences are of the order of 10%. Frequently, buoy SWH_{100} is smaller than model SWH_{100}, which in some cases is probably a result of missing buoy data. This is likely in the case of 42001, 42002, and

42003 where annual maxima of the order of 7m (based on model calculations) were missing. The differences between buoy and model SWH_{100} are certainly lager in the case of 42020. The reasons for this were examined. Figure 6.1 shows a plot of the modeled and buoy annual maximum. It appears that one data point is responsible for this mismatch, i.e. year 1999, where the modeled SWH is 12m as against the buoy SWH of 8m. However, on examination this buoy was found to be close to the track of hurricane Bret, and in a region of considerable wave height variability in model results (Recall the issues pertaining to track uncertainty noted in Chapter IV, and note that the closest grid point in this case is 12.8km away). As an experiment, the effect of replacing the modeled value at this location by the buoy value was studied. The resulting model SWH_{100} were then much closer to buoy SWH_{100}, as shown in Table 6.2 (Model (b)). This demonstrates the effect of errors in a relatively short dataset, as opposed to much smaller effect in the case of buoy 42001, 42002, and 42003 where the dataset better corresponds the rule of thumb. The difference for 42020 between the two models (a) and (b) is smaller as the duration increases (Table 6.2 right), indicating the diminishing importance of an isolated large errors. The table also shows that the differences between buoy and model SWH_{100} are greater for the GEV distributions. The reason for this is that for the GOM, the GEV appears to emphasize the ‘upper tail’, as shown later in Chapter VII.

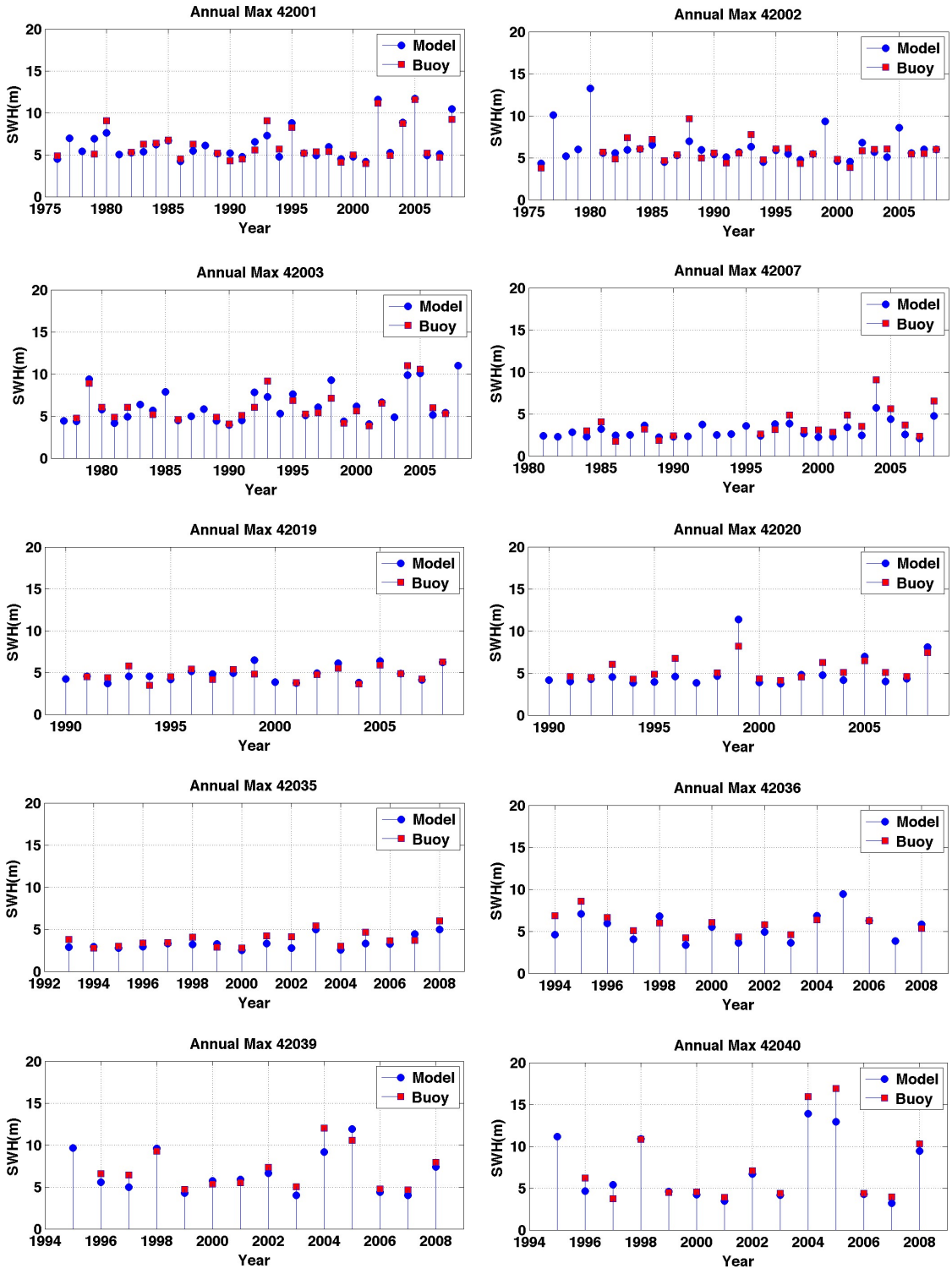

Fig. 6.1. The modeled and buoy annual maxima.

Finally, we see that the effect of the 2004-2008 periods is to increase the SWH_{100} at nearly all locations. The exception is the case of the location of buoy 42040, where the effect is much greater (e.g. using the Gumbel distribution the buoy SWH_{100} increases from 13m to 20m). The reason for this is that very large wave heights were recorded in 2004-2008 and the data length is short. Adding the high wave period of 2004-2008 increases the data length from only 8 years to 13 years. When the datasets are longer the effect of 2004-2008 seasons is smaller.

Overall, the similarity of the model SWH_{100} and buoy SWH_{100} values shown in Table 6.2 for the Gumbel and Weibull distributions for both periods is a validation of the modeling procedure. Further, we see that the effect of individual errors diminishes as the data length increases. As a result, in the next chapter, the three distributions are applied using all the model data developing Chapter IV for 51 years.

CHAPTER VII

RESULTS AND DISCUSSION: SWH_{100} ESTIMATES FOR THE GULF OF MEXICO

After all the simulations were completed, a dataset for each grid point consisting of 51 annual maxima was developed. There was a total of 7676 grid points in the domain. For each grid point, the 3 distributions described in Chapter V were fitted to the data and the SWH_{100} was estimated. The bootstrap technique was used to identify the preferred distribution.

The SWH_{100} estimated by 3 different distributions are shown in Figs. 7.1 – 7.3 using both the pre 2004 data and the data that includes the 2004-2008 seasons. The maximum estimates (spatially) obtained with the Gumbel distribution is the smallest and those with GEV are the largest. In these two cases, the effect of the 2004-2008 seasons is to increase maximum SWH_{100} estimate by 0.9m and 1.3m respectively. The effect of the 2004 – 2008 season is more pronounced in the case of the Weibull distribution (maximum difference of 2.7m) and the spatial variability of the differences is also greater, suggesting that the Weibull distribution has much greater sensitivity to data than the other two.

The estimates of SWH_{100} provided in the older API manual (2000) and the revised manual in 2007 appeared to suggest a difference in the SWH_{100} of the order of 5m. Our calculations provided in this chapter indicate that the effect of the 2004-2008 hurricane season is of the order of only 1-2m based on the choice of distribution.

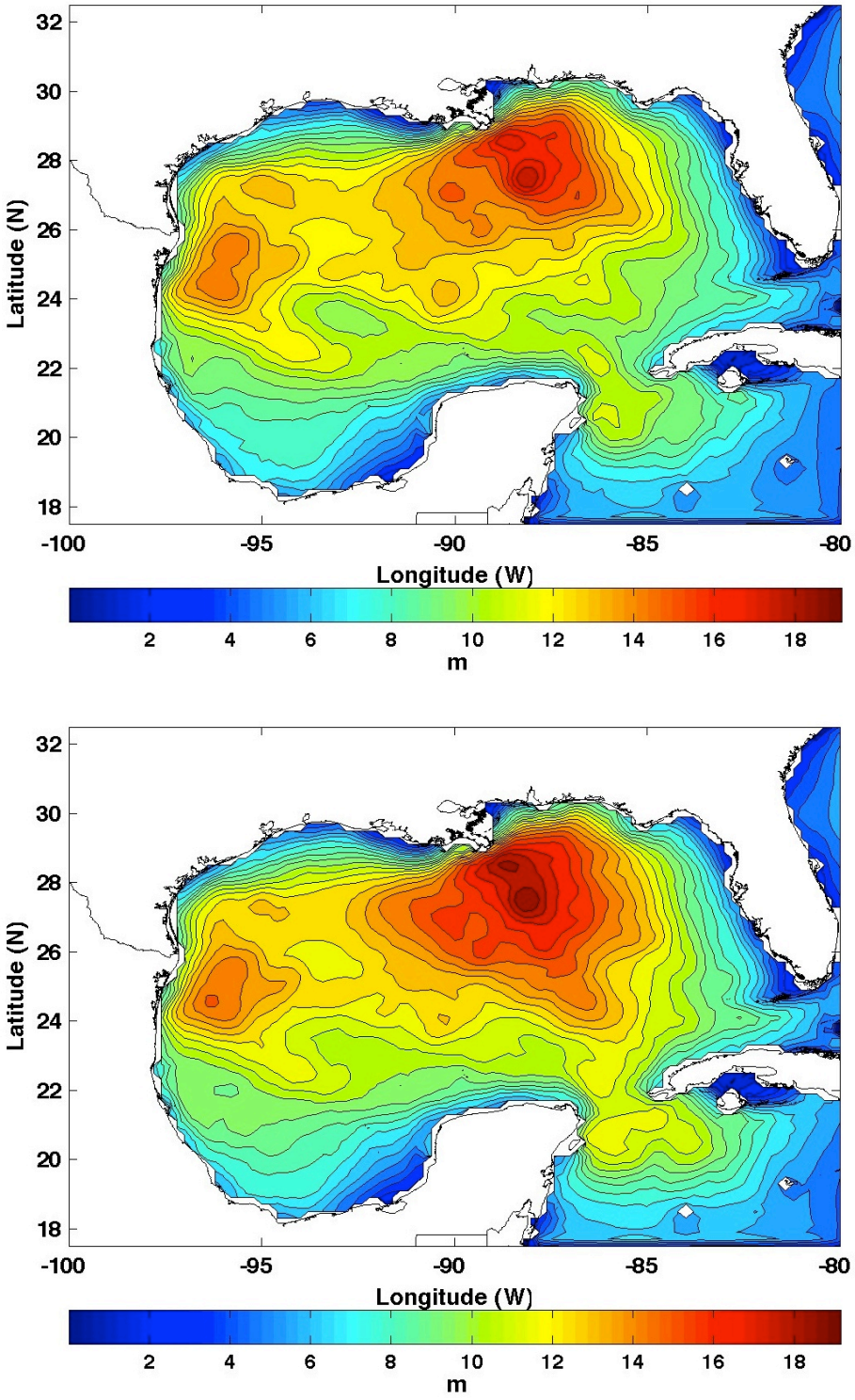

Fig. 7.1. Estimated SWH_{100} with Gumbel method; 46years(top) and 51years (bottom).

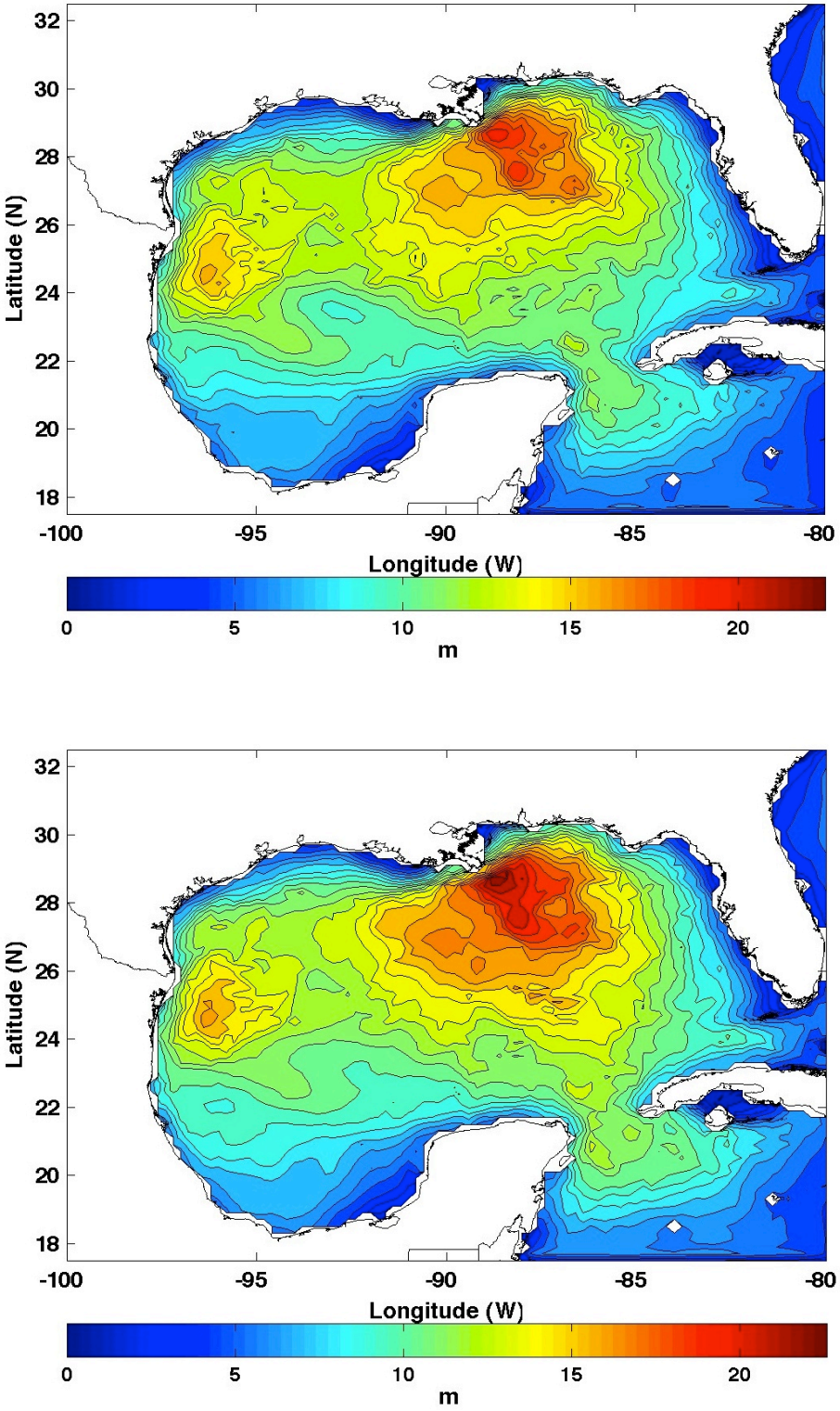

Fig. 7.2. Estimated SWH_{100} with Weibull method; 46years(top) and 51years (bottom).

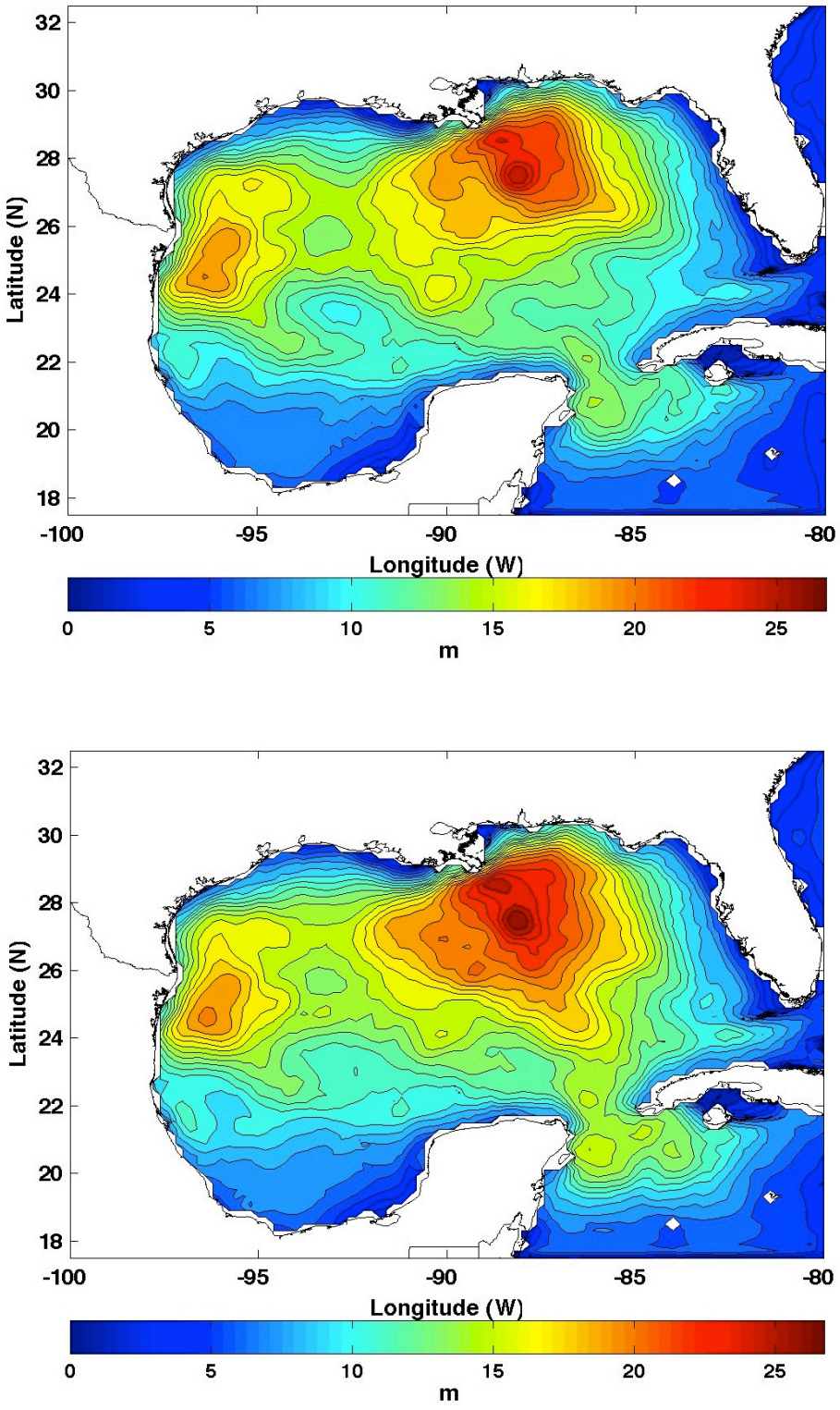

Fig. 7.3. Estimated SWH_{100} with GEV method; 46years(top) and 51years (bottom).

This would suggest that the differences obtained by API are not entirely due to the 2004 - 2008 hurricane season but also may be an effect of the approach taken to obtaining this estimate. i.e. the choice of the data set as well as the distribution used by them in their calculation.

To summarize, Fig 7.1 – 7.3 provides a range of SWH_{100}'s in the Gulf of Mexico. The range for the maximum SWH_{100} is as shown in Table. 7.1.

Table. 7.1. Maximum SWH_{100} for three different methods.

	1958 – 2003	**1958 – 2008**
Gumbel	18.2 m	19.1 m
Weibull	19.9 m	22.6 m
GEV	25.4 m	26.7 m

It is interesting to note from Figs 7.1-7.3 that these maxima occur just south of Louisiana; no estimates for the area have been provided by the API. However, estimates obtained by McAfee and Wong (2007) in this region are of the order of over 20m, which are consistent with the results in Table 7.1.

While multiple estimates have been developed, the question of which distribution is to be preferred remains. While there can be no absolute answer to this question, the bootstrap technique provides some guidance. To implement this technique, 500 samples were generated using the data at each grid point. The three distributions were fitted and the error norm calculated as explained in Chapter V. This was done for different values of *h*, and the distribution with the least error norm is selected.

Results for six values of *h* (0.35, 0.5, 0.75, 1, 1.25, and 1.5) are shown in Fig. 7.4. It is observed that for small values of *h* the Gumbel distribution is the preferred one,

and for $h>1$, the GEV is the preferred distribution. As h increases from small values, at many locations, the Weibull and the GEV are the preferred distributions (Fig.7.4).

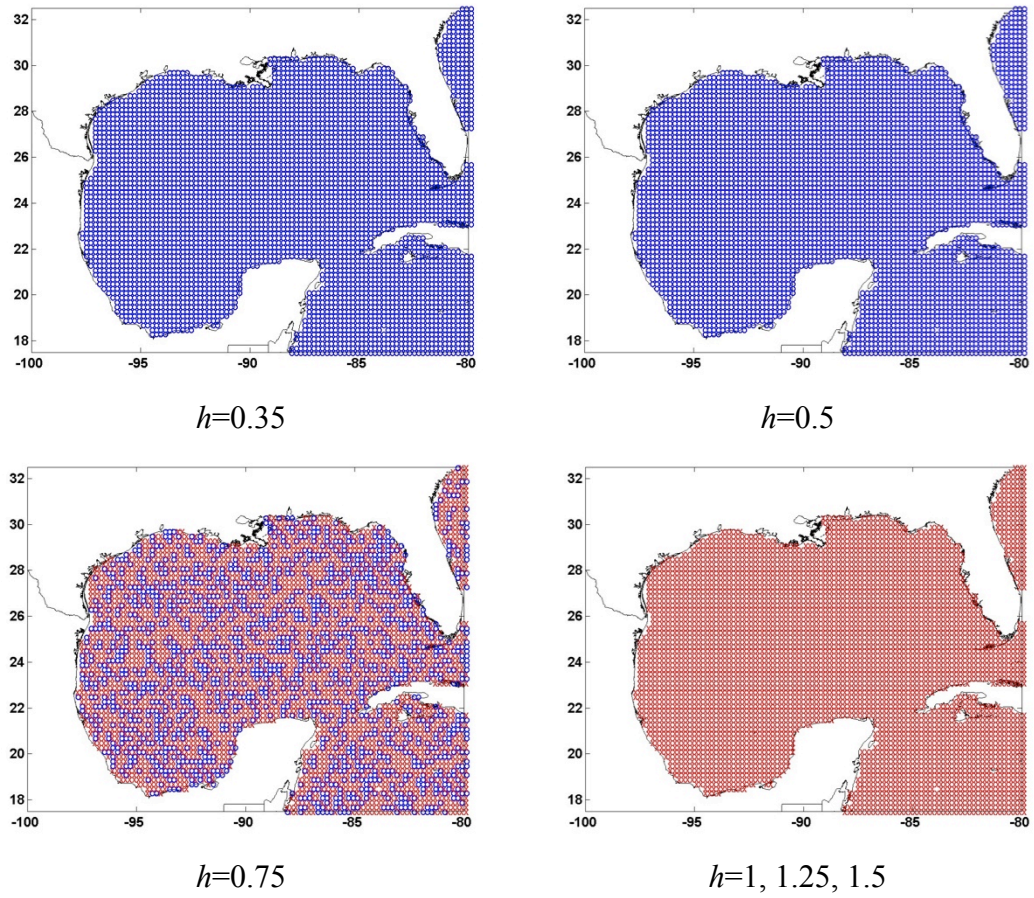

Fig. 7.4. Different distribution with different h values (GEV: red, Gumbel: blue).

Recalling that small values of h correspond to an emphasis on the lower tail and $h>1$ corresponds to an emphasis on the upper tail, the smooth progression between the distributions observed in Fig. 7.4 implies that the Gumbel and the GEV are the two extremes. Based on the engineer's choice, i.e. if one wants to emphasize the lower tail (where most the data lie), then the Gumbel distribution is to be preferred. Fig. 7.5 illustrates this point clearly.

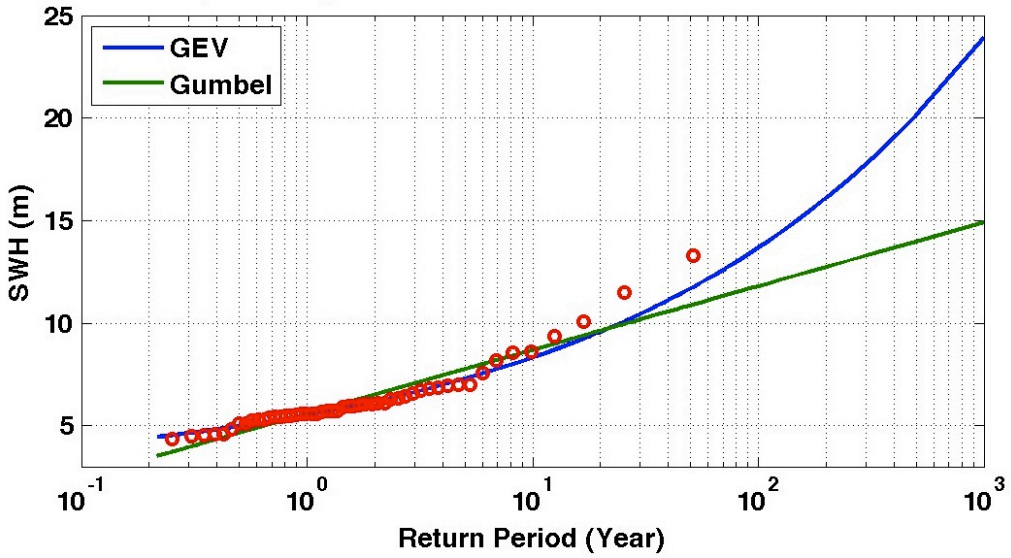

Fig. 7.5. Gumbel and GEV SWH return period.

Table. 7.2. Comparison of estimated SWH_{100} (m) near NDBC buoy locations.

Buoy No.	GEV		Gumbel		Weibull		API		MAX SWH
	46 year	51 year	46 year	51 year	46 year	51 year	RP2 - WSD	2INT - MET	
42001	16.53	17.10	13.35	13.83	14.30	14.97	11.9	15.2	11.63
42002	13.82	13.65	11.88	11.78	11.81	11.69	11.9	12.3	9.7
42003	15.78	16.58	12.42	13.17	13	14.08	11.9	13.03	11.04
42007	7.79	7.87	6.51	6.81	7.07	7.62	NA	NA	9.09
42019	13.37	12.89	10.84	10.65	11.31	11.19	10.5	11.6	6.3
42020	15.48	15.92	11.8	12	11.81	12.19	10.6	11.8	8.2
42035	6.68	6.88	5.75	5.97	5.78	6.08	5.3	7.44	7.1
42036	12.63	12.8	10.5	10.85	11.81	12.34	11.8	10.2	8.6
42039	16.43	18.84	12.75	14.34	14.05	15.79	11.8	13.77	12.05
42040	19.09	20.37	14.28	15.44	16.24	18.33	11.9	NA	16.91
42041	18.78	19.61	14.58	15.26	15.32	16.22	11.9	12.44	12.31

Table 7.2 shows a comparison between the three different methods and API estimations. The API SWH_{100} in Table 7.2 are our estimates from their plots near the locations of the eleven buoys. The GEV estimates are, for the most part, higher than

API's estimated values. Note that in shallow areas (e.g. buoy 42007 and 42035, where the depth is 14m addition of a 5m storm surge results in a 1m increase in SWH_{100})

It is interesting that the Weibull results obtained here (for 51 years) are mostly close to the API revised results. (With the exception buoy 42041, the difference is less than about 2 m). The API study also used the Weibull distribution and though their dataset and modeling methods are different and their statistical analysis could be sensitive to the threshold chosen, it is encouraging that the two sets reinforce each other.

However, the GEV provides a better fit to the larger data values (e.g. Fig 7.5) and may provide a reasonable and conservative alternative.

The new API manual (2000) notes that statistical methods other than those used in their study can yield slightly different results. This study has explored a wide range of alternative estimates. In addition efforts have been directed toward identifying the preferred distribution. In the case of the GEV, we must note that a better fit to the higher data values implies larger estimates if N is much greater than the data length. Because of the nonlinear nature of the curve in Fig. 7.5, it is not reasonable to obtain estimates for return periods of the order of 200, 500 and even 1000 years as provided by the API.

In recent years, Guedes Soares and Scotto (2004) and Sobey and Orloff (1995) have explored methods to maximize the use of the data by including multiple maxima per year instead of one annual maximum. Preliminary studies were conducted, especially when using buoy data of limited duration (Jeong and Panchang 2008). In general, the SWH_{100} were smaller than those obtained with the annual maxima, but additional work is needed in this area, as in the area of including trends in the distribution. Graham

(2005), Wang et al. (2004), Komar and Allan (2007) and Hansoma et al. (2008) have reported increasing trends in the wave climate off both US coasts. For example Komar and Allan report an increase of 1.7 cm/year off the east coast. Figure. 4.11 suggests an increase of 0.6cm/year in the Gulf of Mexico. To accommodate trends in the data, Coles (2004) has indicated that the GEV model parameters σ and μ can be regarded as functions of time. For simplicity, we have used $\mu = \beta_0 + \beta_1 t$, where β_1 = the average trend for the Gulf of Mexico data. Preliminary results using this approach are described in Jeong and Panchang (2008).

CHAPTER VIII

CONCLUSIONS

This thesis is focused on the study on the development of extreme wave height conditions in the GOM using the adjusted parametric wind model, a numerical wave model and multiple statistical methods. The following is a summary of the conclusions from this study:

1. Commonly used parametric models such as the SLOSH, Holland, and Rankine vortex models, do not adequately simulate recent GOM hurricanes such as Katrina and Ike. The size and velocity contour distribution showed substantial mismatch relative to H*WIND measurements.
2. Modifications to the RV model, based on observed discrepancies between H*WIND and the RV contours, for five storms resulted in a "modified RV model". This model, when applied to set of 17 hurricanes in the GOM produced smaller errors (on average 18 % vs. 27%) compared with the original RV model.
3. The SWH's resulting from the use of the model RV resulted in a much better match with buoy data (as opposed to the original RV model which led to errors of approximately 4 m for hurricane Ike).
4. The SWAN wave model was used with the used RV model and the Reanalysis winds for 127 storms covering the maximum duration for which buoy data are available (up to 33 years). This resulted in 2760 monthly maxima. The slope of the buoy data vs. model data plot was 0.82, indicating a high correlation (The

mismatch was due partly to storm track uncertainty, separation between the chosen grid point and the buoy, and the large variability near the storm track).

5. Model results for 51 years at 7676 grid points show that the maximum modeled SWH is 18m. The effect of the 2004-2008 seasons is not big on the maximum, SWH in the GOM, but the frequency of large wave (SWH>10m) increased substantially. Also the eastern part of the GOM shows an increasing trend while the western part a decreasing trend. For the whole GOM, model data show an increasing trend of the order of 0.6cm/year. In contrast, Komar and Allan (2007) indicate an increasing trend in the mid-Atlantic of 1.7 cm/year.
6. SWH_{100} were obtained using annual maximum obtained by modeling and from buoy data. The buoy data lengths varied from 10 years to 33 years. The SWH_{100} estimates mostly increased after adding the 2004 - 2008 hurricane season. The SWH_{100} estimates obtained using the 2 datasets were consistent with a maximum difference of 2m. This consistency is validation of the model-derived data for further statistical analysis.
7. Using buoy 42020 as an example, it was seen that an errors in individual modeled SWH has a decreasing effect on SWH_{100} as the data length increased from 1990-2003 to 1990-2008.
8. SWH_{100} estimates were obtained using 46 and 51 years of model data. The Weibull estimates were very similar to the API estimates (also obtained with the Weibull distribution but using different data and statistical methods).

9. The Bootstrap method indicated that, for all grid points, the GEV distribution is to be preferred if the emphasis is on the larger wave heights where extreme happen, and the Gumbel distribution is to be preferred if the emphasis is on the lower tail.
10. The maximum increase caused by the 2004-2008 season in the SWH_{100} is approximately 2.7m (for the Weibull distribution), 1.3m (for the GEV distribution), and 0.9m (for the Gumbel distribution). These are much smaller than the difference between the old and new API guidelines. The distribution of large SWH_{100}'s is greater because of the 2004-2008 season.
11. Table 7.1 and Fig 7.1 – Fig. 7.3 provided alternative estimates for SWH_{100} in the GOM. The maximum SWH_{100} estimates using the three methods are 19.1m, 22.6m, and 26.7m (Gumbel, Weibull, and GEV).

This information can be used for a variety of applications besides coastal and offshore structure design, such as planning and management of the coastal hazard, safety of marine operations, wave-power studies (Wilson and Beyene 2007), etc.

REFERENCES

American Petroleum Institute (2000), "Recommended Practice for Planning, Designing and Constructing Fixed Offshore Platforms - Working Stress Design", API recommended practice 2A-WSD.

American Petroleum Institute (2007), "Interim Guidance on Hurricane Conditions in the Gulf of Mexico", API Bulletin 2INT-MET.

Bender III L. C., N. L. Guinasso Jr, J. N. Walpert, S.D. Howden (2008), "Wave heights from a 3m discus buoy during hurricane Katrina", Quebec, *Oceans Conference*.

Berek E. P., C. K. Cooper, D. B. Driver, J. C. Heideman, D. A. Mitchell, J. D. Stear, M. J. Vogel (2007), "Development of revised Gulf of Mexico Metocean hurricane conditions for reference by API recommended practices", Houston, *Offshore Technology Conference*.

Borgman, L. E. (1975), "Extremal statistics in ocean engineering", New York, *Civil Engineering in the Oceans Conference*, 117-133.

Booij, N., Holthuijsen, L. H., Doorn N., and Kieftenburg, A. T. M. M. (1997), " Diffraction in a spectral wave model", Virginia, *Ocean Wave Measurements and Analysis: Proc. 3rd International Symposium Waves97*, ASCE, 243-255.

Booij, N., Ris, R. C. and Holthuijsen, L. H. (1999), "A third-generation wave model for coastal regions, 1, model description and validation", *Journal of Geophysical Research*, 104, C4, 7649-7666.

Bretschneider C. L. (1972), “A non-dimensional stationary hurricane wave model”, *Offshore Technology Conference*, I, 55-68.

Carter, D.J.T., Challenor, P.G. (1981), “Estimating return values of environmental parameters”, *Quarterly Journal of Royal Meteorological Society* 107, 259–266.

Cardone, V. J., C. V. Greenwood, and J. A. Greenwood (1992), *Unified program for the specification of hurricane boundary layer winds over surfaces of specified roughness*, Army Engineer Waterways Experiment Station, Contract Report CERC-92-1, Vicksburg, MS.

Cieślikiewicz W. and B. Paplińska-Swerpel (2008), “A 44-year hindcast of wind wave fields over the Baltic Sea”, *Coastal Engineering*, 55, 894-905.

Clayton, B., “Gearing up for Gulf hurricanes”, Houston Chronicle, Apr. 29. 2007.

Coles, S. (2004). An introduction to statistical modeling of extreme values. Springer. New York.

DeMaria M., S. Aberson, K. V. Ooyama, S. J. Lord (1992), “A nested spectral model for hurricane track forecasting”, *Monthly Weather Review*, 120, 1628-1643.

Earle, M. D. (1975), “Extreme wave conditions during hurricane Camille”, *Journal of Geophysical Research,* 80, 377-379.

Federal Emergency Management Agency (2004), “Final draft guidelines for coastal flood hazard analysis and mapping for the Pacific Coast of the United States”, Northwest Hydraulic Consultants, Inc., Washington D.C.

Georgiou P. (1985), *Design wind speeds in tropical cyclone prone regions*. Ph.D. dissertation, University of Western Ontario, 295.

Graham N. (2005), *Coastal impacts of north Pacific winter wave climate variability: The southern California bight and the Gulf of Farallones*, Scripps Institution of oceanography, California Energy Commission, CEC-500-2005-018, 34.

Guedes Soares, C. and Scotto, M. G. (2004), "Application of the *r* largest-order statistics for long-term predictions of significant wave height", *Coastal Engineering*, 51, 387-394.

Hansoma J. D., N. D. P. Barltropb, A. M. Hallc (2008), "Modeling the processes of cliff-top erosion and deposition under extreme storm waves", *Marine Geology,* 253, 36-50.

Harris, P. T. and Coleman, R. (1998), "Estimating global shelf sediment mobility due to swell waves", *Marine Geology*, 150, 171-177.

Heideman, J. C. and D. A. Mitchell (2009), "Grid point pooling in extreme value analysis of hurricane hindcast data", *Journal of Waterway, Port, Coastal, and Ocean Engineering,* 135, 31-37.

Holland G. J. (1980), "An analytic model of the wind and pressure profiles in hurricanes", *Monthly Weather Review*, 108, 1212-1218.

Houston S. H. and M. D. Powell (1994), "Observed and modeled wind and water-level response from tropical storm Marco (1990)", *Weather and Forecasting,* 9, 427-439.

Hovis, G. T. (2005), "Analysis of storm surge measured at water level stations from hurricanes Charley, Frances, Ivan, and Jeanne", Reston, VA, *Proc. Solutions of Coastal Disasters 2005*, ASCE, 1–15.

Jeong C. K. and V. G. Panchang (2008), "Measurement-based estimates of extreme wave conditions for the Gulf of Mexico", Quebec, *Oceans Conference*.

Kalnaya M. K. E., R. Kistlera, W. Collinsa, D. Deavena, L. Gandina, M. Iredella, S. Sahaa, G. Whitea, J. Woollena, Y. Zhua, A. Leetmaaa, R. Reynoldsa, M. Chelliahb, W. Ebisuzakib, W. Higginsb, J. Janowiakb, K.C. Mob, C. Ropelewskib, J. Wangb, Roy Jennec, Dennis Josephc (1996), "The NCEP/NCAR 40-year reanalysis project", *American Meteorological Society*, 77, 437-471.

Kennedy A., S. Rogers, A. Sallager, V. Gravois, B. Zachry, M. Dosa, and F. Zarama (2010), "Building destruction from wave & surge on the Bolivar Peninsula during hurricane Ike", *Journal of Waterway, Port, Coastal & Ocean Engineering, (to appear)*

Komar, P. D. and J. C. Allan (2007), "Higher waves along US East Coast linked to hurricanes." *EOS Transactions*, AGU, 88, 30, 301.

Li, D., V. G. Panchang, and J. Jin (2005), "Development of an on-line wave forecasting system", Charleston, SC, *ASCE Conference, Solutions to Coastal Disasters*.

Li, Y., D. Simmonds, D. Reeve (2008), "Quantifying uncertainty in extreme values of design parameters with resampling techniques," *Ocean Engineering,* 35, 1029-1038.

Linhart, H., Zucchini, W. (1986), *Model selection*. Wiley, New York.

Liu H., L. Xie, L. J. Pietrafesa, and S. Bao (2007), "Sensitivity of wind waves to hurricane wind characteristics", *Ocean Modelling*, 18, 37-52.

MacAfee A. W. and G. M. Pearson (2006), "Development and testing of tropical cyclone parametric wind models tailored for midlatitude application - Preliminary Results", *Applied Meteorology and Climatology*, 45, 1244-1260.

MacAfee, A. W. and S. W. K. Wong (2007), "Extreme value analysis of tropical cyclone trapped-fetch waves", *Journal of Applied Meteorology and Climatology*, 46, 1501–1522.

Millar, D. L., H. C. M. Smith and D. E. Reeve (2006), "Modeling analysis of the sensitivity of shoreline change to a wave farm", *Ocean Engineering,* 34, 5-6, 884-901.

Music S. and S. Nickovic (2008), "44-year wave hindcast for the Eastern Mediterranean", *Coastal Engineering*, 55, 872-880.

Oliveira, F. S. B. F. (2002), "Wave climate modeling south of Rio de Janeiro in Brazil", *Continental Shelf Research*, 22, 2021-2034.

Palao I. M., C. C. Teng, and D. A. Brown (1994), "An extremal analysis of significant wave height data measured from NDBC buoys", Rep. 1804-07.01, NDBC, Stennis Space Center, MS, 46.

Panchang, V.G., B. R. Pearce & K. K. Puri (1990), "Hindcast estimates of extreme wave conditions in the Gulf of Maine", *Applied Ocean Research*, 12, 1, 43-49.

Panchang, V. G., L. Zhao, & Z. Demirbilek (1999), "Estimation of extreme wave heights using GEOSAT measurements", *Ocean Engineering*, 26, 205-225.

Panchang, V. G. and D. Li (2006), "Large waves in the Gulf of Mexico caused by hurricane Ivan", *Bulletin of the American Meteorological Society*, 87, 4, 481-489.

Perez, O. M., Telfer, T. C. and Ross, L. G. (2003), "On the calculation of wave climate for offshore cage culture site selection: a case study in Tenerife", *Aquacultural Engineering*, 29, 1-21.

Petruaskas, C. and P. M. Aagaard (1971), "Extrapolation of historical storm data for estimating design wave heights", *Society of Petroleum Engineers*, 251, 23-37.

Phadke A. C., C. D. Martino, K. F. Cheung, S. H. Houston (2003), "Modeling of tropical cyclone winds and waves for emergency management", *Ocean Engineering*, 30, 553-578.

Pilar P., C. G. Soares, J. C. Carretero (2008), "44-year wave hindcast for the north east Atlantic European coast", *Coastal Engineering*, 55, 861-871.

Pontes, M. T., Aguiar, R. and Oliverira Pires, H. (2005), "A nearshore wave energy atlas for Portugal." *Journal of Offshore Mechanics and Arctic Engineering*, 127, 249-255.

Powell M. D., S. H. Houston (1996), "Hurricane Andrew's landfall in South Florida. Part II: Surface wind fields and potential real-time applications", *Weather and Forecasting,* 11, 329-349.

Powell M. D., S. H. Houston, L. R. Amat, Morisseau-Leroy, N. (1998), "The HRD real-time surface wind analysis system", *Journal of Wind Engineering and Industrial Aerodynamics,* 77&78, 53-64.

Powell M. D., S. Murillo, P. Dodge, E. Uhlhorn (2010), "Reconstruction of hurricane Katrina's wind fields for storm surge and water hindcasting", *Ocean Engineering*, 37, 26-36.

Ris, R. C., Booij, N., Holthuijsen, L. H., Padilla-Hernandez, R., Haagsma, IJ. G. (1998), "SWAN Cycle 2 Users' Manual" for SWAN version 30.75, Unauthorized Electronic Version, Delft Univ. Technology, Delft.

Ris, R. C.,Holthuijsen, L. H. and Booij, N. (1999). "A third-generation wave model for coastal regions 2, verification", *Journal of Geophysical Research,* 104, C4, 7667-7681.

Rogers, W. E., J. M. Kaihatu, H. A. H. Petit, N. Booij and L. H. Holthuijsen (2002), "Diffusion reduction in an arbitrary scale third generation wind wave model", *Ocean Engineering*, 1357-1390.

Rogers W. E., J. M. Kaihatu, L. Hsu, R. E. Jensen, J. D. Dykes and K. T. Holland (2007), "Forecasting and hindcasting wave with the SWAN model in the Southern California Bight", *Coastal Engineering*, 54, 1-15.

Sebastião P., C. G. Soares, E. Alvarez (2008), "44 years hindcast of sea level in the Atlantic Coast of Europe", *Coastal Engineering*, 55, 843-848.

Sobey, R. J. and L. S. Orloff (1995), "Triple annual maximum series in wave climate analyses", *Coastal Engineering,* 26, 135-151.

Sorenson, R. M. (1993). Basic wave mechanics for coastal and ocean engineers. John Wiley & Sons, New York.

Van Vledder, G., Y. Goda, P. Hawkes, E. Mansard, M. J. Martin, M. Mathiesen, E. Peltier, E. Thompson (1993), "Case studies of extreme wave analysis: a comparative analysis", *Proc. 2nd International Symposium on Ocean Wave Measurement and Analysis*. ASCE, New York, 978–992.

Wang, D. W., D. A. Mitchell, W. J. Teague, E. Jarosz, and M. S. Hulbert (2005), "Extreme waves under hurricane Ivan", *Science*, 309, 896.

Wang X. L., F. W. Zwiers, and V. R. Swail (2004), "North Atlantic ocean wave climate change scenarios for the twenty-first century", *Journal of Climate*, 17, 12, 2368–2383.

Wang X. L. and V. R. Swail (2002), "Trends of Atlantic wave extremes as simulated in a 40-Yr wave hindcast using kinematically reanalyzed wind fields", *Journal of Climate*, 15, 1020-1035.

Willoughby H. E. and M. E. Rahn (2002), "A new parametric model of hurricane wind profiles", San Diego, *Preprints, 25th Conf. on Hurricanes and Tropical Meteorology*, 553-554.

Wilson, J. H. and A. Beyene (2007), California wave energy resource evaluation. *Journal of Coastal Researc.,* 23, 3, 679–690.

Xie L., S. Bao, L. J. Pietrafesa, K. Foley, M. Fuentes (2006), "A real-time hurricane surface wind forecasting model: Formulation and verification", *Monthly Weather Review*, 134, 1355-1370.

Zubier, K., V. G. Panchang & Z. Demirbilek (2003), "Simulation of waves at Duck (North Carolina) using two numerical models", *Coastal Engineering Journal*, 45, 3, 439-469.

APPENDIX A

COMPARISON FOR 17 HURRICANE WINDS

[1] Carla (1961)

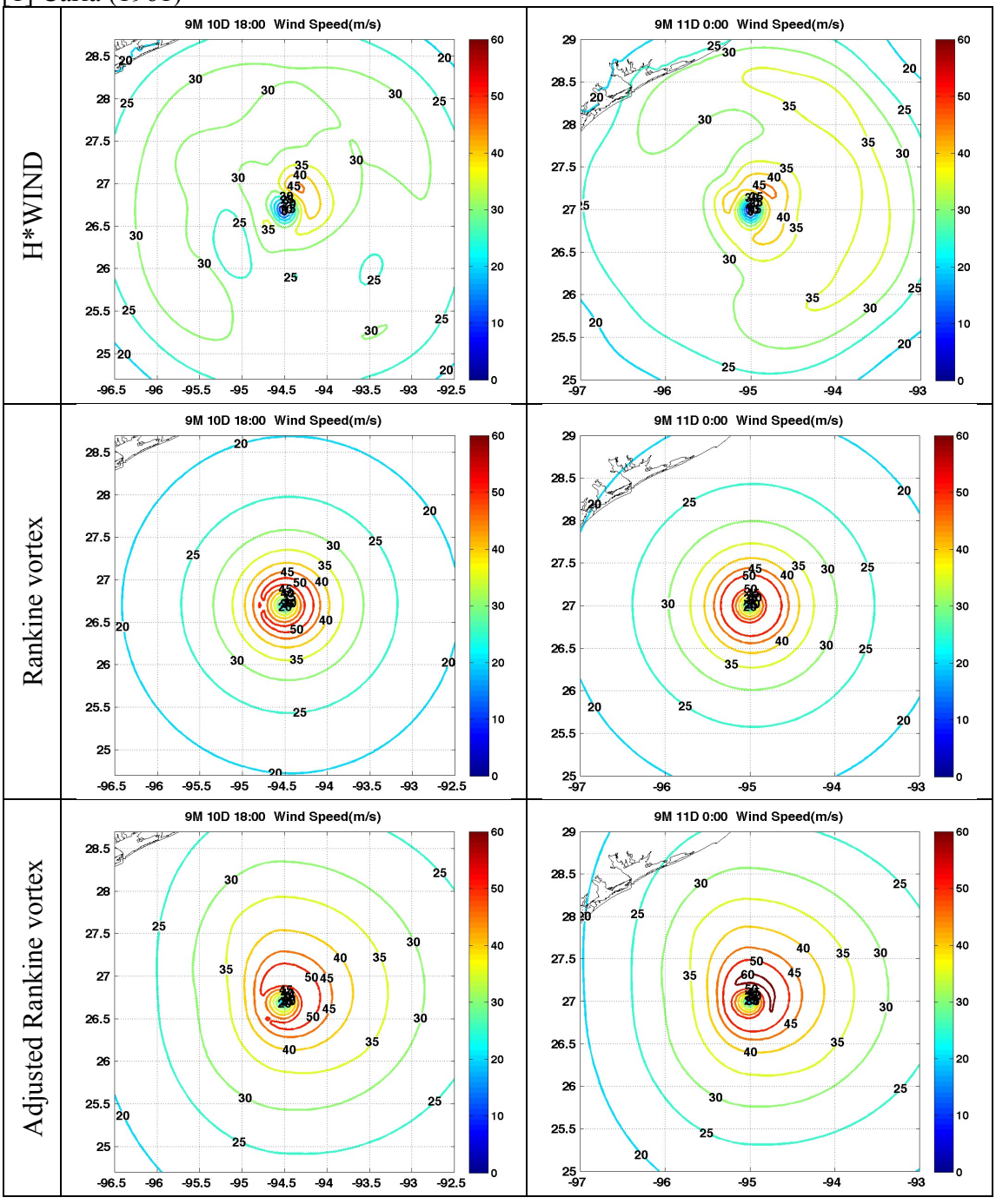

[2] Georges (1998)

H*WIND	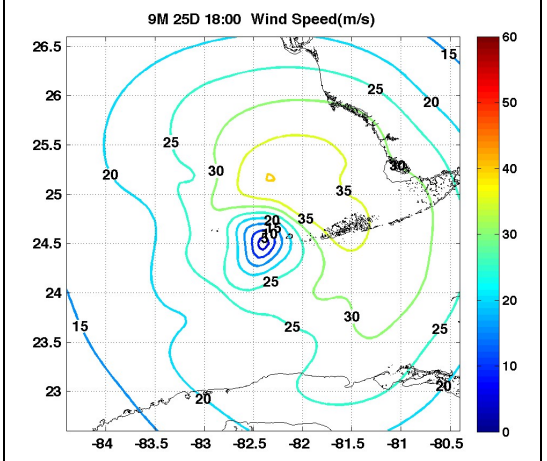	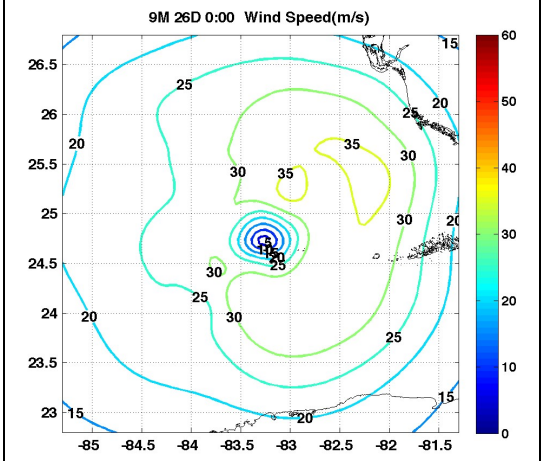
Rankine vortex	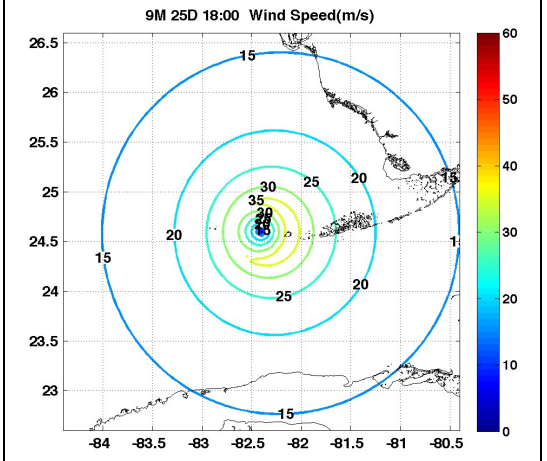	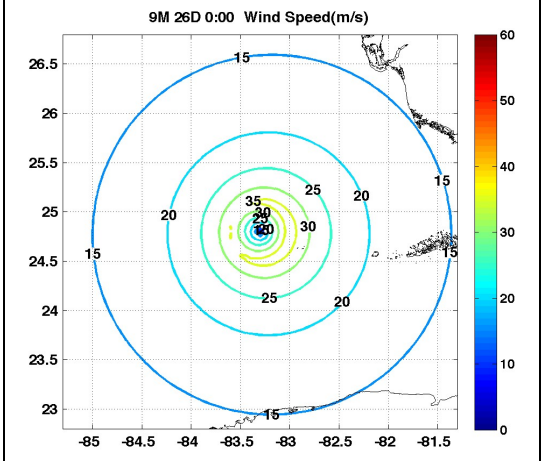
Adjusted Rankine vortex	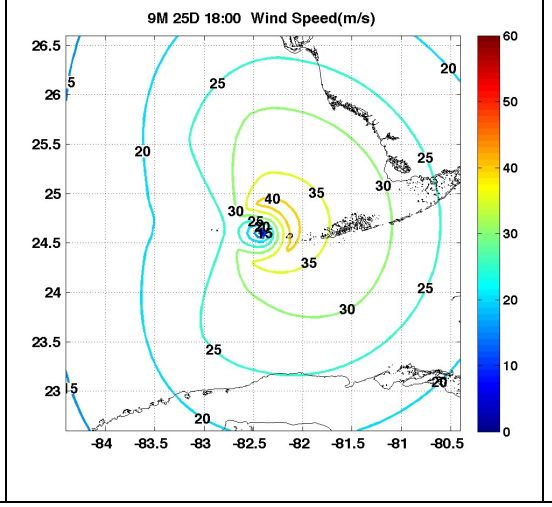	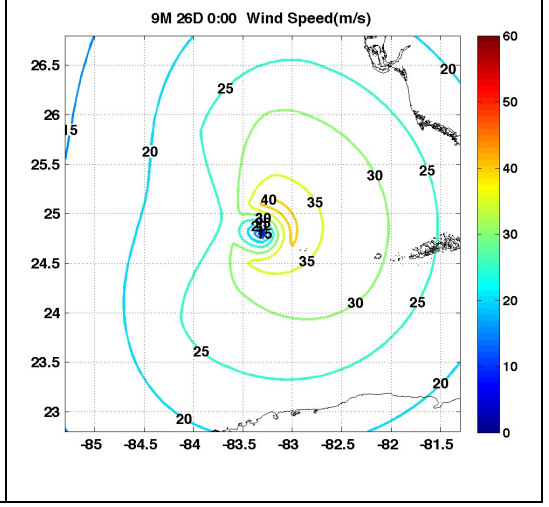

H*WIND	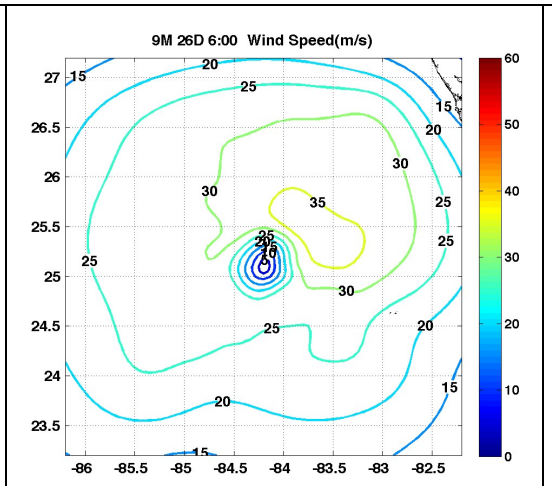	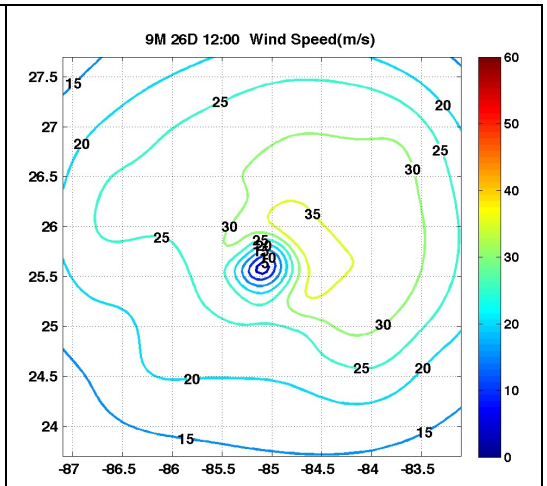
Rankine vortex	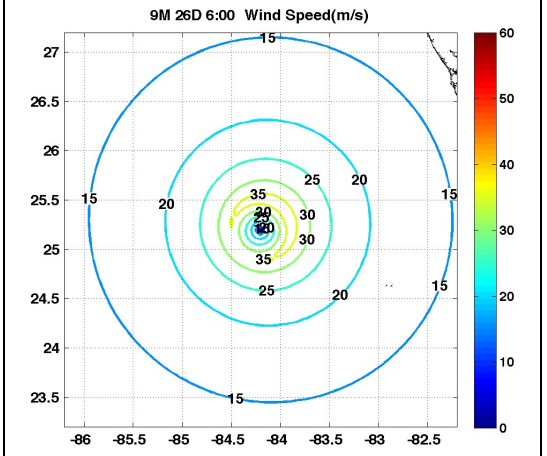	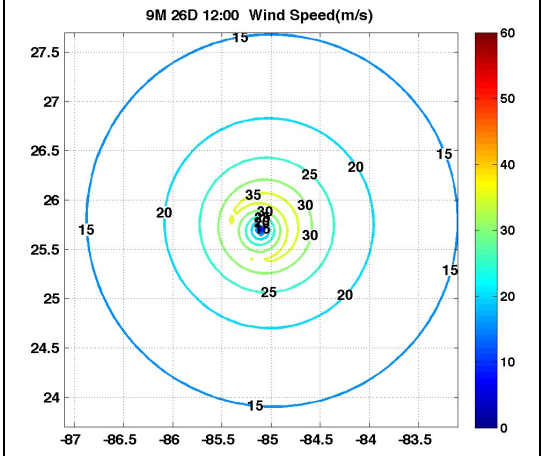
Adjusted Rankine vortex	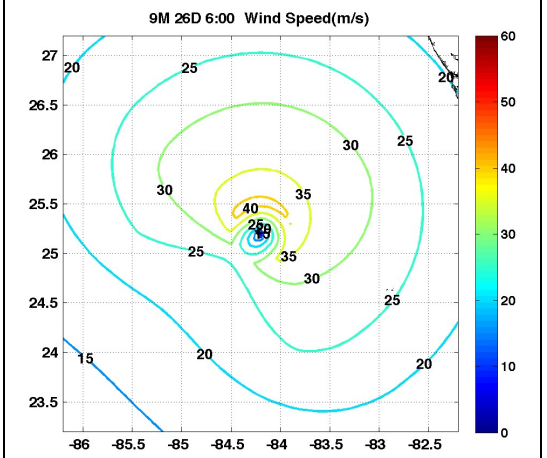	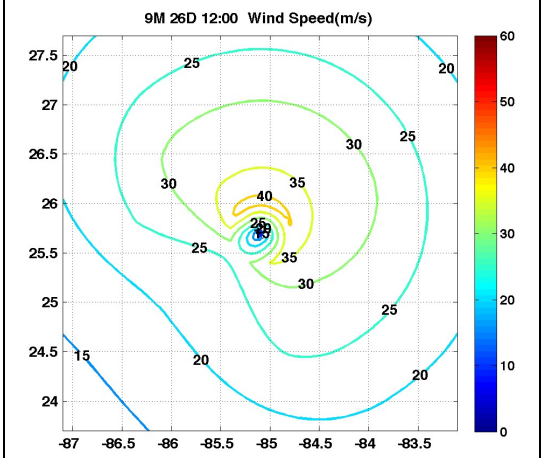

H*WIND	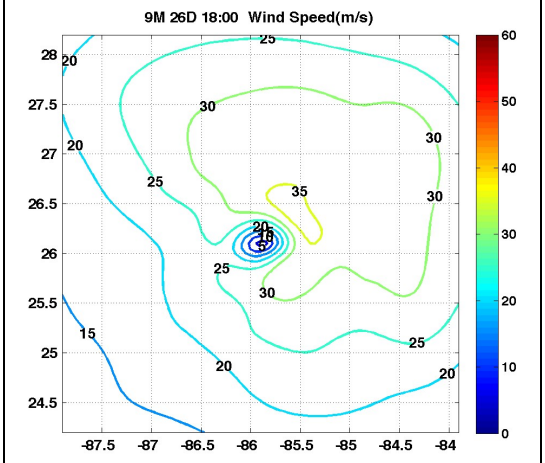	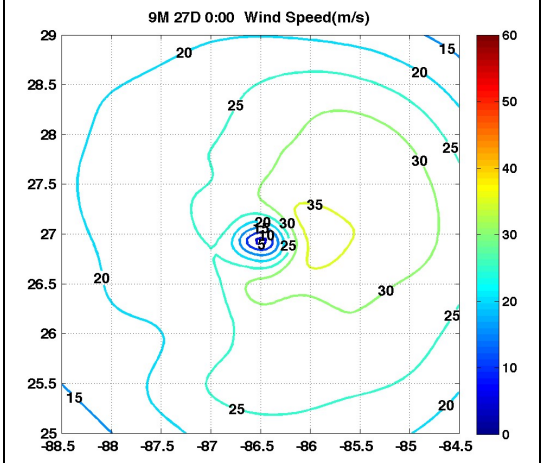
Rankine vortex	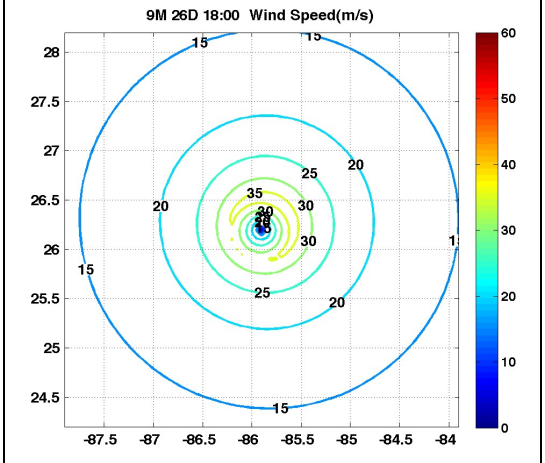	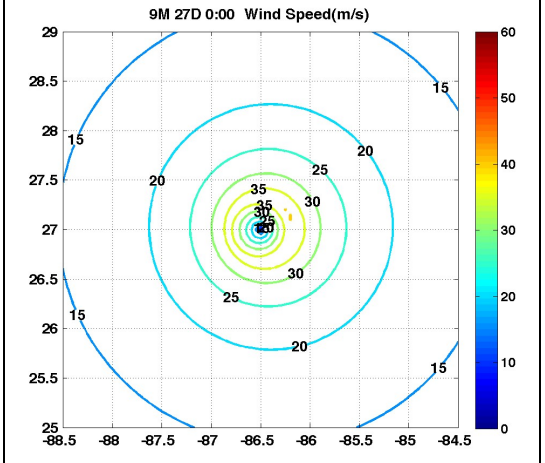
Adjusted Rankine vortex	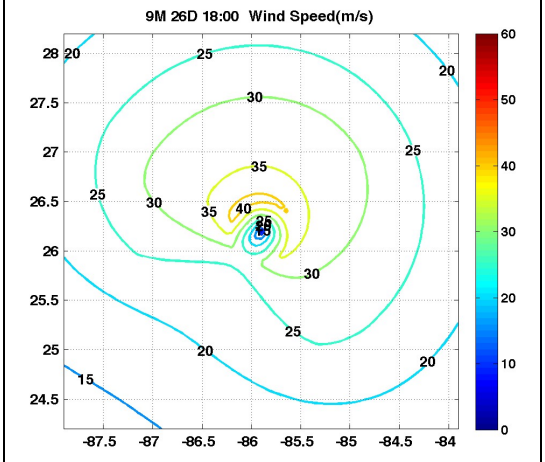	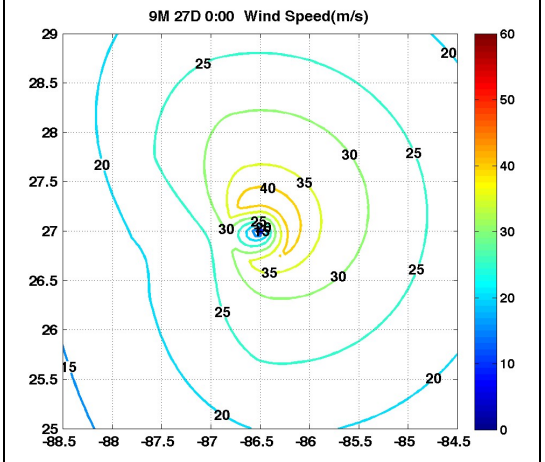

H*WIND	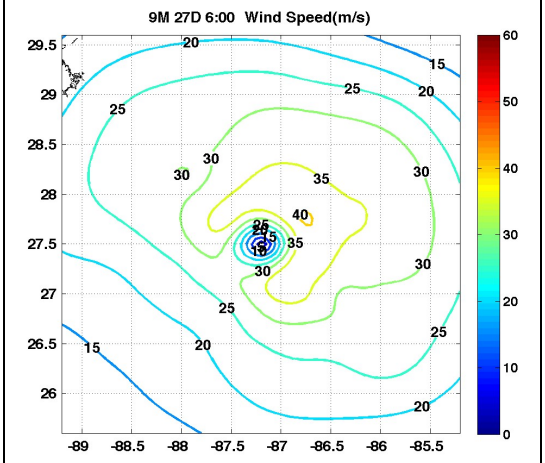	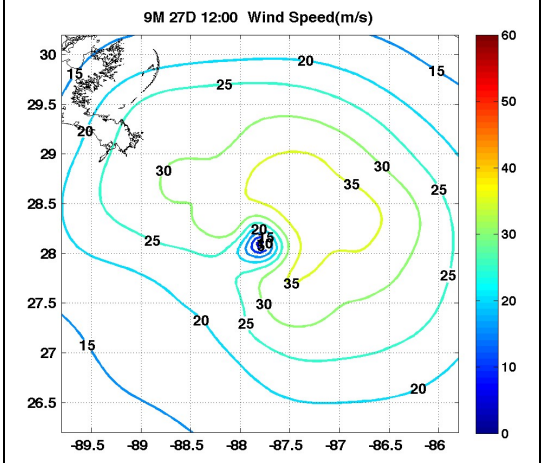
Rankine vortex	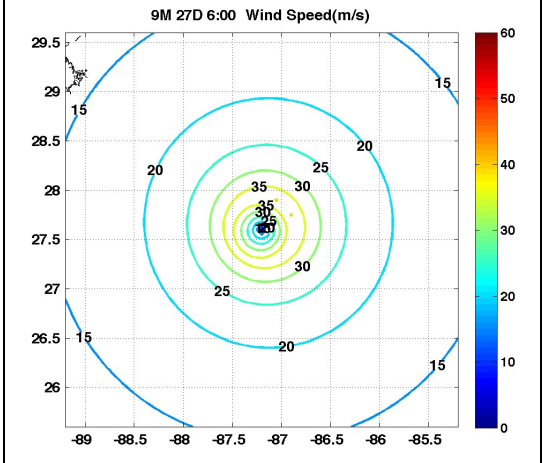	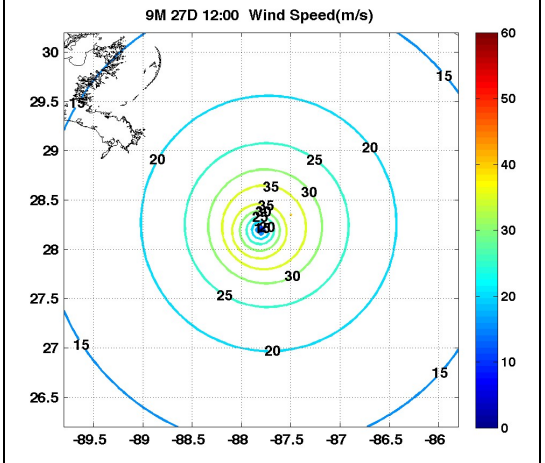
Adjusted Rankine vortex	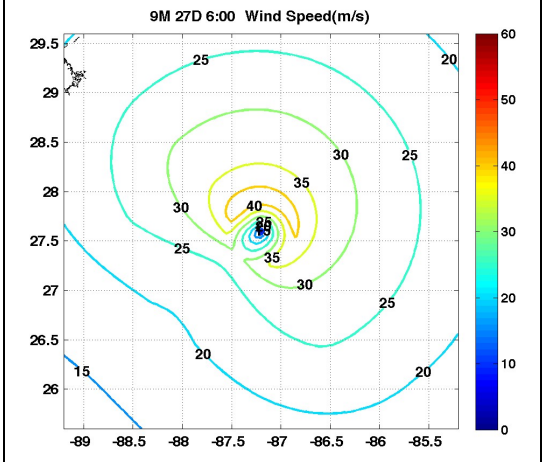	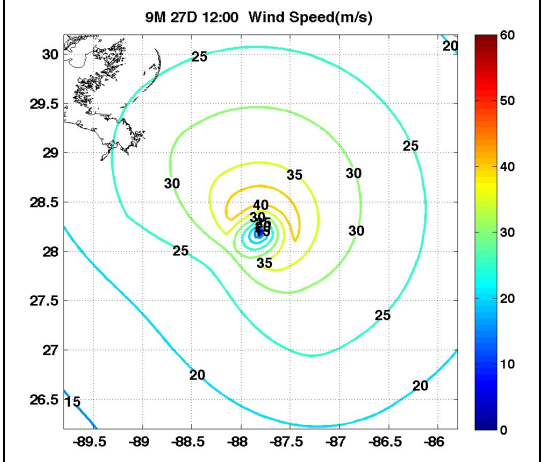

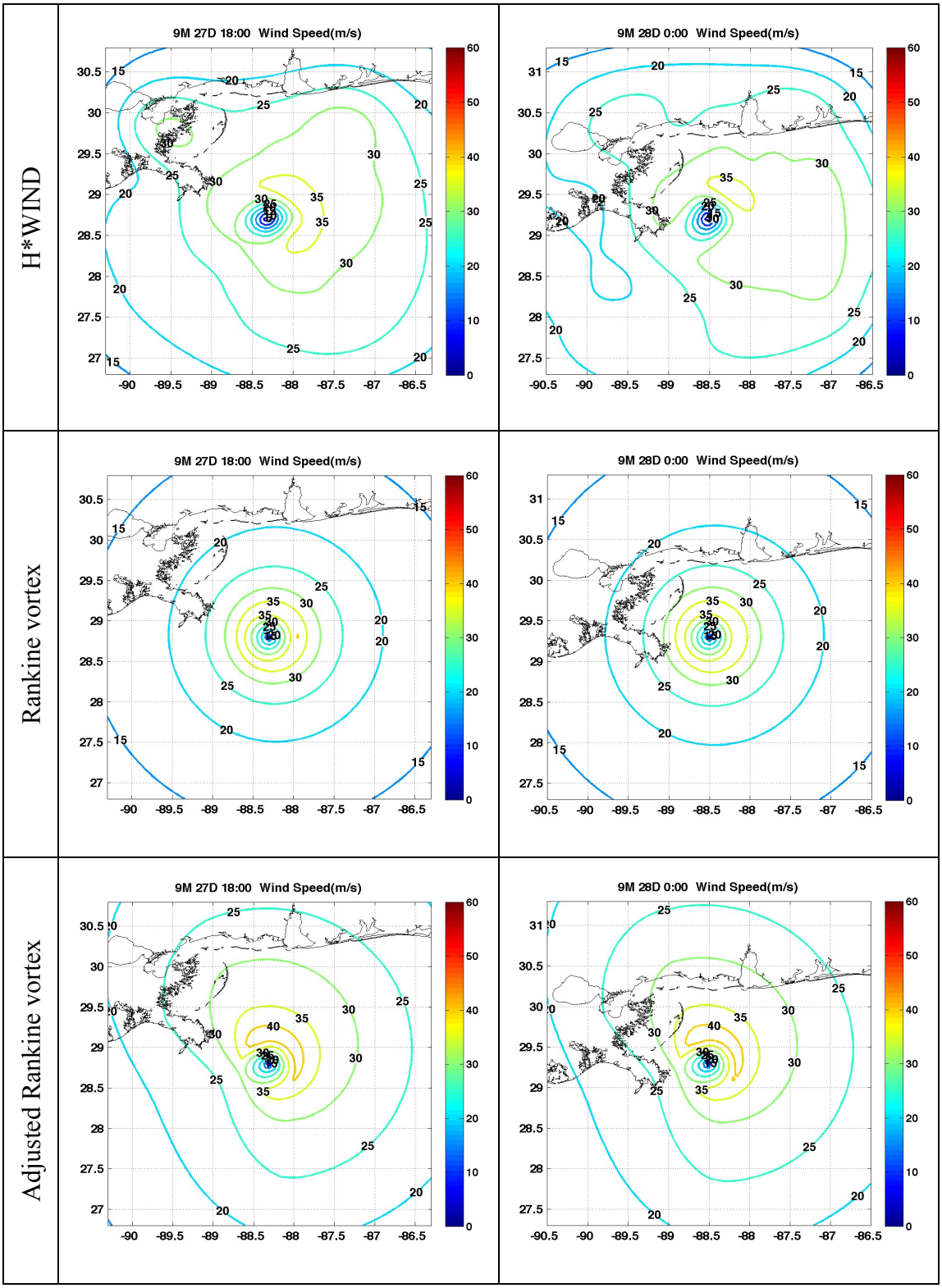
H*WIND
Rankine vortex
Adjusted Rankine vortex
9M 27D 18:00 Wind Speed(m/s)
9M 28D 0:00 Wind Speed(m/s)

[3] Gordon (2000)

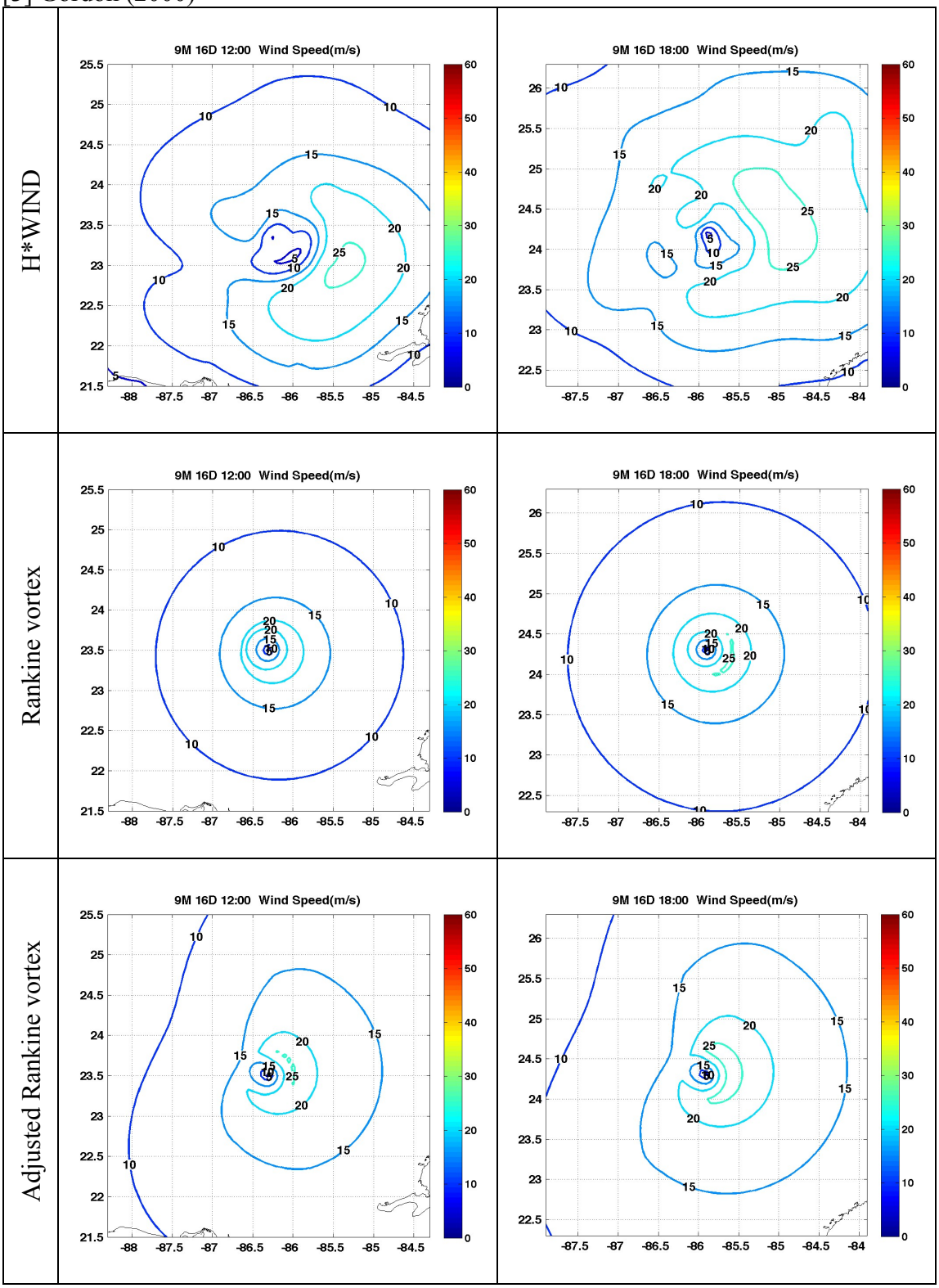

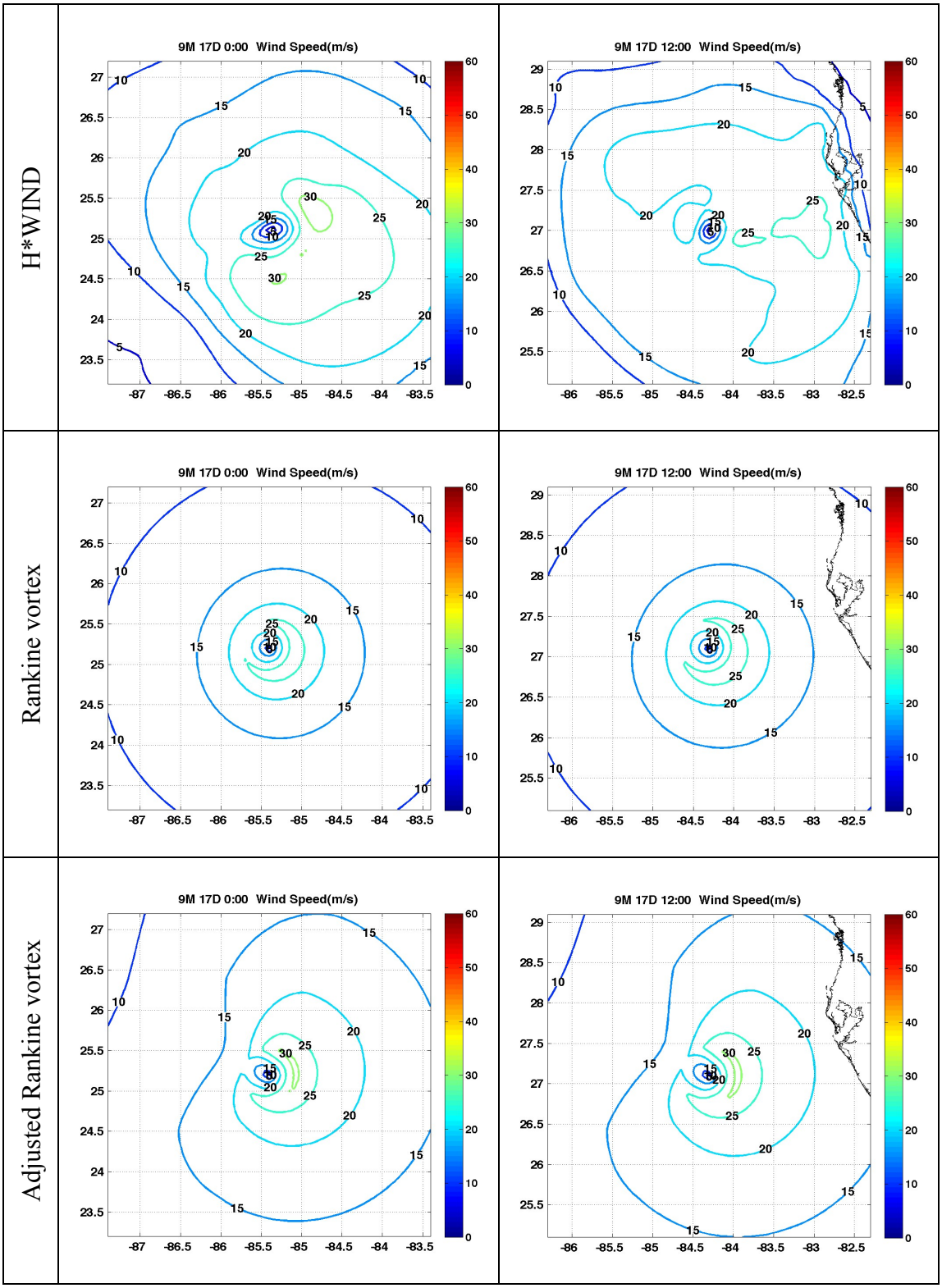
H*WIND
Rankine vortex
Adjusted Rankine vortex
9M 17D 0:00 Wind Speed(m/s)
9M 17D 12:00 Wind Speed(m/s)

[4] Isidore (2002)

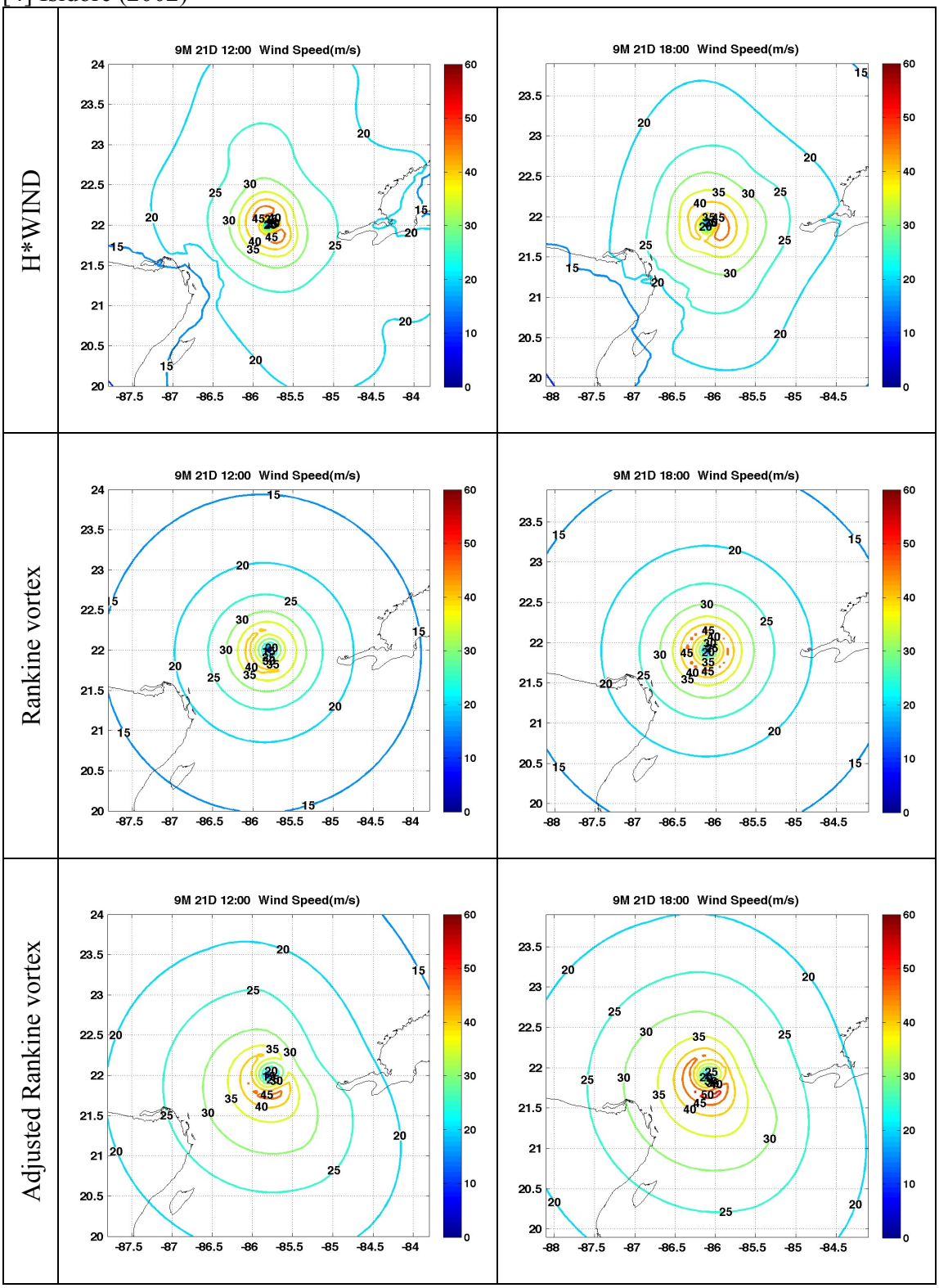

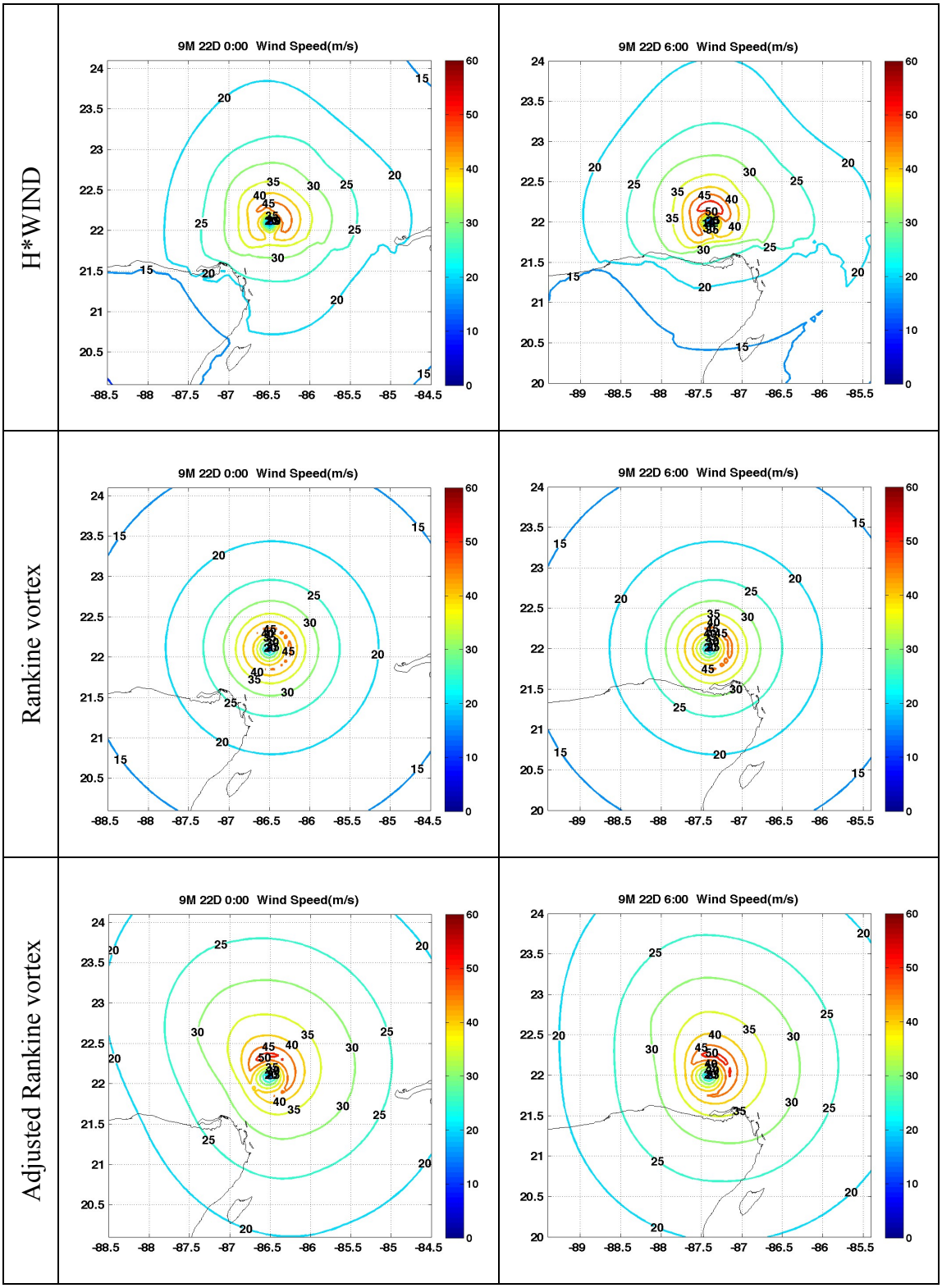
H*WIND
Rankine vortex
Adjusted Rankine vortex
9M 22D 0:00 Wind Speed(m/s)
9M 22D 6:00 Wind Speed(m/s)

[5] Lili (2002)

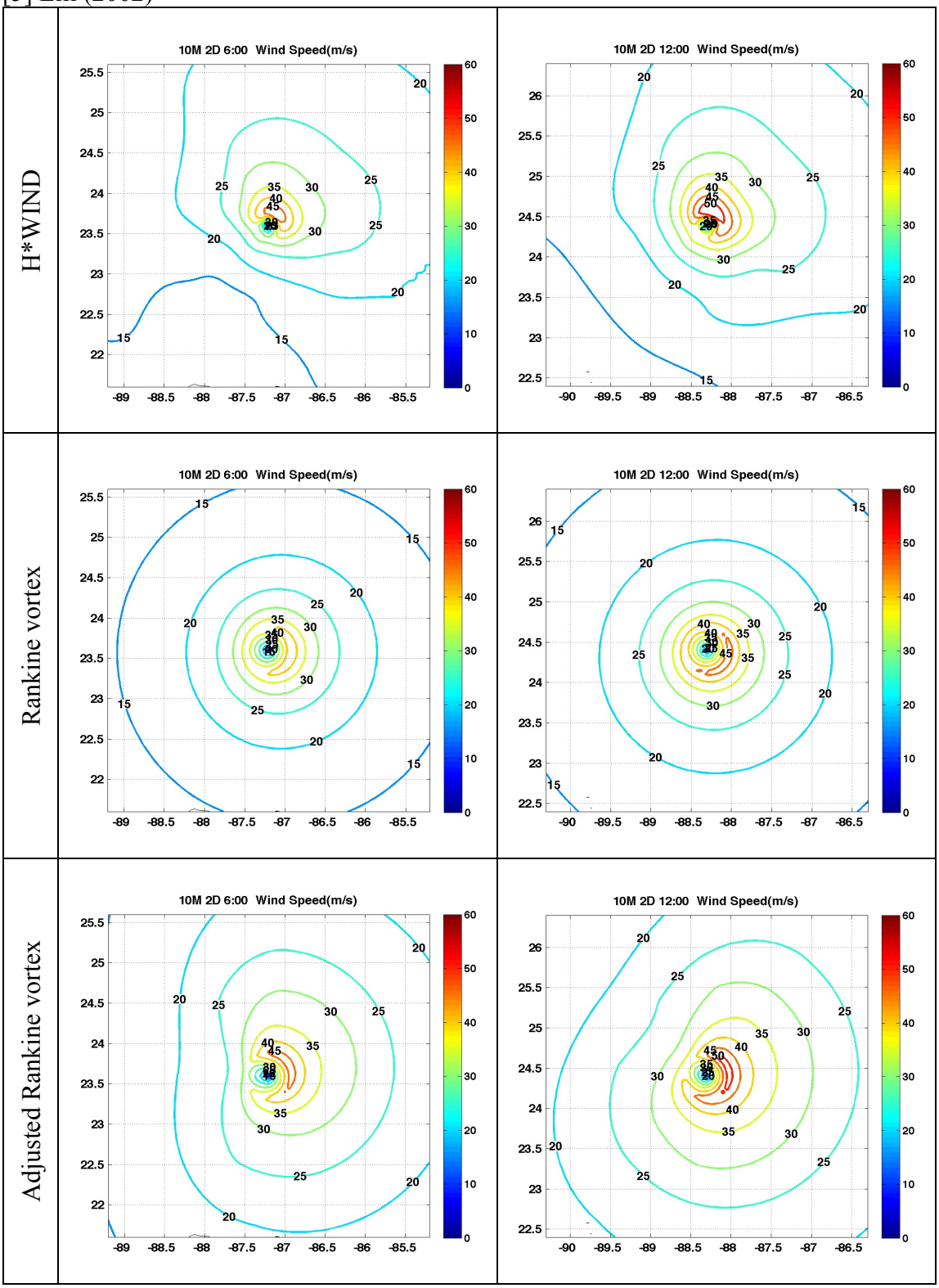
H*WIND
Rankine vortex
Adjusted Rankine vortex
10M 2D 6:00 Wind Speed(m/s)
10M 2D 12:00 Wind Speed(m/s)

H*WIND	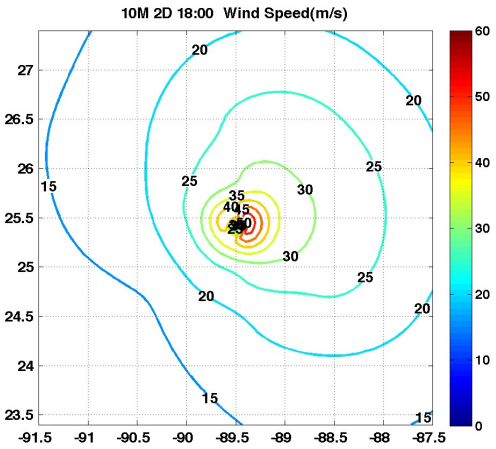	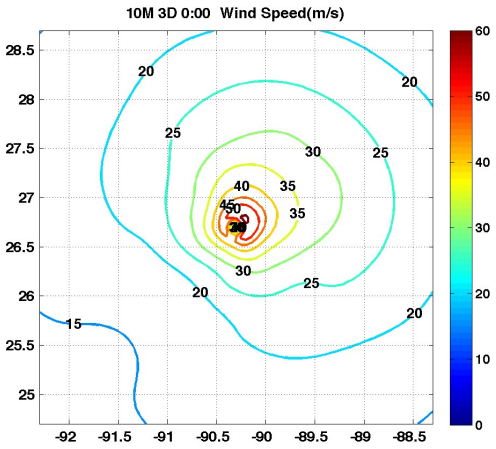
Rankine vortex	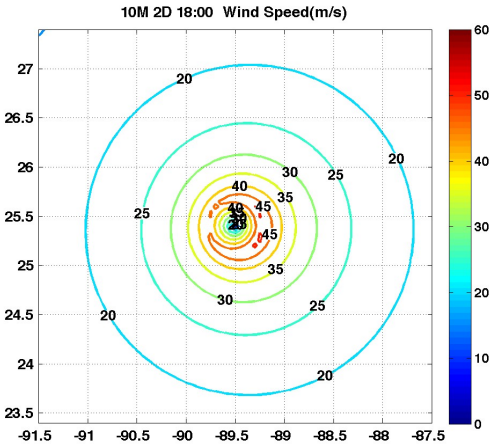	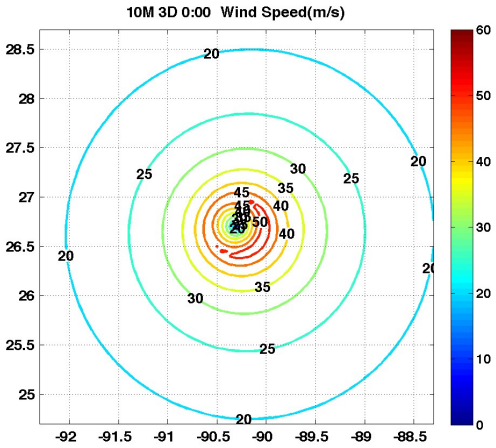
Adjusted Rankine vortex	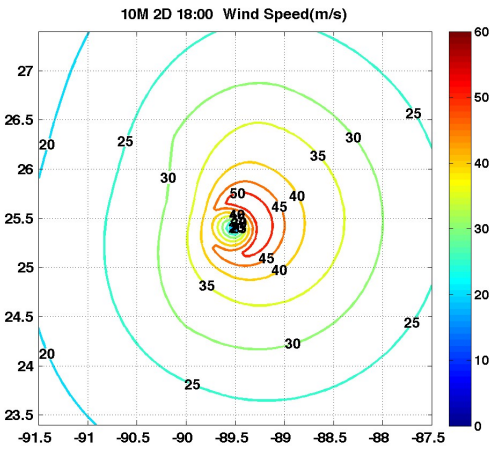	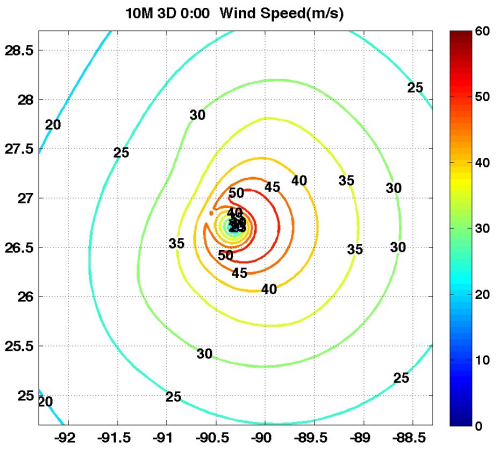

[6] Ivan (2004)

H*WIND	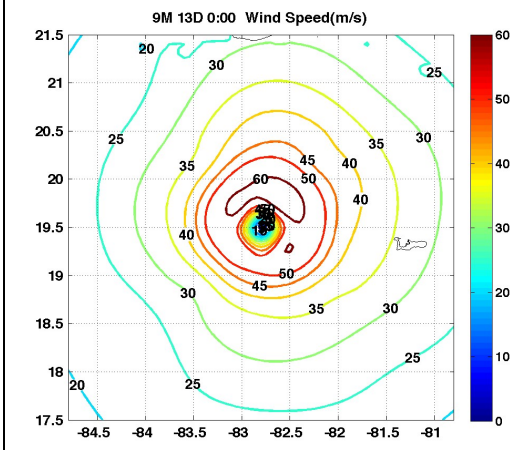	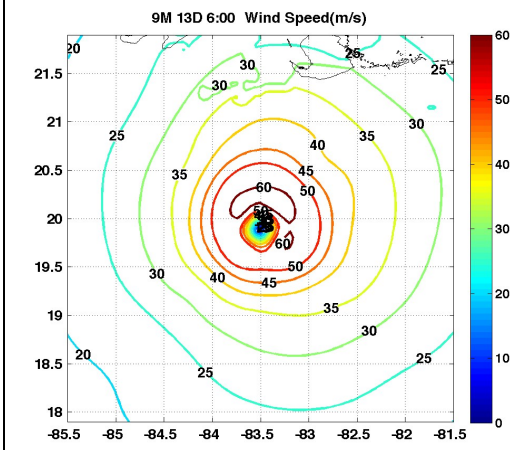
Rankine vortex	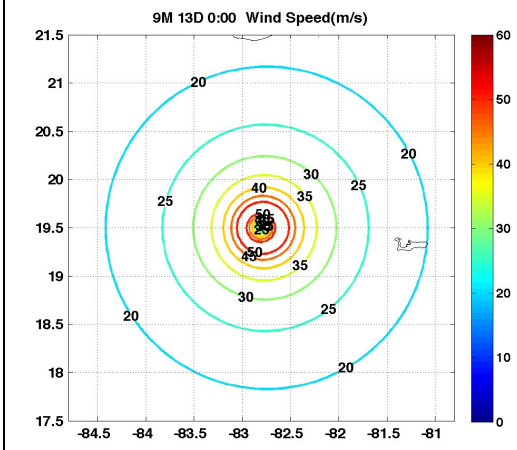	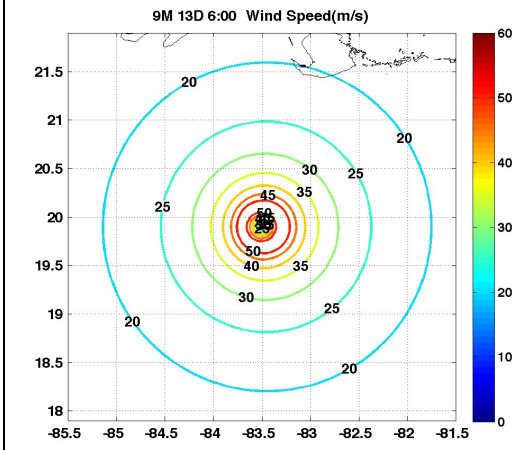
Adjusted Rankine vortex	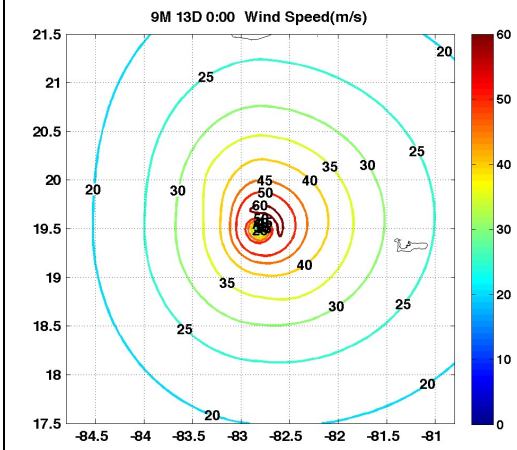	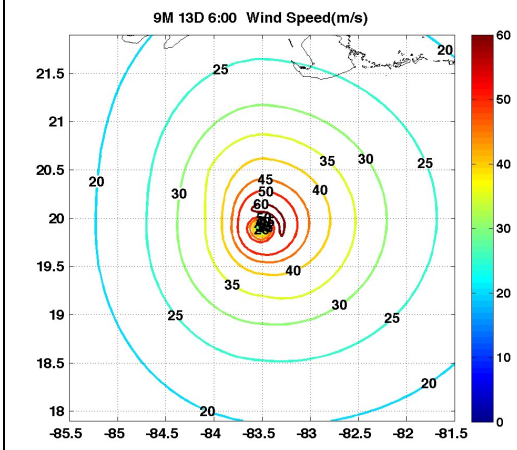

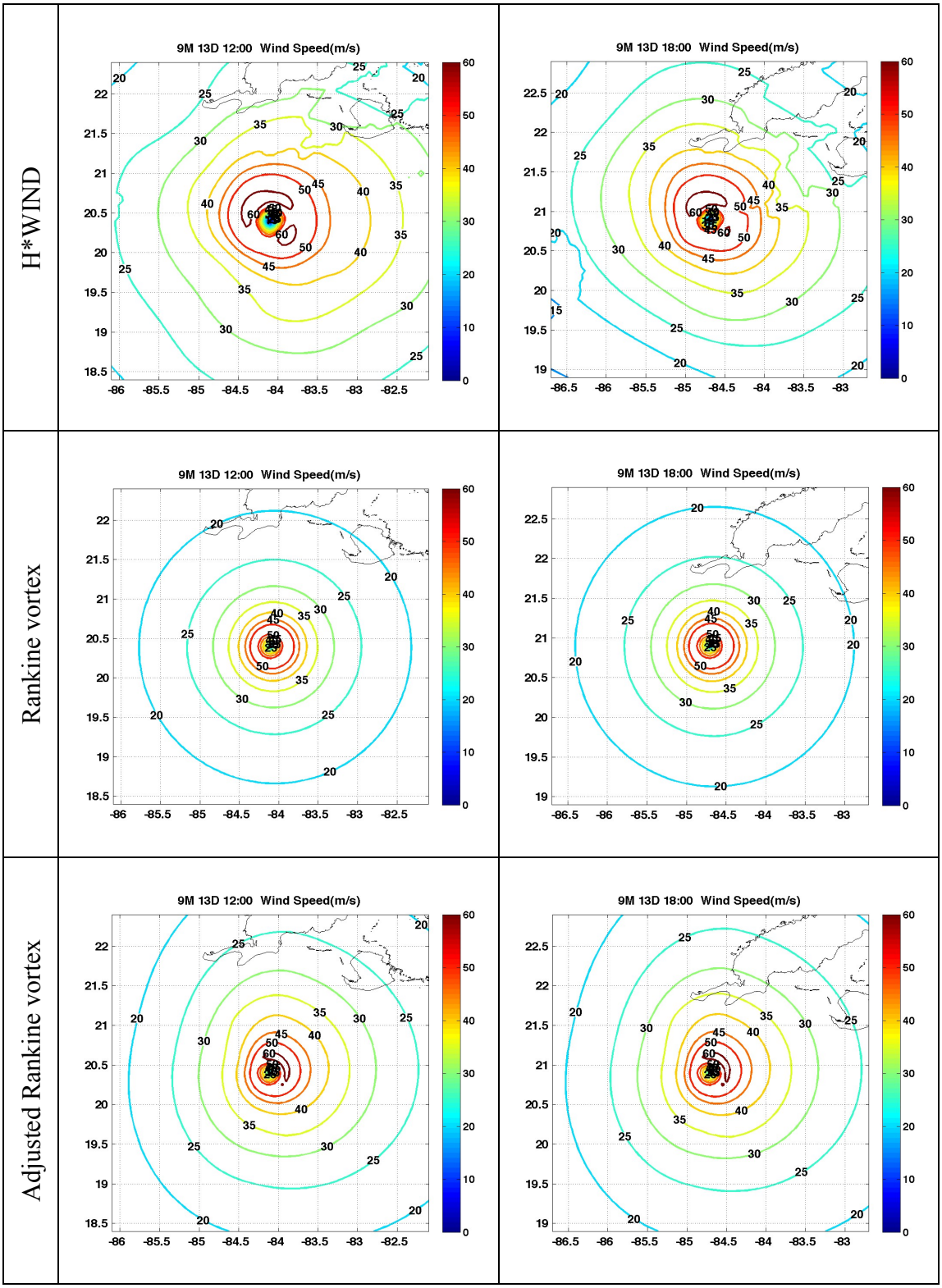
H*WIND
Rankine vortex
Adjusted Rankine vortex
9M 13D 12:00 Wind Speed(m/s)
9M 13D 18:00 Wind Speed(m/s)

H*WIND	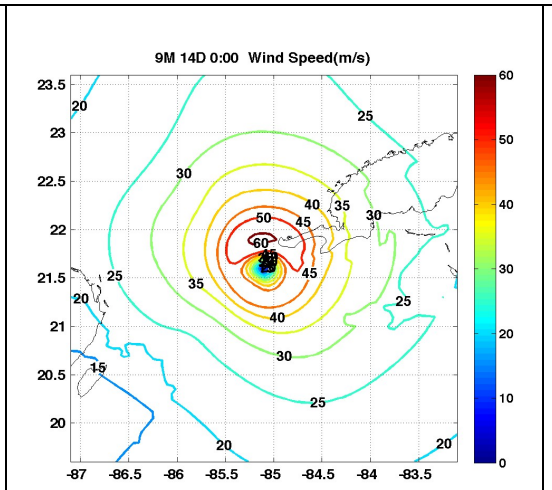	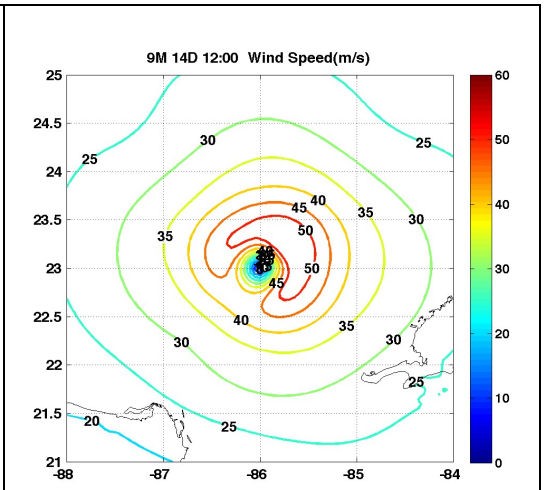
Rankine vortex	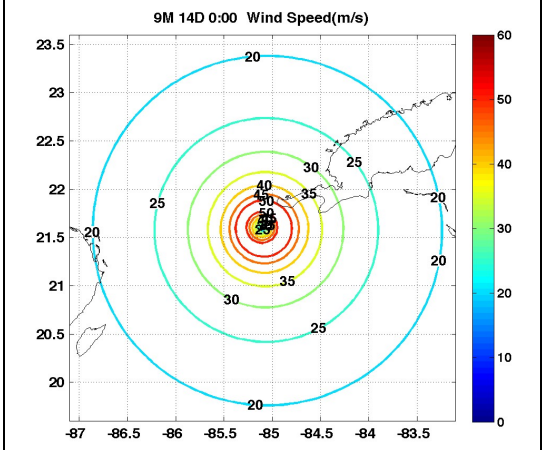	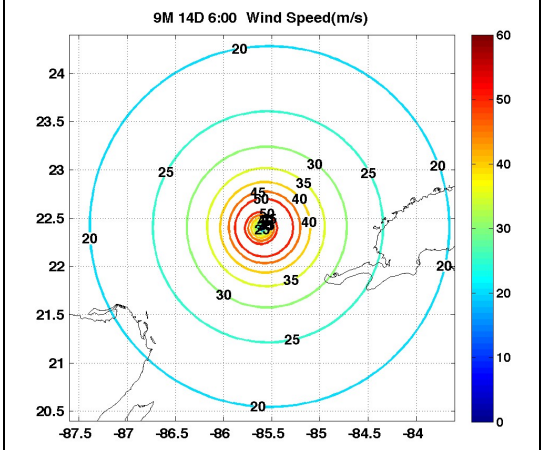
Adjusted Rankine vortex	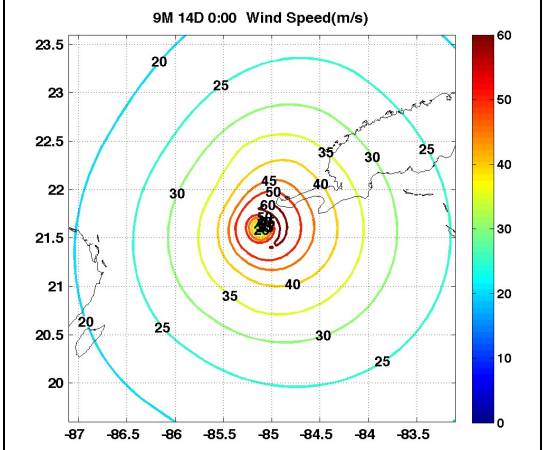	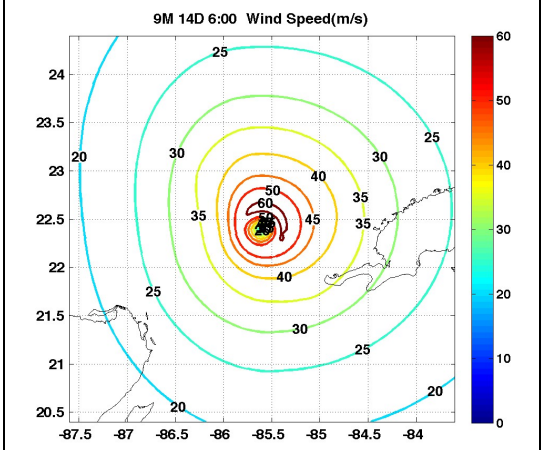

H*WIND	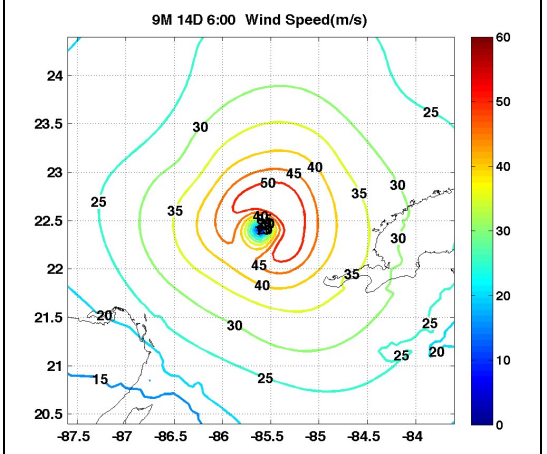	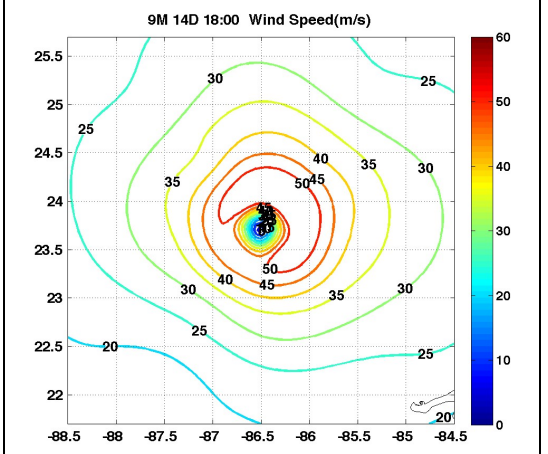
Rankine vortex	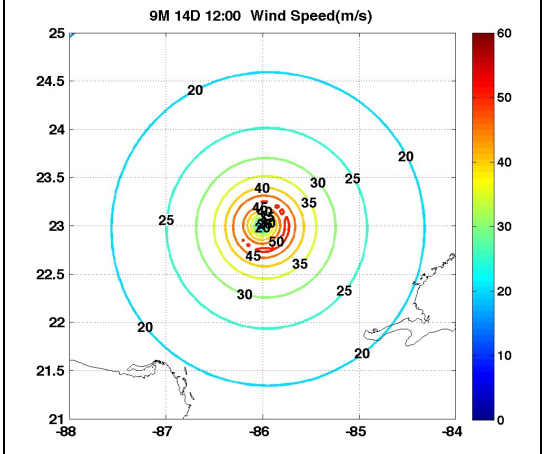	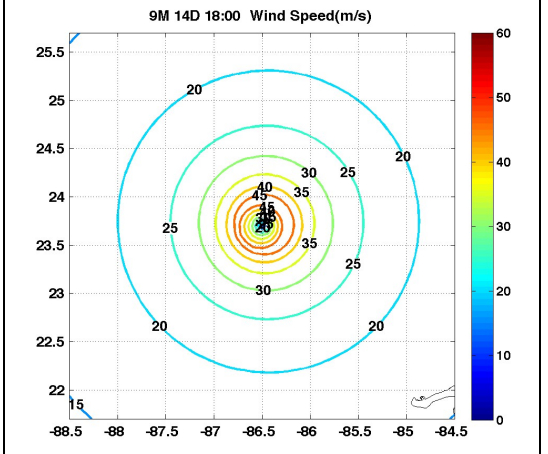
Adjusted Rankine vortex	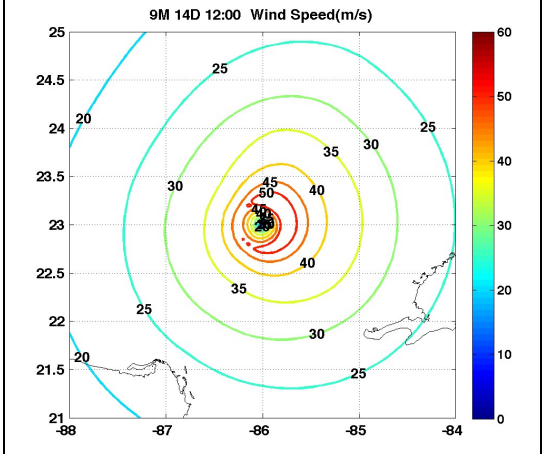	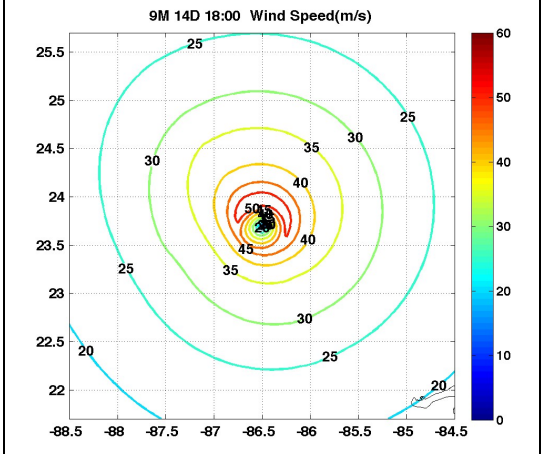

H*WIND	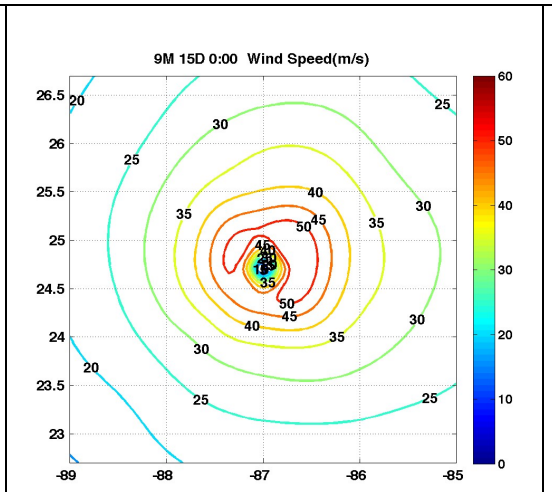	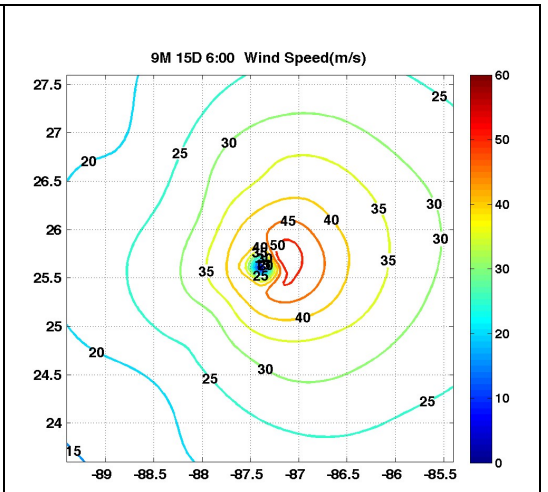
Rankine vortex	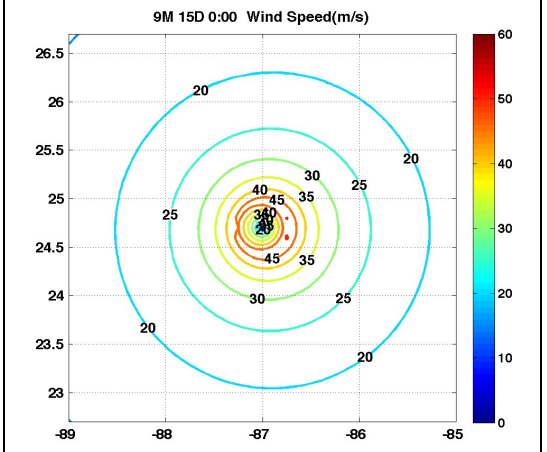	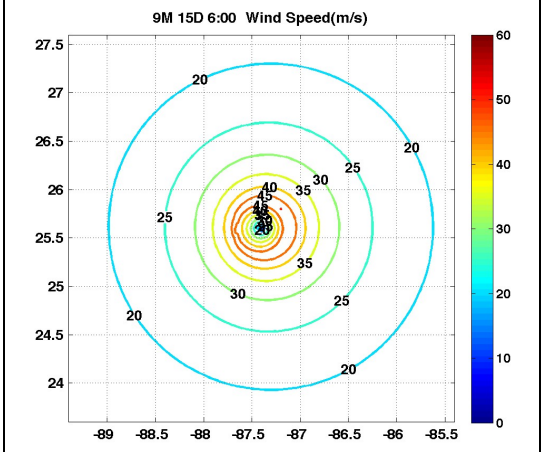
Adjusted Rankine vortex	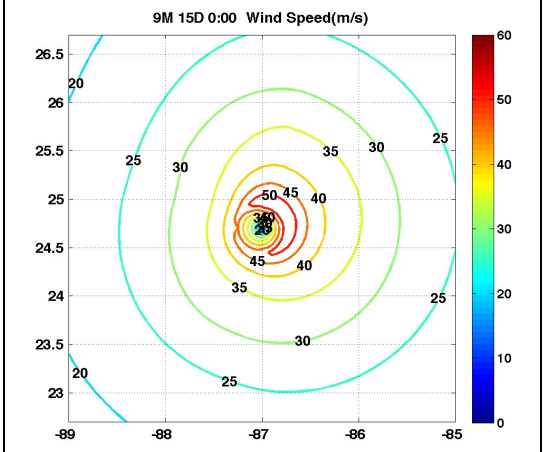	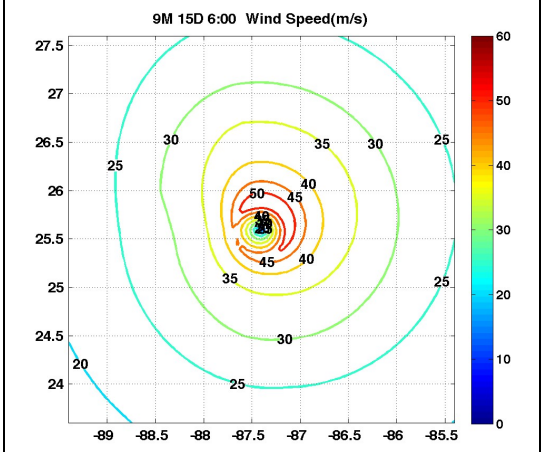

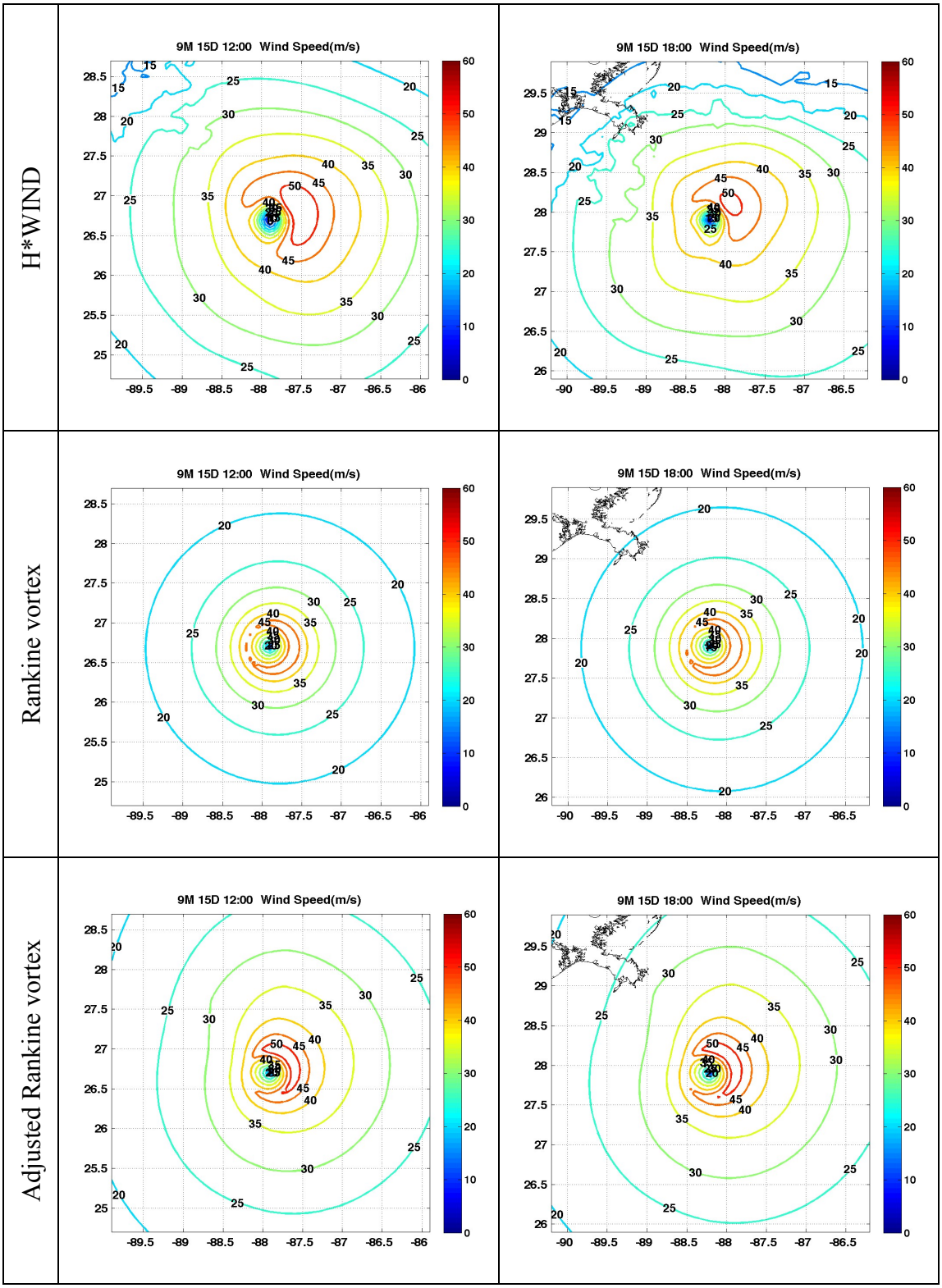
H*WIND
Rankine vortex
Adjusted Rankine vortex
9M 15D 12:00 Wind Speed(m/s)
9M 15D 18:00 Wind Speed(m/s)

[7] Arlene (2005)

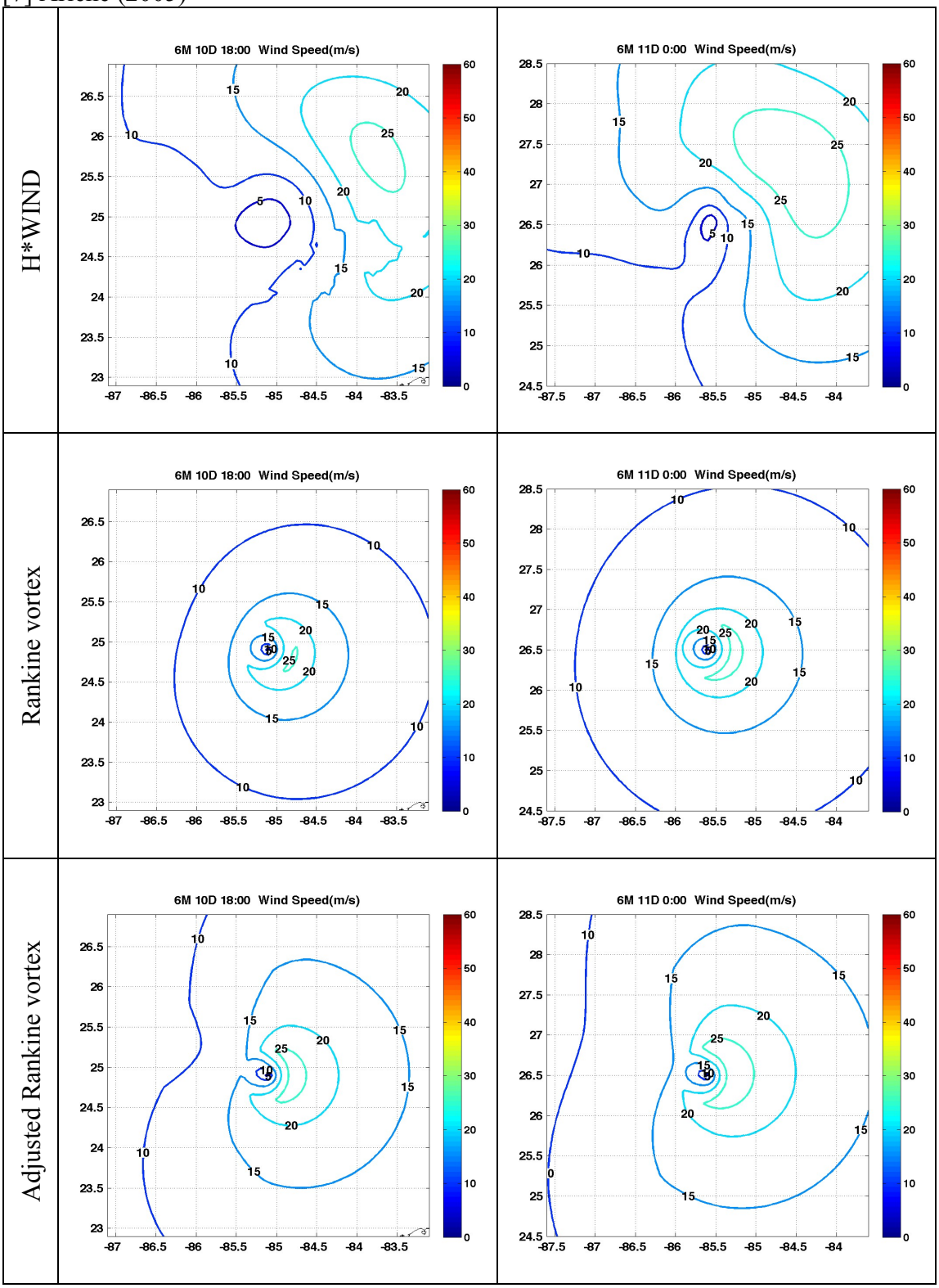

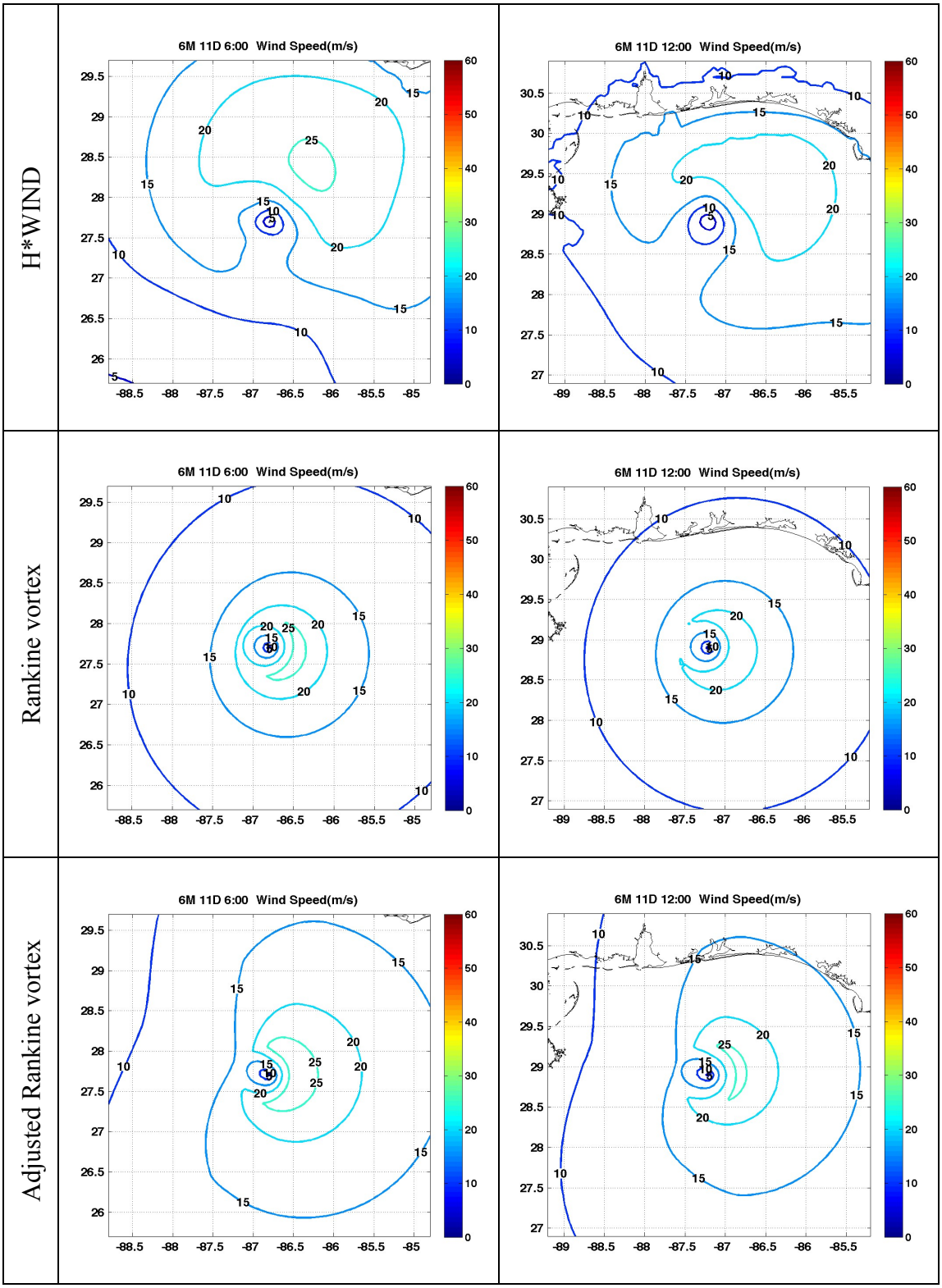
H*WIND
Rankine vortex
Adjusted Rankine vortex
6M 11D 6:00 Wind Speed(m/s)
6M 11D 12:00 Wind Speed(m/s)

[8] Dennis (2005)

H*WIND	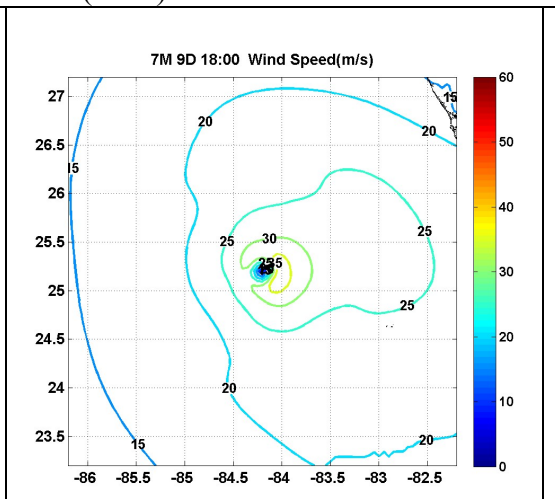	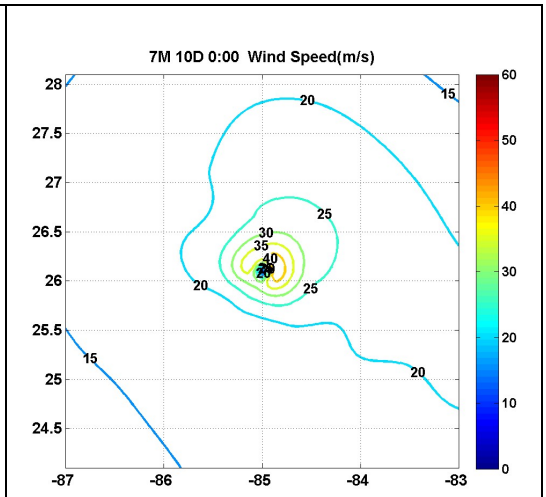
Rankine vortex	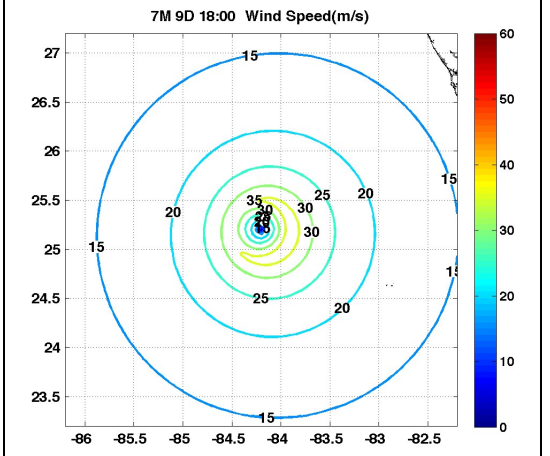	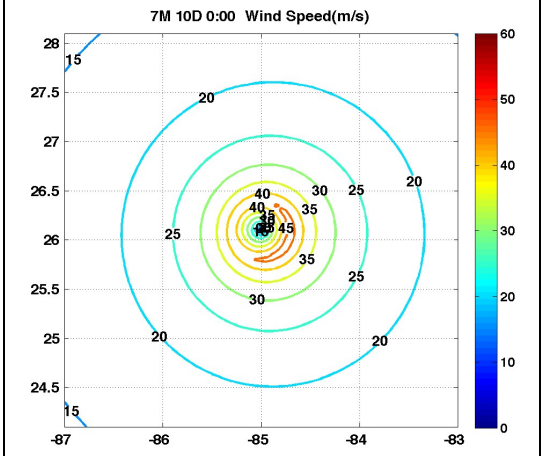
Adjusted Rankine vortex	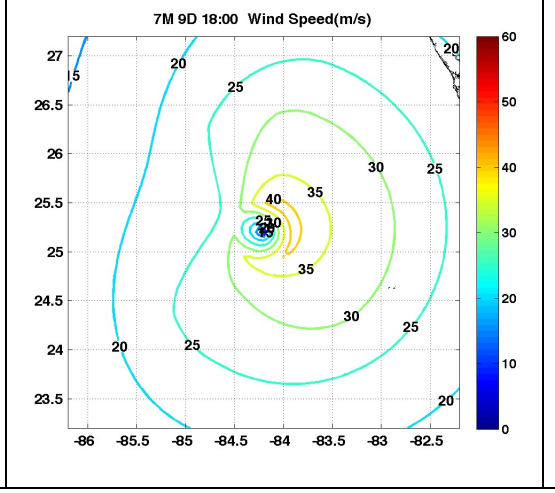	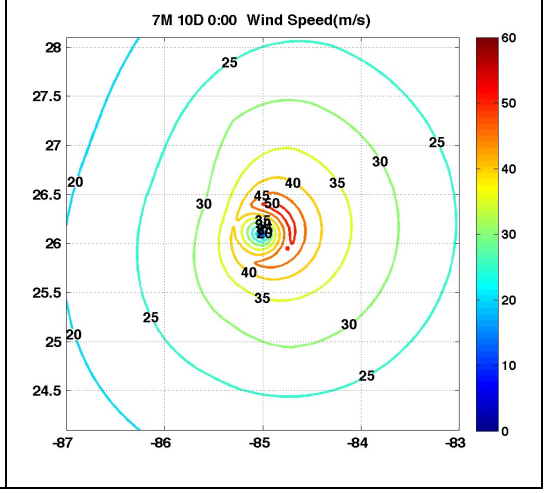

H*WIND	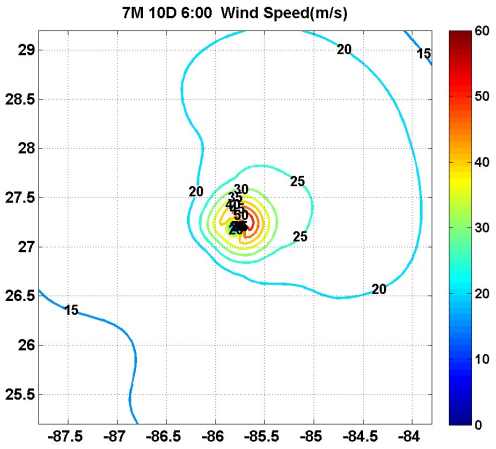	
Rankine vortex	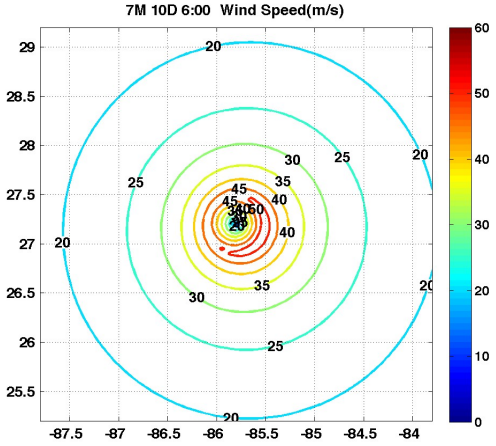	
Adjusted Rankine vortex	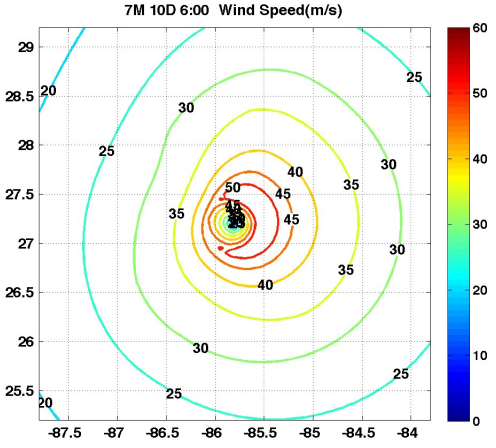	

[9] Emily (2005)

H*WIND	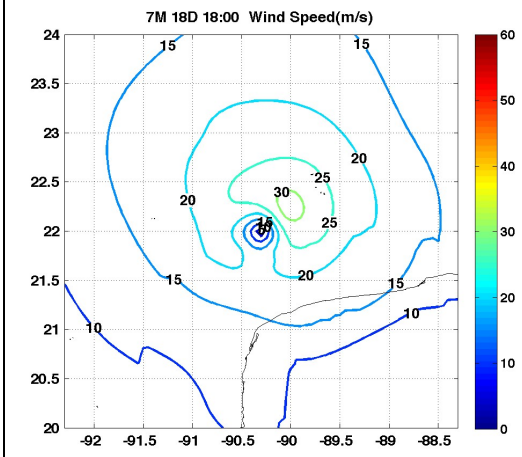	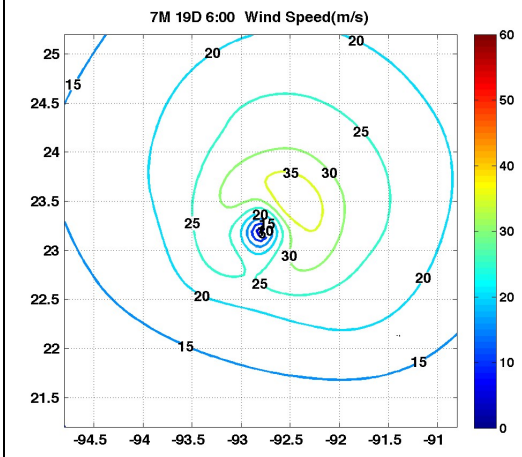
Rankine vortex	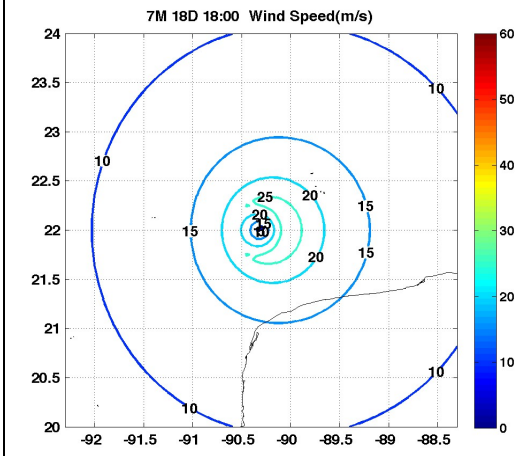	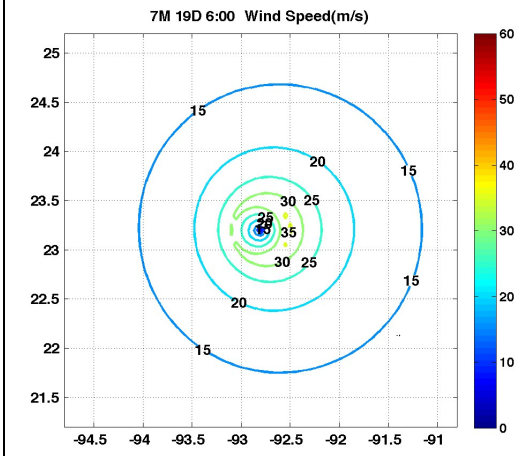
Adjusted Rankine vortex	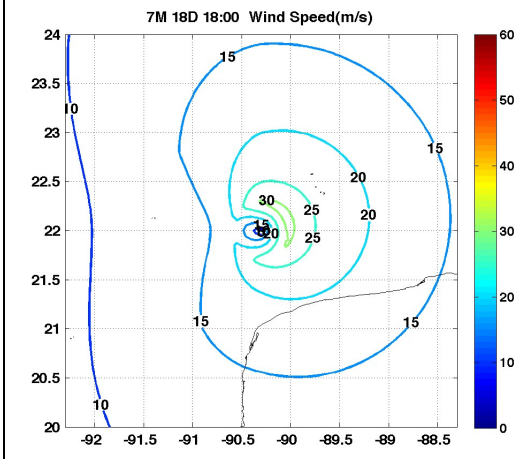	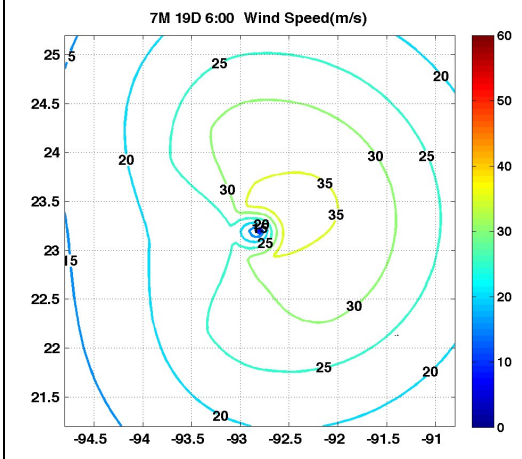

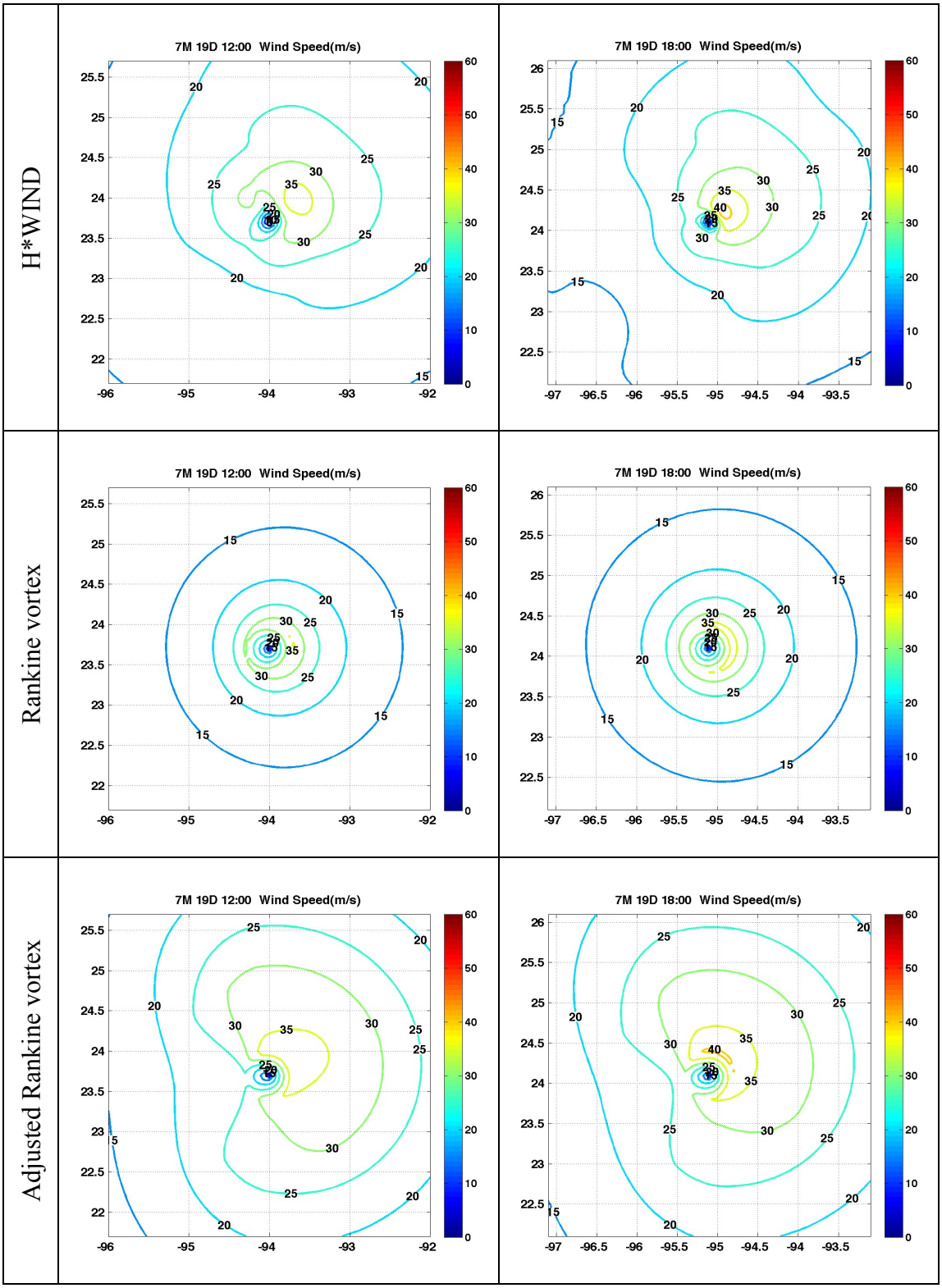
H*WIND
Rankine vortex
Adjusted Rankine vortex
7M 19D 12:00 Wind Speed(m/s)
7M 19D 18:00 Wind Speed(m/s)

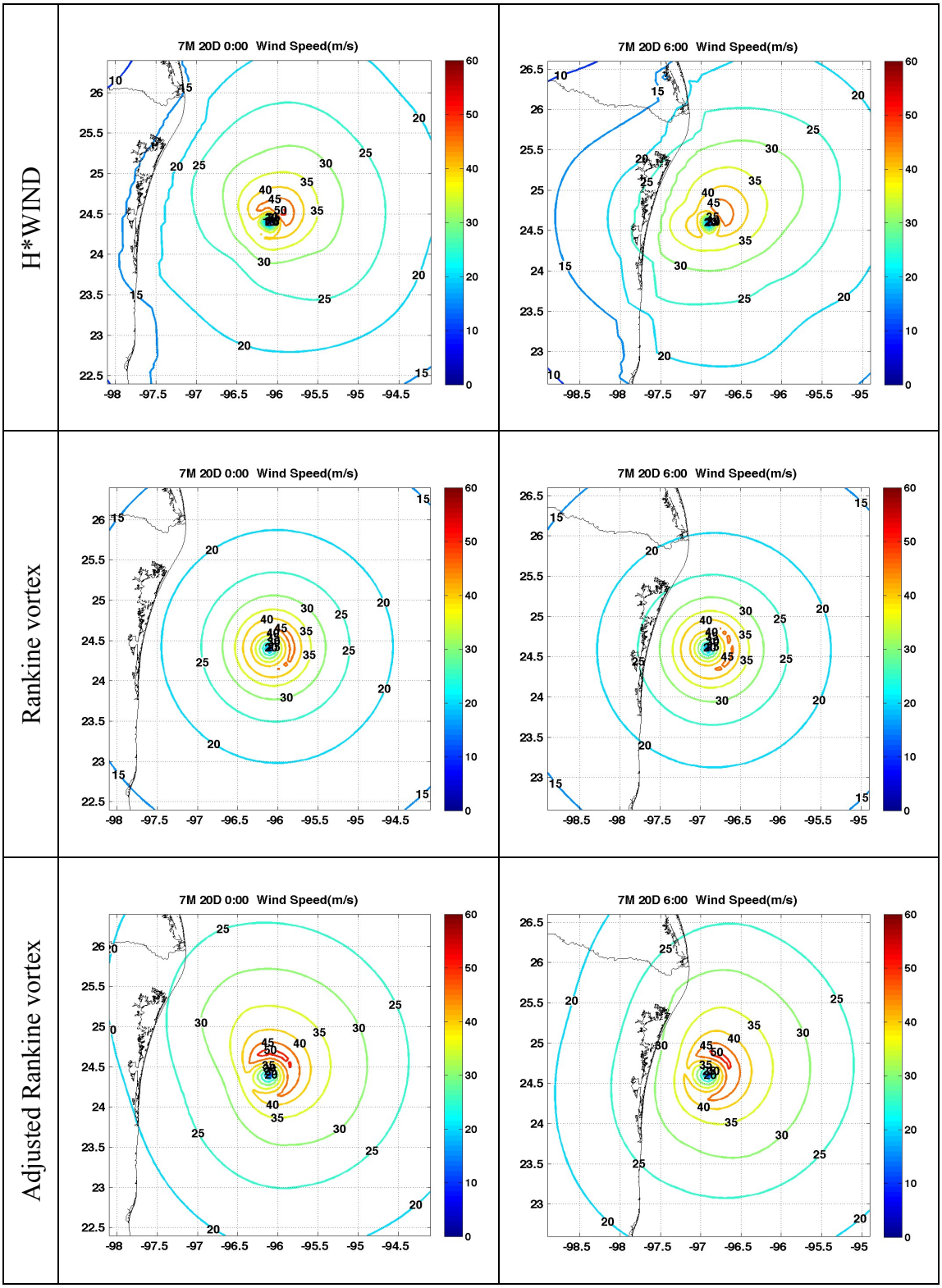
H*WIND
Rankine vortex
Adjusted Rankine vortex
7M 20D 0:00 Wind Speed(m/s)
7M 20D 6:00 Wind Speed(m/s)

[10] Katrina (2005)

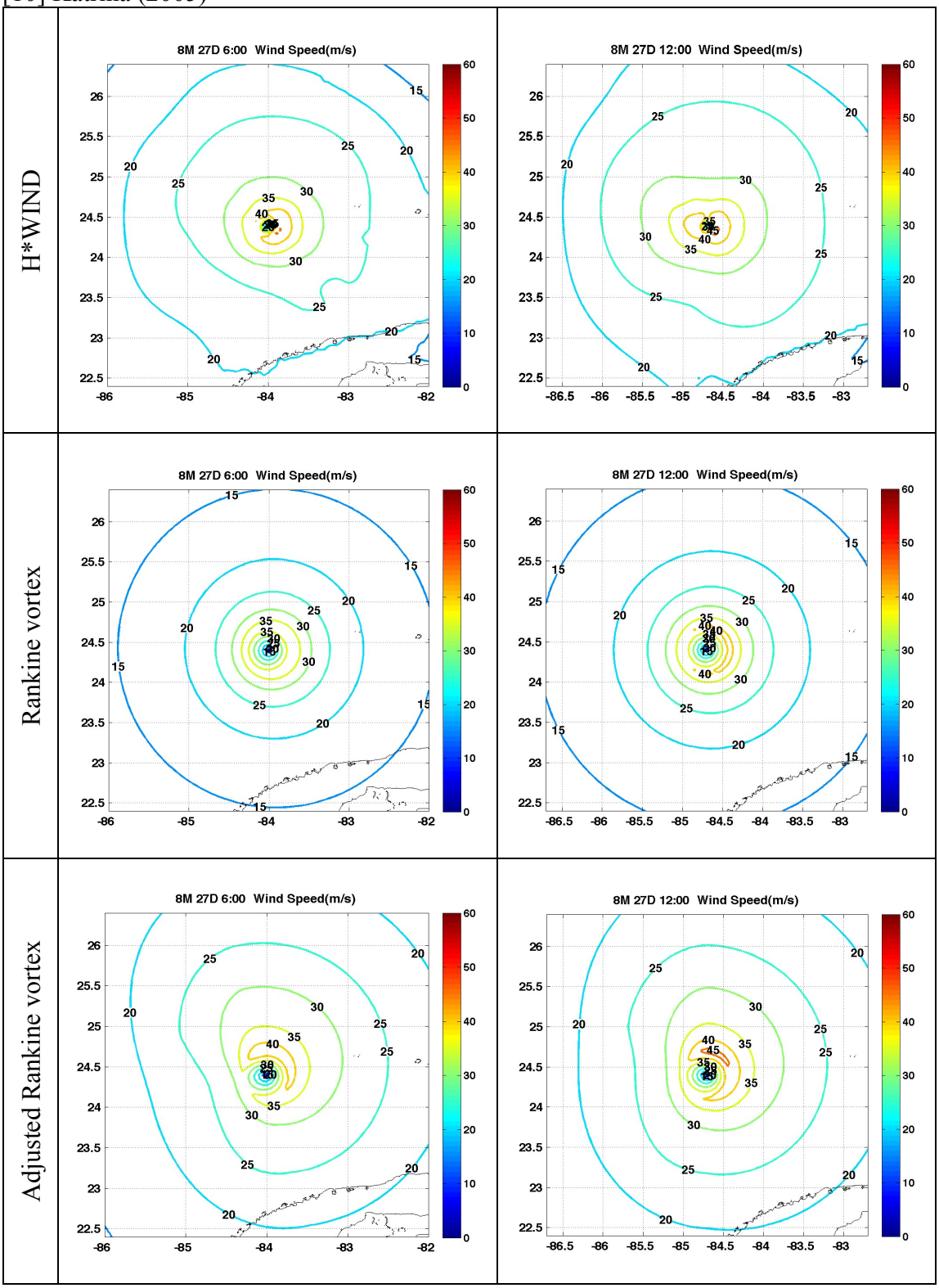

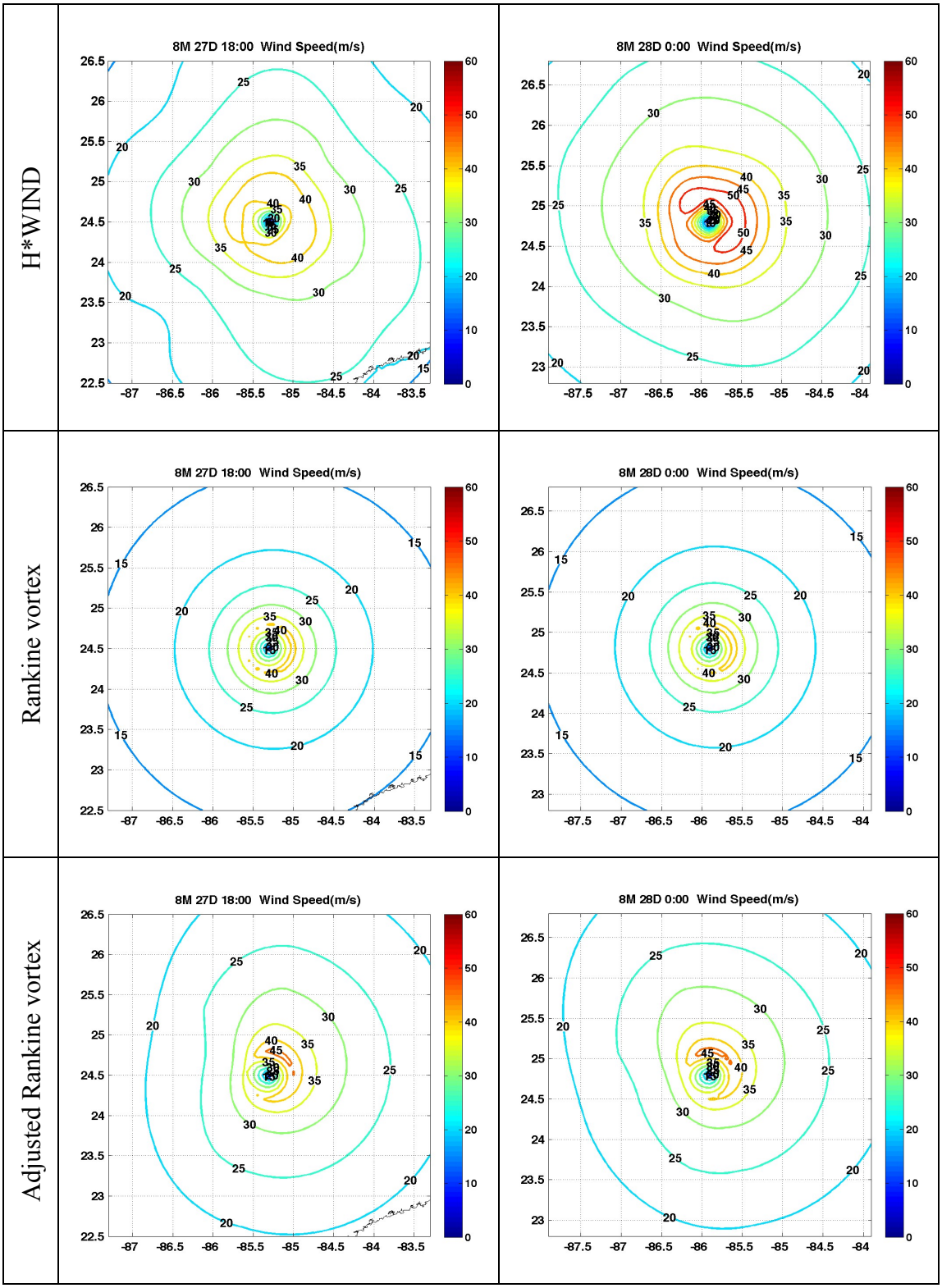
H*WIND
Rankine vortex
Adjusted Rankine vortex
8M 27D 18:00 Wind Speed(m/s)
8M 28D 0:00 Wind Speed(m/s)

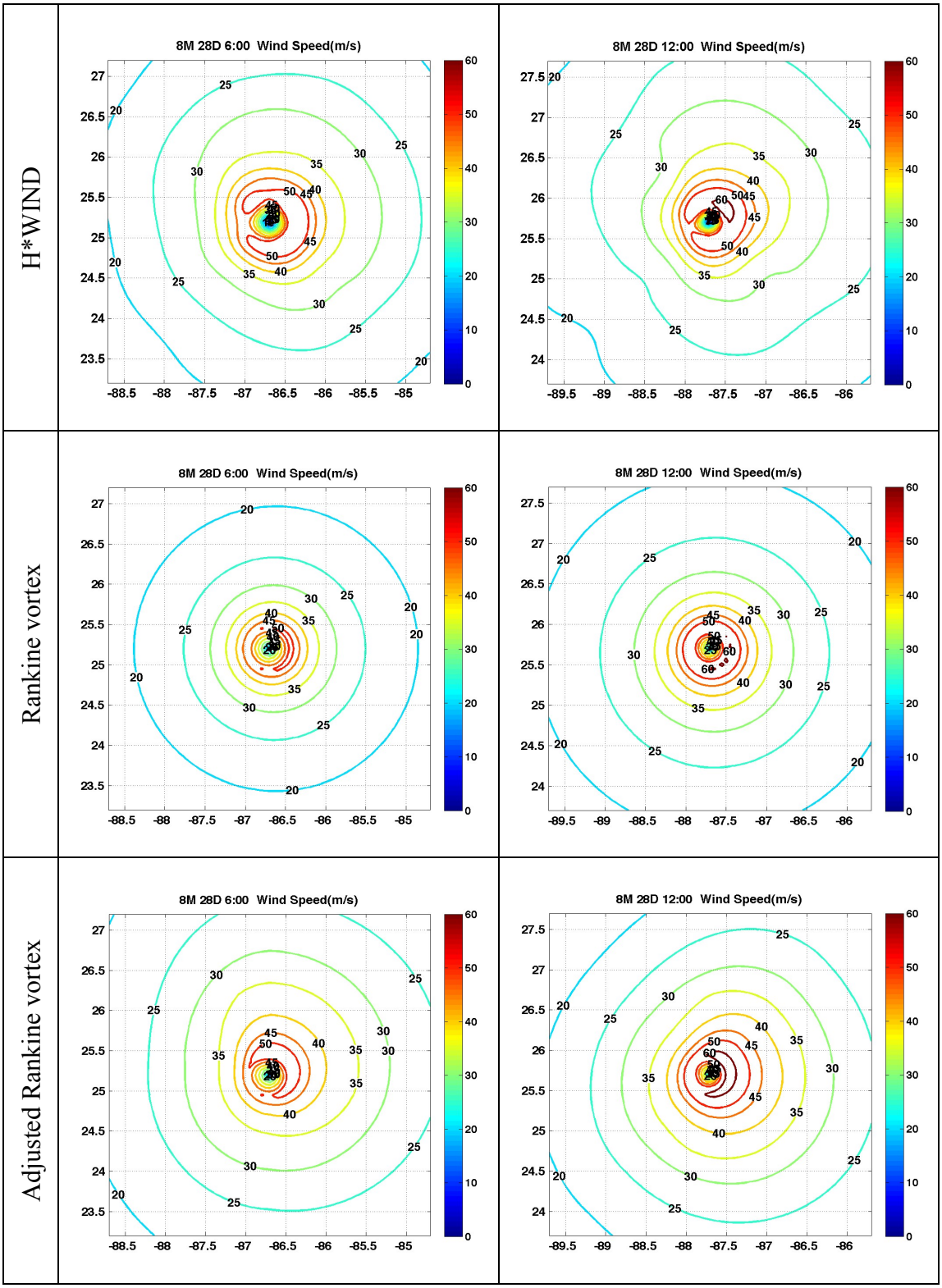
H*WIND
Rankine vortex
Adjusted Rankine vortex
8M 28D 6:00 Wind Speed(m/s)
8M 28D 12:00 Wind Speed(m/s)

H*WIND	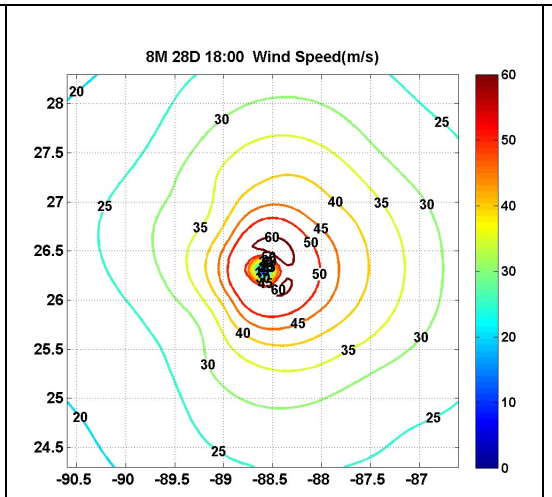	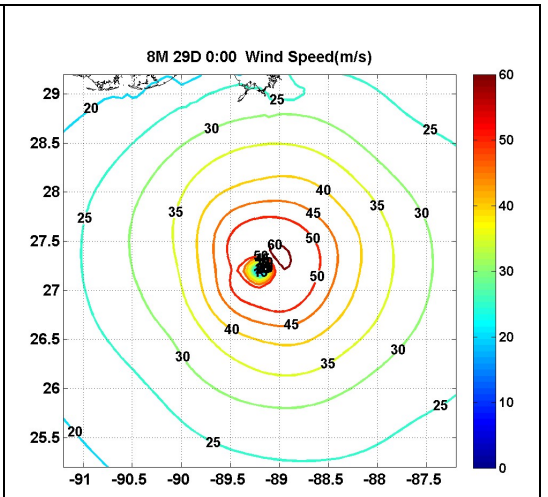
Rankine vortex	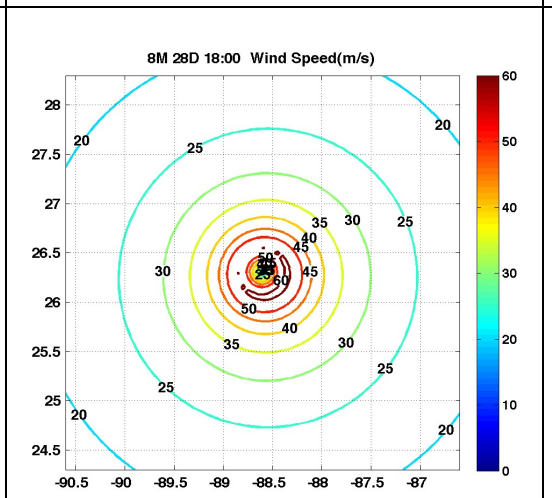	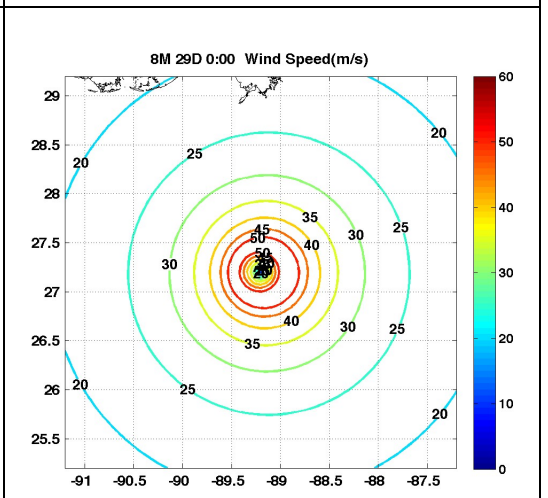
Adjusted Rankine vortex	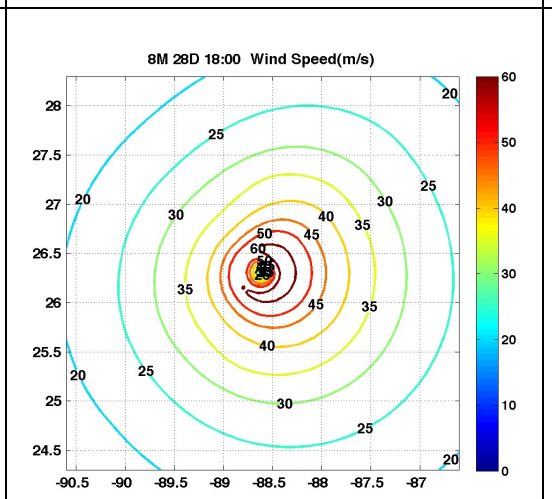	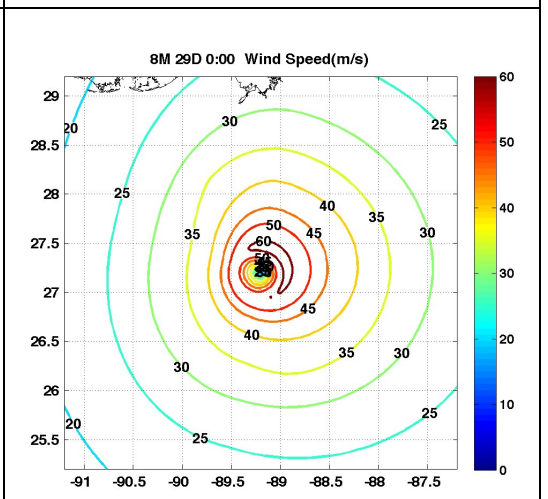

H*WIND	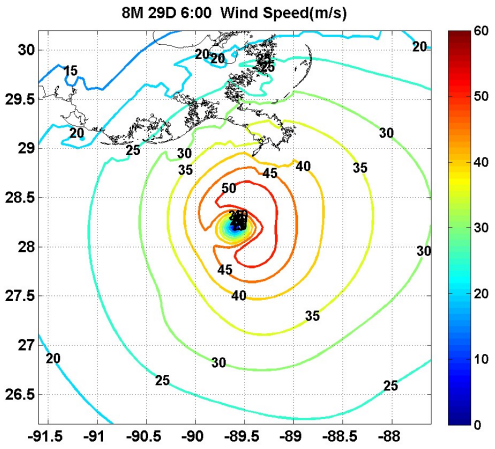	
Rankine vortex	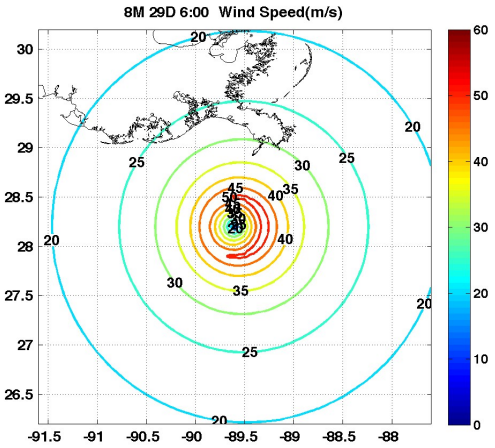	
Adjusted Rankine vortex	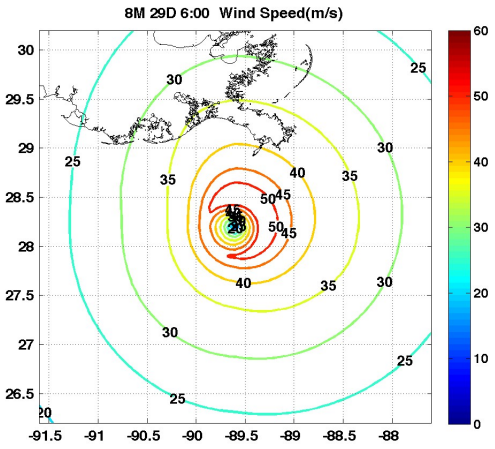	

[11] Rita (2005)

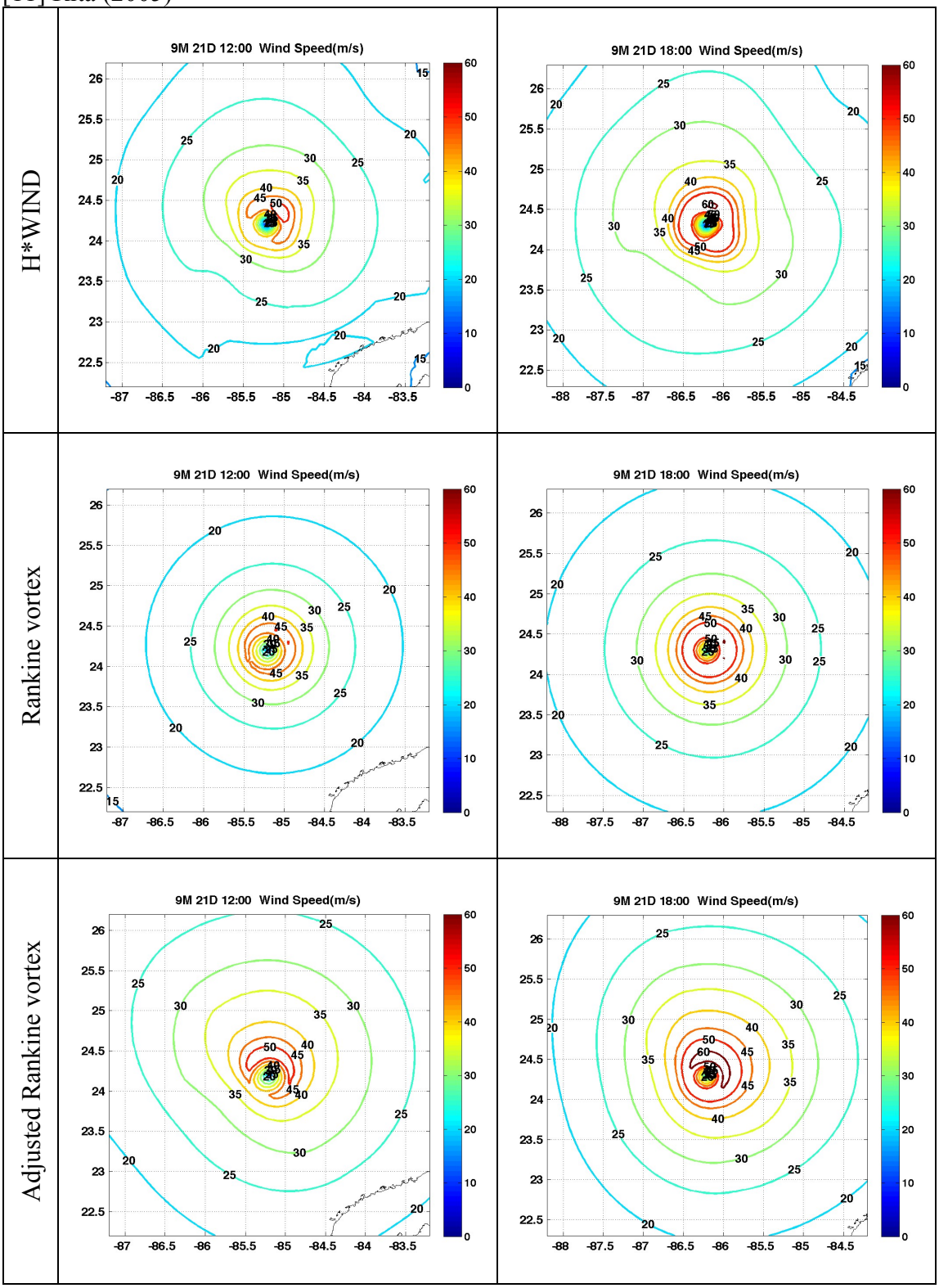
H*WIND
Rankine vortex
Adjusted Rankine vortex
9M 21D 12:00 Wind Speed(m/s)
9M 21D 18:00 Wind Speed(m/s)

H*WIND	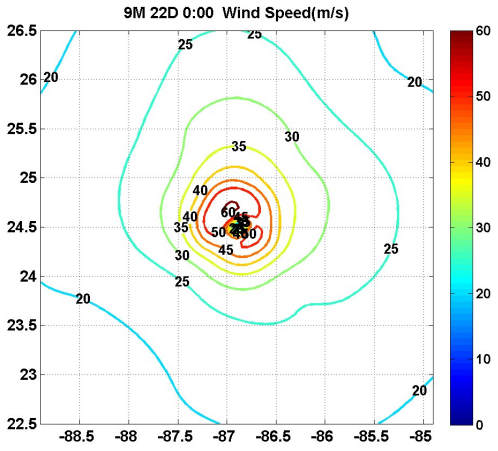	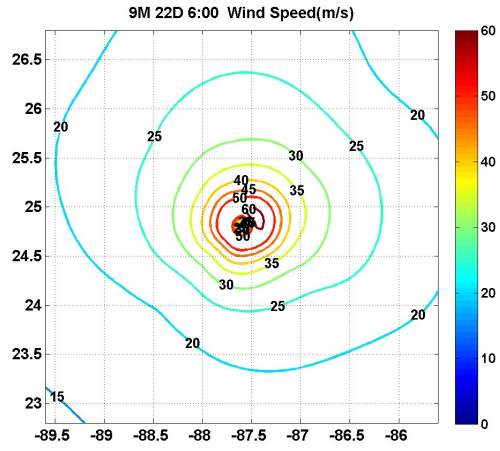
Rankine vortex	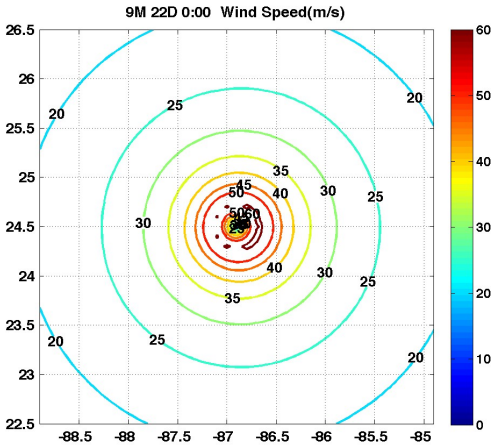	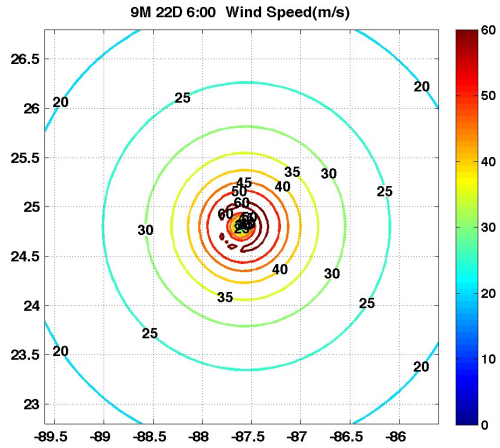
Adjusted Rankine vortex	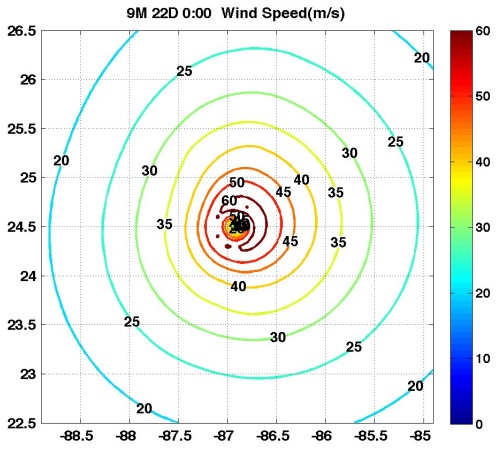	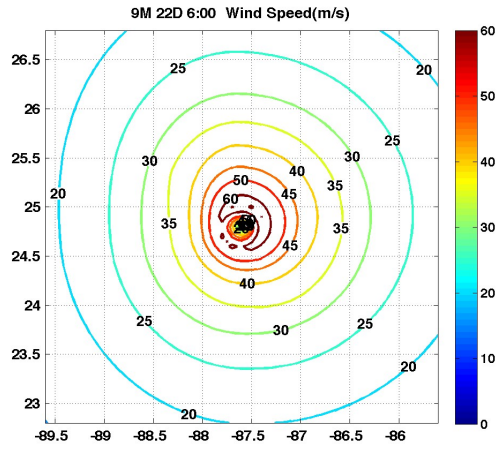

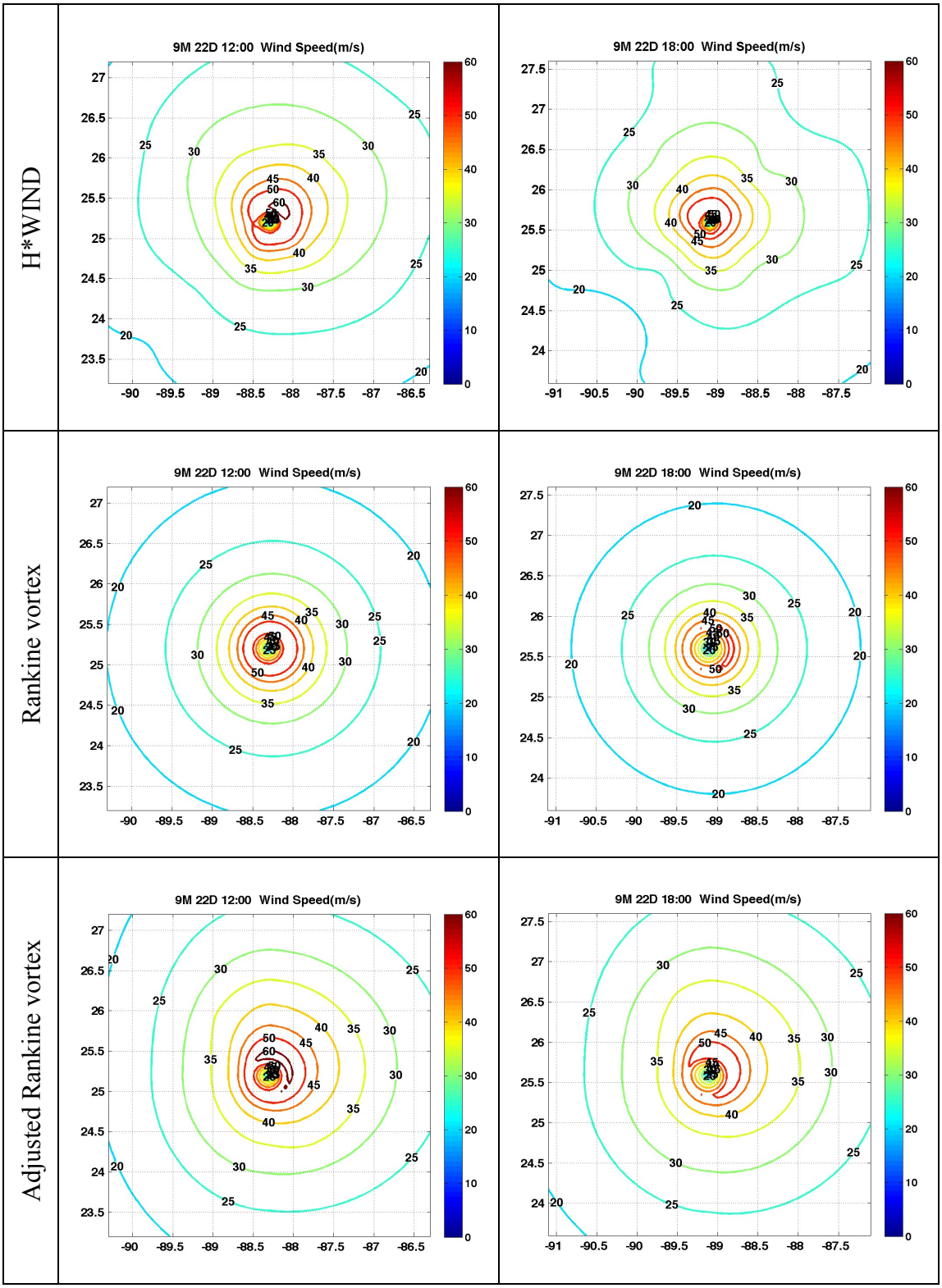
H*WIND
Rankine vortex
Adjusted Rankine vortex
9M 22D 12:00 Wind Speed(m/s)
9M 22D 18:00 Wind Speed(m/s)

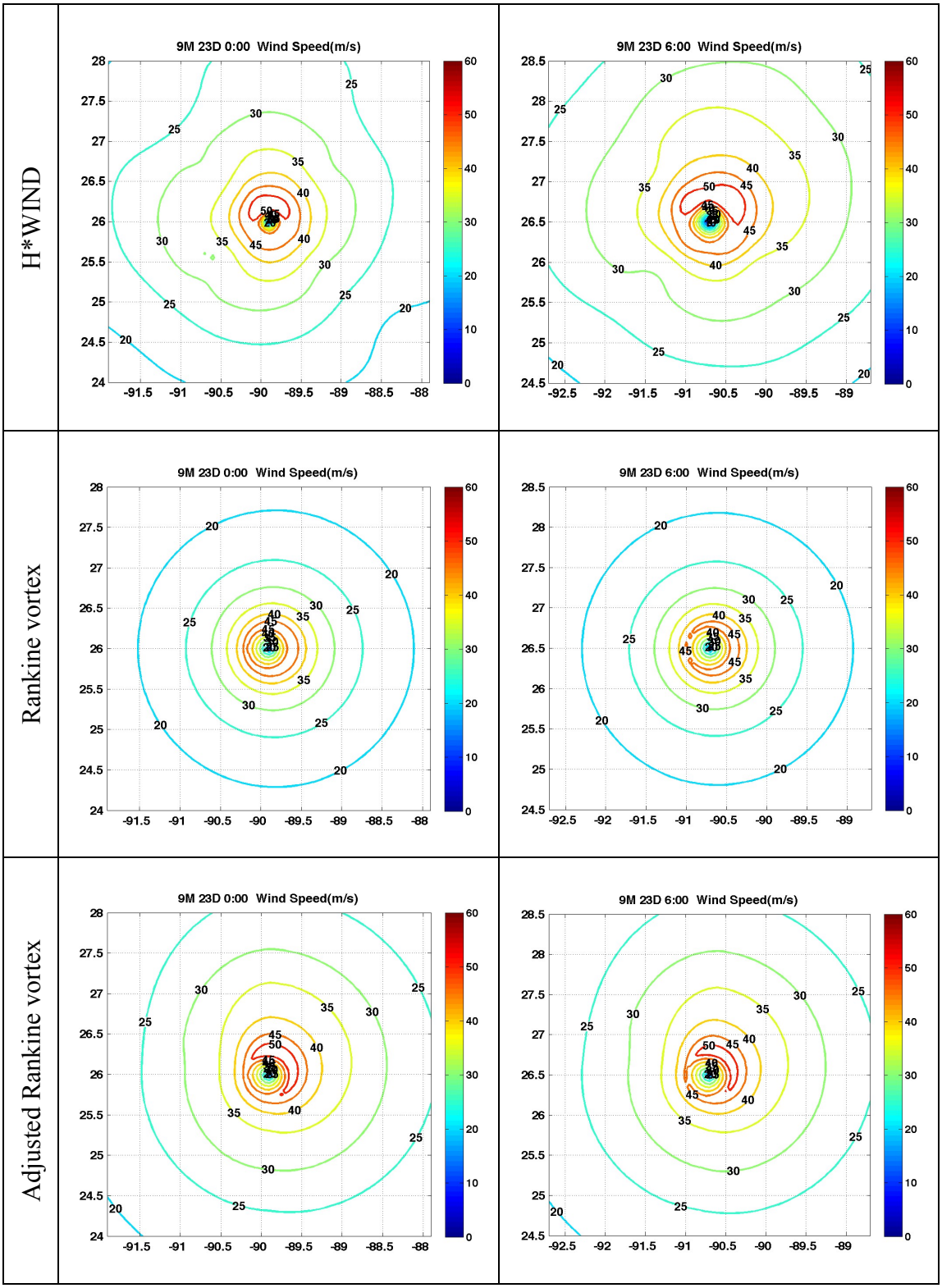
H*WIND
Rankine vortex
Adjusted Rankine vortex
9M 23D 0:00 Wind Speed(m/s)
9M 23D 6:00 Wind Speed(m/s)

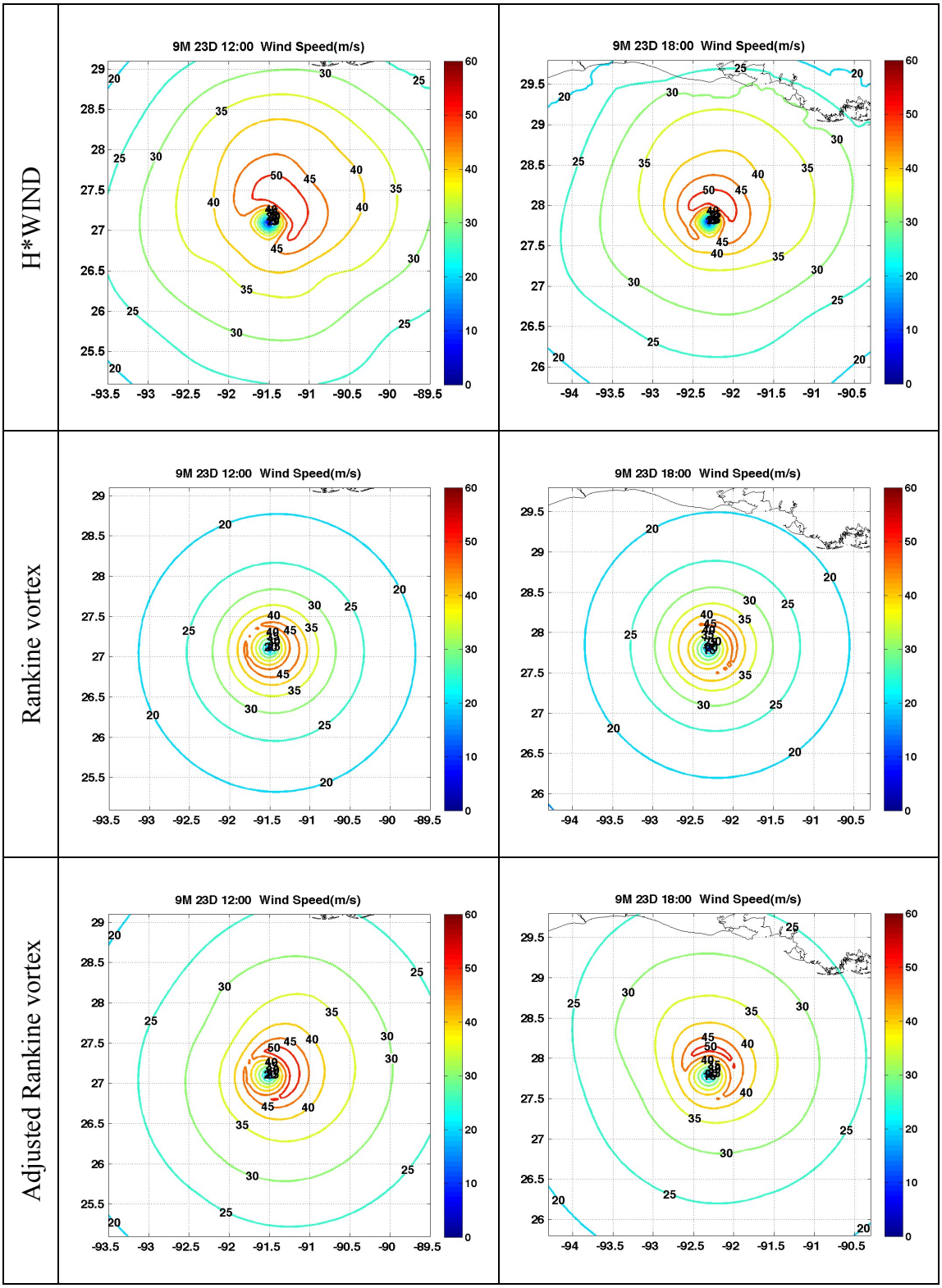
H*WIND
Rankine vortex
Adjusted Rankine vortex
9M 23D 12:00 Wind Speed(m/s)
9M 23D 18:00 Wind Speed(m/s)

[12] Wilma (2005)

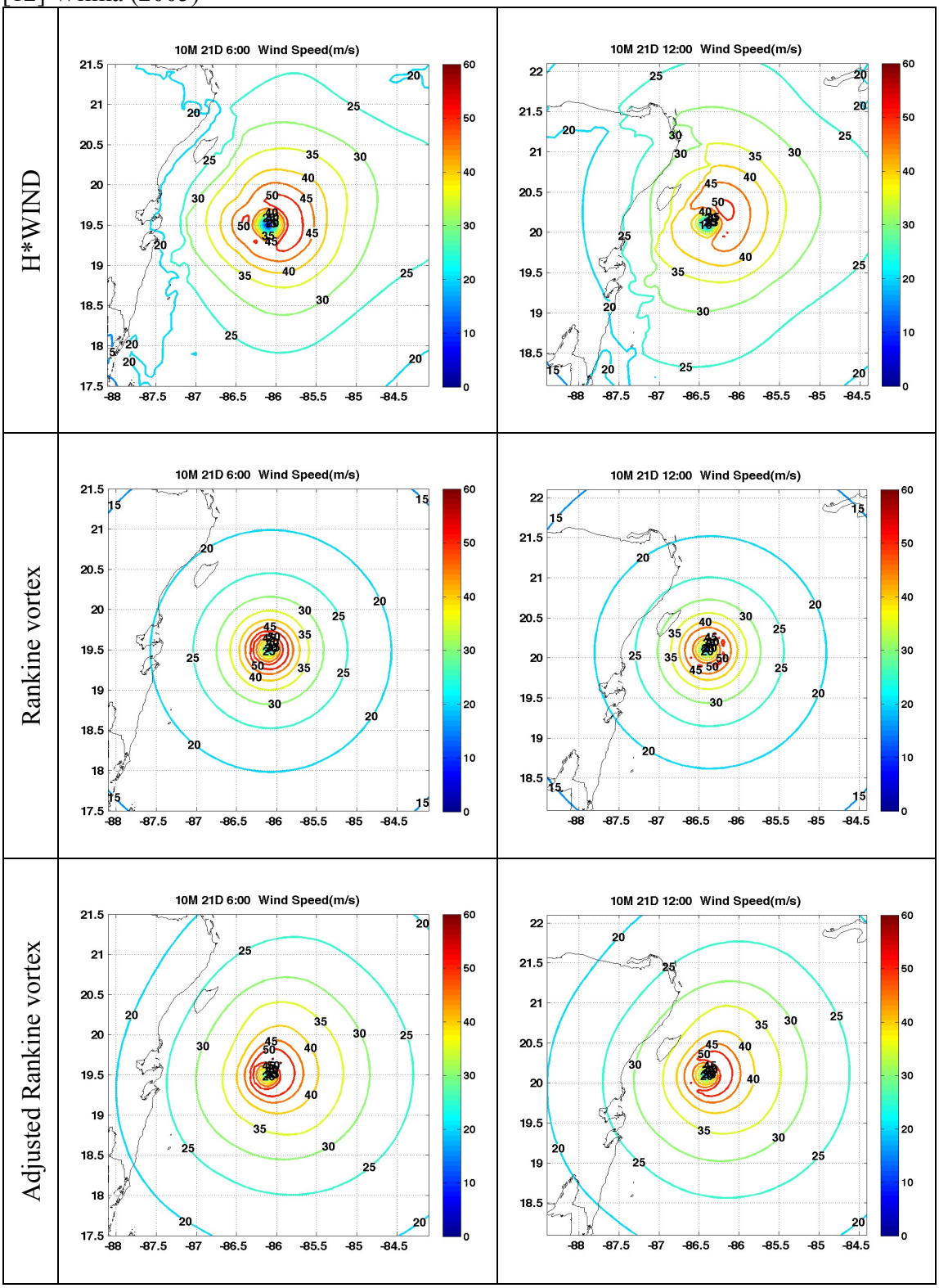

H*WIND	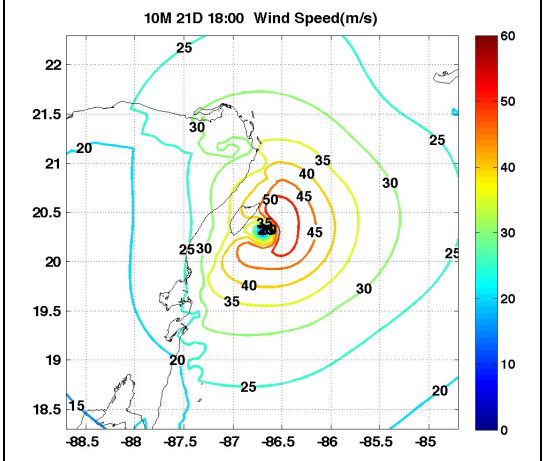	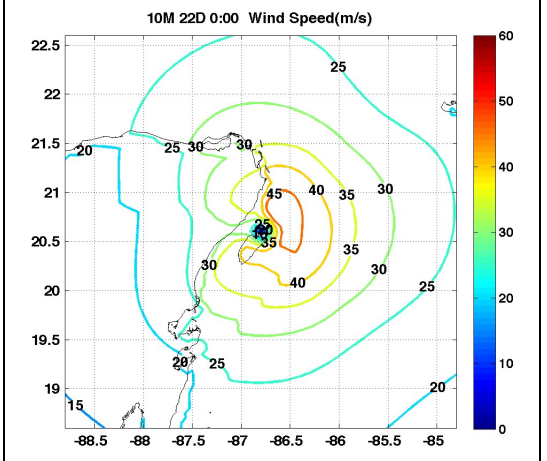
Rankine vortex	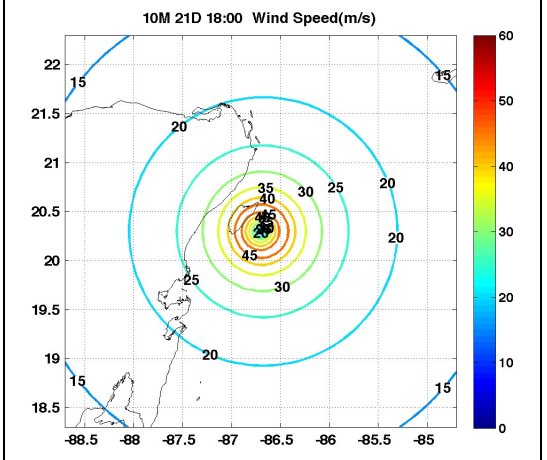	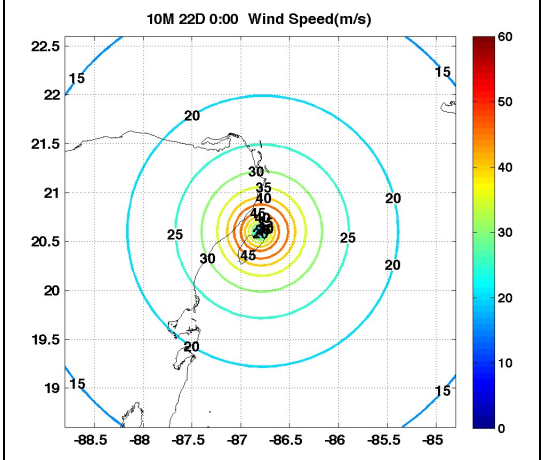
Adjusted Rankine vortex	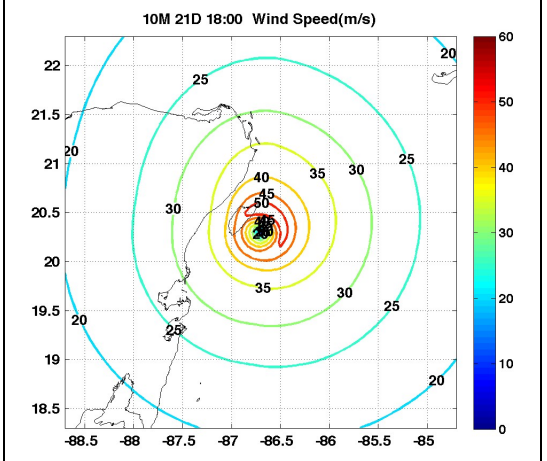	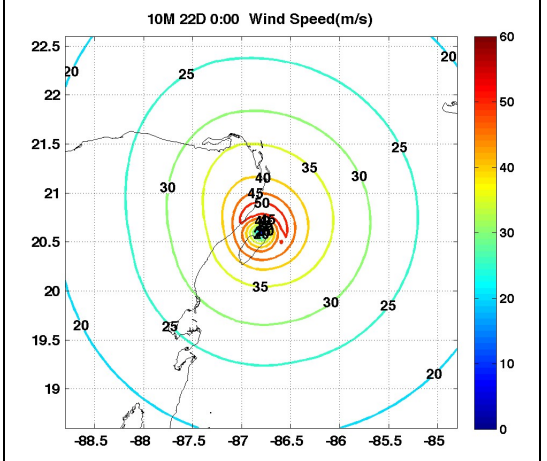

H*WIND	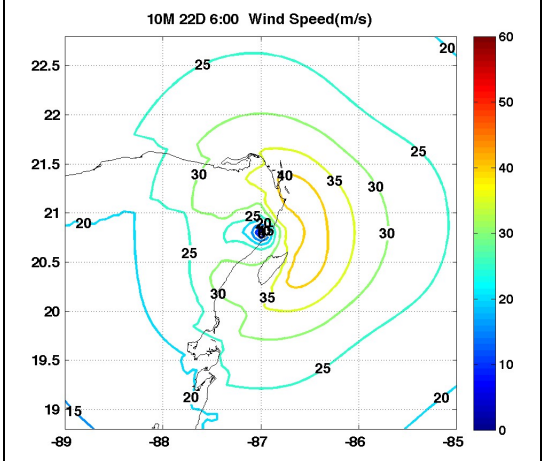	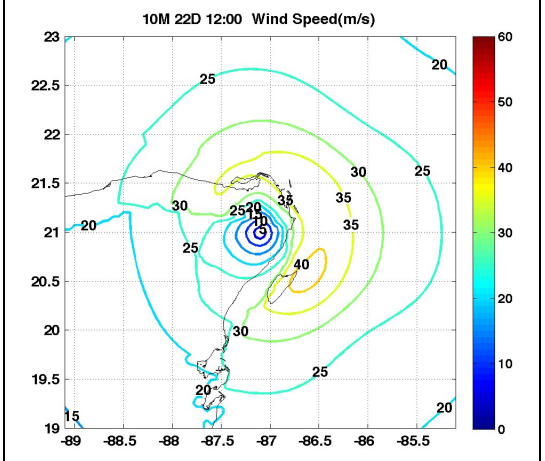
Rankine vortex	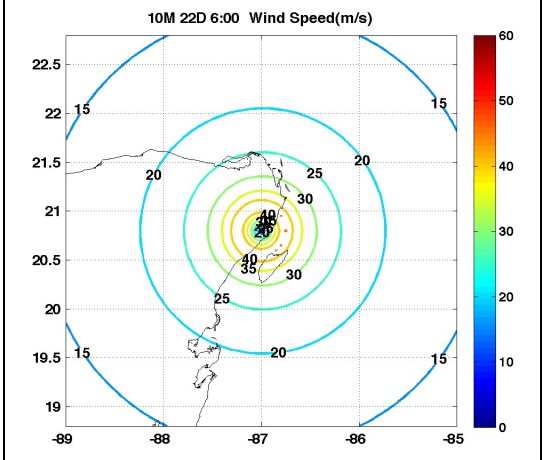	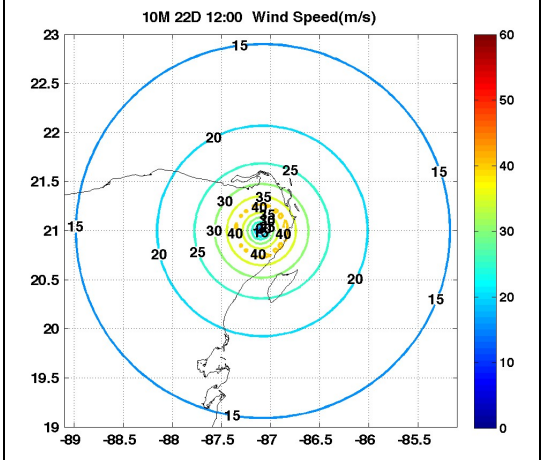
Adjusted Rankine vortex	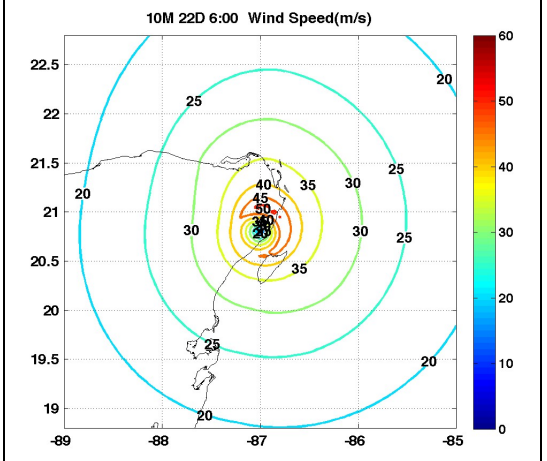	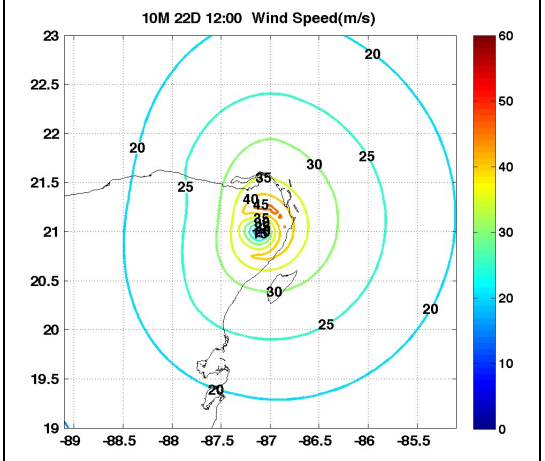

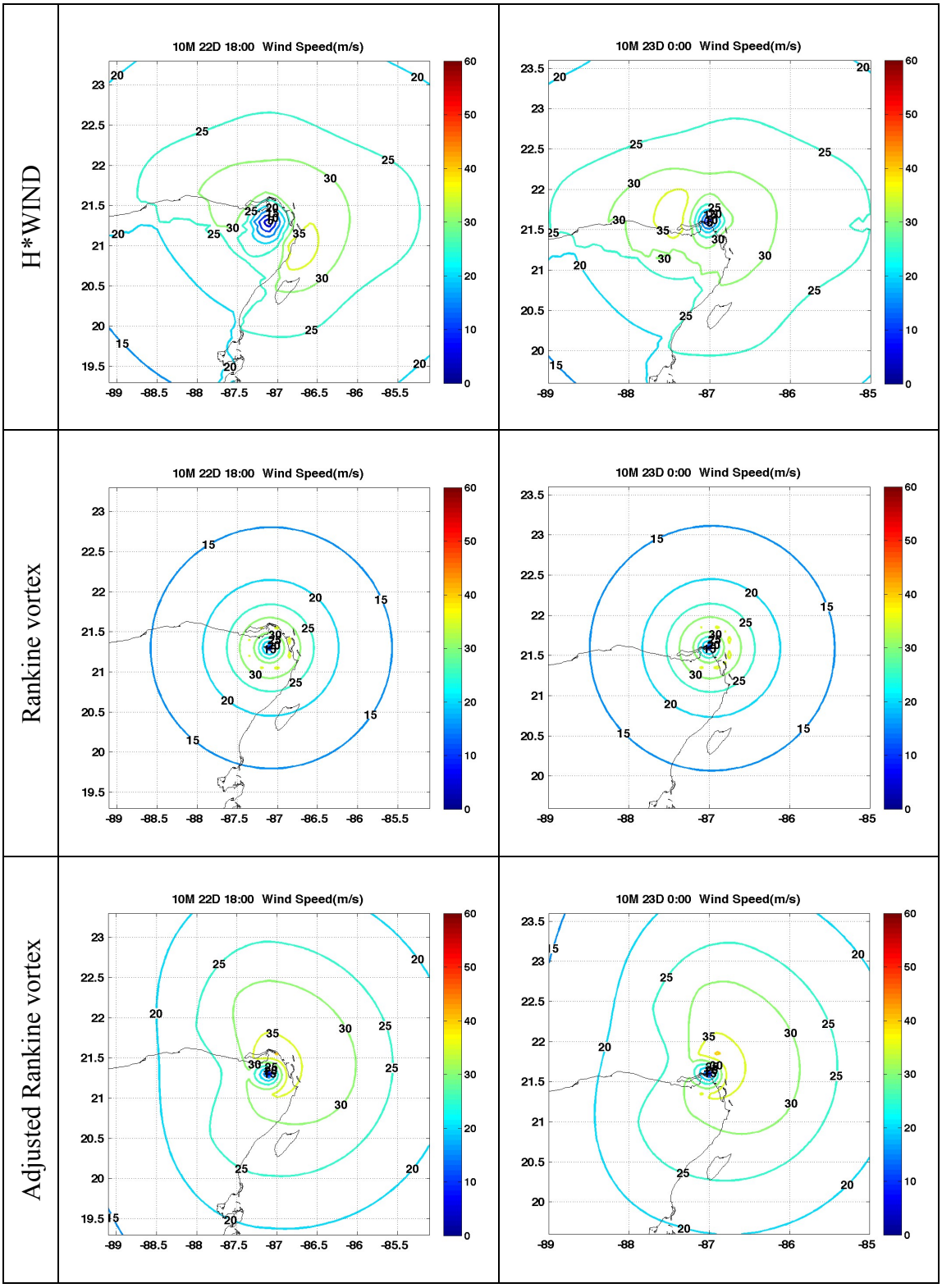
H*WIND
Rankine vortex
Adjusted Rankine vortex
10M 22D 18:00 Wind Speed(m/s)
10M 23D 0:00 Wind Speed(m/s)

H*WIND	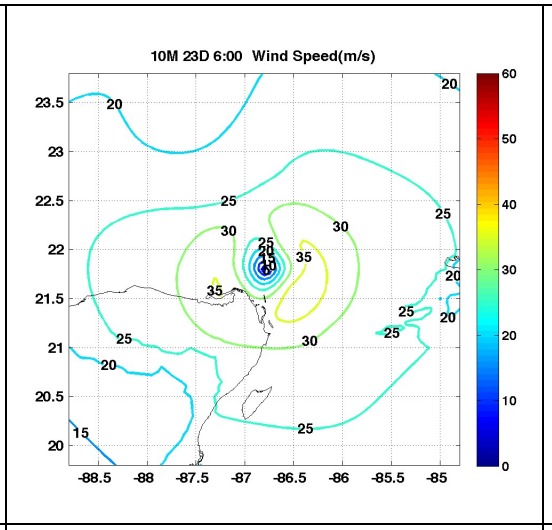	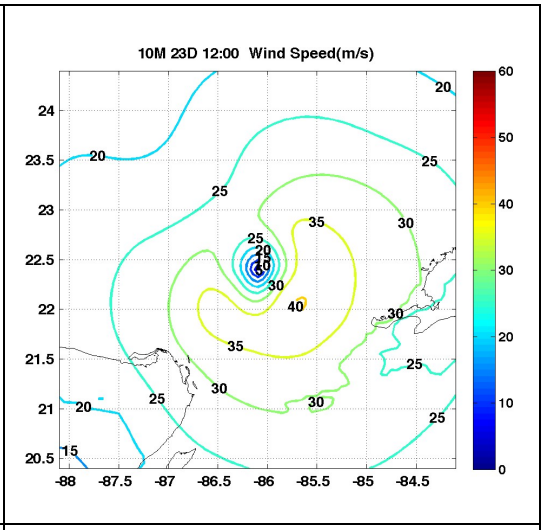
Rankine vortex	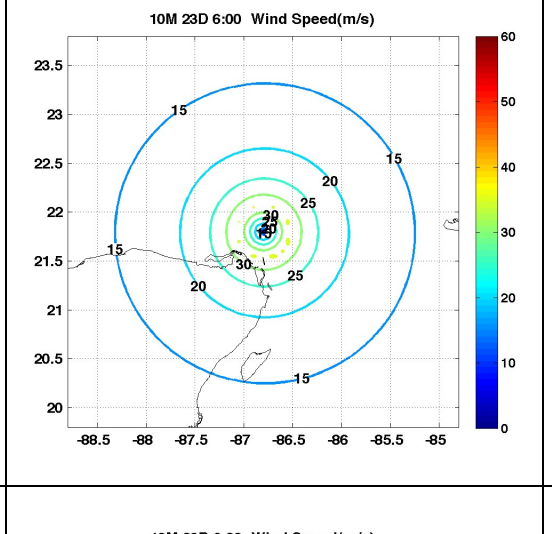	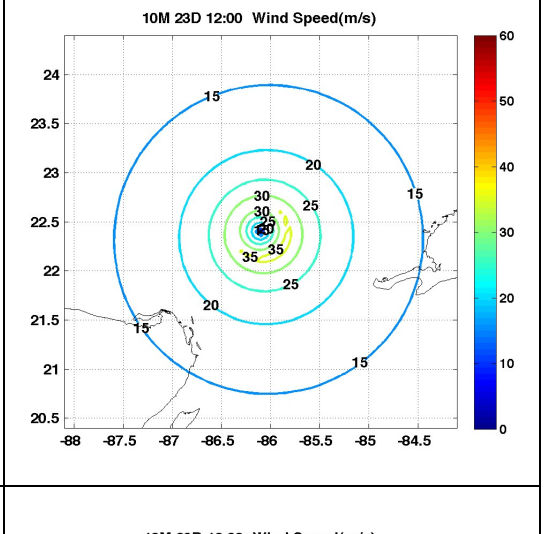
Adjusted Rankine vortex	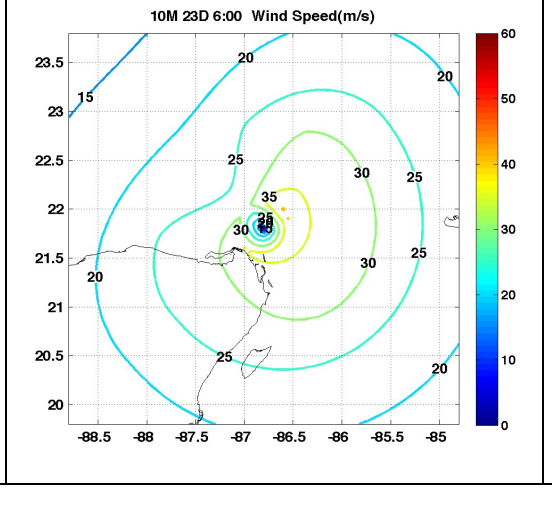	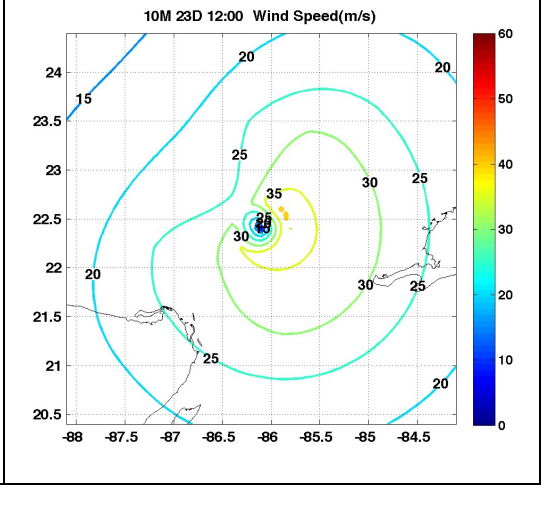

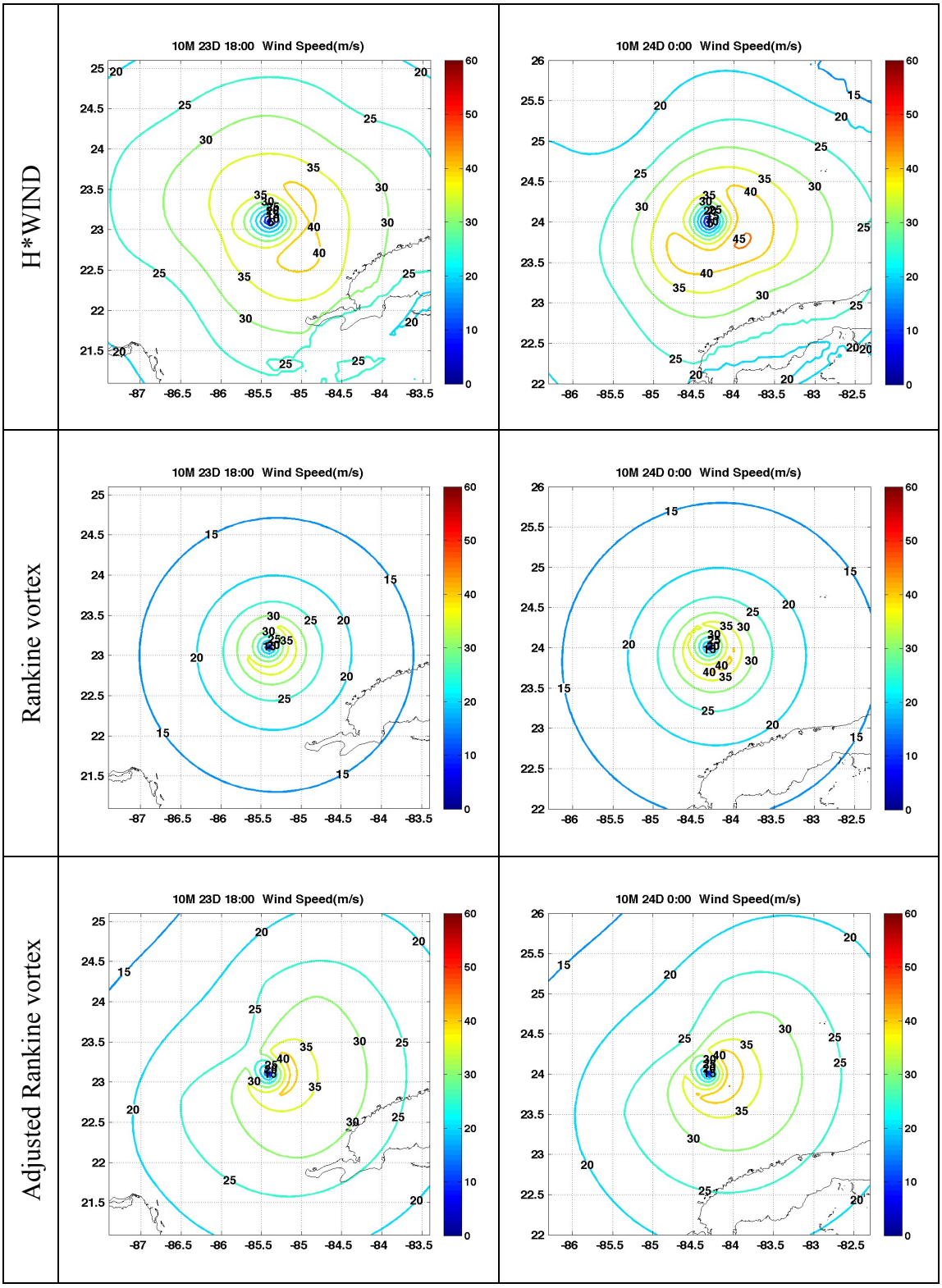
H*WIND
Rankine vortex
Adjusted Rankine vortex
10M 23D 18:00 Wind Speed(m/s)
10M 24D 0:00 Wind Speed(m/s)

[13] Alberto (2006)

H*WIND	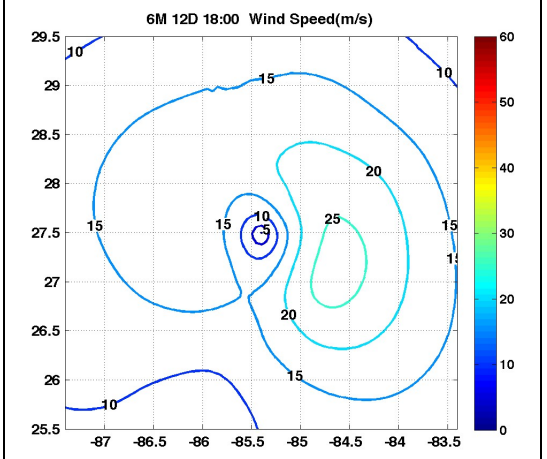	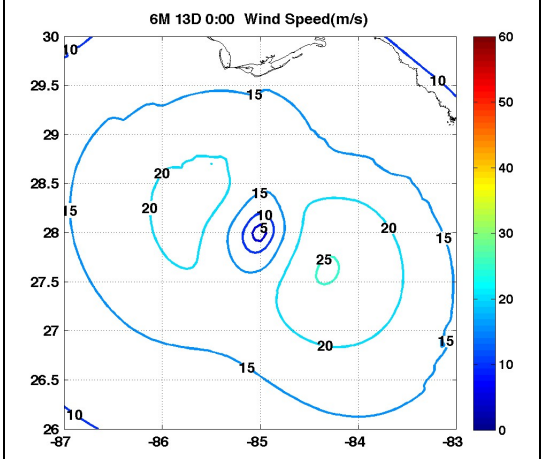
Rankine vortex	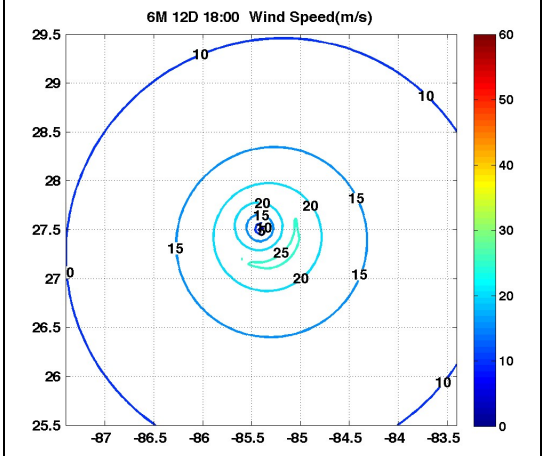	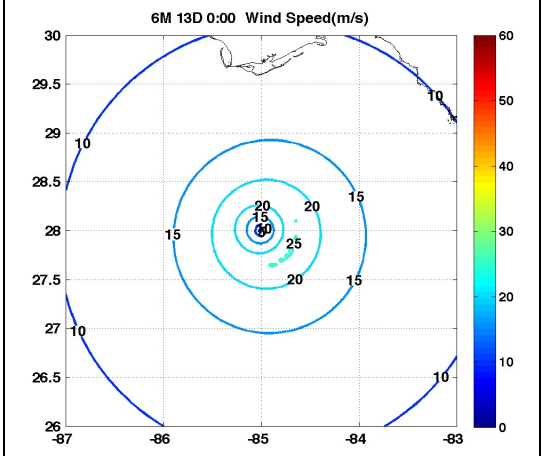
Adjusted Rankine vortex	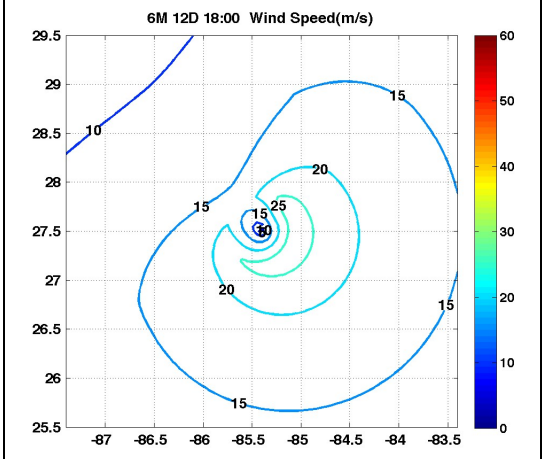	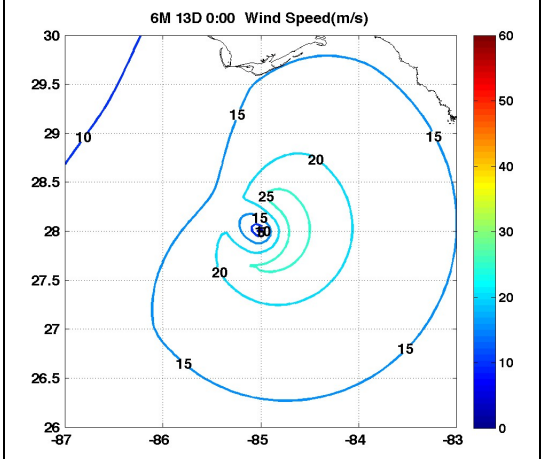

H*WIND	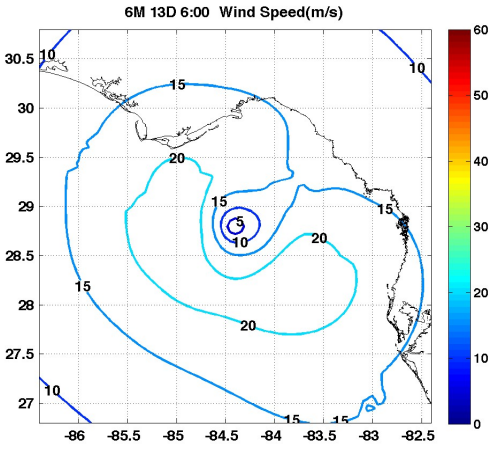	
Rankine vortex	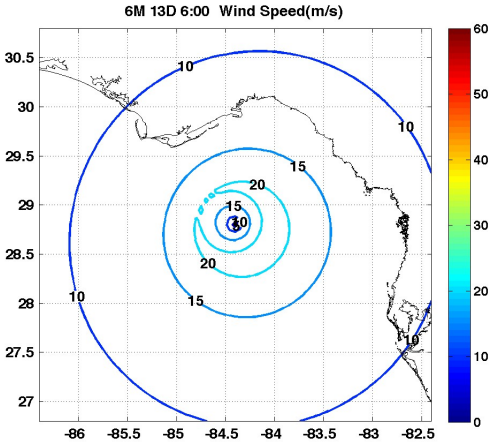	
Adjusted Rankine vortex	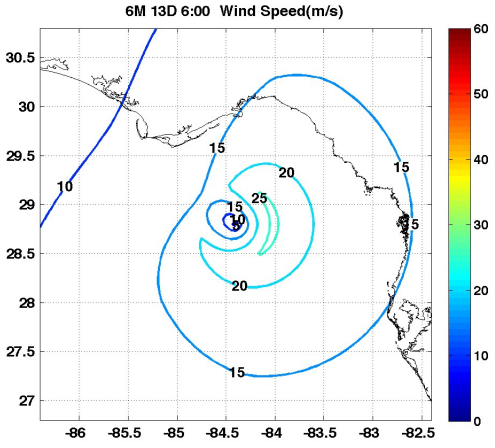	

[14] Dean (2007)

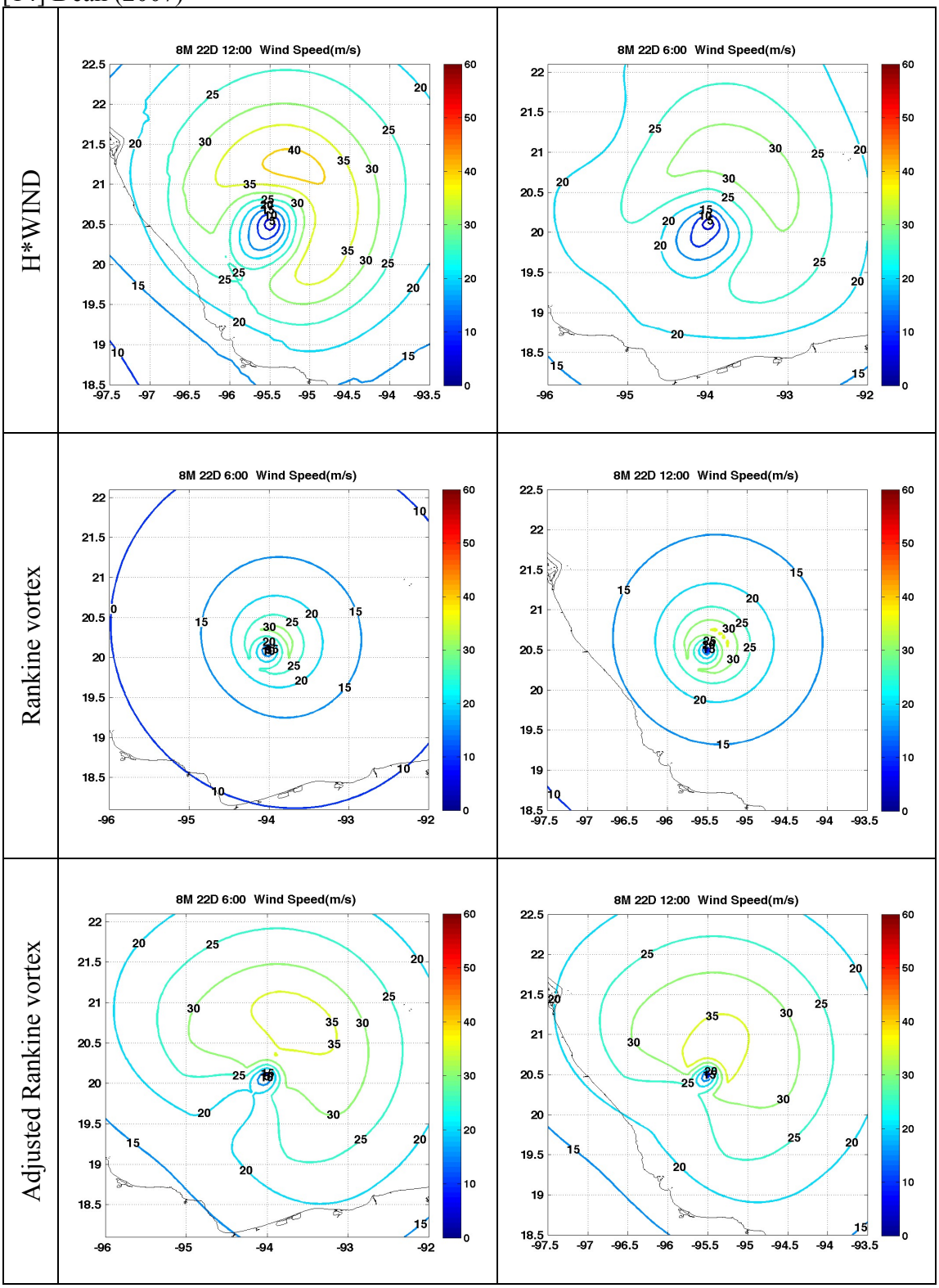
H*WIND
Rankine vortex
Adjusted Rankine vortex
8M 22D 12:00 Wind Speed(m/s)
8M 22D 6:00 Wind Speed(m/s)
8M 22D 6:00 Wind Speed(m/s)
8M 22D 12:00 Wind Speed(m/s)
8M 22D 6:00 Wind Speed(m/s)
8M 22D 12:00 Wind Speed(m/s)

[15] Dolly (2008)

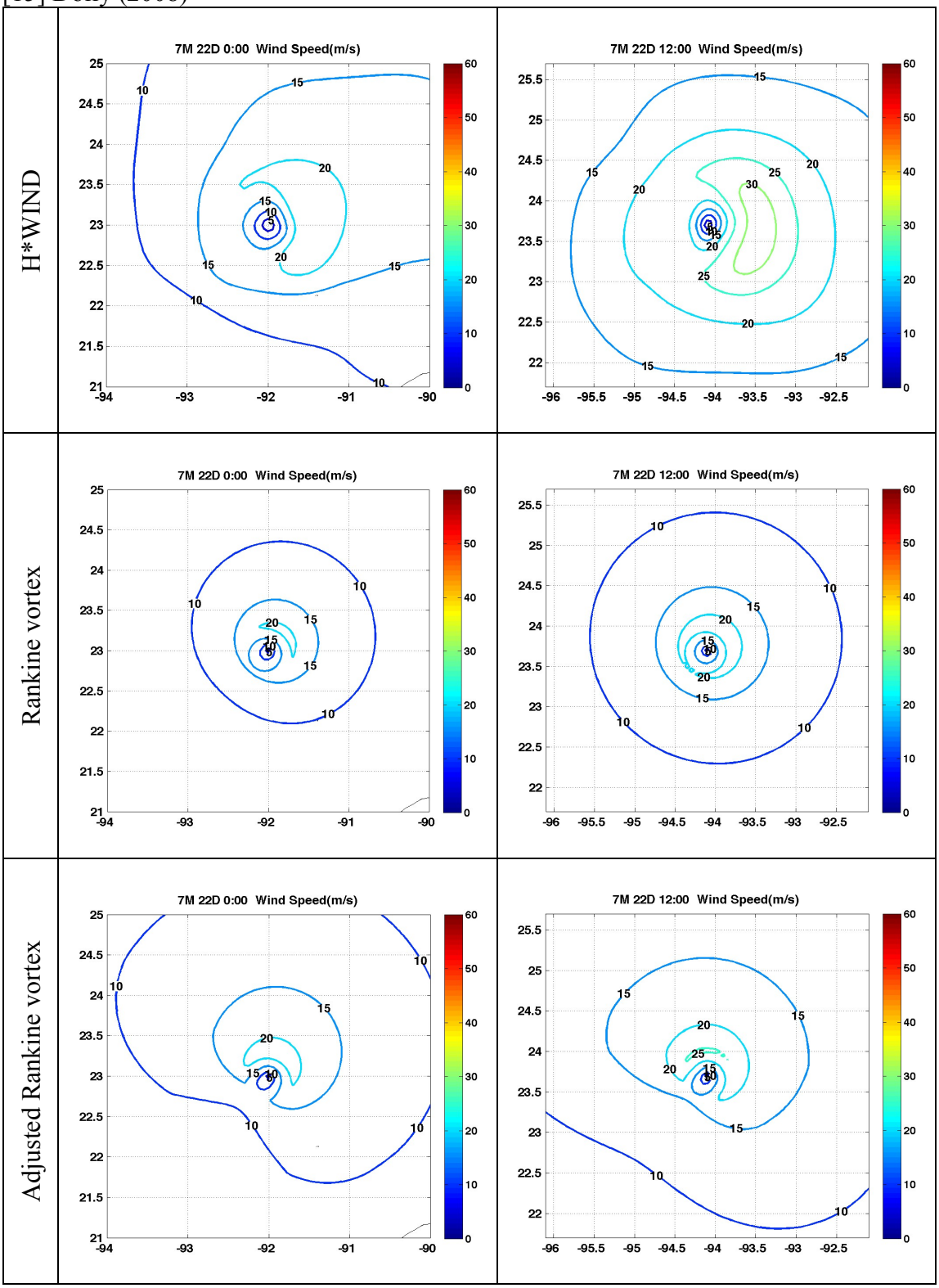

H*WIND	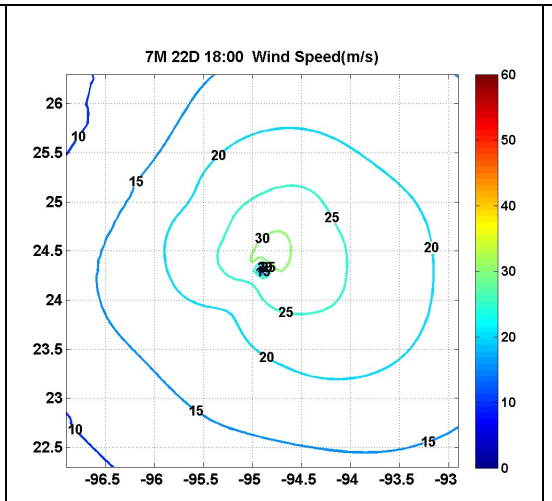	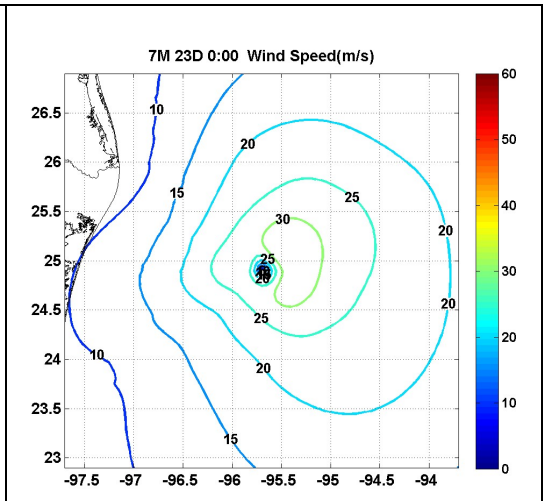
Rankine vortex	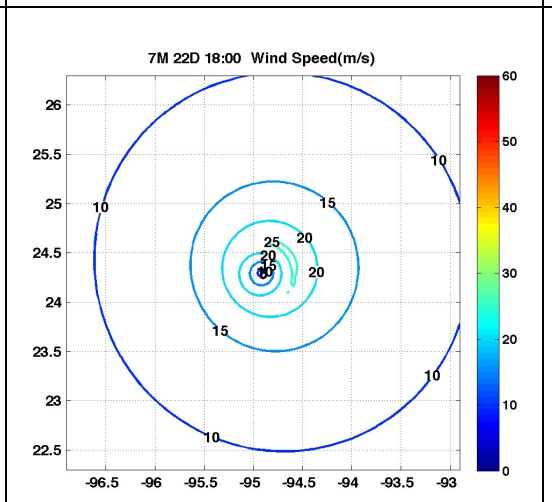	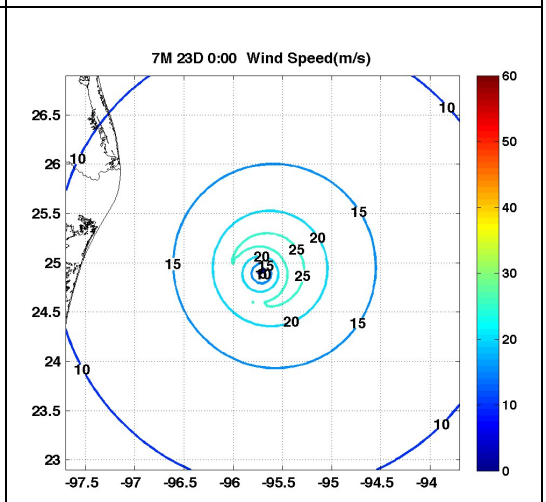
Adjusted Rankine vortex	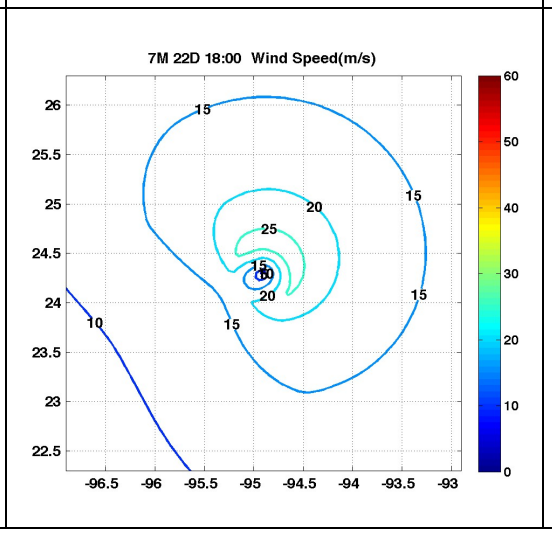	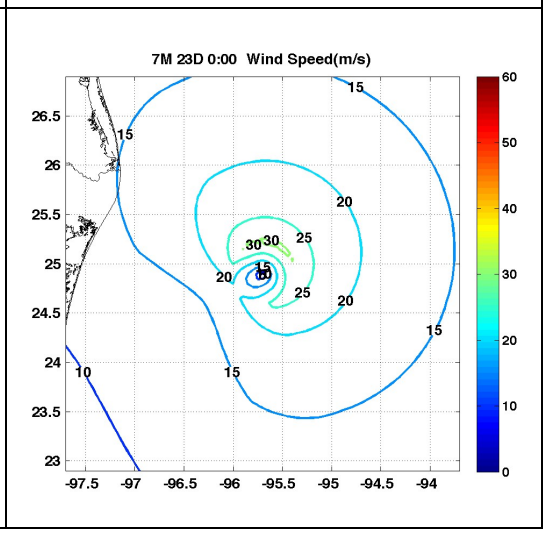

[16] Gustav (2008)

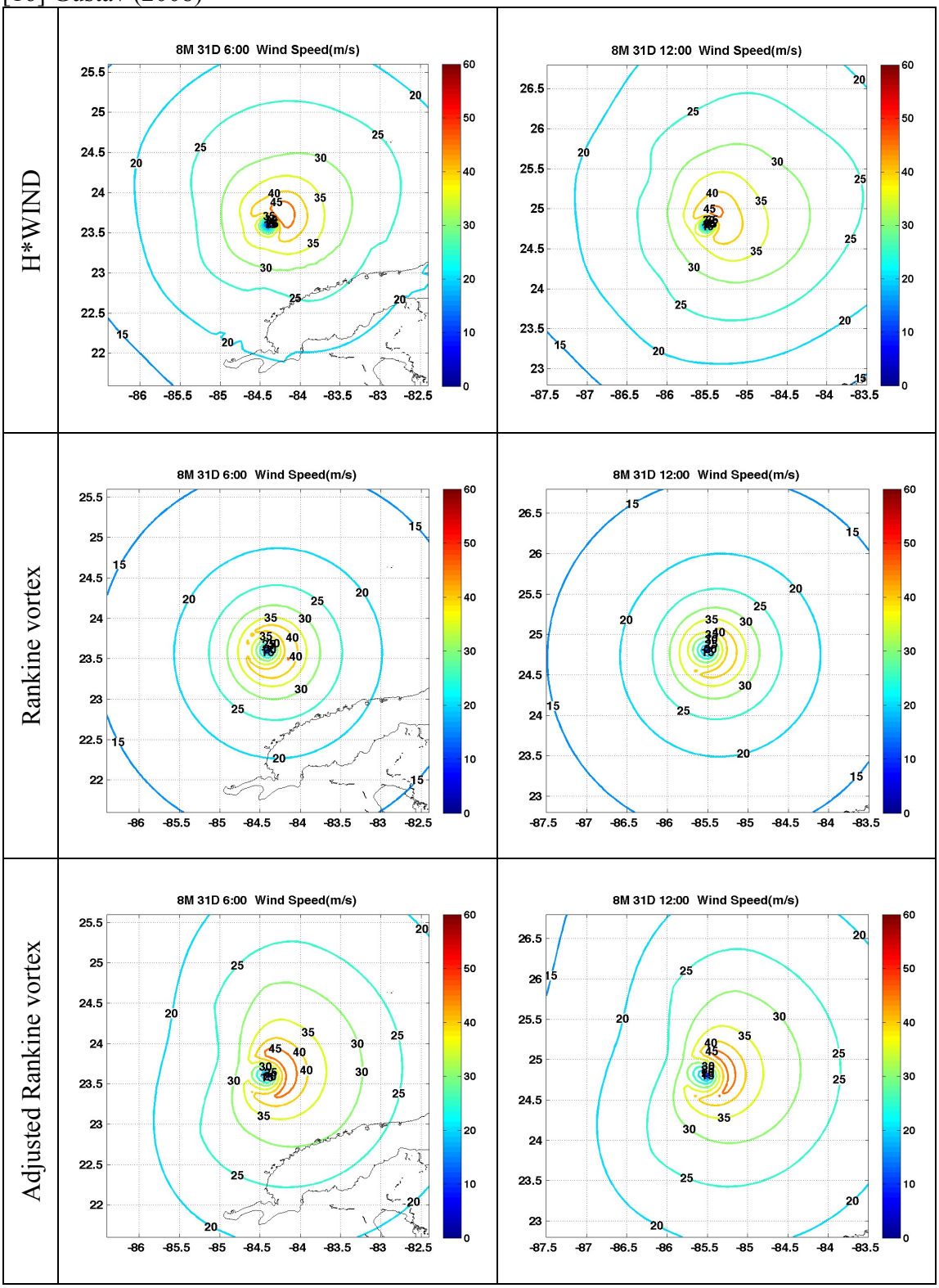

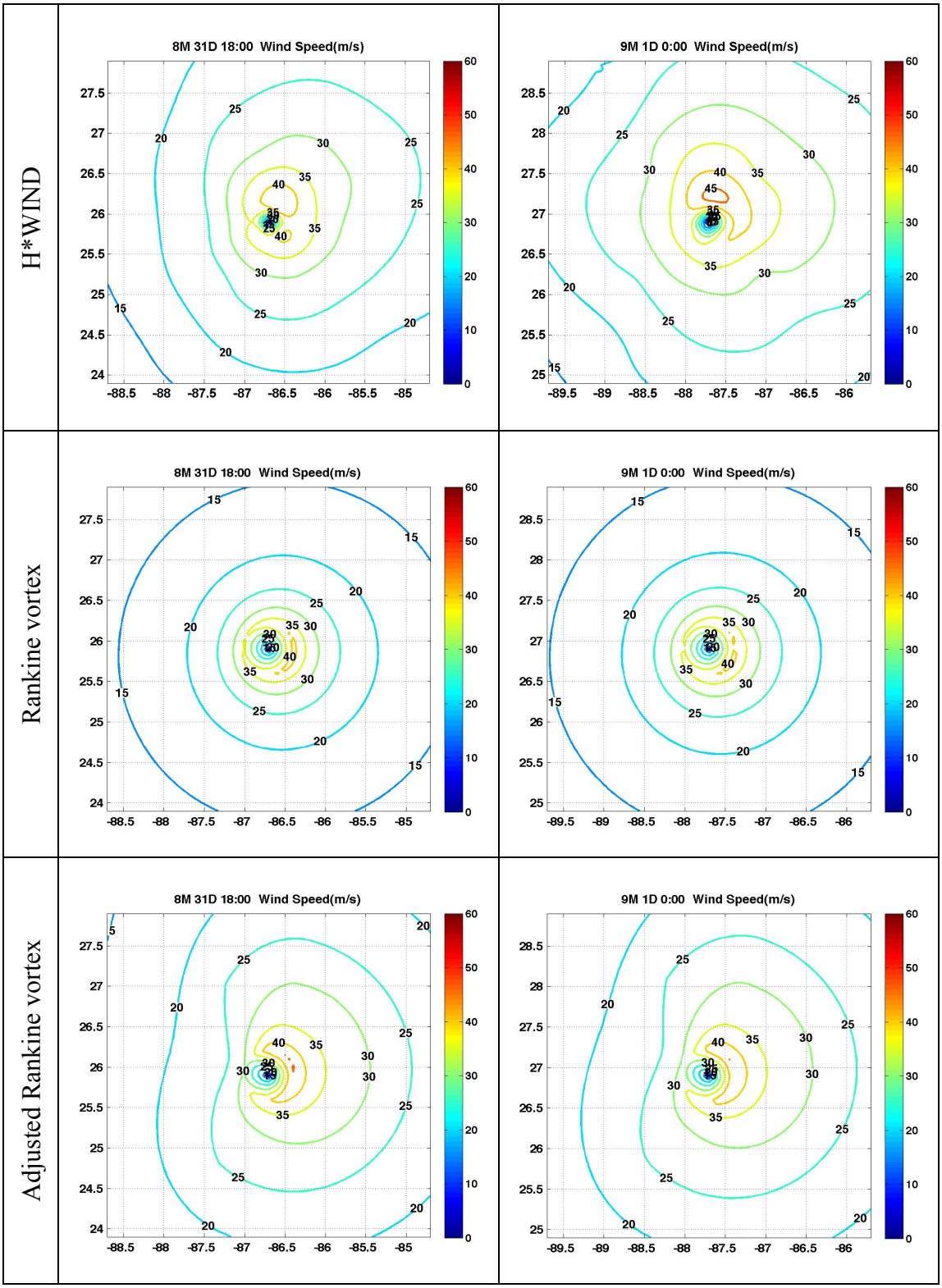
H*WIND
Rankine vortex
Adjusted Rankine vortex
8M 31D 18:00 Wind Speed(m/s)
9M 1D 0:00 Wind Speed(m/s)

H*WIND	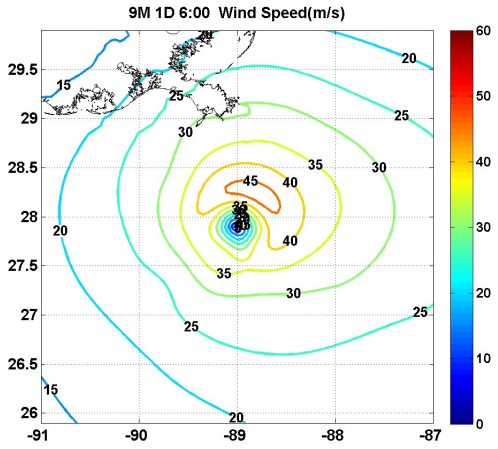	
Rankine vortex	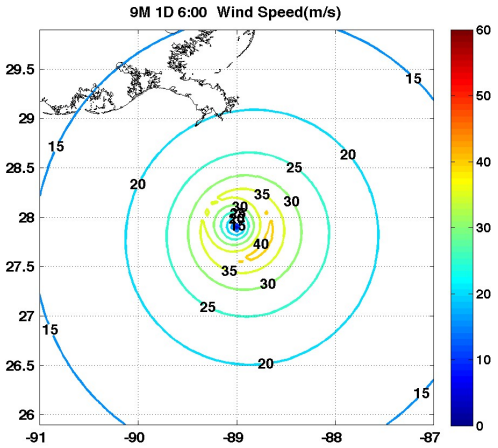	
Adjusted Rankine vortex	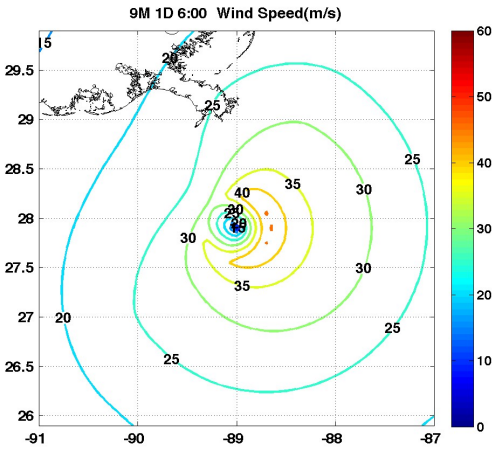	

[17] Ike (2008)

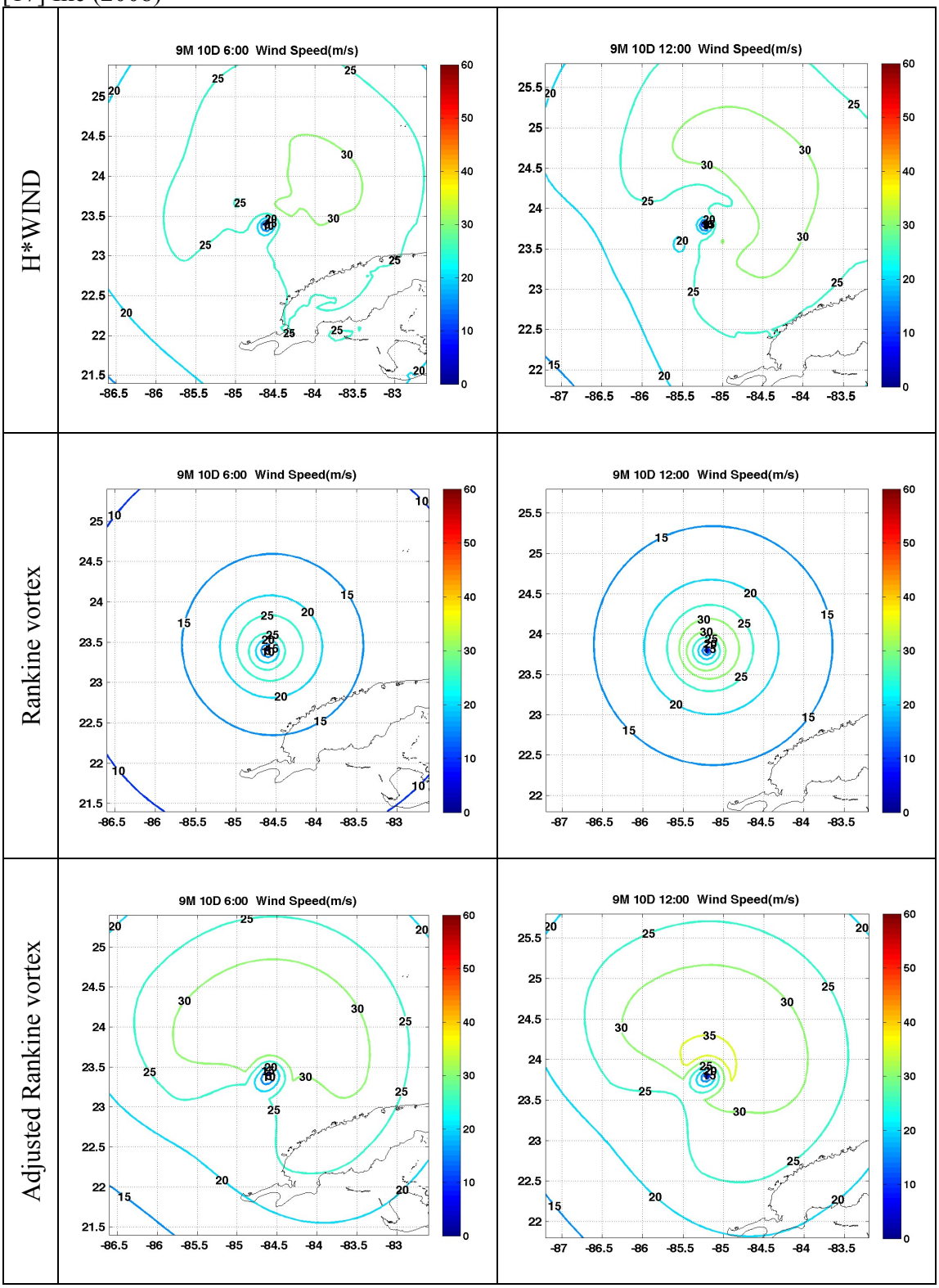
H*WIND
Rankine vortex
Adjusted Rankine vortex
9M 10D 6:00 Wind Speed(m/s)
9M 10D 12:00 Wind Speed(m/s)

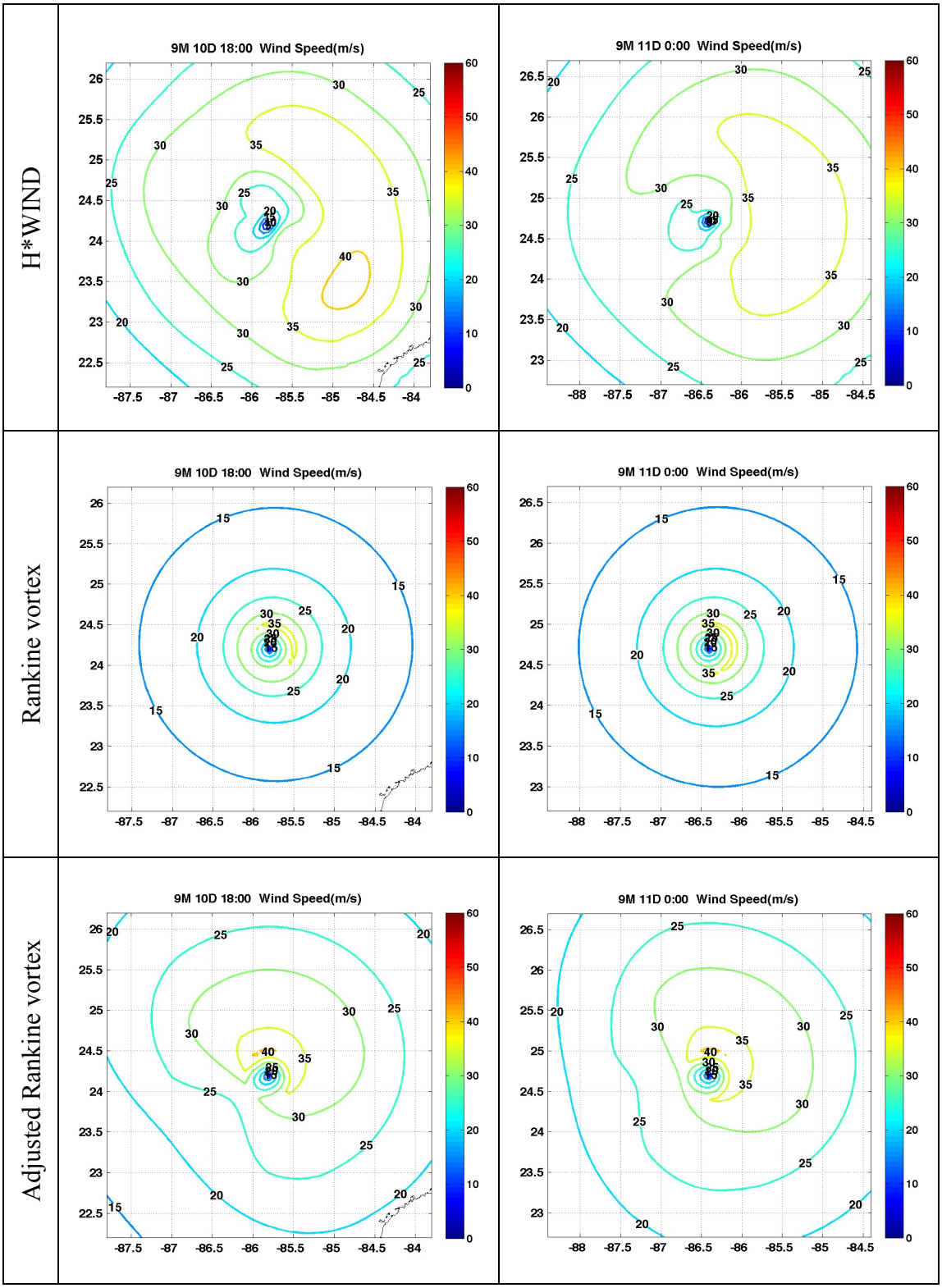
H*WIND
Rankine vortex
Adjusted Rankine vortex
9M 10D 18:00 Wind Speed(m/s)
9M 11D 0:00 Wind Speed(m/s)

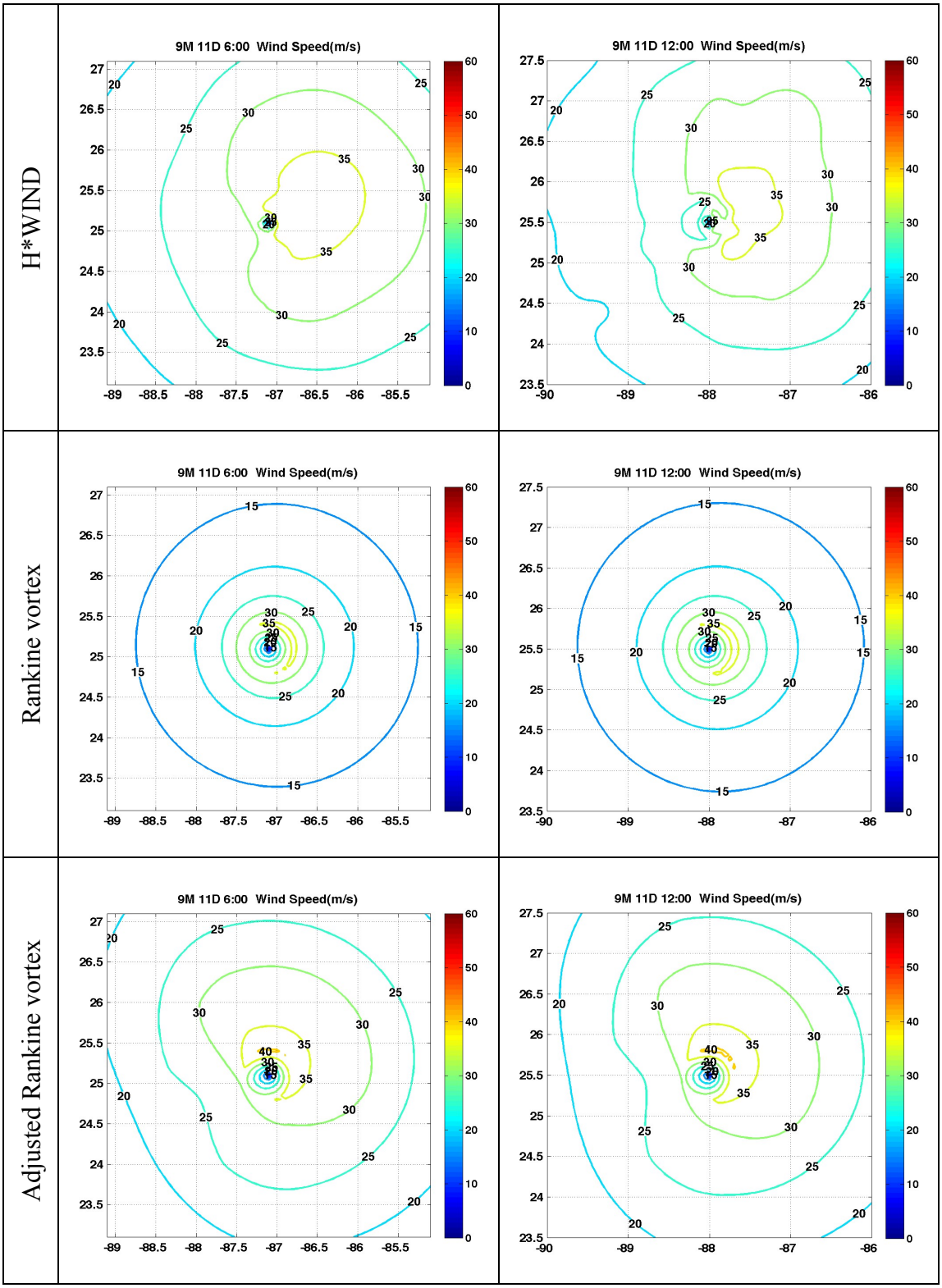
H*WIND
Rankine vortex
Adjusted Rankine vortex
9M 11D 6:00 Wind Speed(m/s)
9M 11D 12:00 Wind Speed(m/s)

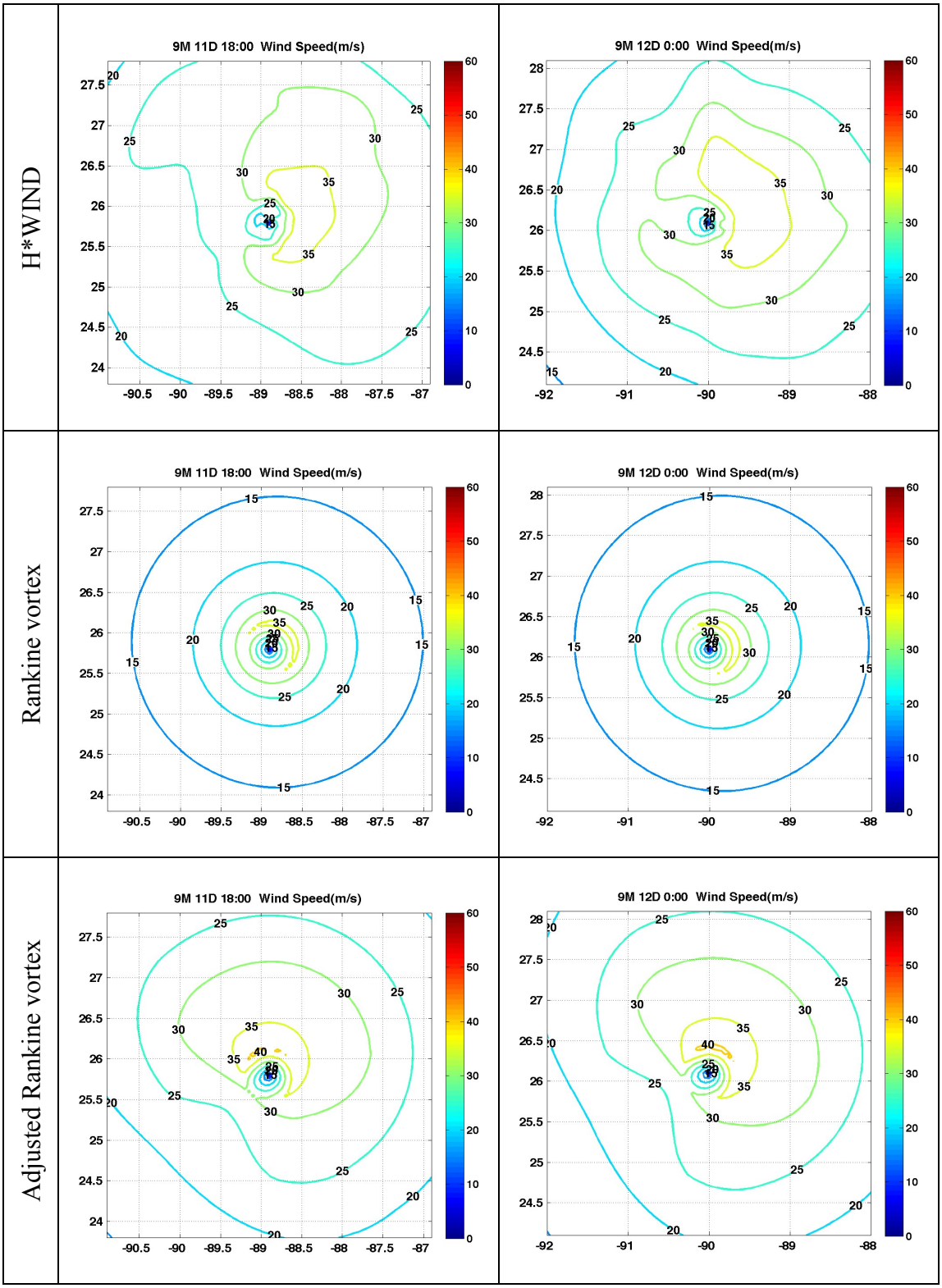
H*WIND
Rankine vortex
Adjusted Rankine vortex
9M 11D 18:00 Wind Speed(m/s)
9M 12D 0:00 Wind Speed(m/s)

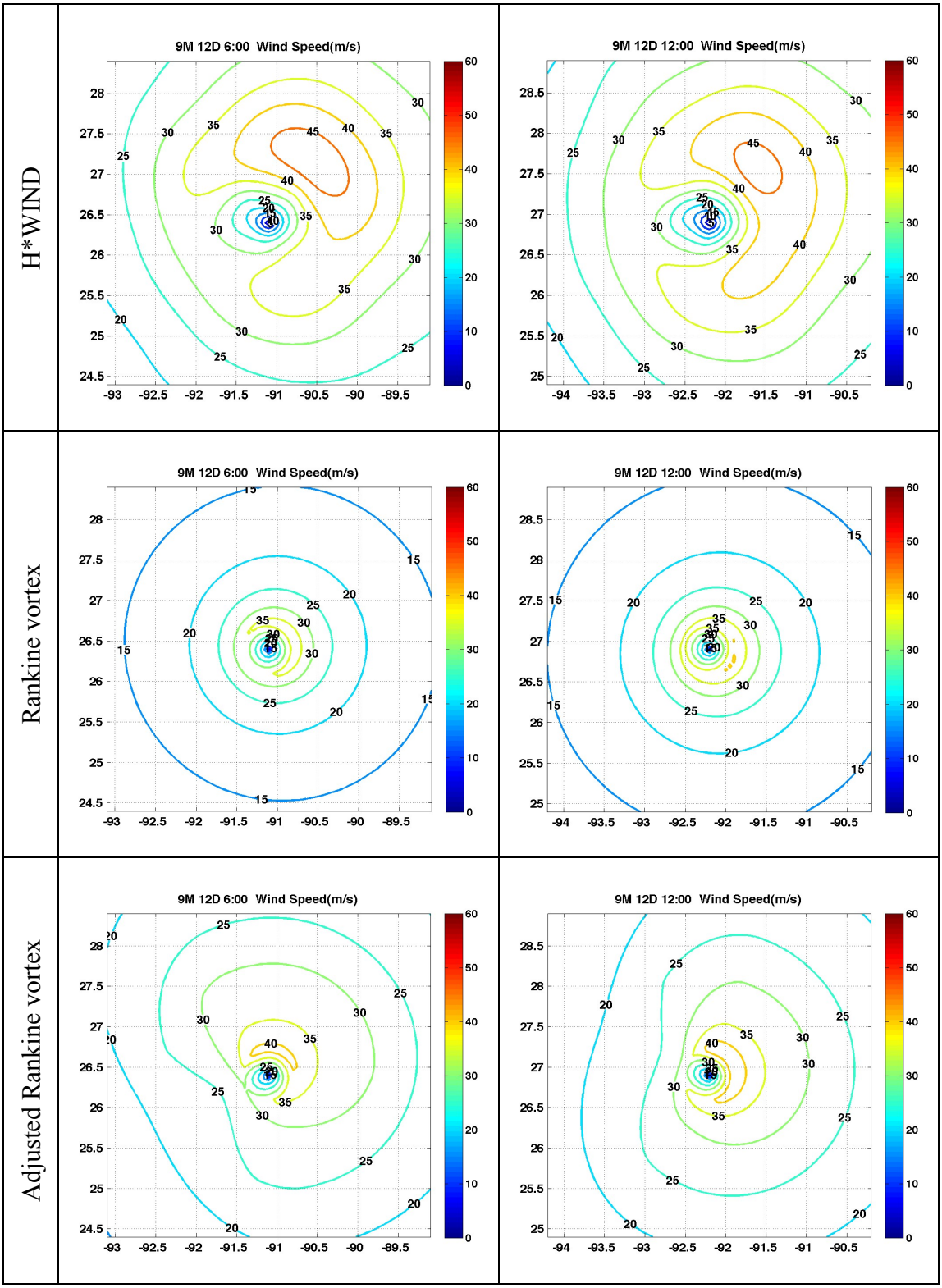
H*WIND
Rankine vortex
Adjusted Rankine vortex
9M 12D 6:00 Wind Speed(m/s)
9M 12D 12:00 Wind Speed(m/s)

H*WIND	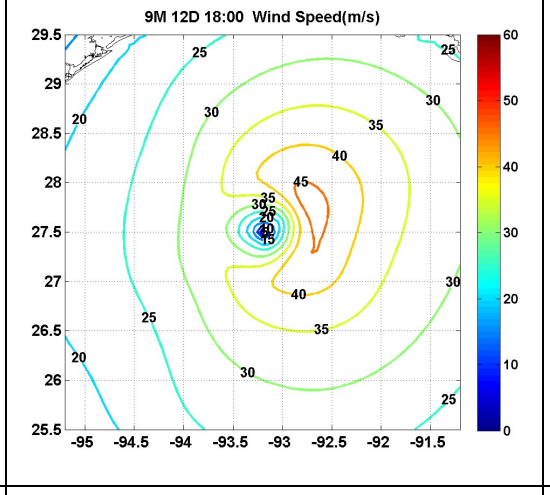	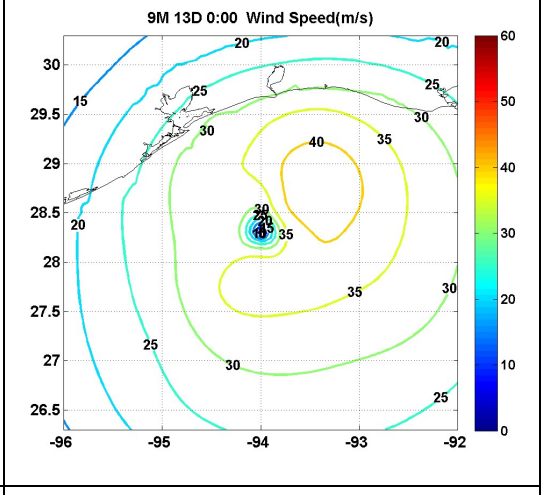
Rankine vortex	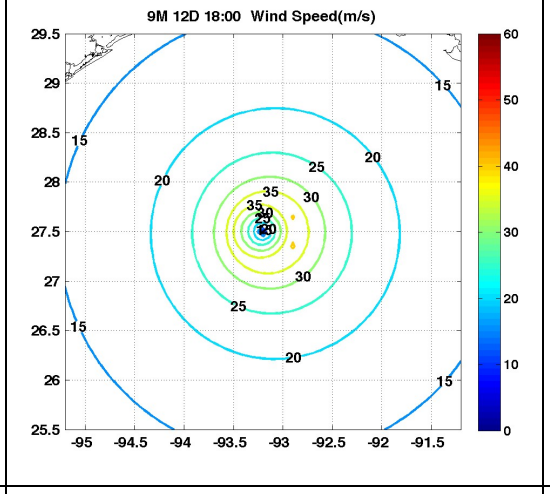	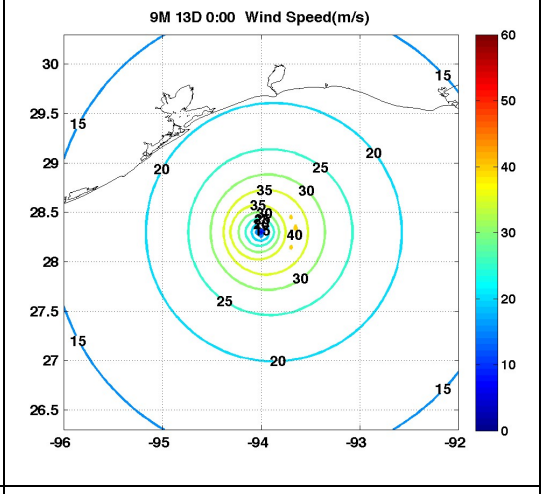
Adjusted Rankine vortex	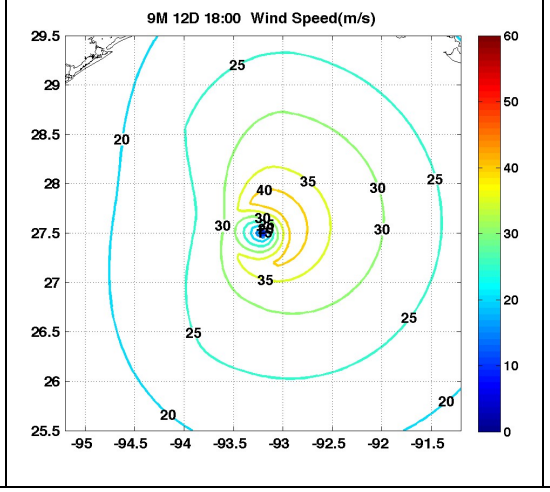	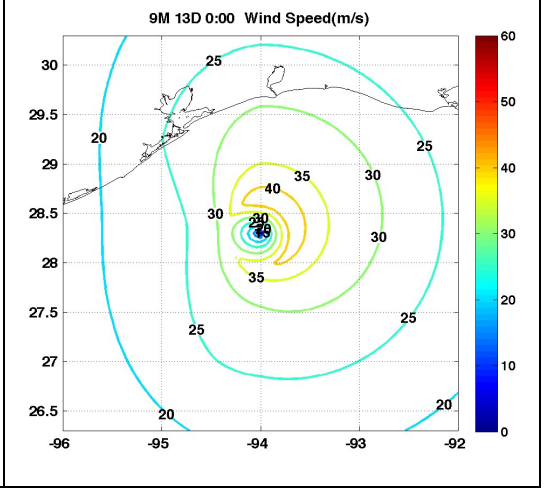

APPENDIX B

AVAILABLE HURDAT DATA FOR GULF OF MEXICO

No.	Year	Name	Data	Start		End		Peak of intensity
1	1958	ALMA	NAN	June	14d06h		16d18h	Tropical storm
2	1958	ELLA	NAN	Aug.	30d06h	Sep.	6d18h	Category 3
3	1959	ARLENE	NAN	May	28d12h	June	2d18h	Tropical storm
4	1959	BEULAH	NAN	June	15d18h		18d18h	Tropical storm
5	1959	NaN	NAN	June	18d00h	June	21d18h	Category 1
6	1959	DEBRA	NAN	July	23d00h	July	28d06h	Category 1
7	1959	IRENE	NAN	Oct.	6d18h		9d06h	Tropical storm
8	1959	JUDITH	NAN	Oct.	17d12h		21d18h	Category 1
9	1960	NaN	NAN	June	22d06h		29d00h	Tropical storm
10	1960	BRENDA	NAN	July	28d18h	Aug.	01d01h	Tropical storm
11	1960	ETHEL	NAN	Sep.	14d12h		17d18h	Category 5
12	1960	FLORENCE	NAN	Sep.	17d06h		27d06h	Tropical storm
13	1961	CARLA	O	Sep.	03d12h		16d00h	Category 5
14	1963	CINDY	NAN	Sep.	16d12h		20d00h	Category 1
15	1964	NaN	NAN	June	02d12h		11d18h	Tropical storm
16	1964	ABBY	NAN	Aug.	05d18h		08d18h	Tropical storm
17	1964	HILDA	O	Sep.	28d12h	Oct.	05d18h	Category 4
18	1964	ISBELL	O	Oct.	08d12h		17d00h	Category 3
19	1965	NaN	NAN	June	11d06d		18d06h	Tropical storm
20	1965	BETSY	O	Aug.	27d00h	Sep.	13d00h	Category 4
21	1965	DEBBIE	O	Sep.	24d12h		30d00h	Tropical storm
22	1966	ALMA	O	June	04d06h		14d12h	Category 3
23	1966	INEZ	O	Sep.	21d12h	Oct.	11d12h	Category 4
24	1967	BEULAH	O	Sep.	05d12h		22d18h	Category 5
25	1967	FERN	O	Oct.	01d18h		04d18h	Category 1
26	1968	ABBY	O	June	01d06h		13d18h	Category 1
27	1968	CANDY	NAN	June	22d18h		26d06h	Tropical storm
28	1968	GLADYS	O	Oct.	13d12h		21d18h	Category 1
29	1969	CAMILLE	O	Aug.	14d18h		22d12h	Category 5
30	1969	SUBTROP 1	O	Sep.	29d12h	Oct.	01d18h	Subtropical Storm
31	1969	JENNY	NAN	Oct.	01d12h		06d18h	Tropical storm
32	1969	LAURIE	O	Oct.	17d00h		27d06h	Category 2
33	1970	ALMA	O	May	17d18h		27d06h	Category 1
34	1970	BECKY	O	July	19d00h		23d12h	Tropical storm
35	1970	CELIA	O	July	31d00h	Aug.	05d18h	Category 3
36	1970	ELLA	O	Sep.	08d12h		13d06h	Category 3
37	1970	FELICE	O	Sep.	12d00h		17d12h	Tropical storm
38	1970	GRETA	O	Sep.	26d12h	Oct.	05d00h	Tropical storm
39	1971	EDITH	O	Sep.	05d18h		18d06h	Category 5
40	1971	FERN	O	Sep.	03d12h		13d00h	Category 1
41	1972	AGNES	O	June	14d12h		23d00h	Category 1
42	1973	DELIA	O	Sep.	01d18h		07d06h	Tropical storm
43	1974	CARMEN	O	Aug.	29d06h	Sep.	10d06h	Category 4

No.	Year	Name	Data	Start		End		Peak of intensity
44	1975	CAROLINE	O	Aug.	24d12h	Sep.	01d12h	Category 3
45	1975	ELOISE	O	Sep.	13d06h		24d18h	Category 3
46	1976	SUBTROP 1	O	May	21d12h		25d18h	Subtropical Storm
47	1977	ANITA	O	Aug.	29d12h	Sep.	03d06h	Category 5
48	1977	BABE	O	Sep.	03d06h		09d00h	Category 1
49	1978	BESS	O	Aug.	05d12h		08d12h	Tropical storm
50	1978	DEBRA	O	Aug.	26d12h		29d18h	Tropical storm
51	1979	BOB	O	July	09d12h		16d12h	Category 1
52	1979	CLAUDETTE	O	July	15d12h		29d12h	Tropical storm
53	1979	ELENA	O	Aug.	30d00h	Sep.	02d00h	Tropical storm
54	1979	FREDERIC	O	Aug.	29d06h	Sep.	15d00h	Category 4
55	1979	HENRI	O	Sep.	15d00h		24d12h	Category 1
56	1980	ALLEN	O	July	31d12h	Aug.	11d18h	Category 5
57	1980	DANIELLE	O	Sep.	04d18h		07d12h	Tropical storm
58	1980	JEANNE	O	Nov.	07d18h		16d06h	Category 2
59	1982	ALBERTO	O	June	02d12h		06d12h	Category 1
60	1982	SUBTROP 1	O	June	18d00h		20d18h	Subtropical Storm
61	1982	CHRIS	O	Sep.	09d00h		12d18h	Tropical storm
62	1983	ALICIA	O	Aug.	15d12h		21d06h	Category 3
63	1983	BARRY	O	Aug.	23d18h		29d12h	Category 1
64	1985	BOB	O	July	21d06h		26d00h	Category 1
65	1985	DANNY	O	Aug.	12d00h		20d18h	Category 1
66	1985	ELENA	O	Aug.	28d00h	Sep.	04d18h	Category 3
67	1985	JUAN	O	Oct.	26d00h	Nov.	01d18h	Category 1
68	1986	BONNIE	O	June	23d18h		28d12h	Category 1
69	1987	NaN	O	Aug.	09d12h		17d06h	Tropical storm
70	1988	DEBBY	O	Aug.	31d18h	Sep.	08d18h	Category 1
71	1988	FLORENCE	O	Sep.	07d06h		11d12h	Category 1
72	1988	GILBERT	O	Sep.	08d18h		20d00h	Category 5
73	1988	KEITH	O	Nov.	17d18h		26d18h	Tropical storm
74	1989	ALLISON	O	June	24d00h	July	01d18h	Tropical storm
75	1989	CHANTAL	O	July	30d00h	Aug.	03d18h	Category 1
76	1989	JERRY	O	Oct.	12d06h		16d18h	Category 1
77	1990	DIANA	O	Aug.	04d00h		09d12h	Category 2
78	1990	MARCO	O	Oct.	09d12h		13d12h	Tropical storm
79	1992	ANDREW	O	Aug.	16d18h		28d06h	Category 5
80	1993	ARLENE	O	June	18d00h		21d06h	Tropical storm
81	1993	GERT	O	Sep.	14d18h		21d18h	Category 2
82	1994	ALBERTO	O	June	30d06h	July	07d18h	Tropical storm
83	1994	BERYL	O	Aug.	14d00h		19d00h	Tropical storm
84	1995	ALLISON	O	June	03d00h		11d00h	Category 1
85	1995	DEAN	O	July	28d00h	Aug.	02d18h	Tropical storm
86	1995	ERIN	O	July	31d00h	Aug.	06d12h	Category 1
87	1995	GABRIELLE	O	Aug.	09d00h		12d00h	Tropical storm
88	1995	OPAL	O	Sep.	27d00h	Oct.	06d18h	Category 4
89	1996	DOLLY	O	Aug.	19d06h		25d00h	Category 1
90	1996	JOSEPINE	O	Oct.	04d18h		16d00h	Tropical storm

No.	Year	Name	Data	Start		End		Peak of intensity
91	1997	DANNY	O	July	16d12h		27d12h	Category 1
92	1998	CHARLEY	O	Aug.	21d06h		24d00h	Tropical storm
93	1998	EARL	O	Aug.	31d12h	Sep.	08d18h	Category 2
94	1998	FRANCES	O	Sep.	08d18h		13d18h	Tropical storm
95	1998	GEORGES	O	Sep.	15d12h	Oct.	01d06h	Category 4
96	1998	HERMINE	O	Sep.	17d12h		20d18h	Tropical storm
97	1998	MITCH	O	Oct.	22d00h	Nov.	09d18h	Category 5
98	1999	BRET	O	Aug.	18d18h		25d00h	Category 4
99	1999	HARVEY	O	Sep.	19d06h		22d00h	Tropical storm
100	2000	BERTL	O	Aug.	13d18h		15d18h	Tropical storm
101	2000	GORDON	O	Sep.	14d12h		21d06h	Category 1
102	2000	HELENE	O	Sep.	15d12h		25d18h	Tropical storm
103	2000	KEITH	O	Sep.	28d18h	Oct.	06d12h	Category 4
104	2001	ALLISON	O	June	05d12h		19d00h	Tropical storm
105	2001	BARRY	O	Aug.	02d12h		08d06h	Tropical storm
106	2001	GABRIELLE	O	Sep.	11d18h		21d18h	Category 1
107	2002	BERTHA	O	Aug.	04d18h		09d12h	Tropical storm
108	2002	EDOUARD	O	Sep.	01d18h		06d12h	Tropical storm
109	2002	FAY	O	Sep.	05d18h		11d06h	Tropical storm
110	2002	HANNA	O	Sep.	12d00h		15d12h	Tropical storm
111	2002	ISIDORE	O	Sep.	14d18h		27d18h	Category 3
112	2002	LILI	O	Sep.	21d18h	Oct.	04d12h	Category 4
113	2003	BILL	O	June	28d06h	July	03d00h	Tropical storm
114	2003	CLAUDETTE	O	July	07d00h		17d12h	Category 1
115	2003	ERIKA	O	Aug.	14d18h		17d00h	Category 1
116	2003	GRACE	O	Aug.	30d12h	Sep.	02d06h	Tropical storm
117	2003	HENRI	O	Sep.	03d18h		08d18h	Tropical storm
118	2003	LARRY	O	Sep.	27d18h	Oct.	07d18h	Tropical storm
119	2004	BONNIE	O	Aug.	03d12h		14d00h	Tropical storm
120	2004	CHARLEY	O	Aug.	09d12h		15d12h	Category 4
121	2004	FRANCES	O	Aug.	25d00h	Sep.	10d18h	Category 4
122	2004	IVAN	O	Sep.	02d18h		24d06h	Category 5
123	2004	MATTTHEW	O	Oct.	08d12h		11d06h	Tropical storm
124	2005	ARLENE	O	June	08d18h		14d06h	Tropical storm
125	2005	BRET	O	June	28d18h		30d00h	Tropical storm
126	2005	CINDY	O	July	03d18h		11d06h	Category 1
127	2005	DENNIS	O	July	04d18h		18d06h	Category 4
128	2005	EMILY	O	July	11d00h		21d12h	Category 5
129	2005	GERT	O	July	23d18h		25d18h	Tropical storm
130	2005	KATRINA	O	Aug.	23d18h		31d06h	Category 5
131	2005	RITA	O	Sep.	18d00h		26d06h	Category 5
132	2005	STAN	O	Oct.	01d12h		05d06h	Category 1
133	2005	WILMA	O	Oct.	15d18h		26d18h	Category 5
134	2006	ALBERTO	O	June	10d06h		19d06h	Tropical storm
135	2007	BARRY	O	May	31d00h	June	05d12h	Tropical storm
136	2007	DEAN	O	Aug.	13d06h		23d00h	Category 5
137	2007	ERIN	O	Aug.	15d00h		19d18h	Tropical storm

No.	Year	Name	Data	Start		End		Peak of intensity
138	2007	HUMBERTO	O	Sep.	12d06h		14d12h	Category 1
139	2007	LORENZO	O	Sep.	25d18h		28d18h	Category 1
140	2007	OLGA	O	Dec.	10d12h		16d06h	Tropical storm
141	2008	DOLLY	O	July	20h12h		27d00h	Category 2
142	2008	EDOUARD	O	Aug.	03d12h		06d18h	Tropical storm
143	2008	GUSTAV	O	Aug.	25d00h	Sep.	05d12h	Category 4
144	2008	IKE	O	Sep.	01d06h		15d12h	Category 4
145	2008	PALOMA	O	Nov.	05d18h		14d06h	Category 4

VITA

Chan Kwon Jeong graduated with a Bachelor of Science degree from the Department of Naval Architecture and Ocean Engineering at HongIk University, Korea, in 1997. During his bachelor degree, he joined Korean Army as a soldier and served between 1992 and 1995. He entered the Department of Naval Architecture at Inha University in January 1997 and received his Master of Science degree in January 1999. After finishing his master degree, he started his professional career as a researcher at SONCY engineering in 1999. He came to Texas A&M University in the fall of 2002 to pursue his doctoral degree in Ocean Engineering. His research interests include numerical wave forecast and hindcast, hurricane wind and wave and extreme condition analysis.

Permanent address: Texas A&M University at Galveston
Department of Maritime Systems Engineering,
200 Seawolf Parlway, Galveston, TX 77554

Email Address: chankwon.jeong@gmail.com